Chemical Biology Tools to Study Bacterial Cell Surface Glycans

By

Victoria M. Marando

B.S. Chemical Biology
McMaster University 2018

Submitted to the Department of Chemistry
in Partial Fulfillment of the Requirements for the Degree of

DOCTOR OF PHILOSOPHY IN CHEMISTRY

at the

MASSACHUSETTS INSTITUTE OF TECHNOLOGY

June 2023

Authored By: _____
Victoria M. Marando
Department of Chemistry
April 6, 2023

Certified By: _____
Laura L. Kiessling
Novartis Professor of Chemistry
Thesis Supervisor

Accepted By: _____
Adam P. Willard
Associate Professor of Chemistry
Graduate Officer
Chair, Department Committee on Graduate Students

This doctoral thesis has been examined by a committee of professors
from the Department of Chemistry as follows:

Professor Ronald T. Raines _____

Thesis Committee Chair
Roger and Georges Firmenich Professor of Chemistry

Professor Laura L. Kiessling _____

Thesis Supervisor
Novartis Professor of Chemistry

Professor Bryan Bryson _____

Thesis Committee Member
Associate Professor of Biological Engineering

Chemical Biology Tools to Study Bacterial Cell Surface Glycans

By
Victoria M. Marando

Submitted to the Department of Chemistry
on May 12, 2023 in Partial Fulfillment of the Requirements for the Degree of
Doctor of Philosophy in Chemistry

Abstract

Cell surface glycans are ubiquitous and serve as the first point of contact between a cell and the surrounding environment. Many of the carbohydrate-mediated interactions that occur at this interface regulate key signaling processes such as cell-cell recognition, communication, and adhesion. Bacterial glycans in particular play critical roles in maintaining cellular structure and are implicated in infections and pathogenesis. Understanding molecular determinants of these important biological functions is critical for both fundamental and translational research. Despite the need to better understand these important biological structures, methods for probing glycan structure and function remain limited. Glycans are incompatible with common strategies for studying other biomacromolecules, which often exploit chemoselective reactions for covalent modification, capture, or imaging. Unlike the amino acid residues that constitute proteins, glycan building blocks are composed primarily of polyol isomers and lack distinguishing reactivity required for selective labeling. Moreover, unlike protein synthesis, glycan biosynthesis is not templated, making perturbation through genetic manipulation is often convoluted. Finally, the molecular complexity of glycan composition presents an added challenge. Unlike the 20 canonical amino acids used in proteins, bacteria use more than 600 distinct monosaccharide building blocks. To address this open challenge, we developed novel chemical biology tools to study bacterial cell surface glycans. We have established a new, generalizable strategy for chemoselective glycan modification to enable the study of specific bacterial cell wall glycans. Our method relies on the direct incorporation of reactive glycan building block surrogates by cell surface glycosyltransferases, a technique termed “biosynthetic incorporation”. We first validated this approach by labeling the arabinan (Chapter 2), which enabled several important downstream applications, including assay development and controlled cell surface perturbation (Chapter 3). We then demonstrated the generalizability of this approach by developing probes for mannose-containing glycans using this strategy (Chapter 4). In this work, we have also targeted modification of the cell wall assembly enzymes themselves (Chapter 5), in addition to the structures they produce. Ultimately, we envision that the chemical biology tools developed in this work will be useful for both answering fundamental biological questions and towards efforts to develop new antibiotics.

Thesis Supervisor: Laura L. Kiessling
Title: Novartis Professor of Chemistry

Acknowledgments

This Ph.D. would not have been possible without so many people. First and foremost, thank you to the Toronto Maple Leafs for teaching me that no matter how many times you fail, the only thing that matters is that you keep working hard, chasing pucks behind the net, and coming back next game (or next season) with all the confidence in the world. Being a fan of this team has taught me about resilience, dedication, and passion, all things that carried me through this Ph.D.

My real first thank you is to the one and only Prof. Laura L. Kiessling. Thank you for the opportunity to work in your research group where I have learned countless lessons and numerous skills. I am constantly inspired by your passion and excitement for science, and your ability to share that with everyone you meet. I am grateful for the freedom you have provided to follow the science in any direction it took and for having faith that I could drive my projects. Thank you for the support you have given, for all the opportunities that you have provided, and for shaping me into the scientist I am today.

Thank you to my scientific mentors at McMaster, Karolinska, and NMX, who are the reason I went to graduate school. I would not have had the confidence or skills to even imagine being here without you. In particular, thank you to Prof. Alex Adronov for being the first person to teach me about the excitement of scientific research. Even more, thank you for being a constant source of support and guidance, for many years after I left McMaster.

Thank you to my thesis committee members Prof. Ronald T. Raines and Prof. Bryan Bryson. Thank you to Ron for years of light-hearted taunting about the Toronto Maple Leafs and Boston Bruins and anything sport related, but also for thoughtful scientific feedback. Thank you to Bryan for the support and feedback at every key step of this process.

Thank you to the facilities staff across MIT's campus who made the research in this thesis possible. Thank you to the DCIF staff (Walt, Bruce, John and Mohan) for your tireless troubleshooting and for Thursday morning bagels. Thank you to all the microscopy staff that I have had the pleasure to work with, including at the Whitehead Keck Core (Wendy, Brandyn and Cassandra), the Koch Microscopy Core (Jeffrey) and the Koch Nanotechnology EM facility (Peggy and Abigail).

Thank you to all of the members of the Kiessling Group, past and present. I am grateful to have had the privilege to work with many incredible scientists. To my collaborators in the Kiessling Group, Phil Calabretta, Daria Kim, Stephanie Smelyansky, So Young Lee, Teddy Warner, Alby Joseph and Nutchapong Suwanwong, without you, the work in this thesis would not have been possible. To my mentors, I am grateful to all of you who took the time to teach me key skills and talk through experiments throughout my PhD. To the senior members of the lab when I started in the group, thank you for being so welcoming and patient. Special thank you to Spencer Brucks for helping me set up my first reaction in graduate school. To Deepsing, I am so grateful to have gone through this process beside you. To my mentees, I am so excited to see the new and exciting directions that you take

these projects. To all of the current Kiessling Group members, thank you for making the end of my Ph.D. so memorable. And, a huge thank you to Heather Hodges, who despite never overlapping with me in the Kiessling group, has been an incredible source of knowledge and support over the course of my Ph.D.

I am thankful for my community in Boston and the friends I have made along the way. To the Annihilation Operators intramural hockey team, thanks for the opportunity to pretend I am a Toronto Maple Leaf. To the members of my cohort, in particular, JoLynn, Mikaila, Evans, and Nile, thank you for countless hours of ranting, listening, and laughing. I am so grateful for our friendships. To Spencer, thank you for all of the walks to Flour, hockey commiseration and endless support. To Janet, Cassie, and Azin, thank you for so many adventures, beach days and memories. To Christine, thank you for teaching me how to move with motion. To Lyle, thank you for helping me start my week off right with Monday morning coffee runs. To Carolyn, Sunhee, and Valerie, thanks for keeping me calm at the end of my time in the Kiessling group. To Deena, Murshid, and Aara, thank you for welcoming me into your family with open arms. To Taylor and Brian, thank you for making me feel so welcome when I first moved here; I am very grateful for all of our lasting traditions. And finally, thank you to Alex Brown for your unwavering support and for countless hours spent watching (or sleeping in front of) Toronto Maple Leafs games. Thank you for your calmness during the chaotic moments in graduate school. Can't wait to take on the rest of the terrifying twenty-five together!

I am so thankful for my people back home who have been with me from afar throughout this process. Thank you to the McMaster ChemBio Boys, especially Elise, and Daniel, for making my formative years as a scientist so fun and for your continued support during grad school. Thank you to Julia and Natalie for always being down to reminisce about countless adventures or to go on a new adventure. Thank you to my incredible family. I feel so lucky and proud to have been raised in a big, loving, and supportive family. I am grateful for the traditions and celebrations. To my parents and grandparents, thank you for instilling in me the importance of hard work. To my grandparents who moved from Italy to Canada with an elementary school education, I hope you are proud. Thank you to my mom for being a role model of success in all aspects of life. Thank you to my dad for teaching me the importance of being the first one on the ice and the last one off. Thank you to my brother Josh for constantly reminding me that I am not nearly as smart or cool as I think I am.

And last, but certainly not least, thank you to Area4 for keeping me caffeinated throughout my Ph.D. I am too ashamed to put into writing how much of my time and money were spent in this café but I am grateful nonetheless for the countless iced coffees, pastries, and pizza that fueled late nights watching the Toronto Maple Leafs, and the research described in the following chapters.

Table of Contents

Abstract 3
Acknowledgments 4
Table of Contents 6
List of Figures 9
List of Schemes 11
List of Tables 12
List of Abbreviations 12

Chapter 1: Chemical Biology Tools to Study the Structure and Biological Function of Bacterial Cell Envelope Glycans

1.1 Summary 17
1.2 Introduction 18
1.2.1: Bacterial Cell Envelope Glycans: Structural Overview 18
1.2.2: Bacterial Glycans Play Important Roles 20
1.2.3: Challenges Associated with Studying Bacterial Glycans 23
1.3 Chemical Strategies to Label and Probe Bacterial Glycans 24
1.3.1: Probe Development Based on Known Antibiotics 24
1.3.2: Probes Based on Metabolic Glycan Labeling 26
1.3.3: Probes Based on Biosynthetic Glycan Labeling 30
1.3.4: Probes Relying on Glycan Remodeling 31
1.3.5: Fluorogenic Probes 33
1.4 Biological Insights Uncovered by Chemical Probes 35
1.4.1: Understanding Cell Wall Biogenesis and Assembly 35
1.4.2: Understanding Cell Wall Remodeling 36
1.4.3: Applying Probes for Antibiotic Discovery and Development 37
1.4.3.1: Screening and Target Identification 37
1.4.3.2: Glycan-Based Inhibitor Design 38
1.4.4: Application to Microbiome Research 40
1.5 Conclusions and Outlook 42
1.6 References 44

Chapter 2: Development of Biosynthetic Glycan Labeling Probes Targeting Mycobacterial Arabinan

2.1 Abstract 55
2.2 Introduction 56
2.3 Results & Discussion 59

2.3.1: Optimizing a Synthetic Lipid 59
2.3.2: Design and Synthesis of Azide-Functionalized Probe 61
2.3.3: Validation of AzFPA Probes 62
2.3.4: Visualizing Incorporation of AzFPA Probes by Microscopy 65
2.4 Conclusions 69
2.5 Experimental Details 70
2.5.1: Chemical Synthesis and Characterization 70
2.5.2: Strains and Growth Conditions 71
2.5.3: Growth Inhibition Experiments 71
2.5.4: Flow Cytometry and Fluorescence Microscopy 72
2.5.5: mAGP Isolation 73
2.5.6: Uptake into THP-1 Cells 74
2.6 Acknowledgments 75
2.7 References 76

Chapter 3: Applications Enabled by AzFPA Probes

3.1 Abstract 82
3.2 Introduction 83
3.3 Results & Discussion 86
3.3.1: Use of AzFPA for *In Vitro* Assay Development 86
3.3.2: Enablement of AzFPA Labeling in *Mtb* 88
3.3.3: Use of AzFPA to Perturb mAGP Structure *In Cellulo* 89
3.3.3.1: Mass Spectrometry to Assess Arabinan Truncation 91
3.3.3.2: Treatment with 5-AzFPA Induces Phenotypic Changes 92
3.3.3.3: Transmission Electron Microscopy Reveals Mild Changes in Cell Wall Thickness 95
3.4 Conclusions 97
3.5 Experimental Details 98
3.5.1: Strains and Growth Conditions 98
3.5.2: mAGP Isolation 98
3.5.3: mAGP Fluorescence Release Assay 99
3.5.4: Flow Cytometry 99
3.5.5: Super-Resolution Microscopy 100
3.5.6: Cell Viability Assay 101
3.5.7: mAGP Isolation and Composition Analysis 101
3.5.8: Transmission Electron Microscopy Sample Preparation 103
3.5.9: Transmission Electron Microscopy Data Analysis 104
3.6 References 105

Chapter 4: Biosynthetic glycan labeling of mannose-containing glycans in mycobacteria

4.1 Abstract 111
4.2 Introduction 112
4.3 Results & Discussion 116
4.3.1: Design and Synthesis of Azido-Mannose Probes 116

4.3.2: AzFPM Probes Label Mannose-Containing Glycans *In Cellulo* 117
4.3.3: Position of Azide Substitution Mediates Selectivity of Labeling for PIMs 121
4.3.4: Understanding Biosynthesis of Mannose-Containing Glycans 122
4.3.5: Tracking Diffusion of Mannose-Containing Glycans 125
4.3.6: Applying FPM Probes in *Mtb* 128
4.4 Conclusions 129
4.5 Experimental Details 130
4.5.1: Chemical Synthesis and Characterization 130
4.5.2: Strains and Growth Conditions 131
4.5.3: Growth Inhibition Experiments 131
4.5.4: Flow Cytometry and Fluorescence Microscopy 132
4.5.5: Super-Resolution Microscopy 133
4.5.6: Dynabead Streptavidin Enrichment 134
4.5.7: Fluorescence Recovery After Photobleaching 135
4.5.8: Cloning Vectors Encoding C-terminal mCherry *M. smegmatis* Mannosyltransferse Fusion Proteins 136
4.5.9: mCherry *M. smegmatis* Mannosyltranferase Fusion Protein Microscopy 136
4.5.10: *Mtb* Flow Cytometry and Microscopy 137
4.6 References 139

Chapter 5: Mechanistic Investigation into N-QTF, Harnessing Carbamate-Containing Probes

5.1 Abstract 144
5.2 Introduction 145
5.3 Results & Discussion 147
5.3.1: Probe Design and Synthesis 147
5.3.2: Carb-QTF is Processed *in cellulo* 149
5.3.3: Understanding the Mechanism of Carb-QTF Processing 150
5.3.4: Carb-QTF Structure-Activity Relationship Analysis 152
5.3.5: Carb-QTF Allows for Target Protein Enrichment 153
5.4 Conclusions 154
5.5 Experimental Details 155
5.5.1: Chemical Synthesis and Characterization 155
5.5.2: Strains and Growth Conditions 176
5.5.3: In-culture Fluorescence Assay 176
5.5.4: Cell Viability Assay 177
5.5.5: Confocal Microscopy 177
5.5.6: Dynabead Streptavidin Enrichment 178
5.6 References 179

Appendix 1: Investigation of Binding and Internalization of Synthetic N-Terminal Domain of Pyocin S2 in *Pseudomonas aeruginosa*

A1.1 Abstract 183
A1.2 Introduction 184
A1.3 Results & Discussion 188
A1.3.1: AFPS Enables Rapid Single-Shot Synthesis of PyS2^{NTD} 188
A1.3.2: Site-Specific PyS2^{NTD} Labeling with AZDye 488 191
A1.3.3: PyS2^{NTD}-Fluorophore Conjugate Binds and Internalizes into the *P. aeruginosa* Periplasm 192
A1.4 Conclusions 195
A1.5 Experimental Details 197
A1.5.1: Protein Synthesis and Purification 197
A1.5.2: Staining of *P. aeruginosa* with PyS2-488 198
A1.5.3: Flow Cytometry 198
A1.5.4: Fluorescence Microscopy 198
A1.6 Acknowledgments 199
A1.7 References 200

List of Figures

1.1: Schematic comparison of different bacterial cell envelope structures 19
1.2: Bacterial cell wall modifications to protect against antibiotics 21
1.3: Structures of antibiotic-derived fluorescent probes of the PG 25
1.4: Biosynthesis of PG from GlcNAc precursor and probe processing pathway 27
1.5: Metabolic incorporation probes targeting LPS 28
1.6: Contrasting metabolic and biosynthetic incorporation 30
1.7: Labeling of the PG with fluorescent D-amino acid probes via glycan remodeling 31
1.8: Trehalose-based probes for real-time imaging of the mycomembrane 33
1.9: Core mAGP structure of the mycobacterial cell wall and probes of key components 35
1.10: Structures of Lipid II and the FRET-based probe 38
1.11: Two mechanistic classes of metabolic inhibitors 39
1.12: Chemical tools for visualizing components of a microbiome 41
2.1: Overview of the problem of glycan bioconjugation and our proposed solution 56

2.2: Biosynthetic labeling of arabinose schematic 58
2.3: Optimization and validation of a lipid-linked scaffold for arabinose incorporation 60
2.4: Effect of probe on cell viability 63
2.5: Flow cytometry data to assess cellular labeling 64
2.6: Quantification of cellular and substructure labeling 65
2.7: Fluorescence confocal microscopy to assess cellular labeling 66
2.8: Assessment of AzFPA localization 68
2.9: Proof-of-concept of applications in macrophage infection models 69
3.1: Synthetic donor and acceptor substrates used to study AftA activity *in vitro* 84
3.2: Fluorescence release assay to test arabinan hydrolase activity on mAGP 86
3.3: AzFPA can be used to label *Mtb* 88
3.4: AzFPA staining is dose-dependent 89
3.5: Effect of AzFPA probes on cell viability at high concentrations 90
3.6: Extent of arabinose truncation determined by cell wall composition analysis 92
3.7: Super-resolution microscopy of *C. glutamicum* treated with 5-AzFPA 93
3.8: Super-resolution microscopy of *C. glutamicum Δpks13* 94
3.9: Transmission electron micrographs of *C. glutamicum* 96
4.1: Overview schematic of biosynthetic labeling strategy targeting biologically important mannose-containing glycans 115
4.2: Validation of AzFPM labeling 116
4.3: Cell viability upon AzFPM treatment 118
4.4: Super-resolution microscopy of AzFPM labeled cells 119
4.5: SDS-PAGE analysis of glycans from streptavidin enrichment upon biotin labeling following AzFPA labeling 120
4.6: SDS-PAGE analysis of proteins from streptavidin enrichment upon biotin labeling following AzFPA or AzFPM labeling 121
4.7: Demonstration of azide position dictating target glycan 122

4.8: Analysis of localization of AzFPM and AzFPA probes was visualized via confocal fluorescence microscopy 123
4.9: Flow cytometry histograms of mCherry-fusion expressing *M. smegmatis* 124
4.10: Fluorescence microscopy of mCherry-fusion expressing *M. smegmatis* 124
4.11: FRAP analysis to track glycan diffusion 125
4.12: Fluorescence recovery traces for live and fixed cells 126
4.13: Representative FRAP profile of 2-AzFPM treated *M. smegmatis* 127
4.14: Quantification of fluorescence recovery 127
4.15: AzFPM probes label *Mtb* 128
5.1: Overview schematic of endogenous biosynthetic donor and probes 146
5.2: Carb-QTF processing *in cellulo* 149
5.3: Inhibition of Carb-QTF processing by co-treatment with Ebselen 150
5.4: Confocal fluorescence microscopy images of *C. glutamicum* and *M. smegmatis* grown with Carb-QTF 151
5.5: Structure-activity relationship of linker length in Carb-QTF probes 152
5.6: SDS-PAGE analysis of streptavidin enrichment of Carb-QT-N_3 targets 153
A1.1: PyS2^{NTD} was rapidly synthesized in 9.2 hours using automated fast-flow peptide synthesis (AFPS) 189
A1.2: Synthetic PyS2^{NTD} was conjugated to fluorophore AZDye 488 and folded 191
A1.3: Synthetic PyS2^{NTD}-488 binds *P. aeruginosa* with expected species- and receptor-specificity 192
A1.4: PyS2-488 binds *P. aeruginosa* and achieves periplasmic localization 194

List of Schemes

2.1: Synthesis of AzFPA regioisomers 62
3.1: Alditol acetate preparation from mAGP isolates 91
4.1: Synthesis of AzFPM monomers from Cyrene 117
5.1: Formation of the key carbamate moiety in Carb-QTF probes and synthesis of Carb-QT-N_3 for target enrichment 148
5.2: Synthesis of Carb-QTF for fluorescence read-out assays. 149

5.3: Synthesis of QT-N_3 149

List of Tables

2.1: Extent of arabinose incorporation determined by cell wall composition analysis 60
3.1: Arabinosyltransferases involved in mAGP biosynthesis and the linkages they form 85
4.1: Primers used to generate mCherry fusions of *M. smegmatis* mannosyltransferases 136

List of Abbreviations

Ac_4GlcNAz	1,3,4,6-tetra-*O*-acetyl-*N*-azidoacetyl-α,β-D-glucosamine
AF405	Alexa Fluor 405
AF488	Alexa Fluor 488
AF647	Alexa Fluor 647
AFPS	automated fast-flow peptide synthesis
AG	arabinogalactan
D-Ara*f*	D-arabinofuranose
AzFPA	azido-(*Z,Z*)-farnesyl phosphoryl-β-D-arabinofuranose
AzFPM	azido-(*Z,Z*)-farnesyl phosphoryl-β-D-mannose
AzKdo	8-azidoKdo
Bac	bacillosamine
BHI	brain heart infusion
BHIS	brain heart infusion with sorbitol
BSA	bovine serum albumin
Carb-QTF	carbamate-containing quencher-trehalose-fluorophore
CCCP	cyanide *m*-chlorophenyl hydrazone
CDI	Carbonyldiimidazole
CPS	capsular polysaccharide

DABCO	1,4-diazabicyclo[2.2.2]octane
DART	direct analysis in real time
DAT	2,4-diacetamindo-2,4,6-trioxygalactose
DBCO	dibenzocyclooctyne
DMF	*N*,*N*-dimethylformamide
DMSO	dimethyl sulfoxide
DPA	decaprenyl phosphoryl-β-D-arabinofuranose
DTT	dithiothreitol
ESI-TOF	electrospray ionization time-of-flight
FDAA	fluorescent D-amino acid
Fmoc	fluorenylmethyloxycarbonyl
FPA	(*Z*,*Z*)-farnesyl phosphoryl-β-D-arabinofuranose
FpvA	Ferripyoverdine receptor
FRAP	fluorescence recovery after photobleaching
FucNAc	*N*-acetylfucosamine
GalNAz	*N*-azidoacetylgalactosamine
GlcNAc	*N*-acetylglucosamine
GT-C	glycosyltransferase C fold
HADA	7-hydroxycoumarin-3-carboxylic acid-3-amino-D-alanine
HRMS	High-resolution mass spectra
IC-PAD	ion chromatography with pulsed amperometirc detection
InoAz	Azido inositol
IPTG	Isopropyl β-D-1-thiogalactopyranoside
KAHA	α-ketoacid-hydroxylamine ligation
Kdo	2-keto-3-deoxy-octonate
LAM	lipoarabinomannan
LB	Luria broth
LC-MS	liquid chromatography-mass spectrometry
LM	lipomannan
LPS	lipopolysaccharide
mAG	mycolyl-arabinogalactan

mAGP	mycolyl-arabinogalactan-peptidoglycan complex
MALDI	matrix-assisted laser desorption ionization
D-Man	D-mannose
ManLAM	mannosylated lipoarabinomannan
MFI	mean fluorescence intensity
MOI	multiplicity of infection
MRSA	methicillin-resistant *S. aureus*
MurNAc	*N*-acetylmuramic acid
Mtb	*Mycobacterium tuberculosis*
MTX	methylthio-D-xylose
Myt	mycolyltransferase
NCL	native chemical ligation
NMR	nuclear magnetic resonance
N-QTF	amide-containing quencher-trehalose-fluorophore
PBP	penicillin-binding proteins
PBS	phosphate buffered saline
PEtn	phosphoethanolamine
PIM	phosphatidylinositol mannoside
PG	peptidoglycan
PGT	phosphoglycosyltransferase
PMA	phorbol-12-myristate-13-acetated
ppm	parts per million
PUL	polysaccharide utilization loci
PVDF	polyvinylidene fluoride
QTF	quencher-trehalose-fluorophore
RFU	relative fluorescence units
RP-HPLC	reverse-phase high-performance liquid chromatography
SEC	Size exclusion chromatography
SIM	structured illumination microscopy
SPAAC	strain-promoted azide-alkyne cycloaddition
SPPS	solid-phase peptide synthesis

TB	tuberculosis
TBTA	tris(benzyltriazolylmethyl)amine
TEM	transmission electron microscopy
TGase	transglycosylase
TLC	thin layer chromatography
TDM	trehalose dimycolate
TMM	trehalose monomycolate
TPase	transpeptidase
WT	wild type
WTA	wall teichoic acid
ZFP	(*Z*,*Z*)-farnesyl phosphate

Chapter 1: Chemical Biology Tools to Study the Structure and Biological Function of Bacterial Cell Envelope Glycans

1.1 Summary

Bacteria are protected by a rigid, glycan-rich cell envelope critical for maintaining cell shape and orchestrating cell growth and division. The structures that constitute this cell envelope have garnered great research interest due to their essentiality for survival and their absence in eukaryotic cells. These properties render the biosynthetic proteins that generate bacterial cell envelope glycans ideal targets for effective and specific antimicrobials. Because glycans are the dominant feature displayed on bacterial cell surfaces, strategies developed to chemically label and perturb cell surface biomolecules, have facilitated covalent capture, labeling, and imaging. However, such strategies have unfortunately been hard to translate to glycans, especially bacterial glycans. This difficulty is in part due to two key challenges: 1) the non-templated biosynthesis of bacterial glycans makes perturbation via genetic manipulation intractable, and 2) bacterial glycans are composed of isomeric monomers, complicating their analysis. Despite these challenges, many creative strategies have been developed to study historically elusive bacterial glycans. The following sections highlight the strategies developed to study bacterial cell surface glycans, as well as the biological insights these tools have uncovered. The findings enabled by these chemical biology studies highlight exciting opportunities for a deeper fundamental understanding of bacterial physiology. Moreover, they can be leveraged for advances that impact human health.

1.2 Introduction

1.2.1 Bacterial Cell Envelope Glycans: Structural Overview

The bacterial cell envelope displays profound structural diversity, both between substructures of the same biomolecule and between different species of bacteria. One structure that is conserved across bacteria is the peptidoglycan (PG) layer.[1] The PG consists of polysaccharide strands of *N*-acetylglucosamine (GlcNAc) and *N*-acetylmuramic acid (MurNAc) monomers. Adjacent polysaccharide strands are crosslinked by short stem peptides extending from MurNAc residues, creating a mesh-like matrix structure. Though present in all bacteria, the chemical structure and size of this polysaccharide vary greatly.

Hans Christian Gram separated bacteria into two broad groups: those stained with crystal violet dye, termed Gram-positive bacteria, and those that fail to stain, termed Gram-negative.[2-3] The basis for these staining differences is rooted in their distinct cell envelope composition which prevents or allows dye permeation, the structure of the PG, and structures elaborated from this that make up the cell envelope (**Figure 1.1**). Gram-positive bacteria have a cell envelope with a thick, highly-crosslinked PG (20-80 nm), which helps protect the cells from the environment.[3] These bacteria also display teichoic acids, anionic polymers composed of phosphorylated glycerol, glucose, or ribitol that can be covalently tethered to the peptidoglycan (wall teichoic acids, WTA) or lipid anchors (lipoteichoic acids). In contrast, Gram-negative bacteria have a much thinner PG (1-3 nm) and contain an outer membrane appended to the PG with membrane-anchored lipoproteins. The outer leaflet of the outer membrane displays tightly packed lipopolysaccharides (LPS) that form a permeability barrier via crosslinking salt bridges.[4]

Bacteria also ubiquitously produce capsular polysaccharides (CPS), glycans associated with the cell surface usually via covalent attachment to lipids associated with the membrane.[5]

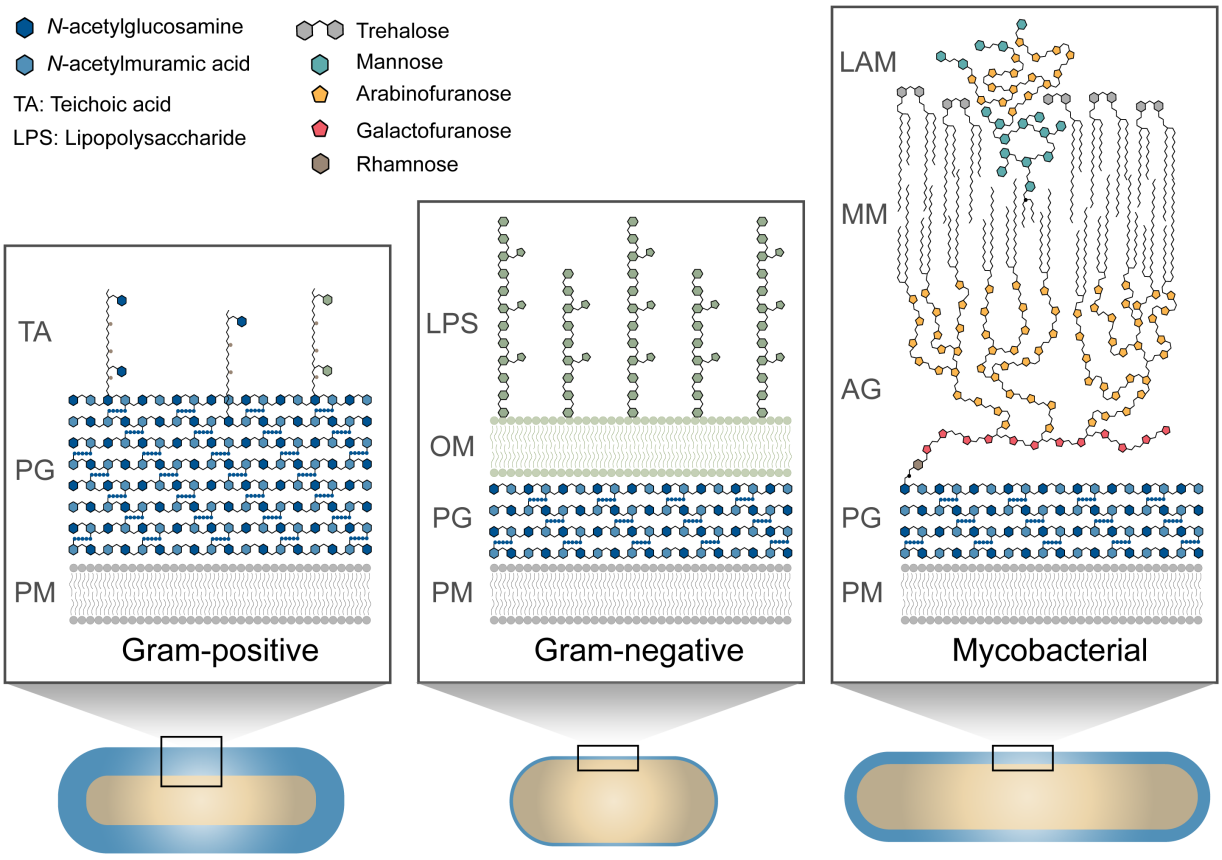

Figure 1.1 Schematic comparison of different bacterial cell envelope structures. TA: teichoic acids, PG: peptidoglycan, PM: phospholipid membrane, LPS: lipopolysaccharides, OM: outer membrane, LAM: lipoarabinomannan, MM: mycolic acid membrane, AG: arabinogalactan. Figure reproduced with permission from reference [2].

A third distinct structural class of bacteria includes mycobacterial species which are poorly stained by crystal violet but their cell envelopes have features that distinguish them from other Gram-negative species. Often referred to as "acid-fast bacteria," mycobacteria and related species are insensitive to the acid treatment used to stain Gram-positive bacteria.[6] Acid-fast bacteria contain an outer membrane composed of

long-chain fatty acids known as mycolic acids appended to a core component of their cell wall, the mycolyl-arabinogalactan-peptidoglycan complex (mAGP).[7] Within the mAGP, the arabinogalactan (AG) layer plays a critical structural role.[8] A family of mannose-containing glycolipids consisting of the phosphatidylinositol mannosides (PIM), lipomannan (LM), and lipoarabinomannan (LAM) are also displayed on the outer membrane of these bacteria. This unique mycobacterial cell envelope structure contributes to the difficulty eradicating this pathogen.

1.2.2 Bacterial Glycans Play Important Roles

Cell envelope glycans are the first point of contact between a bacterium and its environment, other bacteria, a potential host, or antibiotics. These structures have evolved to serve a wide range of functions, including maintaining the cell envelope's structural integrity, providing a physical barrier against environmental threats, and driving disease pathogenesis as virulence factors during infection.[1, 9-10]

Polysaccharides, especially PG, are critical for maintaining the structural organization of bacteria.[11] This macromolecule is cross-linked, which protects the bacteria against turgor pressure and osmotic rupture and dictates cell shape and size. Elaborated from the PG, additional cell surface glycans help maintain and protect the cell from external threats. For instance, WTAs of Gram-positive bacteria aid in regulating cell morphology and division.[12] Mutants lacking WTA grow more slowly and exhibit morphological abnormalities, including increased cell size and defects in septal position and number.[13] Moreover, WTAs are critical for proper localization and assembly of the cell division machinery.[14] An additional example of the bacterial cell envelope's critical structural role is evident in mycobacteria. The characteristic thick,

waxy mycomembrane is largely impermeable, protecting mycobacteria against small molecule antibiotics during treatment and the acidic phagosome during infection.[7, 15]

Beyond maintaining bacterial homeostasis, glycan modification, synthesis, or degradation can drive survival during infection and resistance against antibiotics. For instance, the LPS of Gram-negative bacteria can drive bacterial pathogenesis by dampening a host's immune response.[16] LPS is a potent activator of the innate immune system in mammalian cells and can induce activation of signal transduction cascades which lead to the production of proinflammatory cytokines. LPS can undergo structural changes that protect bacteria during infection.[17] For example, to evade the host immune system, bacteria can install a phosphoethanolamine moiety (PEtN) at anionic positions on their LPS via PEtn transferases. The result is a dramatically altered cell surface charge density (from anionic to more cationic). This change reduces the efficacy of host-derived cationic antimicrobial peptides, such as cathelicidin-2, and promotes bacterial survival (**Figure 1.2A**).[18]

Another cell envelope glycan-mediated survival mechanism is exemplified by *S. aureus* PG modification.[19] During infection, lysozyme can be released by the infected host cell to degrade the cell envelope of an invading bacterium. The *O*-acetylation

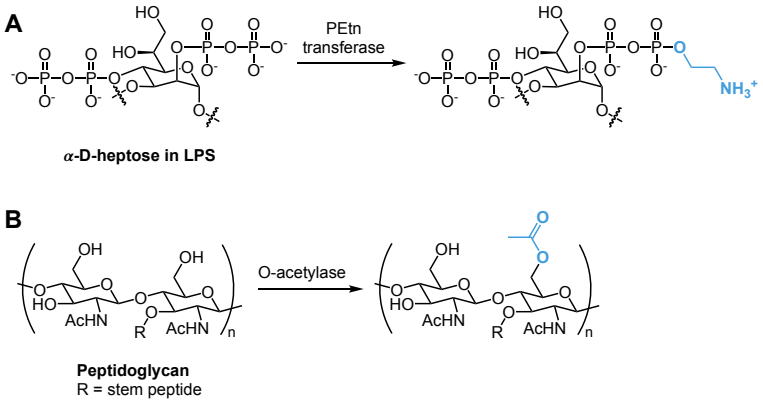

Figure 1.2 Bacterial cell wall modifications to protect against antibiotics. (A) Phosphoethanolamine (PEtn) installation on heptose in LPS as observed in *Pasteurella multocida* to modulate charge density. **(B)** *O*-acetylation of muramic acid in peptidoglycan as observed in *S. aureus* to protect against host lysozyme.

of PG muramic acid catalyzed by *O*-acetyltransferases results in lysozyme resistance, thus protecting the bacterium from the host defenses (**Figure 1.2B**).

Antibiotic resistance can also be induced by glycosylation. Methicillin-resistant *S. aureus* (MRSA) is a frequent cause of fatal infections in humans.[20] MRSA clones encode a unique WTA glycosyltransferase that installs GlcNAc on the WTAs.[21] This glycosylation modulates immunogenicity and leads to immune evasion to cause severe infections. Mycobacteria also vary glycosylation to modulate pathogenicity, as seen in species-specific variations in their LAM. Certain mycobacterial species produce LAM containing a polymannose cap composed of α-(1-2) mannose residues. In *Mycobacterium tuberculosis* (*Mtb*), which causes the disease tuberculosis, these mannose caps can be further elaborated with an α-(1-4) methylthio-D-xylose (MTX) residue.[22] This modification is only observed in pathogenic members of this family. Commonly used non-pathogenic model organisms such as *Mycobacterium smegmatis* are lacking MTX. This selectivity implies MTX has a role in pathogenesis, though direct evidence is still lacking.[23] These and other examples highlight the relevance of glycan-mediated mechanisms in enhanced virulence in bacteria which has implications for the development of antibiotic resistance.

1.2.3 Challenges Associated with Studying Bacterial Glycans

The unclear correspondence between genome sequence and glycan sequences makes it both difficult to decipher what glycans a cell can make and to encode glycan variations. Of the three major biopolymers–polynucleotides, polypeptides, and polysaccharides–the latter remains the most understudied. While five nucleotide monomers are used to assemble oligonucleotides and twenty canonical amino acids are

used to assemble proteins and peptides, the bacterial kingdom uses hundreds of unique monosaccharide building blocks in glycan biosynthesis.[24] Moreover, numerous modifications including alkylation, acylation, amine acylation, and phosphorylation have been characterized on bacterial glycans.[24] Additionally, polysaccharides can branch at several positions and be connected by diverse linkages, in contrast with the strictly linear polymers that form nucleotides and peptides built by consistent bond formation. Thus, bacterial glycans are diverse.

There are no simple, predictable genetic methods to modify or study glycans. Because glycans are not biosynthesized in a templated manner, changes in their structure cannot be encoded directly. Their biosynthesis is dictated by the activity of numerous glycosyltransferases, mutases, and hydrolases. Moreover, the biosynthesis of monosaccharides into high-energy precursors (i.e., sugar nucleotide donors or lipid-linked sugar donors) often involves intermediates that can act as points for crosstalk between different metabolic pathways.[25] Bacteria, in particular, have evolved to survive in diverse and often harsh ecological niches and have therefore developed complex pathways for nutrient acquisition and carbohydrate metabolism which complicated glycan prediction.[26]

Glycans are primarily composed of stereo- and constitutional isomers of polyol monomers. Monosaccharides or even subsets of polysaccharides often cannot be distinguished based on complementary reactivity. This functional group redundancy makes selective bioconjugation methods on endogenous glycans challenging. The similarity in monomers demands sophisticated analytical techniques, as many of the monosaccharide building blocks have the same molecular masses.[27] Taken together,

these challenges have led to the need for creative chemical strategies to understand these important biological structures better.[28]

1.3 Chemical Strategies to Label and Probe Bacterial Glycans

1.3.1 Probe Development Based on Known Antibiotics

The utility of chemical tools for studying cell envelope glycans emerged from using natural-product-based antibiotics. Some of the first probes of PG biosynthesis were fluorophore-labeled antibiotics (**Figure 1.3**).[29-32] In one example, the Walker group compared fluorophore-labeled ramoplanin (**1.1**) with fluorophore-labeled vancomycin (**1.2**) to visualize antibiotics that bind to different PG components.[30] Vancomycin binds D-Ala-D-Ala residues in the PG.[29, 33] Ramoplanin binds to Lipid II and can interact with the reducing ends of the growing PG polymer. Fluorophore-labeled ramoplanin and vancomycin gave rise to similar, though not identical, staining patterns. Such probes revealed a helical wall staining of PG uncovering new information about spatial localization and organization of biosynthetic complexes.[30, 34] These agents have been used to highlight the sites of PG remodeling or new PG biosynthesis.

Rather than target the cell envelope itself, alternative antibiotic-based probes were developed to target cell envelope biosynthetic enzymes. For instance, different β-lactam antibiotic derivatives exhibit selectivity for different penicillin-binding proteins (PBPs)[35] and, therefore, can be converted to probes for distinct PBPs, which participate in PG synthesis and remodeling.[36-40] BOCILLIN (**1.3**), penicillin bearing a fluorophore, has been used for PBP activity-based profiling and imaging (**Figure 1.3**).[41-42] This reagent acts broadly with most PBPs. To complement this approach, the Carlson group examined a variety of substituted β-lactam derivatives to determine their PBP selectivity

in *Escherichia coli,*[43] *Bacillus subtilis,*[44] and *Streptococcus pneumoniae.*[45] Profiling β-lactam reactivity in different species is relevant because the number of PBPs per organism varies, and often, their specific functions are difficult to dissect. Indeed, fluorescent β-lactams have revealed differences in the localization of distinct PBPs, highlighting the utility of these probes for understanding localized PBP activity in replicating and dormant bacteria.[39, 44, 46]

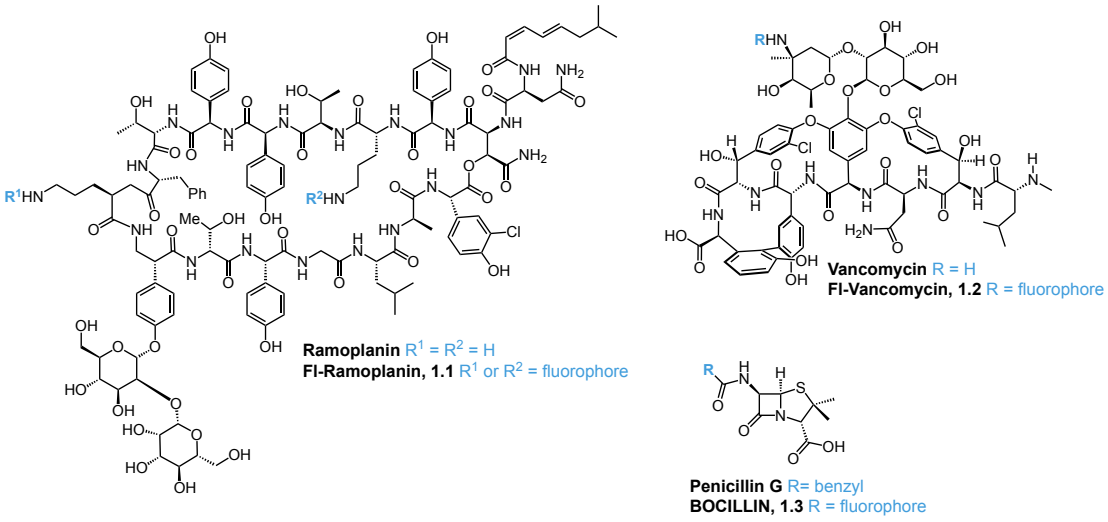

Figure 1.3 Structures of antibiotic-derived fluorescent probes of the PG. The sites of fluorophore attachment (R groups) to convert vancomycin, ramoplanin, and penicillin derivatives into probes of PG biosynthesis.

1.3.2 Probes Based on Metabolic Glycan Labeling

Metabolic incorporation or metabolic oligosaccharide engineering is a useful strategy for monitoring and labeling cell surface glycans.[47-49] This strategy involves feeding cells a metabolic precursor with a bioorthogonal handle or direct reporter for uptake. As many of the glycan building blocks are acetylated to promote mammalian cell uptake, initial processing often proceeds through intracellular deprotection by non-specific

esterases. The free sugar can then undergo processing into a nucleotide sugar donor via metabolic enzymes. The resulting donor can be incorporated into growing glycans by glycosyltransferases followed by extracellular transport and display. Since the Reutter Group first demonstrated non-natural monosaccharide incorporation in mammalian cells, the technique has become widespread.[50-51] Bertozzi and coworkers demonstrated that a range of monosaccharides with functional groups could be employed, demonstrating the generality of this method.[52-53] This strategy has even been applied to visualize glycans in higher-order organisms such as zebrafish and mice.[54-55]

Though very successful in mammalian cells, this strategy is more challenging to translate to bacterial systems.[49] Firstly, many bacteria lack the non-specific reactivity of cellular esterases required to unmask membrane-permeable versions of metabolic probes, this limits probe uptake mechanisms.[56-59] Additionally, due to evolution to survive in diverse ecological niches, glycan metabolism in bacteria often involves complex uptake and scavenging pathways with overlapping intermediates.[25] Therefore, promiscuous labeling is a significant concern for many applications of metabolic probes in bacteria. Despite these important considerations, the metabolic incorporation of some probes has been successful in bacteria.

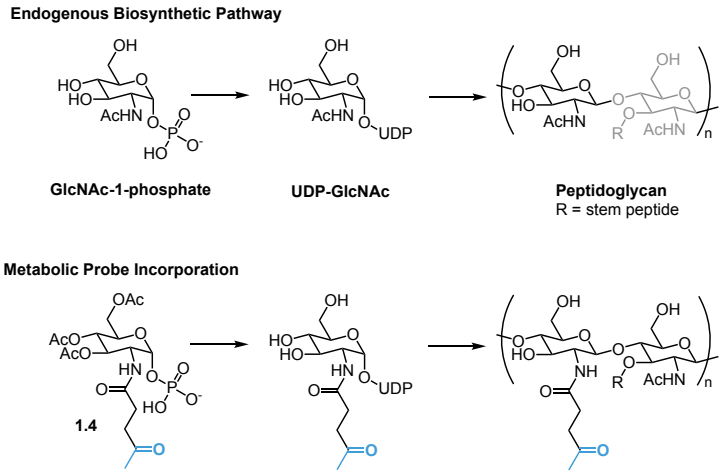

Figure 1.4 Biosynthesis of PG from GlcNAc precursor and probe processing pathway. Metabolic incorporation probe (**1.4**) which showed the greatest staining by flow cytometry,[60] designed based on endogenous biosynthetic pathway. Ketone group introduced into the N-acetyl position.

For ease in synthetic accessibility, preliminary metabolic incorporation probes were designed to intercept early steps within biosynthetic pathways. This approach allowed for relatively facile synthesis of the simplest monosaccharide reporters. However, these probes often suffer from low cell permeability and require a large number of biosynthetic steps for incorporation into the target structure. An early example of this approach is the use of GlcNAc-1-phosphate analogs to label the glycan backbone of the PG (**Figure 1.4**).[60] In this case, the labeling was facilitated through the installation of the ketone on the monosaccharide (**1.4**) and reaction with hydrazine to install a biotin moiety for labeling with a streptavidin-fluorophore conjugate. Taking advantage of peracetylated derivates to improve cellular uptake, at high probe concentrations, a subset of Gram-positive bacteria was labeled.

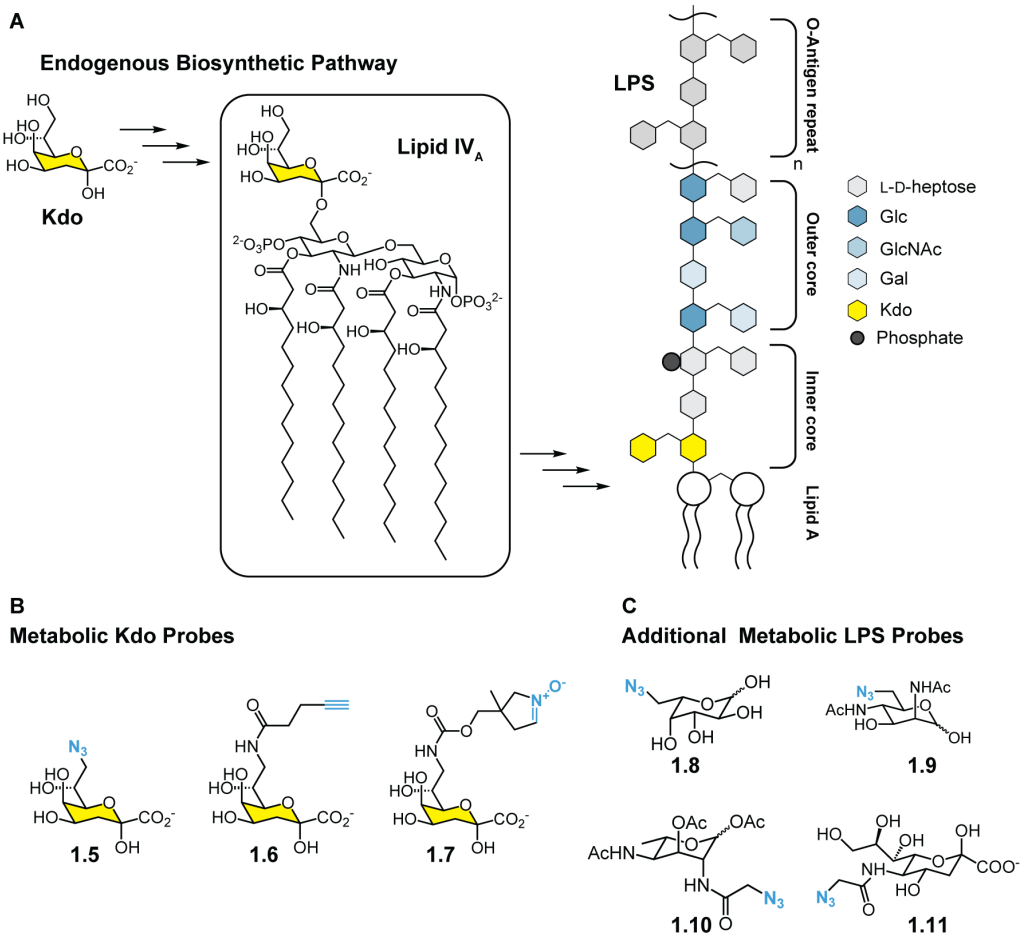

Figure 1.5 Metabolic incorporation probes targeting LPS. (A) Biosynthesis of LPS highlighting Kdo. **(B)** Alternative biorthogonal handles appended to Kdo for metabolic incorporation (**1.5–1.7**). **(C)** LPS targeting metabolic incorporation probes based on alternate monosaccharides (**1.8–1.11**). Figure adapted from reference [2].

An elegant example of rational design to improve selectivity involved 2-keto-3-deoxy-octonate (Kdo), a component of the inner core of LPS (**Figure 1.5A**).[61-62] A non-natural azide-containing derivative, 8-azidoKdo (AzKdo, **1.5**) (**Figure 1.5B**) was chemically synthesized and tested for LPS incorporation.[63] This probe has an azide modification installed at the C8-position specifically, a design feature that prevents reverse metabolism by Kdo-8-P phosphatase. Without this modification, the divergent metabolism of a Kdo analog could limit probe specificity if it could be converted into other carbohydrates and metabolites. Selective labeling of Gram-negative over Gram-positive bacteria was achieved, which is particularly useful when studying mixed

cultures. Notably, the Gram-negative bacterium *Shewanella oneidensis*, which utilizes 8-amino-8-deoxyKdo, was unlabeled. Finally, analysis of *E. coli* LPS by mass spectrometry revealed the presence of Kdo-N_3-Lipid IV_A and (Kdo-N_3)$_2$-Lipid IV_A.[64] This probe demonstrates an example of specifically labeling a glycan substructure via metabolic incorporation in bacteria. Kdo-based reporters with complementary biorthogonal handles have also been synthesized and characterized, including Kdo bearing an alkyne (**1.6**) and an endocyclic nitrone (**1.7**) (**Figure 1.5B**).[65] Thus, the LPS biosynthetic machinery can tolerate functionalities beyond an azide. Additional LPS targeting probes have been disclosed based on other constituent monosaccharides, including fucose (**1.8**)[66], legionaminic acid (**1.9**)[67], pseudominic acid (**1.10**),[68] and sialic acid (**1.11**)[69] (**Figure 1.5C**). New metabolic incorporation probes for a range of targets are still being identified. A recent report disclosed metabolic incorporation probes targeting capsular polysaccharides in *E. coli* and *B. subtilis*.[70] This work demonstrated the utility of such probes in macrophage and mouse models.

A useful strategy for increasing the specificity of metabolic probe incorporation is the use of genetically modified model organisms. By deleting off-target pathways, probes can specifically label glycans on interest. A recent example of this is the disclosure of azido inositol probes (InoAz) in mycobacteria.[71] In this work, an inositol auxotroph strain of mycobacteria with disrupted *de novo* inositol was used to test InoAz incorporation. Though no staining was observed in wild-type *M. smegmatis*, robust glycan labeling was validated in an *M. smegmatis* auxotroph. This probe enabled the discovery of a new inositol importer in this organism highlighting the utility of metabolic incorporation probes, even in cases that require genetic manipulation.

Not all metabolic probes need to label a single structure to be useful for the field. One elegant application of the metabolic incorporation strategy has been demonstrated by the Dube group. This work takes advantage of the promiscuity of metabolic probes in bacteria, rather than trying to avert this feature.[72] A metabolic labeling-based assay was designed using a peracetylated azide-containing derivatize of GlcNAz (Ac_4GlcNAz) in *Helicobacter pylori* to reveal a glycoprotein "fingerprint". Wild-type *H. pylori* were compared to a library of glycosyltransferase mutant strains, which uncovered 13 genes in a novel glycoprotein biosynthesis pathway. In this approach, broad labeling is beneficial allowing a comprehensive fingerprint to identify differences in glycosylation patterns. These examples highlight the broad utility of metabolic incorporation probes in bacteria, specifically focusing on key design considerations.

1.3.3 Probes Based on Biosynthetic Glycan Labeling

As a complement to metabolic incorporation probes, late-stage building blocks have been harnessed to label specific glycans. The direct, extracellular processing of such non-natural substrates by cellular enzymes is termed "biosynthetic incorporation" (**Figure 1.6**).[73-74] The application of glycolipid substrates in biosynthetic incorporation

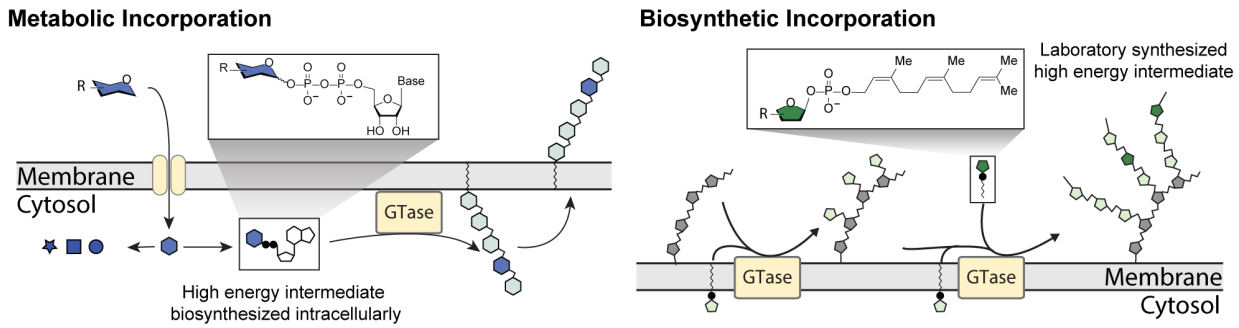

Figure 1.6 Contrasting metabolic and biosynthetic incorporation. In metabolic incorporation, a monosaccharide probe is converted to a nucleotide sugar by the cell, leading to competition with endogenous metabolites and diversion from the desired biosynthetic pathway. Biosynthetic incorporation utilizes a sugar donor that eliminates cytosolic processing and decreases competition. Figure adapted from Reference [73].

offers advantages as cell surface-associated glycosyltransferases (GT-Cs) can directly use them as substrates rather than relying on multiple processing steps. The first demonstration of this strategy to label bacterial glycans was demonstrated to site-selectively introduce D-arabinofuranose (D-Ara*f*) into the arabinan of mycobacteria (See **Chapter 2**).[75] This strategy shows a lot of promise to be applied to a wide range of monosaccharides (See **Chapter 4**). Any structures installed via decaprenyl donors may be viable and accessible to labeling using the previously described farnesyl-based scaffold, such as MTX in *Mtb*.[22]

1.3.4 Probes Relying on Glycan Remodeling

The most ubiquitously used cell wall probes are the D-amino acid derivatives which label the crosslinks between the glycan backbone of the PG (**Figure 1.7**).[76] PG labeling is achieved via D-amino acid analogs bearing biorthogonal handles (**1.12-1.13**), small dyes (e.g., coumarins, **1.14**), and larger reporters such as the rhodamine dyes.[77] The initial model was that fluorescent D-amino acid (FDAAs) were incorporated into the nascent peptidoglycan through a cytosolic "metabolic" manifold by generating a

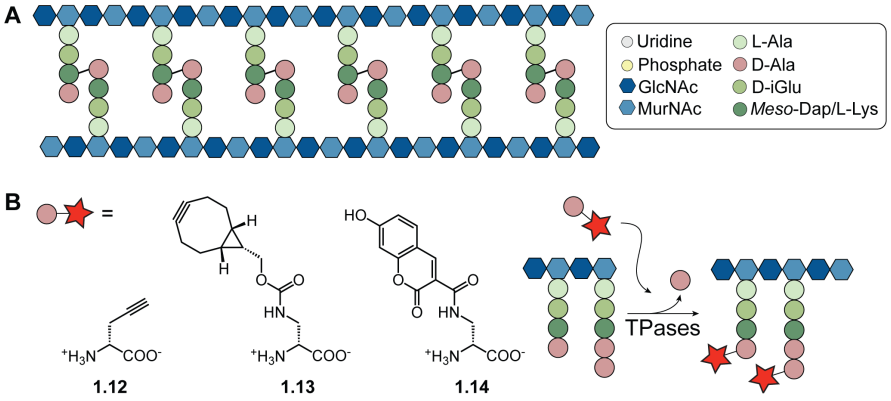

Figure 1.7 Labeling of the PG with fluorescent D-amino acid probes via glycan remodeling. (A) Cartoon schematic the peptidoglycan structure. **(B)** Examples of D-amino acid-based probes and the mechanism of their incorporation through transpeptidase mediated remodeling. Figure adapted from reference [2].

substituted D-Ala-D-Ala dipeptide analog. Mechanistic studies have since indicated that they are incorporated through PG remodeling. They are processed by D,D-transpeptidases (D,D-TPases) or L,D-transpeptidases (L,D-TPases).[78] While an increased fluorescent signal is often accurately inferred to be indicative of cell growth, FDAA incorporation can occur under nutrient starvation or in a growth-independent manner which is consistent with a remodeling mechanism.[78] This example highlights the importance of understanding the molecular basis of probe processing and incorporation for interpreting the results of glycan labeling experiments.

Due to the diversity of carbohydrate acquisition in bacteria, metabolic incorporation probes have also been developed to harness monosaccharide salvage pathways. Salvage pathways are critical in avoiding metabolic waste during PG assembly. During PG remodeling, some bacteria exploit characterized salvage pathways and process released saccharide fragments back into nascent PG.[79] Based on knowledge of the pathway, the Grimes group designed metabolic probes that are incorporated via the MurNAc salvage pathway.[80] Using MurNAc probes bearing an azide or an alkyne, the carbohydrate of the PG was labeled with a fluorophore for super-resolution microscopy and tracking of bacterial infections in macrophages. Salvage pathways have also been harnessed to produce homogeneously modified structures. In *E. coli*, it has been demonstrated that native *de novo* biosynthetic pathways can be replaced with exogenous salvage pathways (first validated with LPS labeling).[66]

1.3.5 Fluorogenic Probes

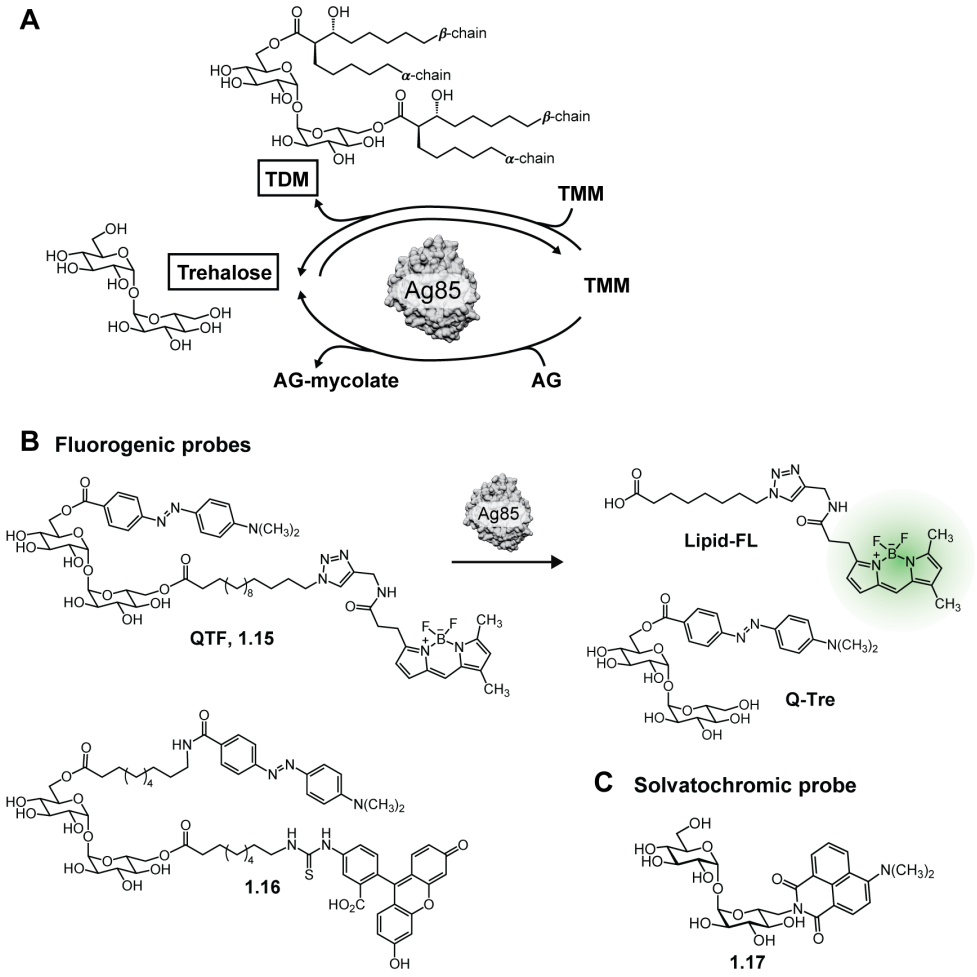

Figure 1.8 Trehalose-based probes for real-time imaging of the mycomembrane. (A) The pathway for trehalose uptake and TMM/TDM processing. (B) A fluorogenic probe of mycolyltransferase and hydrolase activity. (C) Solvatorchromic probes based on trehalose recognition.

Most of the chemical tools mentioned above are designed to install a biorthogonal handle into a desired glycan structure for subsequent installation of a reporter. This two-step process allows for a modular approach where a variety of reporters can be installed (i.e. fluorophore for visualization, biotin for enrichment, photoaffinity handle for binding partner identification, etc.). The major disadvantage to these probes is that they require multiple reactions and wash steps, limiting the time-scale resolution that can be achieved. An effective strategy to overcome this challenge is using fluorogenic

probes that fluoresce upon processing. For example, fluorogenic probes have been developed to report on mycobacterial growth and division based on knowledge of the biosynthetic activity of Ag85 enzymes (**Figure 1.8A**).[81-82] The quencher-trehalose-fluorophore (QTF, **1.15**) probe is an analog of the endogenous mycolyltransferase donor TMM and is hydrolyzed by mycolyltransferases providing a real-time fluorescent read out of mycolyltransferase activity and mycolic acid membrane assembly (**Figure 1.8B**).[82] Additionally, this and other fluorogenic labeling agents (**1.16**) have little background fluorescence until processing by the mycolyltransferases, which unleash the fluorescence.[81] These probes also have the advantage of not needing to be taken into the cytosol, avoiding the risk of off-target labeling. Solvatochromic probes (**1.17**) have also been applied as a complementary strategy to label the mycolate of mycobacteria. The Bertozzi group developed trehalose analogs with a solvatochromic dye (**Figure 1.8C**) whose fluorescence increases in the hydrophobic environment of the mycomembrane relative to free in solution.[83-86] Such probes that do not require washing steps allow for real-time imaging and enable unique screening opportunities (as will be discussed in **section 1.4.3**).

1.4 Biological Insights Uncovered by Chemical Probes

1.4.1 Understanding Cell Envelope Biogenesis and Assembly

The chemical tools highlighted in the previous sections have enabled a nuanced understanding of the careful orchestration of bacterial cell envelope biosynthesis by enabling direct visualization of distinct structures. For instance, it has been demonstrated using FDAA labeling that bacteria can exhibit distinct and diverse growth patterns that may provide selective advantages in different environments.[87] In the case of mycobacteria, it has been demonstrated that cell envelope glycan biosynthesis occurs in an asymmetric fashion with enhanced biosynthetic activity at the older of the two poles. By labeling individual components of the core mAGP (**Figure 1.9**), this phenomenon has been shown to hold true for the peptidoglycan,[88] arabinan,[75] and mycolate layer.[82]

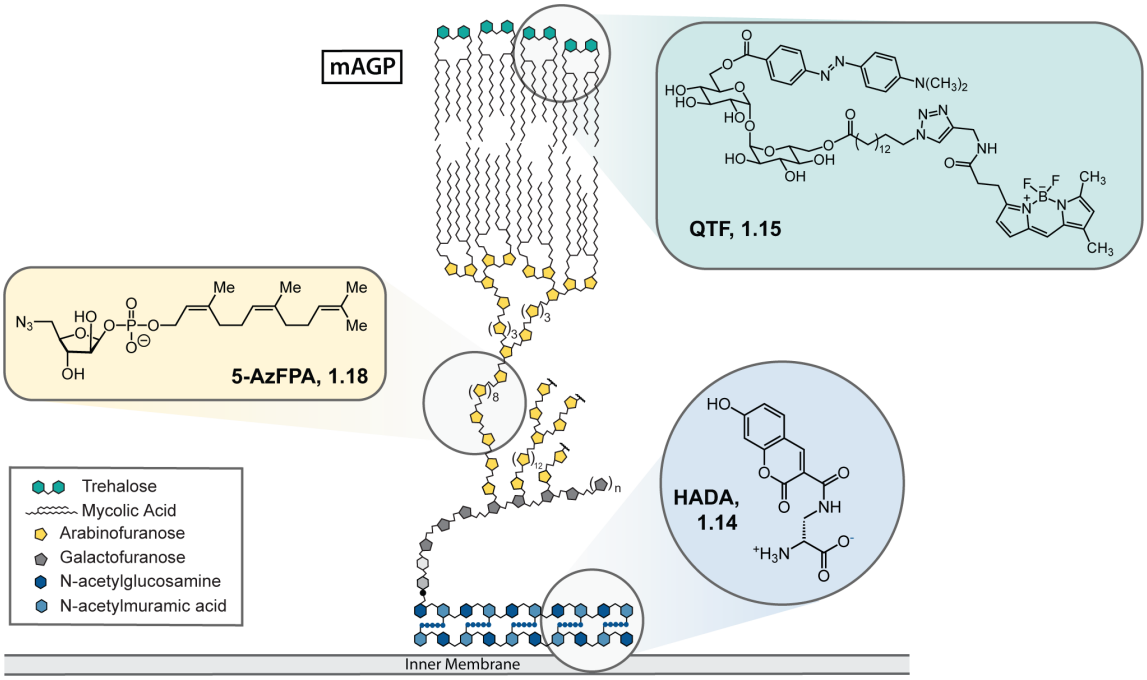

Figure 1.9 Core mAGP structure of the mycobacterial cell wall and probes of key components. QTF (**1.15**) reports of mycolyltransferase activity at the mycolic acid layer, 5-AzFPA (**1.18**) is incorporated into the arabinan by arabinosyltransferases at the cell membrane and HADA (**1.14**) is incorporated by transpeptidases into the peptidoglycan.

Chemical installation of a fluorophore via D-alanine analogs into *Listeria monocytogenes* allowed for visualization of incorporation into nascent PG both *in vitro* and during macrophage infection.[89] This experiment uncovered that the localization of resultant fluorescence on intracellular *L. monocytogenes* was consistent with observations *in vitro* with bacteria alone. This work highlights the utility of such probes to study bacteria in diverse and highly relevant environments.

1.4.2 Understanding Cell Envelope Remodeling

Installing a reporter into the bacterial cell envelope allows observation of the subsequent cell envelope remodeling processes. For example, bacterial cell envelope probes illuminated mycobacterial membrane remodeling dynamics under antibiotic stress. This insight can help uncover new therapeutic strategies to address the growing threat of mycobacterial antibiotic resistance. For example, N-QTF, a more hydrolytically stable derivative of QTF described in **section 1.3.5**, was leveraged to uncover spatial and temporal fluorogenic phenotypes in response to treatment by several antibiotics in mycobacteria.[90] In this work, time-lapse microscopy revealed distinct spatial and temporal changes in the mycobacterial membrane upon treatment with frontline antibiotics with distinct mechanisms. This probe allowed for the visualization of unique cellular phenotypes. Initially validated by studying antibiotics that act through known mechanisms, this probe could be of great use to help identify new targets of antibiotics through phenotypic screens.

Bacteria are also known to remodel their glycans during infection of the host and can even engage in “molecular mimicry”. For example, *Haemophilus influenzae* is a Gram-negative commensal bacterium that resides in the respiratory microbiome.[91] *H.*

influenzae can switch from a commensal to an opportunistic pathogen causing severe infection. This switch is associated with an uptake and display of host sialic acids and this transfer has been directly visualized through metabolically incorporated sialic acid-based probes.[69] This is the first example of a chemical reporter being used to monitor glycan transfer between a host cell and a bacterial and highlights the wide range of applications such labeling strategies can enable. The insight gained about glycan remodeling through this work allowed for the development of a sialic acid-based inhibitor of *H. influenzae*.

Chemical probes are also useful in providing a readout for *in vitro* assays of relevant enzymatic activities. For instance, a chemical probe can be used to label a specific structure, and then upon isolation, this labeled substructure can be used in enzymatic assays. This approach has been applied recently to assess the activity of newly discovered arabinan hydrolases using FPA-labeled arabinan.[92] This study found distinct promiscuity of these remodeling enzymes derived from different species.

1.4.3 Applying Probes for Antibiotic Discovery and Development

1.4.3.1 Screening and Target Identification

As many antibiotics either target or permeate glycans on the cell envelope of bacteria, there are countless exciting opportunities to use chemical probes of bacterial glycans to aid in therapeutic discovery pipelines. Chemical probes of bacterial glycans have been used as screening tools for antibiotic discovery. For example, based on understanding of PG synthesis, a FRET-based lipid II analog (**1.19**) was designed as a screening tool (**Figure 1.10**).[93] **1.19** contains a coumarin fluorophore in the peptide chain that is covalently bound to a quencher in the lipid chain. Upon processing by a

transglycosylase (TGase), the quencher is released, and fluorescence can be observed. This probe was demonstrated to function as hypothesized *in vitro* in a cell-free system and in bacterial culture. Ultimately this compound was validated for high throughput screening and a 120,000 compound library was tested to identify potent TGase inhibitors based on a facile read-out of loss of fluorescence. Similar FRET-based probes can be envisioned for use in additional high-throughput screening campaigns.[82]

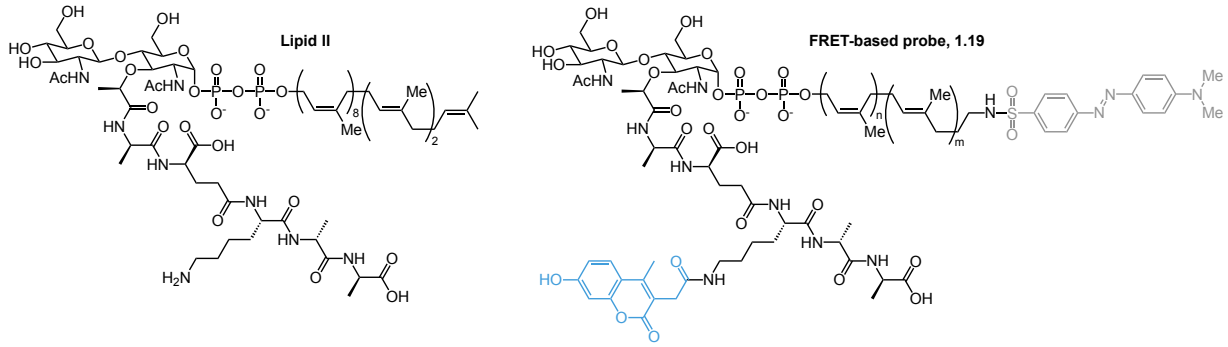

Figure 1.10 Structures of Lipid II and the FRET-based probe. In the probe structure on the right the fluorophore is highlighted in blue and the quencher is denoted in grey.

1.4.3.2 Glycan-Based Inhibitor Design

A number of small molecule inhibitors of bacterial glycan biosynthesis have been rationally designed based on information gained by chemical probes. For instance, the Imperiali group has taken advantage of understanding monosaccharide donor identity to design nucleoside inhibitors of glycan tailoring enzymes.[94] Through this modular approach, novel phosphoglycosyltransferase (PGT) inhibitors were developed with IC_{50}'s in the micromolar range. Similar uridinyl nucleoside analogs have been demonstrated to inhibit a range of glycan-modulating enzymes, including a PGT, a UDP-aminosugar acyltransferase, and a glycosyltransferase highlighting the generality of this inhibition strategy.[95]

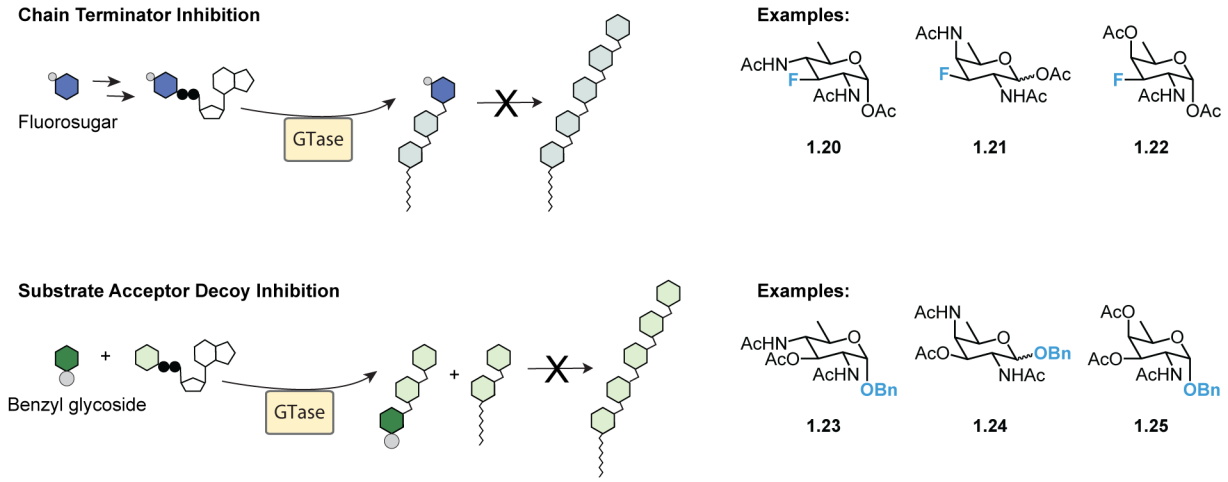

Figure 1.11 Two mechanistic classes of metabolic inhibitors. Fluorosugars terminate glycan elongation. Benzyl glycosides mimic endogenous glycan acceptors and divert precursor onto decoy resulting in truncated glycans. Examples of each mimicking bacillosamine (**1.20, 1.23**), 2,4-diacetamindo-2,4,6-trioxygalactose (**1.21, 1.24**) and N-acetylfucosamine (**1.22, 1.25**). Figure adapted from reference [96].

A distinct inhibitor design strategy is metabolic inhibition. There are two classes of metabolic inhibitors: chain terminators and substrate decoys (**Figure 1.11**).[96] Chain terminators, often fluorosugars (**1.20-1.22**), allow for incorporation into bacterial glycans but prevent further elongation.[69, 97] The substitution of a fluorine most common for these studies as the electronegativity of fluorine preserves the monosaccharide conformation and sterically, fluorine can be easily accommodated by glycosyltransferases. The incorporated residue cannot be further elaborated at positions bearing fluorine, yielding truncated cellular glycans.[94] In contrast, substrate decoy inhibitors serve as an acceptor rather than a donor (**1.23-1.25**). In this case, glycan biosynthesis is diverted onto benzyl glycosides which compete with endogenous substrates and again yield truncated cellular glycans. Both strategies have been demonstrated to lead to glycoprotein defects in *H. pylori*.[98] Metabolic inhibition has also been applied in mycobacteria as non-hydrolyzable derivatives of trehalose 6-phosphate induced growth inhibition.[99]

1.4.4 Application to Microbiome Research

In recent years, a greater appreciation for the roles of microbial communities has emerged, specifically the critical roles that the microbiota plays in human physiology and disease.[100-105] The ability to label and visualize bacteria provides opportunities to explore their localization and dissemination *in vivo*. This strategy is particularly important for commensal bacteria as these strains can be difficult to culture *in vitro*.[106] Moreover, insight into the localization of bacteria within a host is vital for determining their function and how they interact with the host.

Chemical tools outlined in previous sections have been applied to monitor bacteria within the gut. The Kasper group carried out a seminal study in this area with *Bacteroides fragilis*, an anaerobic Gram-negative commensal.[107] They labeled the CPS A on the bacterial surface, as it can modulate immune responses (**Figure 1.12A**). In brief, they cultured *B. fragilis* with an *N*-acetylgalactose derivative bearing an azide (GalNAz, **1.26**) and subsequently reacted with a fluorophore.[108] The labeled bacteria were then administered to germ-free mice, and bacterial colonization followed over time. At early time points, bacteria were detected in the small intestine. At 12 hours, however, most bacteria were in the colon. This approach is generalizable, as shown by its application to nine other commensals and the pathogen *S. aureus*. The Yang group used a variation on this approach to image Gram-positive versus Gram-negative bacteria in the gut microbiota.[109] They employed 8-AzKdo (**1.5**), which can be used to mark LPS and, therefore, Gram-negative species (**Figure 1.12B**). Subsequent exposure to BODIPY-substituted vancomycin (**1.2**) distinguished Gram-positive species. This work demonstrated the ability to track multiple distinct species at once. Recently, fluorescent oligosaccharide metabolic labeling probes have been applied to microbiome samples.[110]

These probes allow for identification of glycan consumers and for the discovery of new carbohydrate processing enzymes.

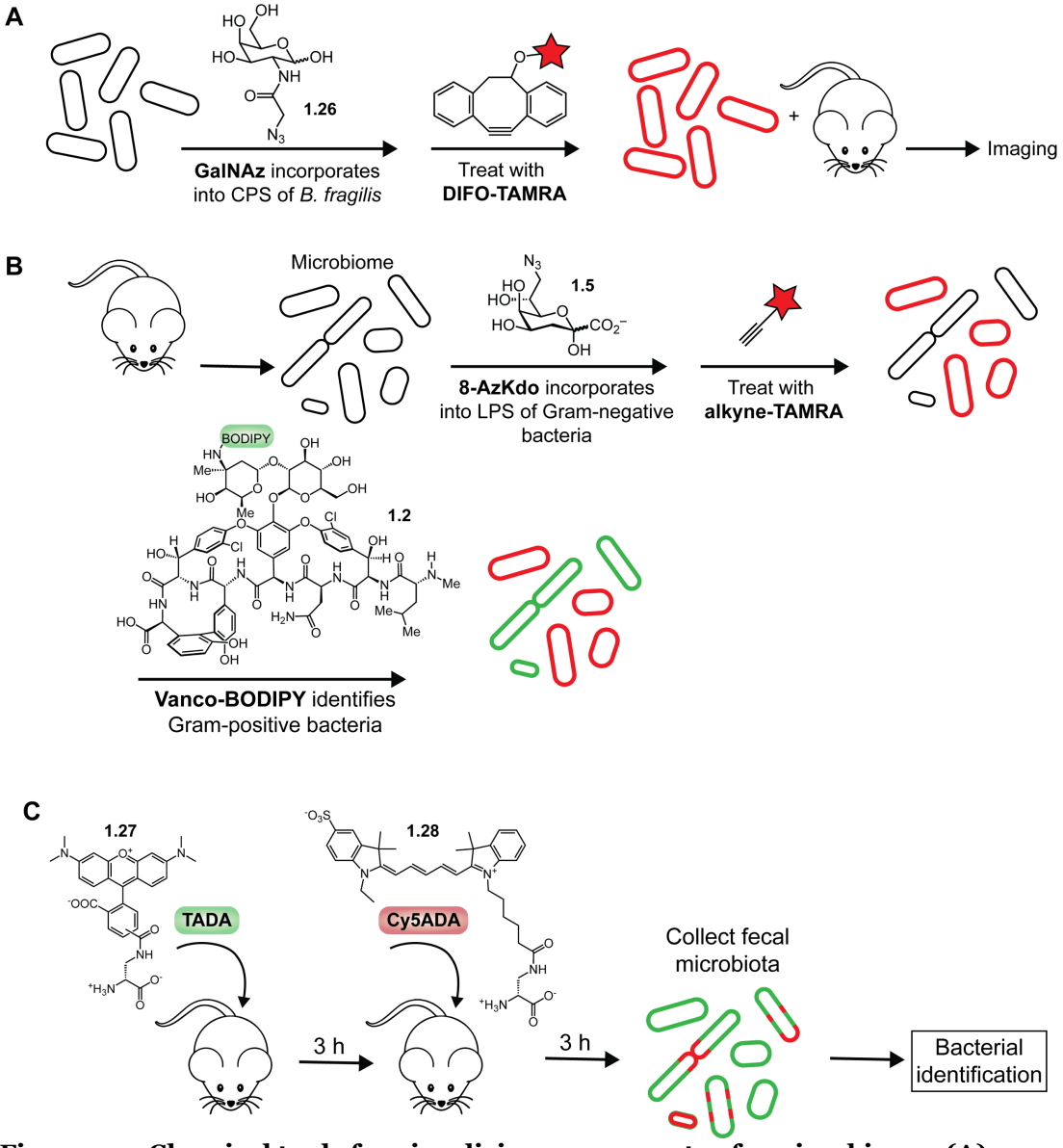

Figure 1.12 Chemical tools for visualizing components of a microbiome. (A) Metabolic labeling of the cell surface capsular polysaccharide of *B. fragilis* can be accomplished with an N-acetylgalactosamine derivative and subsequent click reaction. The bacteria can be followed using intravital microscopy in a live animal. **(B)** Strategy for distinguishing between Gram-negative and Gram-positive bacteria within a microbiome. **(C)** Approach to assess bacterial proliferation kinetics by subsequent treatment with different fluorescent D-amino acids. Figure reproduced with permission from Reference [2].

Given that PG is not present in eukaryotic cells, bacteria labeled with FDAA (**1.27, 1.28**) can be tracked in a host (**Figure 1.12C**).[111] It has been demonstrated that FDAAs can be introduced directly into an animal to follow the growth and division of bacterial species. The rates of *in vivo* proliferation of different bacterial species can therefore be determined. The microbiome studies emphasized above represent a small fraction of the exciting research being carried out by the chemical biology community using newly developed tools.

1.5 Conclusions and Outlook

Great strides have been made towards expanding the chemical biology toolkit for exploring bacterial glycans and the biological roles that they play. Glycobiology has been a challenging field to apply traditional biological or biochemical strategies to study. The non-templated nature of glycan biosynthesis makes these structures challenging to interrogate using conventional genetic manipulation methods. Moreover, the impact that novel sequencing and "-omics" platforms have had on other biomolecules are less informative for glycans. Chemical conjugation strategies have also been challenging due to the lack of distinct chemical functionalities found in glycans. In the face of such challenges, chemical biology strategies have been transformative for the field of bacterial glycobiology, from fundamental research to translational applications. From early efforts based on naturally-derived antibiotics and antibiotic conjugates, to rationally designed metabolic or biosynthetic probes, a number of distinct chemical strategies have been developed. In addition to imaging, probes to specifically perturb glycan structures have been particularly impactful. The modular nature of chemical probes, such as metabolic incorporation or biosynthetic incorporation probes, can

enable attachment of diverse functionality for facile glycan purification, visualization of biosynthesis and trafficking and identification of protein-carbohydrate interactions. It is important to note that, in order for these experiments to be interpreted, there is a need for rigorous characterization of probe activity and specificity.

Ultimately the chemical tools outlined in this chapter have helped highlight the critical importance of bacterial cell envelope glycans. New insights have been uncovered to understand better bacterial growth, cell division, and cell envelope remodeling. These tools initially developed to answer basic research questions have also inspired transformative translational studies uncovering the mechanisms of antibiotics, enabling development of screening platforms, and can serve as starting points for rationally designed inhibitors. One area that will be exciting to see in the future is the application of chemical reporters in tracking bacterial glycans over the course of an infection. This work has begun to be demonstrated but is still actively being developed to better understand relevant models of bacterial infection and pathogenesis and profiling the bacterial microbiota. A key to the innovations outlined in this chapter is the interdisciplinary research spanning synthetic organic chemistry, biochemistry, biology, microbiology, and medicine. Novel advances in the field of chemical microbiology are still needed to address the numerous challenges that remain to be tackled, but it is abundantly clear that the payoffs will be transformative.

1.6 References

1. Dorr, T.; Moynihan, P. J.; Mayer, C., Editorial: Bacterial Cell Wall Structure and Dynamics. *Front Microbiol* **2019,** *10*, 2051.

2. Kiessling, L. L.; Marando, V. M.; Smelyansky, S. R.; Kim, D. E., Chapter 25: Chemical Microbiology. In *Advanced Chemical Biology*, Hang, H. C.; Pratt, M. R.; Prescher, J. A., Eds. Wiley-VCH: 2023.

3. Moyes, R. B.; Reynolds, J.; Breakwell, D. P., Differential staining of bacteria: gram stain. *Curr Protoc Microbiol* **2009,** *Appendix 3*, Appendix 3C.

4. Rojas, E. R.; Billings, G.; Odermatt, P. D.; Auer, G. K.; Zhu, L.; Miguel, A.; Chang, F.; Weibel, D. B.; Theriot, J. A.; Huang, K. C., The outer membrane is an essential load-bearing element in Gram-negative bacteria. *Nature* **2018,** *559* (7715), 617-621.

5. Roberts, I. S., The biochemistry and genetics of capsular polysaccharide production in bacteria. *Annu Rev Microbiol* **1996,** *50*, 285-315.

6. Bloch, H., Acid-fast bacteria. *Annu Rev Microbiol* **1953,** *7.1*, 19-46.

7. Dulberger, C. L.; Rubin, E. J.; Boutte, C. C., The mycobacterial cell envelope - a moving target. *Nat Rev Microbiol* **2020,** *18* (1), 47-59.

8. Justen, A. M.; Hodges, H. L.; Kim, L. M.; Sadecki, P. W.; Porfirio, S.; Ultee, E.; Black, I.; Chung, G. S.; Briegle, A.; Azadi, P.; Kiessling, L. L., Polysaccharide length affects mycobacterial cell shape and antibiotic susceptibility. *Science Advances* **2020,** *6*, eaba4015.

9. Comstock, L. E.; Kasper, D. L., Bacterial glycans: key mediators of diverse host immune responses. *Cell* **2006,** *126* (5), 847-50.

10. Poole, J.; Day, C. J.; von Itzstein, M.; Paton, J. C.; Jennings, M. P., Glycointeractions in bacterial pathogenesis. *Nat Rev Microbiol* **2018,** *16* (7), 440-452.

11. Mueller, E. A.; Levin, P. A., Bacterial cell wall quality control during environmental stress. *mBio* **2020,** *11* (5), e02456-20.

12. Brown, S.; Santa Maria, J. P., Jr.; Walker, S., Wall teichoic acids of gram-positive bacteria. *Annu Rev Microbiol* **2013,** *67*, 313-36.

13. Atilano, M. L.; Pereira, P. M.; Yates, J.; Reed, P.; Veiga, H.; Pinho, M. G.; Filipe, S. R., Teichoic acids are temporal and spatial regulators of peptidoglycan cross-linking in Staphylococcus aureus. *Proc Natl Acad Sci U S A* **2010,** *107* (44), 18991-6.

14. Formstone, A.; Carballido-Lopez, R.; Noirot, P.; Errington, J.; Scheffers, D. J., Localization and interactions of teichoic acid synthetic enzymes in Bacillus subtilis. *J Bacteriol* **2008,** *190* (5), 1812-21.

15. Ehrt, S.; Schappinger, D., Mycobacterial survival strategies in the phagosome: defence against host stresses. *Cellular Microbiology* **2009,** *11* (8), 1170-1178.

16. Huszczynski, S. M.; Lam, J. S.; Khursigara, C. M., The Role of Pseudomonas aeruginosa Lipopolysaccharide in Bacterial Pathogenesis and Physiology. *Pathogens* **2019,** *9* (1).

17. Zgurskaya, H. I.; Lopez, C. A.; Gnanakaran, S., Permeability Barrier of Gram-Negative Cell Envelopes and Approaches To Bypass It. *ACS Infect Dis* **2015,** *1* (11), 512-522.

18. Harper, M.; Wright, A.; St Michael, F.; Li, J.; Deveson Lucas, D.; Ford, M.; Adler, B.; Cox, A. D.; Boyce, J. D., Characterization of Two Novel Lipopolysaccharide Phosphoethanolamine Transferases in Pasteurella multocida and Their Role in Resistance to Cathelicidin-2. *Infect Immun* **2017,** *85* (11).

19. Bera, A.; Herbert, S.; Jakob, A.; Vollmer, W.; Gotz, F., Why are pathogenic staphylococci so lysozyme resistant? The peptidoglycan O-acetyltransferase OatA is the major determinant for lysozyme resistance of Staphylococcus aureus. *Mol Microbiol* **2005,** *55* (3), 778-87.

20. Stefani, S.; Chung, D. R.; Lindsay, J. A.; Friedrich, A. W.; Kearns, A. M.; Westh, H.; Mackenzie, F. M., Meticillin-resistant Staphylococcus aureus (MRSA): global epidemiology and harmonisation of typing methods. *Int J Antimicrob Agents* **2012,** *39* (4), 273-82.

21. Gerlach, D.; Guo, Y.; De Castro, C.; Kim, S. H.; Schlatterer, K.; Xu, F. F.; Pereira, C.; Seeberger, P. H.; Ali, S.; Codee, J.; Sirisarn, W.; Schulte, B.; Wolz, C.; Larsen, J.; Molinaro, A.; Lee, B. L.; Xia, G.; Stehle, T.; Peschel, A., Methicillin-resistant Staphylococcus aureus alters cell wall glycosylation to evade immunity. *Nature* **2018,** *563* (7733), 705-709.

22. Angala, S. K.; McNeil, M. R.; Shi, L.; Joe, M.; Pham, H.; Zuberogoitia, S.; Nigou, J.; Boot, C. M.; Lowary, T. L.; Gilleron, M.; Jackson, M., Biosynthesis of the Methylthioxylose Capping Motif of Lipoarabinomannan in Mycobacterium tuberculosis. *ACS Chem Biol* **2017,** *12* (3), 682-691.

23. Sigal, G. B.; Pinter, A.; Lowary, T. L.; Kawasaki, M.; Li, A.; Mathew, A.; Tsionsky, M.; Zheng, R. B.; Plisova, T.; Shen, K.; Katsuragi, K.; Choudhary, A.; Honnen, W. J.; Nahid, P.; Denkinger, C. M.; Broger, T., A Novel Sensitive Immunoassay Targeting the 5-Methylthio-D- Xylofuranose–Lipoarabinomannan Epitope Meets the WHO's Performance Target for Tuberculosis Diagnosis. *Journal of Clinical Microbiology* **2018,** *56* (12), e01338-18.

24. Imperiali, B., Bacterial carbohydrate diversity - a Brave New World. *Curr Opin Chem Biol* **2019,** *53*, 1-8.

25. Gilormini, P. A.; Batt, A. R.; Pratt, M. R.; Biot, C., Asking more from metabolic oligosaccharide engineering. *Chem Sci* **2018,** *9* (39), 7585-7595.

26. Fraenkel, D. G.; Vinopal, R. T., Carbohydrate metabolism in bacteria. *Annu. Rev. Microbiol.* **1973,** *27*, 69-100.

27. Ohyama, Y.; Nakajima, K.; Renfrow, M. B.; Novak, J.; Takahashi, K., Mass spectrometry for the identification and analysis of highly complex glycosylation of therapeutic or pathogenic proteins. *Expert Rev Proteomics* **2020,** *17* (4), 275-296.

28. Banahene, N.; Kavunja, H. W.; Swarts, B. M., Chemical Reporters for Bacterial Glycans: Development and Applications. *Chem Rev* **2022,** *122* (3), 3336-3413.

29. Daniel, R. A.; Errington, J., Control of cell morphogenesis in bacteria: Two distinct ways to make a rod-shaped cell. *Cell* **2003,** *113* (6), 767-776.

30. Tiyanont, K.; Doan, T.; Lazarus, M. B.; Fang, X.; Rudner, D. Z.; Walker, S., Imaging peptidoglycan biosynthesis in Bacillus subtilis with fluorescent antibiotics. *Proc. Natl. Acad. Sci. U. S. A.* **2006,** *103* (29), 11033-11038.

31. Kocaoglu, O.; Calvo, R. A.; Sham, L. T.; Cozy, L. M.; Lanning, B. R.; Francis, S.; Winkler, M. E.; Kearns, D. B.; Carlson, E. E., Selective Penicillin-Binding Protein Imaging Probes Reveal Substructure in Bacterial Cell Division. *ACS Chem. Biol.* **2012,** *7* (10), 1746-1753.

32. Kocaoglu, O.; Carlson, E. E., Progress and prospects for small-molecule probes of bacterial imaging. *Nat. Chem. Biol.* **2016,** *12* (7), 472-478.

33. Pinho, M. G.; Errington, J., Dispersed mode of Staphylococcus aureus cell wall synthesis in the absence of the division machinery. *Mol. Microbiol.* **2003,** *50* (3), 871-881.

34. Daniel, R. A.; Errington, J., Control of cell morphogenesis in bacteria: two distinct ways to make a rod-shaped cell. *Cell* **2003,** *113* (6), 767-76.

35. Bush, K.; Bradford, P. A., beta-Lactams and beta-Lactamase Inhibitors: An Overview. *Cold Spring Harbor Perspectives in Medicine* **2016,** *6* (8).

36. Bottcher, T.; Sieber, S. A., beta-Lactams and beta-lactones as activity-based probes in chemical biology. *Medchemcomm* **2012,** *3* (4), 408-417.

37. Staub, I.; Sieber, S. A., beta-Lactam Probes As Selective Chemical-Proteomic Tools for the Identification and Functional Characterization of Resistance Associated Enzymes in MRSA. *Journal of the American Chemical Society* **2009,** *131* (17), 6271-6276.

38. Staub, I.; Sieber, S. A., beta-lactams as selective chemical probes for the in vivo labeling of bacterial enzymes involved in cell wall biosynthesis, antibiotic resistance, and virulence. *Journal of the American Chemical Society* **2008,** *130* (40), 13400-13409.

39. Marshall, A. P.; Shirley, J. D.; Carlson, E. E., Enzyme-targeted fluorescent small-molecule probes for bacterial imaging. *Curr. Opin. Chem. Biol.* **2020,** *57*, 155-165.

40. Levine, S. R.; Beatty, K. E., Investigating beta-Lactam Drug Targets in Mycobacterium tuberculosis Using Chemical Probes. *Acs Infectious Diseases* **2021,** *7* (2), 461-470.

41. Zhao, G. S.; Meier, T. I.; Kahl, S. D.; Gee, K. R.; Blaszczak, L. C., BOCILLIN FL, a sensitive and commercially available reagent for detection of penicillin-binding proteins. *Antimicrob. Agents Chemother.* **1999,** *43* (5), 1124-1128.

42. Gee, K. R.; Kang, H. C.; Meier, T. I.; Zhao, G. S.; Blaszcak, L. C., Fluorescent Bocillins: Synthesis and application in the detection of penicillin-binding proteins. *Electrophoresis* **2001,** *22* (5), 960-965.

43. Kocaoglu, O.; Carlson, E. E., Profiling of beta-Lactam Selectivity for Penicillin-Binding Proteins in Escherichia coli Strain DC2. *Antimicrob. Agents Chemother.* **2015,** *59* (5), 2785-2790.

44. Sharifzadeh, S.; Dempwolff, F.; Kearns, D. B.; Carlson, E. E., Harnessing beta-Lactam Antibiotics for Illumination of the Activity o Penicillin-Binding Proteins in Bacillus subtilis. *ACS Chem. Biol.* **2020,** *15* (5), 1242-1251.

45. Kocaoglu, O.; Tsui, H. C. T.; Winkler, M. E.; Carlson, E. E., Profiling of beta-Lactam Selectivity for Penicillin-Binding Proteins in Streptococcus pneumoniae D39. *Antimicrob. Agents Chemother.* **2015,** *59* (6), 3548-3555.

46. Perez, A. J.; Boersma, M. J.; Bruce, K. E.; Lamanna, M. M.; Shaw, S. L.; Tsui, H. C. T.; Taguchi, A.; Carlson, E. E.; VanNieuwenhze, M. S.; Winkler, M. E., Organization of peptidoglycan synthesis in nodes and separate rings at different stages of cell division of Streptococcus pneumoniae. *Mol. Microbiol.* **2021,** *115* (6), 1152-1169.

47. Dube, D. H.; Bertozzi, C. R., Metabolic oligosaccharide engineering as a tool for glycobiology. *Curr Opin Chem Biol* **2003,** *7* (5), 616-25.

48. Kufleitner, M.; Haiber, L. M.; Wittmann, V., Metabolic glycoengineering - exploring glycosylation with bioorthogonal chemistry. *Chem Soc Rev* **2023,** *52* (2), 510-535.

49. Saeui, C. T.; Urias, E.; Liu, L.; Mathew, M. P.; Yarema, K. J., Metabolic glycoengineering bacteria for therapeutic, recombinant protein, and metabolite production applications. *Glycoconj J* **2015,** *32* (7), 425-41.

50. Kayser, H.; Ats, C.; Lehmann, J.; Reutter, W., New amino sugar analogues are incorporated at different rates into glycoproteins of mouse organs. *Experientia* **1993,** *49* (10), 885-7.

51. Cheng, B.; Tang, Q.; Zhang, C.; Chen, X., Glycan Labeling and Analysis in Cells and In Vivo. *Annu Rev Anal Chem (Palo Alto Calif)* **2021,** *14* (1), 363-387.

52. Prescher, J. A.; Bertozzi, C. R., Chemistry in living systems. *Nat Chem Biol* **2004,** *1* (1), 13-21.

53. Prescher, J. A.; Bertozzi, C. R., Chemical technologies for probing glycans. *Cell* **2006,** *126* (5), 851-4.

54. Laughlin, S. T.; Baskin, J. M.; Amacher, S. L.; Bertozzi, C. R., In Vivo Imaging of Membrane-Associated Glycans in Developing Zebrafish. *Science* **2008,** *320*, 664-667.

55. Xie, R.; Dong, L.; Du, Y.; Zhu, Y.; Hua, R.; Zhang, C.; Chen, X., In vivo metabolic labeling of sialoglycans in the mouse brain by using a liposome-assisted bioorthogonal reporter strategy. *Proc Natl Acad Sci U S A* **2016,** *113* (19), 5173-8.

56. Qin, W.; Qin, K.; Fan, X.; Peng, L.; Hong, W.; Zhu, Y.; Lv, P.; Du, Y.; Huang, R.; Han, M.; Cheng, B.; Liu, Y.; Zhou, W.; Wang, C.; Chen, X., Artificial Cysteine S-Glycosylation Induced by Per-O-Acetylated Unnatural Monosaccharides during Metabolic Glycan Labeling. *Angew Chem Int Ed Engl* **2018,** *57* (7), 1817-1820.

57. Laughlin, S. T.; Bertozzi, C. R., Metabolic labeling of glycans with azido sugars and subsequent glycan-profiling and visualization via Staudinger ligation. *Nat Protoc* **2007,** *2* (11), 2930-44.

58. Mathew, M. P.; Tan, E.; Shah, S.; Bhattacharya, R.; Adam Meledeo, M.; Huang, J.; Espinoza, F. A.; Yarema, K. J., Extracellular and intracellular esterase processing of SCFA-hexosamine analogs: implications for metabolic glycoengineering and drug delivery. *Bioorg Med Chem Lett* **2012,** *22* (22), 6929-33.

59. Antonczak, A. K.; Simova, Z.; Tippmann, E. M., A critical examination of Escherichia coli esterase activity. *J Biol Chem* **2009,** *284* (42), 28795-800.

60. Sadamoto, R.; Matsubayashi, T.; Shimizu, M.; Ueda, T.; Koshida, S.; Koda, T.; Nishimura, S., Bacterial surface engineering utilizing glucosamine phosphate derivatives as cell wall precursor surrogates. *Chemistry* **2008,** *14* (33), 10192-5.

61. Lodowska, J.; Wolny, D.; Weglarz, L., The sugar 3-deoxy-d-manno-oct-2-ulosonic acid (Kdo) as a characteristic component of bacterial endotoxin -- a review of its biosynthesis, function, and placement in the lipopolysaccharide core. *Can J Microbiol* **2013,** *59* (10), 645-55.

62. Unger, F. M., The Chemistry and Biological Significance of 3-Deoxy-d-manno-2-Octulosonic Acid (KDO). In *Advances in Carbohydrate Chemistry and Biochemistry Volume 38*, 1981; pp 323-388.

63. Dumont, A.; Malleron, A.; Awwad, M.; Dukan, S.; Vauzeilles, B., Click-mediated labeling of bacterial membranes through metabolic modification of the lipopolysaccharide inner core. *Angew Chem Int Ed Engl* **2012,** *51* (13), 3143-6.

64. Nilsson, I.; Grove, K.; Dovala, D.; Uehara, T.; Lapointe, G.; Six, D. A., Molecular characterization and verification of azido-3,8-dideoxy-d-manno-oct-2-ulosonic acid incorporation into bacterial lipopolysaccharide. *J Biol Chem* **2017,** *292* (48), 19840-19848.

65. Sherratt, A. R.; Chigrinova, M.; McKay, C. S.; Beaulieu, L. B.; Rouleau, Y.; Pezacki, J. P., Copper-catalysed cycloaddition reactions of nitrones and alkynes for bioorthogonal labelling of living cells. *RSC advances* **2014,** *4* (87), 46966-46969.

66. Yi, W.; Liu, X.; Li, Y.; Li, J.; Xia, C.; Zhou, G.; Zhang, W.; Zhao, W.; Chen, X.; Wang, P. G., Remodeling bacterial polysaccharides by metabolic pathway engineering. *Proc Natl Acad Sci U S A* **2009,** *106* (11), 4207-12.

67. Mas Pons, J.; Dumont, A.; Sautejeau, G.; Fugier, E.; Baron, A.; Dukan, S.; Vauzeilles, B., Identification of living Legionella pneumophila using species-specific metabolic lipopolysaccharide labeling. *Angew Chem Int Ed Engl* **2014,** *53* (5), 1275-8.

68. Andolina, G.; Wei, R.; Liu, H.; Zhang, Q.; Yang, X.; Cao, H.; Chen, S.; Yan, A.; Li, X. D.; Li, X., Metabolic Labeling of Pseudaminic Acid-Containing Glycans on Bacterial Surfaces. *ACS Chem Biol* **2018,** *13* (10), 3030-3037.

69. Heise, T.; Langereis, J. D.; Rossing, E.; de Jonge, M. I.; Adema, G. J.; Bull, C.; Boltje, T. J., Selective Inhibition of Sialic Acid-Based Molecular Mimicry in Haemophilus influenzae Abrogates Serum Resistance. *Cell Chem Biol* **2018,** *25* (10), 1279-1285 e8.

70. Wang, Y.; Li, L.; Yu, J.; Hu, H.; Liu, Z.; Jiang, W.; Xu, W.; Guo, X.; Wang, F.; Sheng, J., Imaging of Escherichia coli K5 and glycosaminoglycan precursors via targeted metabolic labeling of capsular polysaccharides in bacteria. *Science Advances* **2023,** *9*, ead4770.

71. Hodges, H.; Obeng, K.; Avanzi, C.; Ausmus, A. P.; Angala, S. K.; Kalera, K.; Palcekova, Z.; Swarts, B. M.; Jackson, M., Azido Inositol Probes Enable Metabolic Labeling of Inositol-Containing Glycans and Reveal an Inositol Importer in Mycobacteria. *ACS Chem Biol* **2023**.

72. Moulton, K. D.; Adewale, A. P.; Carol, H. A.; Mikami, S. A.; Dube, D. H., Metabolic Glycan Labeling-Based Screen to Identify Bacterial Glycosylation Genes. *ACS Infect Dis* **2020,** *6* (12), 3247-3259.

73. Calabretta, P. J.; Hodges, H. L.; Kraft, M. B.; Marando, V. M.; Kiessling, L. L., Bacterial Cell Wall Modification with a Glycolipid Substrate. *J Am Chem Soc* **2019,** *141* (23), 9262-9272.

74. Marando, V. M.; Kim, D. E.; Kiessling, L. L., Biosynthetic incorporation for visualizing bacterial glycans. *Methods Enzymol* **2022,** *665*, 135-151.

75. Marando, V. M.; Kim, D. E.; Calabretta, P. J.; Kraft, M. B.; Bryson, B. D.; Kiessling, L. L., Biosynthetic Glycan Labeling. *J Am Chem Soc* **2021,** *143* (40), 16337-16342.

76. Gautam, S.; Kim, T.; Howell, R.; Spiegel, D. A., Fluorescent stem peptide mimics: In situ probes for peptidoglycan crosslinking. In *Chemical Tools for Imaging, Manipulating, and Tracking Biological Systems: Diverse Methods for Prokaryotic and Eukaryotic Systems*, Chenoweth, D. M., Ed. 2020; Vol. 638, pp 57-67.

77. Hsu, Y.-P.; Rittichier, J.; Kuru, E.; Yablonowski, J.; Pasciak, E.; Tekkam, S.; Hall, E.; Murphy, B.; Lee, T. K.; Garner, E. C.; Huang, K. C.; Brun, Y. V.; VanNieuwenhze, M. S., Full color palette of fluorescent d-amino acids for in situ labeling of bacterial cell walls. *Chem Sci* **2017,** *8* (9), 6313-6321.

78. Kuru, E.; Radkov, A.; Meng, X.; Egan, A.; Alvarez, L.; Dowson, A.; Booher, G.; Breukink, E.; Roper, D. I.; Cava, F.; Vollmer, W.; Brun, Y.; VanNieuwenhze, M. S., Mechanisms of Incorporation for D-Amino Acid Probes That Target Peptidoglycan Biosynthesis. *Acs Chemical Biology* **2019,** *14* (12), 2745-2756.

79. Gisin, J.; Schneider, A.; Nagele, B.; Borisova, M.; Mayer, C., A cell wall recycling shortcut that bypasses peptidoglycan de novo biosynthesis. *Nat Chem Biol* **2013,** *9* (8), 491-3.

80. Liang, H.; DeMeester, K. E.; Hou, C. W.; Parent, M. A.; Caplan, J. L.; Grimes, C. L., Metabolic labelling of the carbohydrate core in bacterial peptidoglycan and its applications. *Nature Communications* **2017,** *8*.

81. Holmes, N. J.; Kavunja, H. W.; Yang, Y.; Vannest, B. D.; Ramsey, C. N.; Gepford, D. M.; Banahene, N.; Poston, A. W.; Piligian, B. F.; Ronning, D. R.; Ojha, A. K.; Swarts, B. M., A FRET-Based Fluorogenic Trehalose Dimycolate Analogue for Probing Mycomembrane-Remodeling Enzymes of Mycobacteria. *ACS Omega* **2019,** *4* (2), 4348-4359.

82. Hodges, H. L.; Brown, R. A.; Crooks, J. A.; Weibel, D. B.; Kiessling, L. L., Imaging mycobacterial growth and division with a fluorogenic probe. *Proceedings of the National Academy of Sciences of the United States of America* **2018,** *115* (20), 5271-5276.

83. Rundell, S. R.; Wagar, Z. L.; Meints, L. M.; Olson, C. D.; O'Neill, M. K.; Piligian, B. F.; Poston, A. W.; Hood, R. J.; Woodruff, P. J.; Swarts, B. M., Deoxyfluoro-D-trehalose (FDTre) analogues as potential PET probes for imaging mycobacterial infection. *Organic & Biomolecular Chemistry* **2016,** *14* (36), 8598-8609.

84. Rodriguez-Rivera, F. P.; Zhou, X.; Theriot, J. A.; Bertozzi, C. R., Acute modulation of mycobacterial cell envelope biogenesis by front-line TB drugs. *Angewandte Chemie (International ed. in English)* **2018,** *57* (19), 5267-5272.

85. Kamariza, M.; Shieh, P.; Ealand, C. S.; Peters, J. S.; Chu, B.; Rodriguez-Rivera, F. P.; Sait, M. R. B.; Treuren, W. V.; Martinson, N.; Kalscheuer, R.; Kana, B. D.; Bertozzi, C. R., F Rapid detection of Mycobacterium tuberculosis in sputum with a solvatochromic trehalose probe. *Sci. Transl. Med.* **2018,** *10* (430).

86. Rodriguez-Rivera, F. P.; Zhou, X. X.; Theriot, J. A.; Bertozzi, C. R., Visualization of mycobacterial membrane dynamics in live cells. *J Am Chem Soc* **2017,** *139* (9), 3488-3495.

87. Kuru, E.; Hughes, H. V.; Brown, P. J.; Hall, E.; Tekkam, S.; Cava, F.; de Pedro, M. A.; Brun, Y. V.; VanNieuwenhze, M. S., In Situ probing of newly synthesized peptidoglycan in live bacteria with fluorescent D-amino acids. *Angew Chem Int Ed Engl* **2012,** *51* (50), 12519-23.

88. Garcia-Heredia, A.; Pohane, A. A.; Melzer, E. S.; Carr, C. R.; Fiolek, T. J.; Rundell, S. R.; Lim, H. C.; Wagner, J. C.; Morita, Y. S.; Swarts, B. M.; Siegrist, M. S., Peptidoglycan precursor synthesis along the sidewall of pole-growing mycobacteria. *Elife* **2018,** *7*.

89. Siegrist, M. S.; Whiteside, S.; Jewett, J. C.; Aditham, A.; Cava, F.; Bertozzi, C. R., (D)-Amino acid chemical reporters reveal peptidoglycan dynamics of an intracellular pathogen. *ACS Chem Biol* **2013,** *8* (3), 500-5.

90. Wuo, M. G.; Dulberger, C. L.; Brown, R. A.; Sturm, A.; Ultee, E.; Bloom-Ackermann, Z.; Choi, C.; Garner, E. C.; Briegel, A.; Hung, D. T.; Rubin, E. J.; Kiessling, L. L., Antibiotic action revealed by real-time imaging of the mycobacterial membrane. *Biorxiv* **2022**.

91. Langereis, J. D.; de Jonge, M. I., Invasive Disease Caused by Nontypeable Haemophilus influenzae. *Emerg Infect Dis* **2015,** *21* (10), 1711-8.

92. Al-Jourani, O.; Benedict, S.; Ross, J.; Layton, A.; van der Peet, P.; Marando, V. M.; Bailey, N. P.; Heunis, T.; Manion, J.; Mensitieri, F.; Franklin, A.; Abellon-Ruiz, J.; Oram, S. L.; Parsons, L.; Cartmell, A.; Wright, G. S. A.; Baslé, A.; Trost, M.; Henrissat, B.; Munoz-Munoz, J.; Hirt, R. P.; Kiessling, L. L.; Lovering, A.; Williams, S. J.; Lowe, E. C.; Moynihan, P. J., Mining the human gut microbiome identifies mycobacterial D-arabinan degrading enzymes. *Biorxiv* **2022**.

93. Huang, S. H.; Wu, W. S.; Huang, L. Y.; Huang, W. F.; Fu, W. C.; Chen, P. T.; Fang, J. M.; Cheng, W. C.; Cheng, T. J.; Wong, C. H., New continuous fluorometric assay for bacterial transglycosylase using Forster resonance energy transfer. *J Am Chem Soc* **2013,** *135* (45), 17078-89.

94. Walvoort, M. T.; Lukose, V.; Imperiali, B., A Modular Approach to Phosphoglycosyltransferase Inhibitors Inspired by Nucleoside Antibiotics. *Chemistry* **2016,** *22* (11), 3856-64.

95. Madec, A. G. E.; Schocker, N. S.; Sanchini, S.; Myratgeldiyev, G.; Das, D.; Imperiali, B., Facile Solid-Phase Synthesis and Assessment of Nucleoside Analogs as Inhibitors of Bacterial UDP-Sugar Processing Enzymes. *ACS Chem Biol* **2018,** *13* (9), 2542-2550.

96. Luong, P.; Dube, D. H., Dismantling the bacterial glycocalyx: Chemical tools to probe, perturb, and image bacterial glycans. *Bioorg Med Chem* **2021,** *42*, 116268.

97. Brown, C. D.; Rusek, M. S.; Kiessling, L. L., Fluorosugar chain termination agents as probes of the sequence specificity of a carbohydrate polymerase. *J Am Chem Soc* **2012,** *134* (15), 6552-5.

98. Williams, D. A.; Pradhan, K.; Paul, A.; Olin, I. R.; Tuck, O. T.; Moulton, K. D.; Kulkarni, S. S.; Dube, D. H., Metabolic inhibitors of bacterial glycan biosynthesis. *Chem Sci* **2020,** *11* (7), 1761-1774.

99. Kapil, S.; Petit, C.; Drago, V. N.; Ronning, D. R.; Sucheck, S. J., Synthesis and in Vitro Characterization of Trehalose-Based Inhibitors of Mycobacterial Trehalose 6-Phosphate Phosphatases. *Chembiochem* **2019,** *20* (2), 260-269.

100. Roy, S.; Trinchieri, G., Microbiota: a key orchestrator of cancer therapy. *Nature Reviews Cancer* **2017,** *17* (5), 271-+.

101. Mowat, A. M.; Agace, W. W., Regional specialization within the intestinal immune system. *Nature Reviews Immunology* **2014,** *14* (10), 667-685.

102. Fung, T. C.; Olson, C. A.; Hsiao, E. Y., Interactions between the microbiota, immune and nervous systems in health and disease. *Nat. Neurosci.* **2017,** *20* (2), 145-155.

103. Coyte, K. Z.; Schluter, J.; Foster, K. R., The ecology of the microbiome: Networks, competition, and stability. *Science* **2015,** *350* (6261), 663-666.

104. Chu, H. T.; Khosravi, A.; Kusumawardhani, I. P.; Kwon, A. H. K.; Vasconcelos, A. C.; Cunha, L. D.; Mayer, A. E.; Shen, Y.; Wu, W. L.; Kambal, A.; Targan, S. R.; Xavier, R. J.; Ernst, P. B.; Green, D. R.; McGovern, D. P. B.; Virgin, H.; Mazmanian, S. K., Gene-microbiota interactions contribute to the pathogenesis of inflammatory bowel disease. *Science* **2016,** *352* (6289), 1116-1120.

105. Sampson, T. R.; Mazmanian, S. K., Control of Brain Development, Function, and Behavior by the Microbiome. *Cell Host Microbe* **2015,** *17* (5), 565-576.

106. Lagier, J. C.; Dubourg, G.; Million, M.; Cadoret, F.; Bilen, M.; Fenollar, F.; Levasseur, A.; Rolain, J. M.; Fournier, P. E.; Raoult, D., Culturing the human microbiota and culturomics'. *Nature Reviews Microbiology* **2018,** *16* (9), 540-550.

107. Geva-Zatorsky, N.; Alvarez, D.; Hudak, J. E.; Reading, N. C.; Erturk-Hasdemir, D.; Dasgupta, S.; von Andrian, U. H.; Kasper, D. L., In vivo imaging and tracking of host-microbiota interactions via metabolic labeling of gut anaerobic bacteria. *Nat. Med.* **2015,** *21* (9), 1091-+.

108. Ning, X. H.; Guo, J.; Wolfert, M. A.; Boons, G. J., Visualizing metabolically labeled glycoconjugates of living cells by copper-free and fast huisgen cycloadditions. *Angewandte Chemie-International Edition* **2008,** *47* (12), 2253-2255.

109. Lin, L. Y.; Du, Y. H.; Song, J.; Wang, W.; Yang, C. Y., Imaging Commensal Microbiota and Pathogenic Bacteria in the Gut. *Acc. Chem. Res.* **2021,** *54* (9), 2076-2087.

110. Dridi, L.; Altamura, F.; Gonzalez, E.; Lui, O.; Kubinski, R.; Pidgeon, R.; Montagut, A.; Chong, J.; Xia, J.; Maurice, C. F.; Castagner, B., Identifying glycan consumers in human gut microbiota samples using metabolic labeling coupled with fluorescence-activated cell sorting. *Nat Commun* **2023,** *14* (1), 662.

111. Hudak, J. E.; Alvarez, D.; Skelly, A.; von Andrian, U. H.; Kasper, D. L., Illuminating vital surface molecules of symbionts in health and disease. *Nat Microbiol* **2017,** *2*, 17099.

Chapter 2: Development of Biosynthetic Glycan Labeling Probes Targeting Mycobacterial Arabinan

Reproduced with permission from:
Calabretta PJ, Hodges HL, Kraft MB, Marando VM, Kiessling LL. Bacterial cell wall modification with a glycolipid substrate. *Journal of the American Chemical Society*. **2019**, 141(23) 9262-72.

Marando VM*, Kim DE*, Calabretta PJ, Kraft MB, Bryson BD, Kiessling LL. Biosynthetic glycan labeling. *Journal of the American Chemical Society*. **2021**, 143(40) 16337-42.
* denotes authors contributed equally

Contributions:
Compounds were synthesized by Daria E. Kim, Matthew B. Kraft and Phillip J. Calabretta. Initial lipid truncation study performed by Phillip J. Calabretta, Heather L. Hodges, Matthew B. Kraft and Victoria M. Marando. Flow cytometry, microscopy and other cell-based assays were performed by Victoria M. Marando. Research designed by Victoria M. Marando, Daria E. Kim, Phillip J. Calabretta, Matthew B. Kraft and Laura L. Kiessling.

2.1 Abstract

Glycans are ubiquitous and play important biological roles, yet chemical methods for probing their structure and function within cells remain limited. Strategies for studying other biomacromolecules, such as proteins, often exploit chemoselective reactions for covalent modification, capture, or imaging. Unlike amino acids that constitute proteins, glycan building blocks lack distinguishing reactivity because they are composed primarily of polyol isomers. Moreover, encoding glycan variants through genetic manipulation is complex. Therefore, we formulated a new, generalizable strategy for chemoselective glycan modification that directly takes advantage of cellular glycosyltransferases. Many of these enzymes are selective for the products they generate yet promiscuous in their donor preferences. Thus, we designed reagents that function as glycosyltransferase substrate surrogates. We validated the feasibility of this approach by synthesizing and testing probes of D-arabinofuranose (D-Ara*f*), a monosaccharide found in bacteria and an essential component of the cell wall that protects mycobacteria, including *Mycobacterium tuberculosis*. In this work we disclose the first probe capable of selectively labeling arabinofuranose-containing glycans with a bioorthogonal handle. This probe revealed an asymmetric distribution of D-Ara*f* residues during mycobacterial cell growth and could be used to detect mycobacteria in THP1-derived macrophages. Our studies serve as a platform for developing new chemoselective labeling agents for other privileged monosaccharides.

2.2 Introduction

Monomer-selective bioconjugation reactions have transformed the study of biomolecules, affording molecular-level insight into structure, function, localization, and dynamics.[1-3] Proteins exhibit significant functional group variation and this diversity has been exploited in bioconjugation reactions. In contrast, glycans and their component sugars cannot easily be distinguished from one another based on complementary reactivity, as their structural diversity derives predominantly from the stereo- and constitutional isomerism of polyol monomers (**Figure 2.1A**). As a result, the systematic interrogation of glycan structure–function relationships at the bacterial cell surface is limited.

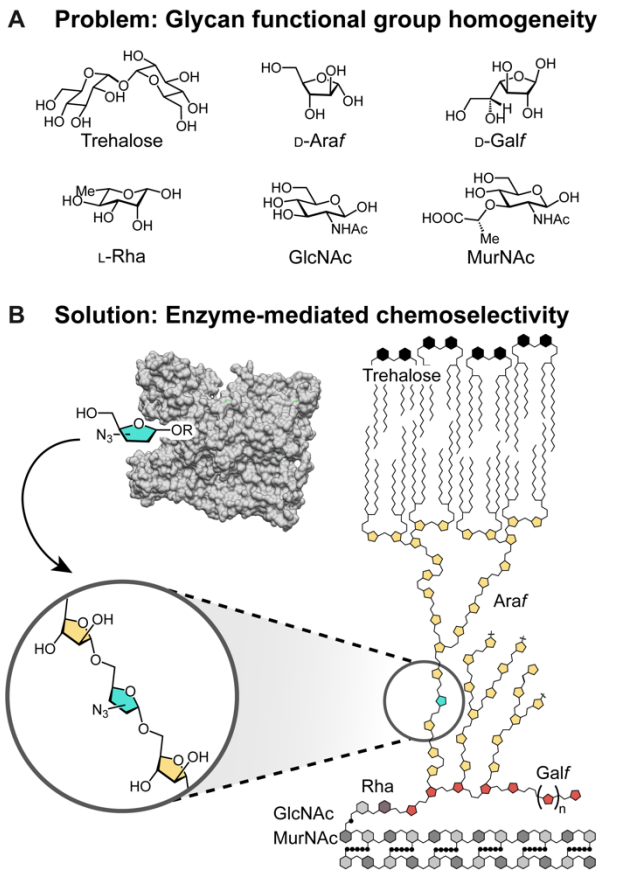

Figure 2.1 Overview of the problem of glycan bioconjugation and our proposed solution. (A) Monosaccharides within glycans derive their identity from polyol stereo- and constitutional isomerism. **(B)** The core cell wall structure of mycobacteria and corynebacteria is comprised of six unique monomers. This structure, termed the mycolyl-arabinogalactan-peptidoglycan complex (mAGP) is a dense glycolipid matrix that protects cells from environmental stresses, including antibiotics. Biosynthetic incorporation directly leverages the activity of cellular glycosyltransferases for specific monosaccharides to introduce modifications into cell surface glycans.

In the absence of a viable chemical approach to site-selective glycan labeling, metabolic engineering has been used to modify and study cell surface glycans in eukaryotic systems.[4-7] This method generally relies on the cellular uptake of non-natural monosaccharides, followed by extensive biosynthetic processing to nucleotide-sugar analogs. As

nucleotide-sugars can serve as donors for cytosolic glycosyltransferases, these intermediates are incorporated into growing glycan chains that are subsequently exported to the cell surface. While effective in eukaryotes, probes can experience unintended fates leading to undesired labeling in many systems.[8-9] The adaptation of metabolic incorporation to prokaryotes in particular has been historically challenging.[10-14] Mammals utilize 35 unique monosaccharide building blocks, while bacteria employ over 600.[15-16] The structural diversity of bacterial monosaccharides and glycans necessitates a complex and often poorly understood carbohydrate metabolism.[17-18] As a result, site-specific modification of bacterial glycans is challenging.[17]

We assumed that unique sugar monomers could be best distinguished through direct enzyme recognition and modification to achieve selective glycan modification.[19] We therefore sought to exploit existing catalysts with the requisite selectivity—the endogenous glycosyltransferases. These biocatalysts have an evolved selectivity for a specific small molecule substrate donor and a specific polysaccharide acceptor (**Figure 2.1B**).[20-24]

Here, we describe the development and application of a new approach to chemoselective glycan bioconjugation. This strategy, termed biosynthetic incorporation, leverages the activity of endogenous extracellular enzymes using substrate surrogates (**Figure 2.2**). This biocatalytic manifold can side-step challenges associated with small molecule-based glycan bioconjugation and metabolic engineering by exploiting the intrinsic selectivity of the target biocatalysts. We assessed the feasibility of our chemoselective labeling strategy by targeting D-arabinofuranose (D-Ara*f*). This arabinose isomer is not found in humans but is present in microbes. D-Ara*f* is an essential component of the cell wall of the order Mycobacteriales.[25-26] Although many

constituents of this order are benign, *Mycobacterium tuberculosis* (*Mtb*), *Corynebacterium diphtheriae*, and *Mycobacterium leprae* are notorious human pathogens.[27-29] These organisms utilize D-Ara*f* for the construction of the core glycolipid component of their cell wall, the mycolyl-arabinogalactan-peptidoglycan complex (mAGP).[30] Within the mAGP, the arabinan is thought to help maintain the structural integrity of the cell envelope. Indeed, mAGP biosynthesis is the target of the front-line antituberculosis drug ethambutol.[31]

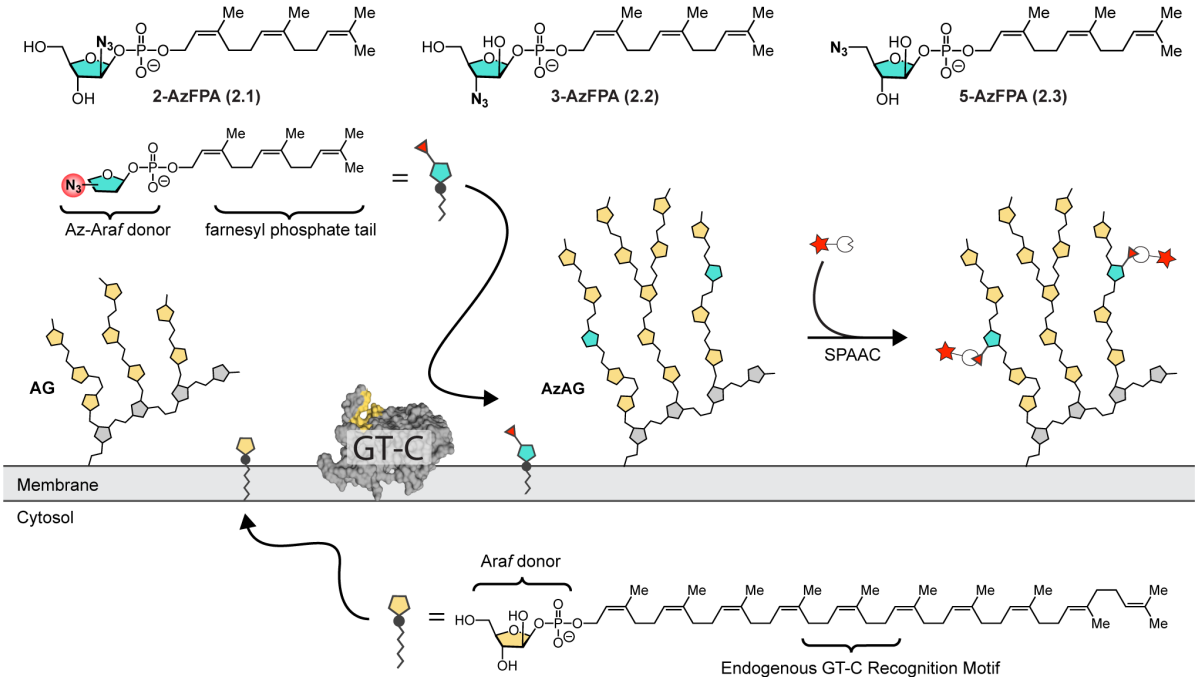

Figure 2.2 Biosynthetic labeling of arabinose schematic. To harness the catalytic activity of arabinofuranosyltransferase GT-Cs for bioconjugation, an azide-modified substrate surrogate was designed based on structural homology to the endogenous D-Ara*f* donor (DPA). Three azide regioisomers were produced (**2.1-2.3**). Exogenous delivery of AzFPA was designed to result in substrate incorporation, which could subsequently be detected and quantified using strain-promoted azide-alkyne click reaction (SPAAC)-mediated fluorophore conjugation.

D-Ara*f* residues are an excellent test of our strategy. First, no methods to selectively visualize D-Ara*f* are known. Second, the biosynthesis of the activated sugar proceeds through late-stage epimerization of the C2 hydroxyl from the ribose-phospholipid to the

corresponding arabinose-phospholipid donor rather than other sources of free arabinose.[32] Consequently, metabolic engineering approaches are unlikely to result in specific D-Ara*f* labeling.[33]

In mycobacteria, integral membrane glycosyltransferases (GT-Cs) mediate D-Ara*f* incorporation into cell-surface glycans.[20-24] In contrast to the nucleotide-sugar substrates of cytosolic glycosyltransferases, these GT-Cs are transmembrane enzymes that recognize polyprenyl phosphate-linked sugar donors.[34] We first identified the non-natural glycolipid donor (*Z*,*Z*)-farnesyl phosphoryl-β-D-arabinofuranose (FPA) as a viable surrogate for the extended (C_{55}) endogenous arabinofuranose donor decaprenyl phosphoryl-β-D-arabinofuranose (DPA) in *C. glutamicum* and *M. smegmatis*. This lipid substitution facilitates exogenous reagent delivery, as extended polyprenyl glycosides are poorly soluble and form micelles.[23, 35] We then employed this non-natural (*Z*,*Z*)-farnesyl phosphoryl donor scaffold as a vehicle to introduce azide-modified D-Ara*f* derivatives into the mAGP. Our work uncovered that surrogates of natural lipid-linked glycans can intervene in the cell's workflow, demonstrating that biosynthetic incorporation is a powerful strategy to label glycans and probe structure–function relationships.

2.3 Results & Discussion

2.3.1 Optimizing a Synthetic Lipid

First, we generated synthetic arabinofuranosyl phospholipids to test the feasibility of a non-natural lipid bearing donor. We rationally designed our reagents based on the structure of the endogenous sugar donor (**Figure 2.3A**). Using a *C. glutamicum* mutant that lacks arabinan, we identified synthetic glycosyl donors whose

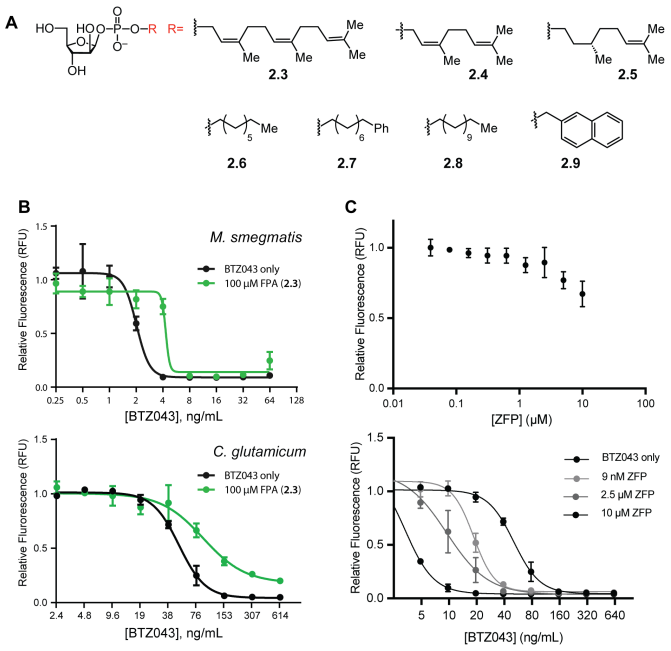

Figure 2.3 Optimization and validation of a lipid-linked scaffold for arabinose incorporation. (A) Library of synthetic arabinose donors. **(B)** Effect of FPA on the antibiotic activity of BTZ043. Bacterial growth was measured, via the Alamar blue assay. Error bars represent the standard deviation, n = 3. **(C)** Effect of ZFP on cell viability and rescue in *C. glutamicum*. Bacterial growth was measured, via the Alamar blue assay. Error bars represent the standard deviation, n = 3.

Table 2.1 Extent of arabinose incorporation determined by cell wall composition analysis. Chemical complementation *of CgΔubiA* was performed by growing cells with each potential donor (250 μM) shown (**2.3-2.9**) for one doubling time. The ratio of arabinose to galactose residues determined by mass spectrometry to calculate degree of incorporation relative to wildtype.

Compound	Degree of Incorporation
2.3	34.7%
2.4	9.5%
2.5	4.7%
2.6	5.6%
2.7	11.9%
2.8	13.4%
2.9	4.5%

addition restores cell wall arabinan by carrying out carbohydrate composition analysis (**Table 2.1**). The appearance of arabinose in the cell walls of treated bacteria indicated that several of the synthetic analogs led to arabinose incorporation. We observed variations in the extent of recovery based on the identity of the lipid tail. The ideal substrate would display a modest degree of incorporation, where there is enough modification to visualize but the non-natural substrate does not make up the majority of the composition. We found that FPA (**2.3**) led to reasonable arabinose incorporation.

We then validated the processing of FPA by wild-type cells by determining whether probe treatment could rescue cells treated with an inhibitor of endogenous donor biosynthesis. We postulated that FPA processing by wild-type cells should compensate for the inhibition of endogenous donor biosynthesis, DPA, and rescue cell viability.

Inhibitors of DPA biosynthesis are known. One class, benzothiazinones, block the enzyme DprE1, which catalyzes an epimerization reaction in the last step of DPA biosynthesis. BTZ043, a commercially available benzothiazinone, is a potent antibiotic against *M. tuberculosis* (MIC = 1–4 ng/mL), *C. glutamicum* (MIC = 20 μg/mL), and *M. smegmatis* (MIC = 0.1–80 ng/mL).[36-37] BTZ043 has been suggested to lead to cell death in *C. glutamicum ATCC 13032* by preventing decaprenyl phosphate recycling by sequestering the lipid in the form of decaprenyl phosphoryl ribose.[36, 38] We hypothesized that FPA processing might facilitate lipid recycling and thereby rescue cells from a lethal dose of BTZ043.[39] To test this hypothesis, we first treated M. smegmatis exposed to BTZ043 and FPA. Indeed, we observed rescue in both *M. smegmatis* and *C. glutamicum* (**Figure 2.3B**).

To probe the mechanism of this observed rescue, we next tested the expected product of FPA processing, (*Z*,*Z*)-farnesyl phosphate (ZFP). When a cell uses the natural substrate DPA, arabinan is produced and decaprenyl phosphate is generated. The mitigating effects of FPA raised the possibility that its activity was due to the production of ZFP. We therefore tested this possibility. No concentration of ZFP afforded any rescue in *C. glutamicum* (**Figure 2.3C**). The inability of ZFP to compensate for the effects of BTZ0243 suggests that FPA's role as a sugar donor is essential to the mechanism of rescue. Taken together, our data indicate that synthetic surrogates of natural lipid-linked glycans can intervene in the cell's traditional workflow.

2.3.2 Design and Synthesis of Azide-Functionalized Probe

We next sought out to apply this scaffold to install a bioconjugation handle. The endogenous monosaccharide donor and polysaccharide acceptors for cell wall arabinosylation have been well-characterized, yet few 3D structures for the target

arabinosyltransferase enzymes have been reported.[40] We reasoned that the efficiency of incorporation could vary between different isomers. Accordingly, we focused on preparing and evaluating all three possible regioisomeric azido-(*Z*,*Z*)-farnesyl phosphoryl-β-D-arabinofuranose (AzFPA) derivatives. The AzFPA regioisomers were synthesized from commercially available arabinofuranose and ribofuranose monomers. The key azide functionality was installed through nucleophilic displacement or nucleophilic epoxide opening.[41] We appended the (*Z*,*Z*)-farnesyl recognition motif and then removed the protecting groups to afford the target compounds (**Scheme 2.1**). The synthetic routes were optimized to provide access to the desired substrate surrogates for microbiological studies.

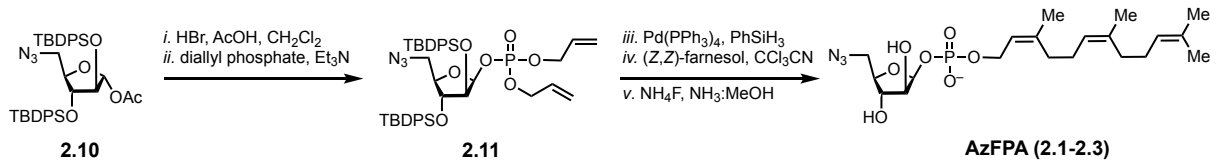

Scheme 2.1 Synthesis of AzFPA regioisomers.

2.3.3 Validation of AzFPA Probes

The collection of AzFPA isomers was evaluated for incorporation in *C. glutamicum* and *M. smegmatis* using fluorescent labeling and flow cytometry. Bacteria were cultured to mid-logarithmic phase with each AzFPA isomer, washed to remove any unassociated probe, and treated with AF647-conjugated dibenzocyclooctyne (DBCO) to install the fluorophore via a strain-promoted azide-alkyne click reaction (SPAAC).[42] At the indicated dose, a minimal effect on bacterial viability was observed due to probe treatment (**Figure 2.4**).

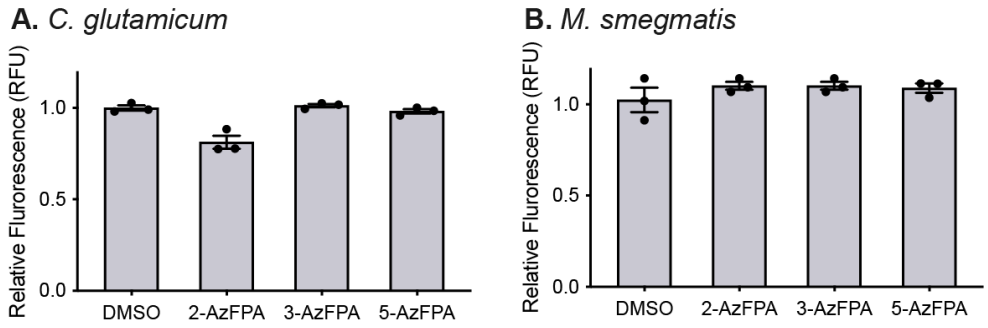

Figure 2.4 Effect of probe on cell viability. Viability of *C. glutamicum* **(A)** and *M. smegmatis* **(B)** measured via the Alamar Blue assay in the presence of 250 μM AzFPA. The Y axis depicts the relative fluorescence compared to an untreated control sample. Error bars denote the standard error of the mean of three replicate experiments.

Analysis of the fixed samples by flow cytometry revealed that cells treated with 2-AzFPA (**2.1**) and 5-AzFPA (**2.3**) could be labeled through a strained azide-alkyne click cycloaddition with a fluorophore (**Figure 2.5**).[42] The 2-azido isomer exhibited the brightest staining in *M. smegmatis*, while the 5-azido derivative led to more *C. glutamicum* labeling (**Figure 2.5 & 2.6A**). The 3-AzFPA (**2**) derivative afforded minimal staining of either species. The observed selectivity is consistent with recently disclosed structural data of the *M. smegmatis* arabinofuranosyltransferase EmbA bound to the endogenous arabinose donor DPA, determined by cryoelectron microscopy.[40] This structure indicates key hydrogen-bonding contacts occur at the C-3 hydroxyl group of DPA in the catalytic pocket. Thus, the poor incorporation of the 3-AzFPA (**2.2**) regioisomer could result from disrupted enzyme-substrate complementarity.

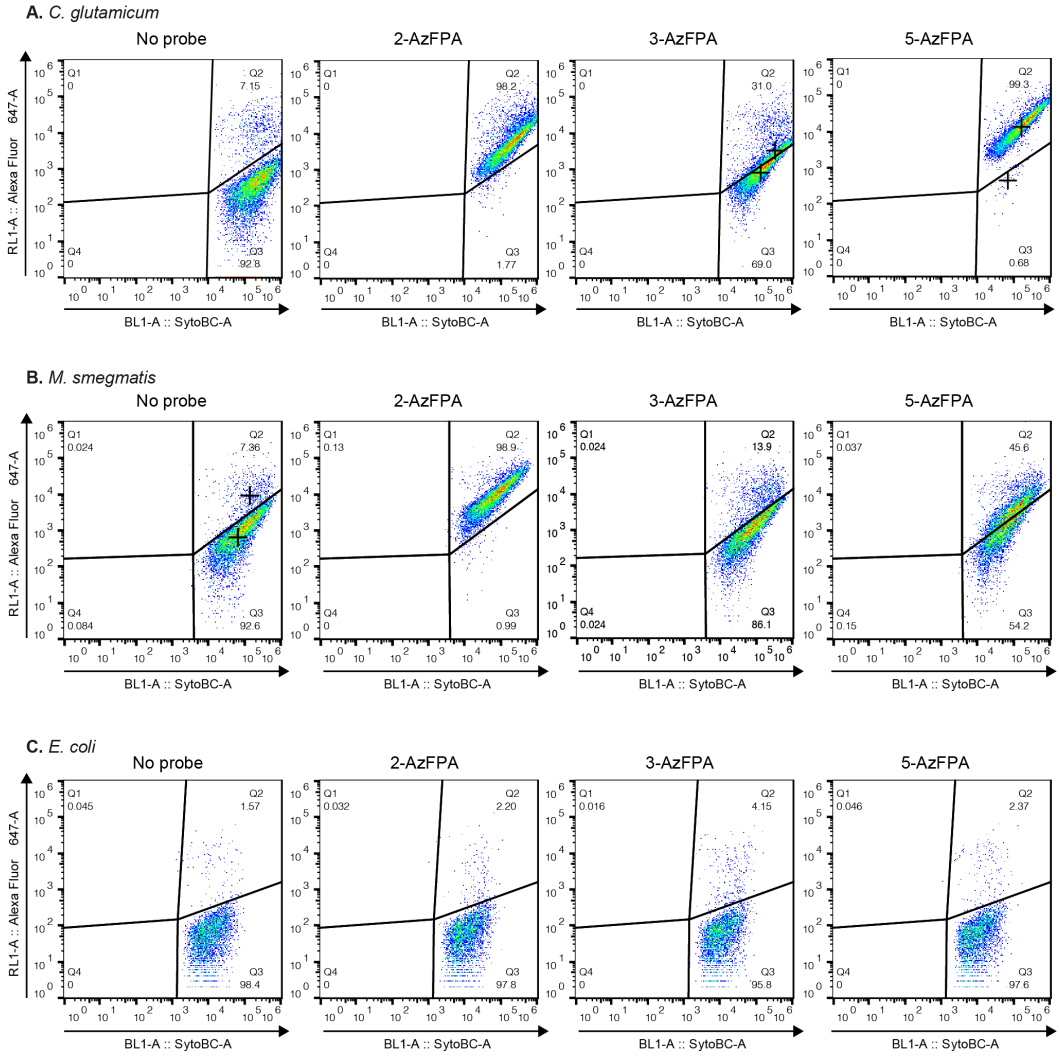

Figure 2.5 Flow cytometry data to assess cellular labeling. Representative scatter plots for *C. glutamicum* **(A)**, *M. smegmatis* **(B)** or *E. coli* **(C)** treated with DBCO-AF647 in the absence or presence of AzFPA probe (250 μM). Plots are representative of two independent experiments with three replicates for each strain and condition.

A critical finding from the experiments above is that each species prefers a different substrate isomer. This observation highlights the value of testing different isomers. We expect such preferences could enable the selective functionalization of distinct glycans within mixed microbial communities.

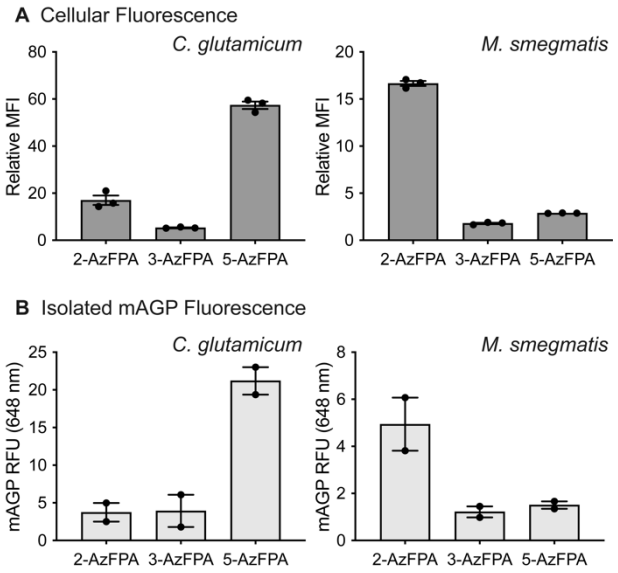

Figure 2.6 Quantification of cellular and substructure labeling. (A) Flow cytometry analysis of AzFPA (250 μM) labeled *C. glutamicum* and *M. smegmatis* treated with DBCO-AF647. Mean fluorescence intensity (MFI) was calculated using the geometric mean and plotted relative to a dye-only control. Error bars denote the standard error of the mean of three replicate experiments. **(B)** Fluorescence emission (633 nm) from isolated mAGP from AzFPA (250 μM) labeled *C. glutamicum* and *M. smegmatis* reacted with DBCO-AF647. Error bars denote the standard error of the mean of two replicate experiments.

To evaluate whether AzFPA was found in the mAGP, we isolated this polysaccharide. We applied a standard procedure to cells exposed to AzFPA and then the strained alkyne dye AF647.[43-44] The fluorescence emission of each isolated polysaccharide fraction was used as a measure of the degree of incorporation (**Figure 2.6B**). The trends in fluorescence for mAGP modification were consistent with the relative cellular fluorescence observed by flow cytometry. The reduced fluorescence intensity across mAGP samples could be attributed to the relatively harsh conditions employed in the isolation protocol. To further probe the specificity of this labeling we tested our protocol with *Escherichia coli*, an organism lacking arabinose-containing glycans, and observed no signal (**Figure 2.5C**).

2.3.4 Visualizing Incorporation of AzFPA Probes by Microscopy

We next tested our probes in confocal fluorescence microscopy to visualize the localization of the mAGP within live cells (**Figure 2.7**). As before, the bacteria were cultured in the presence of AzFPA and stained with AF647-DBCO. The relative incorporation trends determined by flow cytometry were mirrored by the intensities of fluorescence observed by microscopy; the 5-and 2-AzFPA probes afforded the most

pronounced signal in *C. glutamicum* and *M. smegmatis*, respectively. Together, these data indicate that the AzFPA probes are competent substrates for relevant glycosyltransferases and can be selectively incorporated into cell-surface glycans.

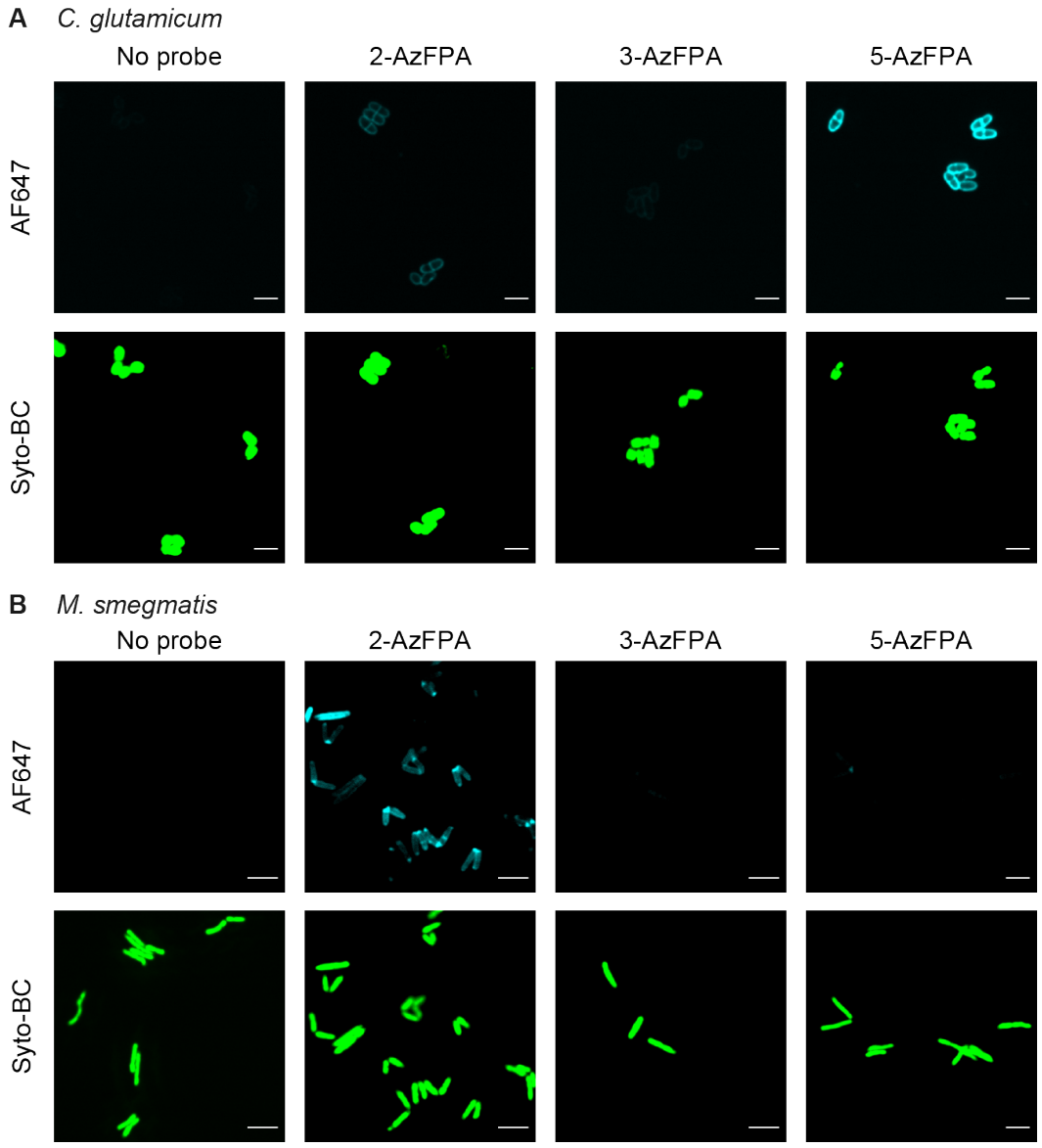

Figure 2.7 Fluorescence confocal microscopy to assess cellular labeling. Images of live AzFPA-labeled (250 μM) *C. glutamicum* **(A)** and *M. smegmatis* **(B)** reacted with DBCO-AF647. Cells were identified using nuclear stain Syto-BC. (Scale bars: 3 μm).

Having validated the utility of our platform for fluorescence-based applications, we used 2-AzFPA (**2.1**) to visualize cell wall biosynthesis. Live-cell confocal imaging of *M. smegmatis* revealed brighter staining at the poles and septum of dividing cells (**Figure 2.8A**). The spatial localization of the probe was quantified across cell length. The resultant fluorescence intensity plot was consistent with that obtained using other cell wall probes in *M. smegmatis*, namely, 7-hydroxycoumarin-3-carboxylic acid-3- amino-D-alanine (HADA), a fluorescent D-alanine analog that is incorporated into nascent peptidoglycan and a mycolic acid probe, quencher-trehalose-fluorophore (QTF).[45-46]

To better understand arabinogalactan biosynthesis, we visualized 5-AzFPA (**3**) incorporation in *C. glutamicum* (**Figure 2.8B**). Because the incorporation of our probes is contingent upon glycosyltransferase activity, we expected to observe brighter staining in areas where cell wall biosynthesis and remodeling are most active. Like *M. smegmatis, C. glutamicum* grows asymmetrically, with peptidoglycan biosynthesis occurring most rapidly at the old pole and slower at the new pole and septal plane.[47] Exposure of cells to 5-AzFPA (**2.3**) over two doubling times afforded pronounced polar and septal staining. As cells underwent multiple division cycles after five doubling times, the staining became distributed across the cell envelope. The ability of cells to continue dividing in the presence of the probes and the morphology of the bacteria indicate that no major deleterious changes to the cell envelope occur.

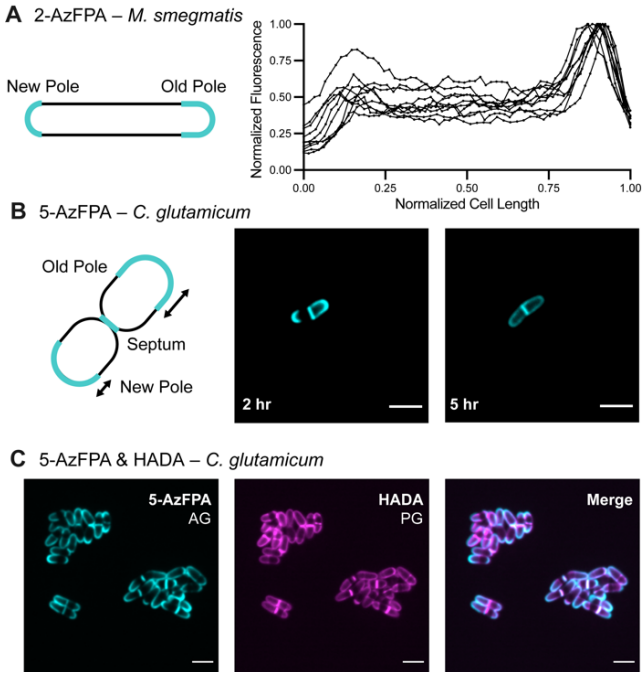

Figure 2.8 Assessment of AzFPA localization. **(A)** Localization analysis of *M. smegmatis* grown with 2-AzFPA (250 μM) and labeled with AF647 (500 μM). Each line denotes an individual cell (n=10). **(B)** Confocal fluorescence microscopy images of *C. glutamicum* grown with 5-AzFPA (250 μM) for 2 or 5 hours. **(C)** Confocal fluorescence microscopy images of *C. glutamicum* grown with 5-AzFPA (250 μM) and HADA (500 μM) for 2 hours. (Scale bars: 3 μm).

The asymmetry in the fluorescence pattern was similar to that observed previously for the peptidoglycan.[46] Because the peptidoglycan serves as the base cell wall structure to which the arabinogalactan is conjugated, we anticipated that arabinogalactan and peptidoglycan assembly would coincide. To test this hypothesis, we incubated *C. glutamicum* with 5-AzFPA (**2.3**) and HADA to visualize the mAGP and peptidoglycan simultaneously.[46] The fluorescent signals co-localized (**Figure 2.8C**). These data support our hypothesis and indicate that our probe can be used in concert with established tools to explore cell envelope assembly.

To assess the utility of our probes in a more complex environment, we examined their efficacy for visualizing bacteria in a phagocytic cell. *Mtb* infection initiates from aerosol particles that enter the lungs of a host.[48] The bacteria then recruit macrophages to the lung that phagocytose the invading pathogen.[49] To examine whether labeled bacteria could be detected, we pre-stained *M. smegmatis* with 2-AzFPA (**2.1**) then

exposed them to THP1-derived macrophages (**Figure 2.9A**). Bacteria were taken up by the phagocytic cells, and the fluorescent signal was stable (**Figure 2.9B**). These data indicate that our probes can be used to visualize D-Ara*f* residues in more complex systems, such as infection models.

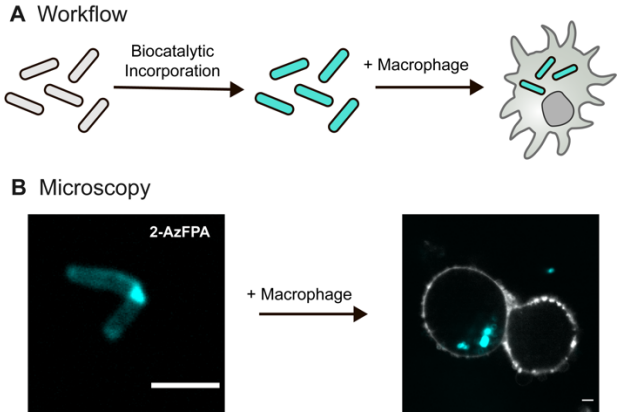

Figure 2.9 Proof-of-concept of applications in macrophage infection models. (A) Schematic of the macrophage uptake workflow. First *M. smegmatis* cells are exposed to AzFPA and then AF647. The resulting labeled cells were mixed with THP1-derived macrophages. **(B)** Confocal fluorescence microscopy images of labeled *M. smegmatis* (cyan) that had been taken up by THP1-derived macrophages (MOI: 10:1). Fluorophore-conjugated (405 nm) Wheat germ agglutinin was used to stain the plasma membrane (white) (Scale bars: 3 μm).

2.4 Conclusions

Our findings highlight the use of synthetic glycolipid donors for selective modification of cell surface glycans. Using a suite of tools for *in cellulo* D-Ara*f* functionalization, we identified probes that afford species-selective glycan modification. These findings indicate that biosynthetic incorporation can be exploited to selectively modify the glycans of different species—even when these glycans are constructed from identical building blocks. The disclosed AzFPA reagents will enable new studies, including: the facile purification of glycans; the visualization of polysaccharide trafficking, biosynthesis, and remodeling, and the identification of new protein-carbohydrate interactions at the cell interface. We anticipate that our findings will serve as a foundation for further expanding the biosynthetic incorporation platform to other monosaccharide components of complex glycans.

2.5 Experimental Details

2.5.1 Chemical Synthesis and Characterization

All chemicals were purchased from Sigma Aldrich unless otherwise stated. Dry solvents were obtained from a solvent purification system (Pure Process Technologies) under argon unless otherwise stated. DMF, MTBE and pyridine were used from sure seal bottles (Sigma Aldrich) without further purification. Triethylamine was distilled from CaH_2 just prior to use.

Analytical thin layer chromatography (TLC) was performed on EMD Millipore TM TLC silica gel 60 F254 (glass-backed). Plates were visualized under UV light and by staining with *p*-anisaldehyde stain with charring. Flash chromatography was performed on SiliCycle ® SiliaFlash ® P60 silica gel and Biotage ® Selekt using Biotage Sfär silica cartridges.

Nuclear magnetic resonance spectra were recorded on a 300 MHz spectrometer (acquired at 300 MHz for ^{1}H and 75 MHz for ^{13}C), 400 MHz spectrometer (acquired at 400 MHz for ^{1}H and 100 MHz for ^{13}C), a 500 MHz spectrometer (acquired at 500 MHz for ^{1}H and 125 MHz for ^{13}C) or a 600 MHz spectrometer (acquired at 600 MHz for ^{1}H and 151 MHz for ^{13}C). Chemical shifts are reported relative to residual solvent peaks in parts per million ($CHCl_3$: ^{1}H, 7.26, ^{13}C, 77.16; MeOH: ^{1}H, 3.31, ^{13}C, 49.00; C_6D_6: ^{1}H, 7.16, ^{13}C, 128.06). High-resolution mass spectra (HRMS) were obtained on an electrospray ionization-time of flight (ESI-TOF) mass spectrometer. All IR spectra were taken on an FT-IR Bruker Alpha II.

2.5.2 Strains and Growth Conditions

For bacterial assays, the strains employed include *Mycobacterium smegmatis mc²155*, *Corynebacterium glutamicum ATCC13032* and *Escherichia coli BL21*. *M. smegmatis* was grown in Middlebrook 7H9 broth (HiMedia, Mumbai, India) supplemented with 0.2% (w/v) dextrose, 0.2% (v/v) glycerol, 0.5% bovine serum albumin (United States Biological, Salem, MA), catalase (4 mg/liter) (Sigma-Aldrich), 15 mM sodium chloride and 0.05 % (v/v) Tween 80 in a shaking incubator at 37 °C. *C. glutamicum* was cultured in brain heart infusion (BHI) medium (BD, Franklin Lake, NJ) supplemented with 9% (w/v) sorbitol (BHIS) and *E. coli* was cultured in Luria broth (LB) liquid medium (Sigma-Aldrich) in a shaking incubator at 30 °C and 37 °C, respectively. Generally, starter cultures were incubated at the relevant temperature with shaking until saturation. Cells were then diluted into fresh media and grown to mid-logarithmic phase (determined by OD_{600} measurement on a BioMate 3S Spectrophotometer).

2.5.3 Growth Inhibition Experiments

Experiments were performed following reported procedures.[44] In brief, a saturated culture was diluted down to the desired starting OD and plated in triplicate in a Corning black 96-well plate. Probes were added at the indicated concentration from DMSO stock solutions. *M. smegmatis* were grown with shaking at 37 °C for 24 h. *C. glutamicum* were grown with shaking at 30 °C for 16 h. Alamar Blue reagent (6 µL, Invitrogen) was added to each well and the plates were incubated again for 1 h at 37 °C or 30 °C. The fluorescence emission of each well was then measured on a Tecan Infinite M1000 Pro microplate reader. Monitoring of resorufin fluorescence was achieved by exciting at 570

nm ± 5 nm and detecting at 585 nm ± 5 nm. Z-position was set to 2 mm, and the fluorimeter gain was optimized and then kept constant between plates. Data are reported in relative fluorescence units (RFU) normalized to untreated controls.

2.5.4 Flow cytometry and Fluorescence Microscopy

Cells were plated from saturated starter cultures (OD_{600} = 0.05) in a Corning black 96-well plate. *M. smegmatis* was cultured in Middlebrook 7H9 containing 0.2% (v/v) glycerol and 0.05 % Tween 80. *C. glutamicum* was cultured in BHIS medium containing 0.05 % Tween 80. *E. coli* was cultured in LB liquid medium containing 0.05 % Tween 80. AzFPA derivatives were added to the desired concentrations from 85 mM stocks in DMSO. Cultures were grown to mid-log (OD_{600} = 1.0-1.2) at 37 °C or 30 °C with shaking. Samples were immediately prepared for flow cytometry or microscopy.

Cells were pelleted for 5 min at 3000 x g. The pellets were washed with ice-cold phosphate-buffered saline (PBS) supplemented with 0.05% Tween 80 (100 µL) once. Cells were washed an additional time with PBS supplemented with 0.05% Tween 80 and 0.5% (w/v) bovine serum albumin (BSA) once then taken up in fresh 7H9 media supplemented with 0.5% Tween 80 (150 µL). AFDye™ 647 DBCO (Click Chemistry Tools #1302) was added from a 10 mM stock solution in DMSO to a final concentration of 500 µM. The samples were stained for 2 h rotating at 37 °C. When 1 h and 45 min had passed, 0.1 µL (1500X dilution) of SytoBC™ Green Fluorescent Nucleic Acid Stain (ThermoFischer #S34855) was added for a 15-min incubation period. The stained cells were pelleted for 5 min at 3000 x g. The supernatant was removed, and the pellet was washed with PBS supplemented with 0.05% Tween 80 and 0.5% (w/v) BSA twice.

For flow cytometry, stained cell pellets were taken up in 4% paraformaldehyde in PBS to be fixed at room temperature for 20 min. Following fixation, cells were pelleted then taken up in sterile PBS supplemented with 0.05% Tween 80 in flow tubes and analyzed using an Attune NxT Flow Cytometer (405 nm, 488 nm, 561 nm, and 640 nm lasers). 10,000 cells were counted at the low flow rate. Flow cytometry analysis was performed in triplicate, representative scatter plots are shown. The unstained controls were analyzed first to set gates. Data were analyzed using the FlowJo software package (FlowJo LLC). Mean fluorescence intensity was calculated using a geometric mean.

For analysis by microscopy, stained cell pellets were taken up in 7H9 supplemented with 0.5% Tween 80 (100 uL). Each sample was spotted onto a glass-bottomed microwell dish (MatTek corporation # P35G-1.5-14-C) and covered with a pre-cooled and 0.6% (w/v) agarose pad. Images were collected RPI spinning-disk confocal microscope (100x oil immersion lens, 1.4 NA). Brightness and contrast were identically adjusted with the open-source Fiji distribution of ImageJ. Images were then converted to an RGB format to preserve normalization and then assembled into panels.

2.5.5 mAGP Isolation

Cell envelope material was extracted similarly to previously described protocols.[43-44] *M. smegmatis* cultures (1 mL) were inoculated from a saturated starter culture (OD_{600} = 0.05) in Middlebrook 7H9 containing 0.05 % Tween 80. AzFPA derivatives were added from DMSO stock solutions to the desired concentrations (250 μM), and the cultures were grown to saturation at 37 °C with shaking. *C. glutamicum* was cultured in BHIS medium (1 mL) in a shaking incubator at 30 °C. Cells were pelleted for 5 min at 3000 x g, normalizing across samples by OD. Cells were washed and reacted with AFDye™ 647

DBCO (Click Chemistry Tools #1302) as described above. After staining, cell pellets were resuspended in lysis buffer (2% Triton X-100 in PBS) and disrupted by sonication (6 x 20 s separated by 2 min off intervals on ice). The cell lysate was then pelleted by centrifugation at 15 000 g for 15 min. The supernatant was removed and the pellet was taken up in 2% SDS in PBS and heated to 95 °C for 1 hr before pelleting as above and discarding the supernatant. The pellet was then washed with water, 80% acetone/water and then acetone. After isolation, the mAGP complex was suspended in 2% SDS in PBS and the fluorescence was detected on a Tecan M1000 plate reader. Plates were shaken for 3 s (6 mm, orbital) immediately before the well fluorescence was read (λ_{ex} = 648 nm ±5, λ_{em} = 671 ± 5 nm).

2.5.6 Uptake into THP-1 Cells

The monocyte cell line THP-1 (ATCC TIB-202) was cultured in ATCC RPMI-1640 medium supplemented with 10% fetal bovine serum, 0.05 mM 2-mercaptoethanol and P/S in a 5% CO_2 humidified atmosphere. Monocyte cells were differentiated into macrophages by induction with phorbol-12-myristate-13-acetated (PMA, Sigma-Aldrich). Cells were seeded in six-well cell non-treated cell culture plates in complete RPMI with 100 ng/mL PMA. After 48 h of PMA stimulation, cells were adherent to the plate. They were washed with PBS and allowed to recover in complete RPMI media for another 24 h before using THP-1-derived macrophages for infection experiment. *M. smegmatis* cells were added at the indicated multiplicity of infection (MOI) and the co-cultures were incubated at 37 °C with 5% CO_2 for 1 h. Following infection, samples were incubated with 1.5 μg/mL fluorophore conjugated wheat germ agglutinin (CF®405S WGA, Biotium) on ice for 30 min. Macrophages were then washed PBS with 1% (w/v)

BSA in PBS three times and spotted onto a glass-bottomed microwell dish. Images were collected RPI spinning-disk confocal microscope (100x oil immersion lens, 1.4 NA). Brightness and contrast were identically adjusted with the open-source Fiji distribution of ImageJ. Images were then converted to an RGB format to preserve normalization and then assembled into panels.

2.6 Acknowledgments

The authors thank H. L. Hodges, R. L. McPherson, C. M. Jarvis, C. R. Isabella and K. I. Taylor for helpful scientific discussions as well as R. L. McPherson, S. D. Brucks and S. M. Smelyansky for their assistance in reviewing the manuscript. The authors thank the NIH-NIAID (Al-126592 to L.L.K.), the NIH Common Fund (UO1GM125288 to L.L.K.), the NIH (R01A1022553 and R01AR073252 to B.D.B.) NIH-NIGMS (F32 GM142288) to D.E.K.), and the NSERC (PGSD Fellowship for V.M.M.) for financial support.

2.7 References

1. Boutureira, O.; Bernardes, G. J., Advances in chemical protein modification. *Chem Rev* **2015,** *115* (5), 2174-95.

2. Gunnoo, S. B.; Madder, A., Bioconjugation - using selective chemistry to enhance the properties of proteins and peptides as therapeutics and carriers. *Org Biomol Chem* **2016,** *14* (34), 8002-13.

3. Roy, S.; Cha, J. N.; Goodwin, A. P., Nongenetic Bioconjugation Strategies for Modifying Cell Membranes and Membrane Proteins: A Review. *Bioconjug Chem* **2020,** *31* (11), 2465-2475.

4. Gilormini, P. A.; Batt, A. R.; Pratt, M. R.; Biot, C., Asking more from metabolic oligosaccharide engineering. *Chem Sci* **2018,** *9* (39), 7585-7595.

5. Cioce, A.; Bineva-Todd, G.; Agbay, A. J.; Choi, J.; Wood, T. M.; Debets, M. F.; Browne, W. M.; Douglas, H. L.; Roustan, C.; Tastan, O.; Kjaer, S.; Bush, J. T.; Bertozzi, C. R.; Schumann, B., Metabolic Engineering Optimizes Bioorthogonal Glycan Labeling in Living Cells. *ChemRxiv* **2021**.

6. Dube, D. H.; Bertozzi, C. R., Metabolic oligosaccharide engineering as a tool for glycobiology. *Curr Opin Chem Biol* **2003,** *7* (5), 616-25.

7. Kayser, H.; Ats, C.; Lehmann, J.; Reutter, W., New amino sugar analogues are incorporated at different rates into glycoproteins of mouse organs. *Experientia* **1993,** *49* (10), 885-7.

8. Boyce, M.; Carrico, I. S.; Ganguli, A. S.; Yu, S. H.; Hangauer, M. J.; Hubbard, S. C.; Kohler, J. J.; Bertozzi, C. R., Metabolic cross-talk allows labeling of O-linked beta-N-acetylglucosamine-modified proteins via the N-acetylgalactosamine salvage pathway. *Proc Natl Acad Sci U S A* **2011,** *108* (8), 3141-6.

9. Qin, W.; Qin, K.; Fan, X.; Peng, L.; Hong, W.; Zhu, Y.; Lv, P.; Du, Y.; Huang, R.; Han, M.; Cheng, B.; Liu, Y.; Zhou, W.; Wang, C.; Chen, X., Artificial Cysteine S-Glycosylation Induced by Per-O-Acetylated Unnatural Monosaccharides during Metabolic Glycan Labeling. *Angewandte Chemie International Edition* **2018,** *57* (7), 1817-1820.

10. Andolina, G.; Wei, R.; Liu, H.; Zhang, Q.; Yang, X.; Cao, H.; Chen, S.; Yan, A.; David Li, X.; Li, X., Metabolic Labeling of Pseudaminic Acid-Containing Glycans on Bacterial Surfaces. *ACS Chem. Biol.* **2018,** *13* (10), 3030-3037.

11. Clark, E. L.; Emmadi, M.; Krupp, K. L.; Podilapu, A. R.; Helble, J. D.; Kulkarni, S. S.; Dube, D. H., Development of Rare Bacterial Monosaccharide Analogs for Metabolic Glycan Labeling in Pathogenic Bacteria. *ACS Chemical Biology* **2016,** *11* (12), 3365-3373.

12. Demeester, K. E.; Liang, H.; Jensen, M. R.; Jones, Z. S.; Ambrosio, E. A. D.; Scinto, S. L.; Zhou, J.; Grimes, C. L.; D'Ambrosio, E. A.; Scinto, S. L.; Zhou, J.; Grimes, C. L., Synthesis of Functionalized N-Acetyl Muramic Acids to Probe Bacterial Cell Wall Recycling and Biosynthesis. *J. Am. Chem. Soc.* **2018,** *140* (30), 9458-9465.

13. Liang, H.; DeMeester, K. E.; Hou, C. W.; Parent, M. A.; Caplan, J. L.; Grimes, C. L., Metabolic labelling of the carbohydrate core in bacterial peptidoglycan and its applications. *Nat. Commun.* **2017,** *8*, 1-11.

14. Mas Pons, J.; Dumont, A.; Sautejeau, G.; Fugier, E.; Baron, A.; Dukan, S.; Vauzeilles, B., Identification of Living Legionella pneumophila Using Species-Specific Metabolic Lipopolysaccharide Labeling. *Angewandte Chemie International Edition* **2014,** *53* (5), 1275-1278.

15. Herget, S.; Toukach, P. V.; Ranzinger, R.; Hull, W. E.; Knirel, Y. A.; von der Lieth, C.-W., Statistical analysis of the Bacterial Carbohydrate Structure Data Base (BCSDB): Characteristics and diversity of bacterial carbohydrates in comparison with mammalian glycans. *BMC Struct. Biol.* **2008,** *8*, 35-35.

16. Imperiali, B., Bacterial carbohydrate diversity - a Brave New World. *Curr Opin Chem Biol* **2019,** *53*, 1-8.

17. Kolbe, K.; Möckl, L.; Sohst, V.; Brandenburg, J.; Engel, R.; Malm, S.; Bräuchle, C.; Holst, O.; Lindhorst, T. K.; Reiling, N., Azido Pentoses: A New Tool To Efficiently Label Mycobacterium tuberculosis Clinical Isolates. *Chembiochem* **2017,** *18* (13), 1172-1176.

18. Fraenkel, D. G.; Vinopal, R. T., Carbohydrate Metabolism in Bacteria. *Annu Rev Microbiology* **1973,** *27* (1), 69-100.

19. Tommasone, S.; Allabush, F.; Tagger, Y. K.; Norman, J.; Kopf, M.; Tucker, J. H. R.; Mendes, P. M., The challenges of glycan recognition with natural and artificial receptors. *Chem Soc Rev* **2019,** *48* (22), 5488-5505.

20. Alderwick, L. J.; Seidel, M.; Sahm, H.; Besra, G. S.; Eggeling, L., Identification of a novel arabinofuranosyltransferase (AftA) involved in cell wall arabinan biosynthesis in Mycobacterium tuberculosis. *J. Biol. Chem.* **2006,** *281* (23), 15653-61.

21. Seidel, M.; Alderwick, L. J.; Birch, H. L.; Sahm, H.; Eggeling, L.; Besra, G. S., Identification of a novel arabinofuranosyltransferase AftB involved in a terminal step of cell wall arabinan biosynthesis in Corynebacterianeae, such as Corynebacterium glutamicum and Mycobacterium tuberculosis. *J. Biol. Chem.* **2007,** *282* (20), 14729-40.

22. Skovierova, H.; Larrouy-Maumus, G.; Zhang, J.; Kaur, D.; Barilone, N.; Kordulakova, J.; Gilleron, M.; Guadagnini, S.; Belanova, M.; Prevost, M. C.; Gicquel, B.; Puzo, G.; Chatterjee, D.; Brennan, P. J.; Nigou, J.; Jackson, M., AftD, a novel essential arabinofuranosyltransferase from mycobacteria. *Glycobiology* **2009,** *19* (11), 1235-47.

23. Zhang, J.; Angala, S. K.; Pramanik, P. K.; Li, K.; Crick, D. C.; Liav, A.; Jozwiak, A.; Swiezewska, E.; Jackson, M.; Chatterjee, D., Reconstitution of functional mycobacterial arabinosyltransferase AftC proteoliposome and assessment of decaprenylphosphorylarabinose analogues as arabinofuranosyl donors. *ACS Chem. Biol.* **2011,** *6* (8), 819-28.

24. Jankute, M.; Alderwick, L. J.; Moorey, A. R.; Joe, M.; Gurcha, S. S.; Eggeling, L.; Lowary, T. L.; Dell, A.; Pang, P. C.; Yang, T.; Haslam, S.; Besra, G. S., The singular Corynebacterium glutamicum Emb arabinofuranosyltransferase polymerises the alpha(1-->5) arabinan backbone in the early stages of cell wall arabinan biosynthesis. *Cell Surf* **2018,** *2*, 38-53.

25. Kotake, T.; Yamanashi, Y.; Imaizumi, C.; Tsumuraya, Y., Metabolism of L-arabinose in plants. *J Plant Res* **2016,** *129* (5), 781-792.

26. Wolucka, B. A., Biosynthesis of D-arabinose in mycobacteria – a novel bacterial pathway with implications for antimycobacterial therapy. *FEBS J.* **2008,** *275* (11), 2691-2711.

27. Organization, W. H., Global Tuberculosis Report 2019. *World Health Organization* **2019**.

28. Sharma, N. C.; Efstratiou, A.; Mokrousov, I.; Mutreja, A.; Das, B.; Ramamurthy, T., Diphtheria. *Nat Rev Dis Primers* **2019,** *5* (1), 81.

29. Pinheiro, R. O.; de Souza Salles, J.; Sarno, E. N.; Sampaio, E. P., Mycobacterium leprae-host-cell interactions and genetic determinants in leprosy: an overview. *Future Microbiol* **2011,** *6* (2), 217-30.

30. Alderwick, L. J.; Harrison, J.; Lloyd, G. S.; Birch, H. L., The Mycobacterial Cell Wall--Peptidoglycan and Arabinogalactan. *Cold Spring Harb Perspect Med* **2015,** *5* (8), a021113.

31. Takayama, K.; Kilburn, J. O., Inhibition of synthesis of arabinogalactan by ethambutol in Mycobacterium smegmatis. *Antimicrob. Agents Ch.* **1989,** *33* (9), 1493-1499.

32. Mikušová, K.; Huang, H.; Yagi, T.; Holsters, M.; Vereecke, D.; D'Haeze, W.; Scherman, M. S.; Brennan, P. J.; McNeil, M. R.; Crick, D. C., Decaprenylphosphoryl Arabinofuranose, the Donor of the d-Arabinofuranosyl Residues of Mycobacterial Arabinan, Is Formed via a Two-Step Epimerization of Decaprenylphosphoryl Ribose. *J. Bacteriol.* **2005,** *187* (23), 8020-8025.

33. Kolbe, K.; Mockl, L.; Sohst, V.; Brandenburg, J.; Engel, R.; Malm, S.; Brauchle, C.; Holst, O.; Lindhorst, T. K.; Reiling, N., Azido Pentoses: A New Tool To Efficiently Label Mycobacterium tuberculosis Clinical Isolates. *Chembiochem* **2017,** *18* (13), 1172-1176.

34. Lairson, L. L.; Henrissat, B.; Davies, G. J.; Withers, S. G., Glycosyltransferases: structures, functions, and mechanisms. *Annu Rev Biochem* **2008,** *77*, 521-55.

35. Angala, S. K.; Joe, M.; McNeil, M. R.; Liav, A.; Lowary, T. L.; Jackson, M., Use of Synthetic Glycolipids to Probe the Number and Position of Arabinan Chains on Mycobacterial Arabinogalactan. *ACS Chem Biol* **2021,** *16* (1), 20-26.

36. Grover, S.; Alderwick, L. J.; Mishra, A. K.; Krumbach, K.; Marienhagen, J.; Eggeling, L.; Bhatt, A.; Besra, G. S., Benzothiazinones mediate killing of Corynebacterineae by blocking decaprenyl phosphate recycling involved in cell wall biosynthesis. *J. Biol. Chem.* **2014,** *289* (9), 6177-87.

37. Makarov, V.; Manina, G.; Mikusova, K.; Möllmann, U.; Ryabova, O.; Saint-Joanis, B.; Dhar, N.; Pasca, M. R.; Buroni, S.; Lucarelli, A. P.; Milano, A.; De Rossi, E.; Belanova, M.; Bobovska, A.; Dianiskova, P.; Kordulakova, J.; Sala, C.; Fullam, E.; Schneider, P.; McKinney, J. D.; Brodin, P.; Christophe, T.; Waddell, S.; Butcher, P.; Albrethsen, J.; Rosenkrands, I.; Brosch, R.; Nandi, V.; Bharath, S.; Gaonkar, S.; Shandil, R. K.; Balasubramanian, V.; Balganesh, T.; Tyagi, S.; Grosset, J.; Riccardi, G.; Cole, S. T., Benzothiazinones Kill Mycobacterium tuberculosis by Blocking Arabinan Synthesis. *Science* **2009,** *324* (5928), 801-804.

38. Campbell, J.; Singh, A. K.; Swoboda, J. G.; Gilmore, M. S.; Wilkinson, B. J.; Walker, S., An Antibiotic That Inhibits a Late Step in Wall Teichoic Acid Biosynthesis Induces the Cell Wall Stress Stimulon in Staphylococcus aureus. *Antimicrob. Agents Ch.* **2012,** *56* (4), 1810-1820.

39. Kaur, D.; Brennan, P. J.; Crick, D. C., Decaprenyl Diphosphate Synthesis in Mycobacterium tuberculosis. *J. Bacteriol.* **2004,** *186* (22), 7564-7570.

40. Zhang, L.; Zhao, Y.; Gao, Y.; Wu, L.; Gao, R.; Zhang, Q.; Wang, Y.; Wu, C.; Wang, M.; Zhu, Y.; Zhang, B.; Bi, L.; Zhang, L.; Yang, H.; Guddat, L.; Xu, W.; Wang, Q.; Li, J.; Besra, G. S.; Rao, Z., Structures of cell wall arabinosyltransferases with ethambutol. *Science* **2020,** *368* (6496), 1211-1219.

41. Kraft, M. B.; Martinez Farias, M. A.; Kiessling, L. L., Synthesis of lipid-linked arabinofuranose donors for glycosyltransferases. *J. Org. Chem.* **2013,** *78* (5), 2128-33.

42. Agard, N. J.; Prescher, J. A.; Bertozzi, C. R., A Strain-Promoted [3+2] Azide-Alkyne Cycloaddition for Covalent Modification of Biomolecules in Living Systems. *J Am Chem Soc* **2004,** *126*, 15046-15047.

43. Besra, G. S.; Khoo, K.; McNeil, M. R.; Dell, A.; Morris, H. R.; Brennan, P. J., A New Interpretation of the Structure of the Mycolyl-Arabinogalactan Complex of *Mycobacterium tuberculosis* As Revealed through Characterization of Oligoglycosylalditol Fragments by Fast-Aton Bombardment Mass Spectrometry and 1H Nuclear Magnetic Resonance Spectroscopy. *Biochemistry* **1995,** *34*, 4257-4266.

44. Calabretta, P. J.; Hodges, H. L.; Kraft, M. B.; Marando, V. M.; Kiessling, L. L., Bacterial Cell Wall Modification with a Glycolipid Substrate. *J Am Chem Soc* **2019,** *141* (23), 9262-9272.

45. Hodges, H. L.; Brown, R. A.; Crooks, J. A.; Weibel, D. B.; Kiessling, L. L., Imaging mycobacterial growth and division with a fluorogenic probe. *Proc Natl Acad Sci U S A* **2018,** *115* (20), 5271-5276.

46. Kuru, E.; Hughes, H. V.; Brown, P. J.; Hall, E.; Tekkam, S.; Cava, F.; de Pedro, M. A.; Brun, Y. V.; VanNieuwenhze, M. S., In Situ probing of newly synthesized peptidoglycan in live bacteria with fluorescent D-amino acids. *Angew Chem Int Ed Engl* **2012,** *51* (50), 12519-23.

47. Kieser, K. J.; Rubin, E. J., How sisters grow apart: mycobacterial growth and division. *Nat Rev Microbiol* **2014,** *12* (8), 550-62.

48. Cambier, C. J.; Falkow, S.; Ramakrishnan, L., Host evasion and exploitation schemes of Mycobacterium tuberculosis. *Cell* **2014,** *159* (7), 1497-509.

49. Queval, C. J.; Brosch, R.; Simeone, R., The Macrophage: A Disputed Fortress in the Battle against Mycobacterium tuberculosis. *Front Microbiol* **2017,** *8*, 2284.

Chapter 3: Applications Enabled by AzFPA Probes

Sections reproduced with permission from:
Marando VM, Kim DE, Kiessling LL. Biosynthetic incorporation for visualizing bacterial glycans. *Methods in Enzymology*. **2022**, 665, 135-151.

Al-Jourani O, Benedict S, Ross, J, Layton A, van der Peet P, Marando VM, Bailey NP, Heunis T, Manion J, Mensitieri F, Franklin A, Abellon-Ruiz J, Oram SL, Parsons L, Cartmell A, Wright GSA, Baslé A, Trost M, Henrissat B, Munoz-Munoz J, Hirt RP, Kiessling LL, Lovering A, Williams SJ, Lowe EC, Moynihan PJ, Identification of D-arabinan-degrading enzymes in mycobacteria. *Nature Communications*. **2023**, 14, 2233.

Contributions:
Compounds used in this study were synthesized by Daria E. Kim. Enzymatic assays were performed by Victoria M. Marando, using enzymes provided by the Lowe and Moynihan groups. *Mtb* experiments were performed by Stephanie R. Smelyansky. Experiments in *C. glutamicum* were performed by Victoria M. Marando. *C. glutamicum Δpks13* cells were prepared by Heather L. Hodges. Research designed by Victoria M. Marando, Stephanie R. Smelyansky and Laura L. Kiessling.

3.1 Abstract

Cell-surface glycans act as cellular identifications and are central to many biological processes. Reactive functional groups can be introduced into glycans through metabolic oligosaccharide engineering, which involves the generation of substituted nucleotide-sugar building blocks that can be processed intracellularly and incorporated into native polysaccharides. In contrast, lipid-linked building blocks, which are also used in glycan biosynthesis, have the advantage that they can be delivered directly to glycosyltransferases to function as surrogate substrates extracellularly in a late-stage biosynthetic step. This process, termed "biosynthetic incorporation", takes advantage of cell-surface associated glycosyltransferases to install non-natural substrates in a substructure-specific manner. We have developed probes that use this strategy to label arabinofuranose-containing glycans on the surface of mycobacterial cells. Such probes have enabled a wide range of studies including the development of fluorescence-based *in vitro* arabinan assays, visualization of arabinan in *Mtb,* and the use of these compounds to perturb arabinan structure *in cellulo*. These probes have proved useful to the broader community and for research directions being explored within the Kiessling group.

3.2 Introduction

Bacterial cell surface glycans serve as the first point of contact between infected hosts and invading pathogens and can confer numerous protective advantages onto the bacterium, ranging from providing a physical barrier against antimicrobial agents, to facilitating safe entry and sequestration within host cells.[1-3] A molecular-level understanding of glycan structure and function is critical for developing new strategies to combat microbial pathogens.[4] However, the elucidation of the functional roles of bacterial glycans has been historically challenging.[5] A major impediment has been the difficulty of labeling specific glycans via traditional methods.

Incorporating non-natural carbohydrate substrates into mammalian cell surface glycans via metabolic incorporation facilitates the introduction of reporter groups, and as a technique, has been transformative for the field of chemical glycobiology.[6-7] Such probes have many impactful applications, including therapeutic delivery to specific cells and substructure tracking.[8-10] Metabolic incorporation strategies in mammalian cells are continuously undergoing development and optimization,[11-13] but the dissimilarities in mammalian and bacterial glycan metabolism limits simple translation of metabolic incorporation.[14] Specifically, bacteria employ a vastly more diverse set of carbohydrate monomer building blocks and use unique pathways to acquire, metabolize, and monosaccharide components and biosynthesize glycans.[15-17] As a result, metabolic incorporation strategies may result in bacteria funneling non-native carbohydrate probes through a variety of metabolic pathways, leading to non-specific and off-target labeling.

To circumvent the challenges associated with intracellular processing, we have employed modified lipid-linked probes as labeling tools. The direct processing of such

non-natural substrates by cellular enzymes is termed “biosynthetic incorporation”.[18] The application of glycolipid substrates in biosynthetic incorporation is advantageous as cell surface-associated glycosyltransferases can directly use them as substrates. We demonstrated that a synthetic donor, with a truncated lipid, can serve as a viable substrate for GT-Cs in the processing of exogenous arabinose into bacteria from the suborder *Corynebacterianeae*, which contains several human pathogens, including *Mycobacterium leprae*, *Corynebacterium diphtheriae*, and *Mycobacterium tuberculosis (Mtb)*.[18] We anticipated that this biosynthetic incorporation strategy would enable a wide range of novel experiments following the validation of this truncated lipid as a successful donor.

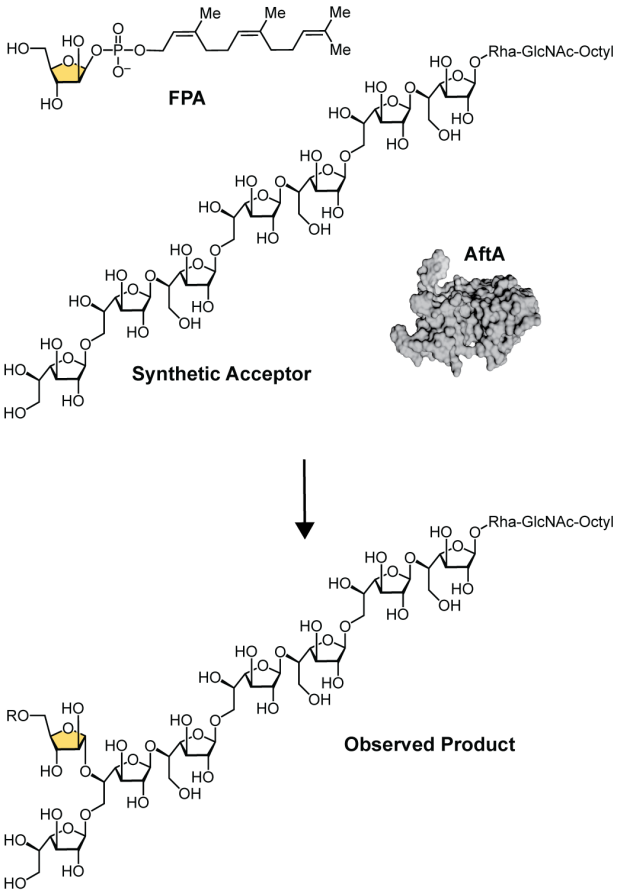

Figure 3.1 Synthetic donor and acceptor substrates used to study AftA activity *in vitro*. FPA as a synthetic arabinose donor substrate, one of the synthetic acceptors used in the described study and product observed indicating the conserved installation of arabinose at residue 6.

The utility of this probe has already been demonstrated by rapid use by other research groups. Upon disclosure of our first biosynthetic incorporation probe, (*Z*,*Z*)-farnesyl phosphoryl-β-D-arabinofuranose (FPA), the Lowary and Jackson groups applied this compound for *in vitro* analysis of arabinogalactan biosynthesis.[19] In this work, they used membrane preparations from *Mycobacterium smegmatis* overexpressing an essential α-(1→5)-arabinosyltransferase, AftA,[20] FPA as an

arabinose donor,[18] and a series of synthetic galactan acceptors[21] (**Figure 3.1**). Using this system, they identified a single priming arabinose residue at the 6th galactofuranosyl residue of the galactan acceptors, regardless of their length. This discovery provides new insight into the structure of the arabinogalactan in mycobacteria. In particular, the authors highlight the conclusion that only one arabinan chain may be present on each AG unit linked to the peptidoglycan, which underlines the value of AftA as a target for the development of novel antimycobacterial therapeutics. This experimental setup would not have been accessible without the use of FPA as a soluble, synthetically accessible donor substrate. Additionally, future studies using these probes will provide opportunities to investigate additional arabinosyltransferases with similar methods (**Table 3.1**).

Table 3.1 Arabinosyltransferases involved in mAGP biosynthesis and the linkages they form.

Enzyme	Linkage Formed
AftA	α 1-5
AftB	β 1-2
AftC	α 1-3
AftD	α 1-5
Emb	α 1-5

Building on our initial FPA probes, we next validated that a biosynthetic incorporation approach can be used to site-selectively introduce non-natural D-arabinofuranose (D-Ara*f)* derivatives bearing azide handles into cell surface glycans (see **Chapter 2**).[22-23] These probes have already been used to shed light on localization of arabinan biosynthesis in *Corynebacterium glutamicum* and *M. smegmatis*. Using confocal microscopy, we observed probe incorporation selectively into the poles and septa, as well as characteristic asymmetric growth. Though the biosynthesis of other cell wall components had previously been visualized, this was the first direct observation of arabinan biosynthesis. Herein, we describe select applications of our azido-arabinose biosynthetic incorporation probes (AzFPA) for *in vitro* and *in cellulo* assays. These

AzFPA probes have allowed for the development of novel enzyme activity assays and investigations into arabinan biosynthesis in a challenging pathogenic organism. Additionally, by installing non-natural functionality, these probes enable structural perturbations and investigation into resulting phenotypic outcomes.

3.3 Results & Discussion

3.3.1 Use of AzFPA for *In Vitro* Assay Development

In a collaborative effort led by the Lowe and Moynihan groups, new arabinofuranosidases were identified by leveraging the diverse carbohydrate-degrading enzymes in the human gut microbiome.[24] The human gut microbiota is responsible for degrading dietary plant polysaccharides and host and microbial glycans. These microorganisms, dominated by *Bacteroidetes*, are among the richest known organisms in terms of the diversity of complex carbohydrate-degrading enzymes.[25] Carbohydrate utilization by *Bacteroidetes* spp. is typically mediated by genes that are organized into polysaccharide utilization loci (PUL), which can be induced upon exposure of the

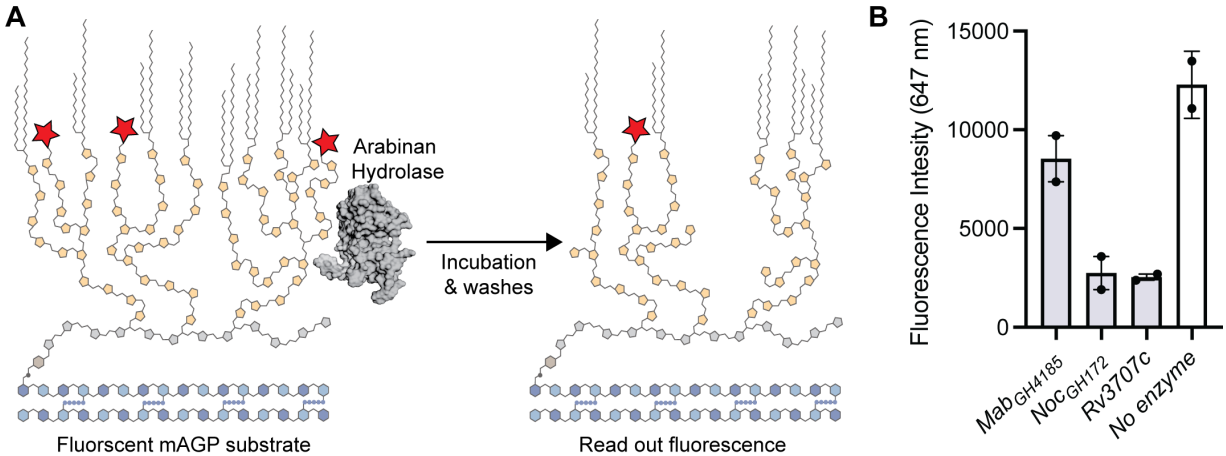

Figure 3.2 Fluorescence release assay to test arabinan hydrolase activity on mAGP. (A) Cartoon schematic of assay workflow. Labeled mAGP is incubated with enzymes followed by three washes to remove any released material. Fluorescence of the resultant mAGP fraction can then be measured to assess enzyme activity on the labeled substrate. **(B)** Fluorescence intensity measured using this activity assay for select acid-fast enzymes. Error bars denote the standard error of the mean of two replicate experiments.

bacterium to a given carbohydrate.[26-30] Arabinogalactan from *M. smegmatis* was used as the sole carbon source for the growth of a panel of 14 *Bacteroidetes* species. Using this approach, the Lowe and Moynihan groups identified and characterized both endo- and exo- acting glycosidases that act on this substrate, including new exo-D-arabinofuranosidases from the DUF2961 family (GH172), and a novel family of glycoside hydrolases (DUF4185) which display endo-D-arabinofuranase activity, the first known endo-D-arabinofuranases.[24]

With these enzymes in hand, initial assays were performed using purified arabinogalactan (AG) and LAM. Products were identified by ion chromatography with pulsed amperometric detection (IC-PAD) analysis. Though informative, these assays are time-intensive and low-throughput. It was observed that most enzymes displayed higher activity against the AG than the LAM. Purified AG lacks key structures present in the intact mAGP complex, specifically the mycolic acids and peptidoglycan. We therefore wanted to assess arabinofuranase activity in a more relevant context. Using biosynthetic incorporation with 5-AzFPA, the mAGP was labeled with an azide *in cellulo* and then conjugated with DBCO-AF647 via strain-promoted azide-alkyne cycloaddition (SPAAC). Labeled mAGP was then isolated as previously described.[22, 31] This material allowed for a fluorescence-based assay for hydrolase activity (**Figure 3.2A**). The assay was initially validated with three of the discovered enzymes representing two classes: those that did not hydrolyze isolated AG (Mab_{GH4185} and Rv3707c) and those that did ($GH172_{Noc}$). It was observed that both Mab_{GH4185} and Rv3707c released fluorescently labeled material from cell walls, in contrast with what was observed using isolated AG (**Figure 3.2B**). Additionally, $GH172_{Noc}$ led to release of fluorescent products, supporting the conclusion that both sets of enzymes can cleave AG in the context of the intact mAGP complex. We

anticipate that due to the fluorescent readout enabled by AzFPA labeling, this assay could be easily scaled up for high-throughput analysis of newly discovered enzymes.

3.3.2 Enablement of AzFPA Labeling in *Mtb*

Initial studies using FPA and AzFPA probes were performed exclusively in *C. glutamicum* and *M. smegmatis*, fast-growing, non-pathogenic model organisms of *Mtb*.[18, 22, 32] Though these models are useful for validation, we hypothesized that our optimized staining protocols could be applied to *Mtb* itself to label and study the AG directly. Applying these probes to *Mtb* required additional optimization as this species is very slow growing, sensitive to growth conditions (media components and culture size), and has a thicker outer lipid layer that dyes can non-specifically associate with.[32] Upon optimization, we performed flow cytometry to investigate regioisomeric preferences of staining in *Mtb* (**Figure 3.3A**). We found that 5-AzFPA gave the brightest staining. As with our previous study in other organisms, we observed that staining is dependent on the position of the azide substitution, corroborating that these probes are labeling cells via enzymatic processing rather than a lipid-mediated interaction. Next, due to the small size of *Mtb*, we used super-resolution structured illumination microscopy (SIM) for increased resolution,[33] to observe localization of probe incorporation. We found that staining was most pronounced at the poles, sites of active cell wall

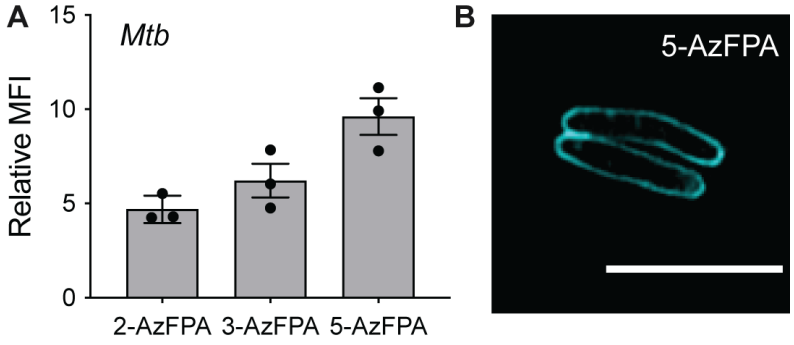

Figure 3.3 AzFPA can be used to label *Mtb*. (A) Flow cytometry analysis of AzFPA (125 μM) *Mtb* treated with DBCO-AF647. Mean fluorescence intensity (MFI) was calculated using the geometric mean and plotted relative to a dye-only control. Error bars denote the standard error of the mean of three replicate experiments **(B)** Structured illumination microscopy (SIM) images of *Mtb* grown with 5-AzFPA (25 μM). (Scale bars: 3 μm).

biosynthesis, consistent with what we had observed in model organisms (**Figure 3.3B**). Notably, the concentration of the probe used was decreased in these experiments as high doses resulted in phenotypic abnormalities (see **section 3.3.3**). This data demonstrates the applications of our probes in a new, more challenging system and will enable future studies using AzFPA in *Mtb*. This also represents the first validation of biosynthetic incorporation as a viable strategy in *Mtb* and highlights the potential for new probes targeting distinct monosaccharides to also be tested in this organism. We envision AzFPA and similar biosynthetic incorporation probes being useful to investigate *Mtb* cell wall remodeling within models of infections in relevant cell types, such as macrophages.

3.3.3 Use of AzFPA to Perturb mAGP Structure *In Cellulo*

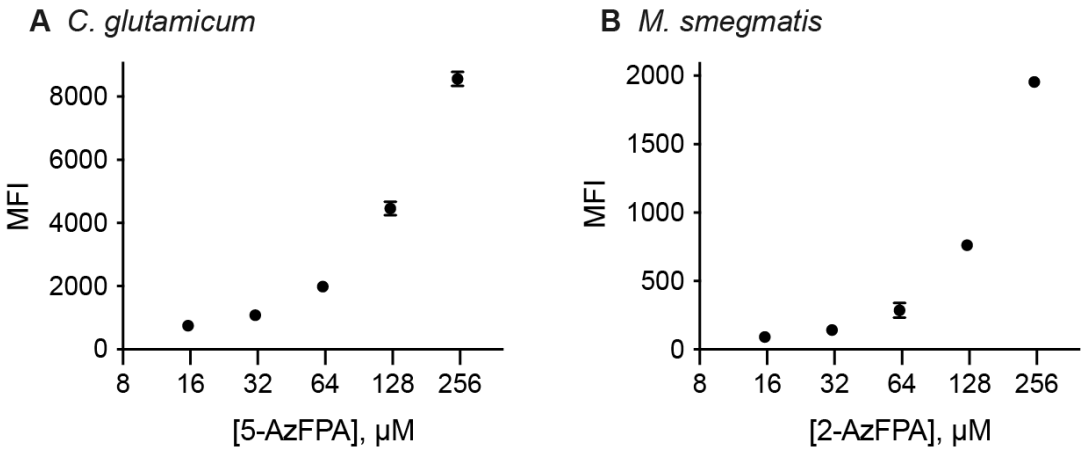

Figure 3.4 AzFPA staining is dose-dependent. Flow cytometry quantification of staining for *C. glutamicum* **(A)**, *M. smegmatis* **(B)** treated with DBCO-AF647 in the presence of increasing concentrations of AzFPA probe. MFI was calculated using the geometric mean. Error bars denote the standard error of the mean of three replicate experiments. Figure reproduced with permission from reference [22].

When performing initial studies with AzFPA probes, we optimized our protocols to stain cells in a manner that would minimize the perturbing effects that introducing non-natural groups may trigger.[22] We first found that probe incorporation was dose-

dependent (**Figure 3.4**). We then optimized growth conditions and probe concentration to ensure that we observed minimal effects on overall cell viability and cell morphology compared to unstained wild-type controls. However, we found that at higher concentrations of 5-AzFPA (500 μM and greater), the increasing levels of azide incorporation led to decreased cell viability in *C. glutamicum* (**Figure 3.5A**). As a control, we tested viability after a similar treatment with 3-AzFPA, a probe that we have shown does not incorporate into *C. glutamicum*. We observed no decrease in viability, even at 500 μM (**Figure 3.5B**) indicating that the observed decrease in viability is dependent on azido-arabinose incorporation. We hypothesized that 5-AzFPA may be

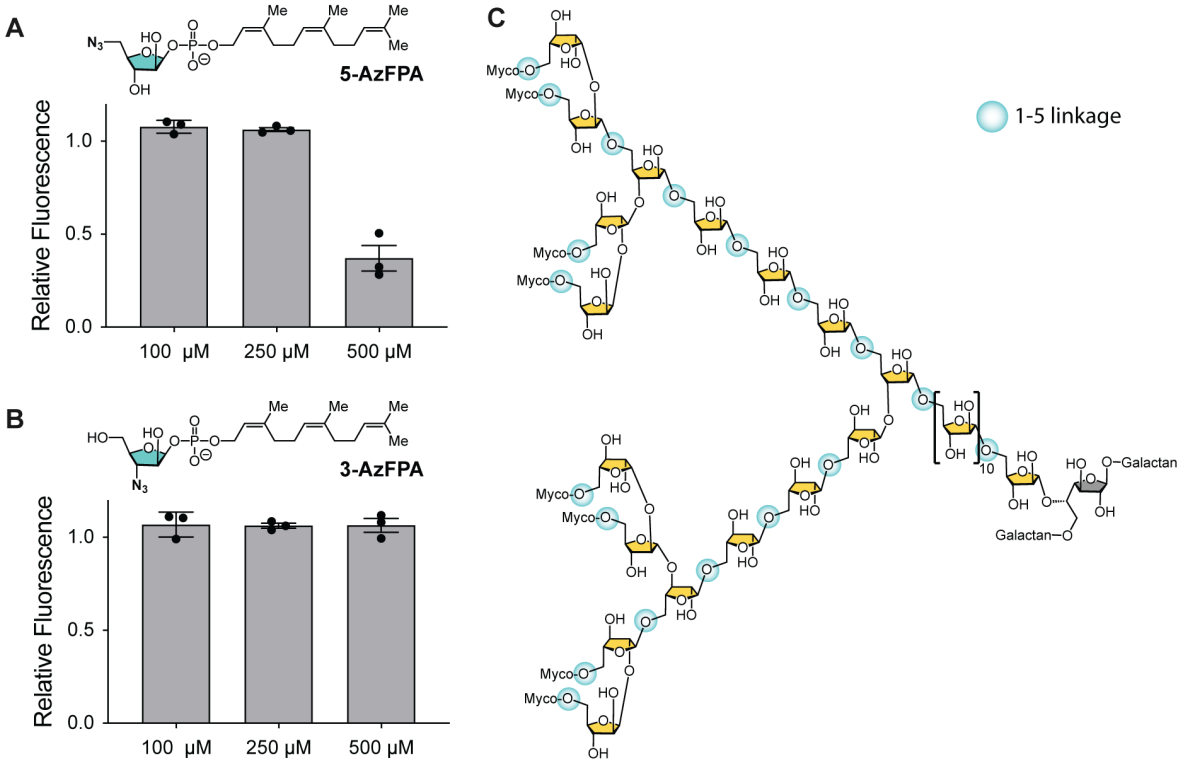

Figure 3.5 Effect of AzFPA probes on cell viability at high concentrations. Viability of *C. glutamicum* was measured via the Alamar Blue assay upon treatment with 5-AzFPA **(A)** which is incorporated and 3-AzFPA **(B)** which is not incorporated. The Y axis depicts the relative fluorescence compared to an untreated control sample. Error bars denote the standard error of the mean of three replicate experiments. **(C)** Chemical structure of the arabinan in *Corynebacterianeae*. 1-5 linkages that would be disrupted by azide installation via 5-AzFPA incorporation are highlighted.

significantly perturbing to the cell wall at high levels of incorporation. Based on structural knowledge of the linkages present in the arabinan, we hypothesized that the installation of an azide group at the 5-position of D-Ara*f* could prevent chain elongation and/or installation of the mycolic acids onto the arabinan (**Figure 3.5C**). This possibility was exciting as previous work has investigated the effect of perturbing the mycolate using genetic manipulations or non-specific antibiotics, such as ethambutol, however, no specific small-molecule modulators of arabinan structure have been reported previously. Small molecules specifically provide a number of advantages for answering biological questions as their administration can be dose- and time-resolved, allowing for more precise perturbations that cannot be achieved using other genetic and biochemical methods, enabling us to test new questions and hypotheses.

3.3.3.1 Mass Spectrometry to Assess Arabinan Truncation

To test the hypothesis that exogenous azide functionality introduced by 5-AzFPA could prevent the extension of arabinan, we carried out carbohydrate composition analysis via mass spectrometry. *C. glutamicum* cells grown either with or without 5-AzFPA (500 μM) were first delipidated, and then the mAGP complex was isolated following literature procedures.[34-35] This material was subjected to acid-catalyzed hydrolysis, reduction, and global acetylation to enable detection (**Scheme 3.1**).[18]

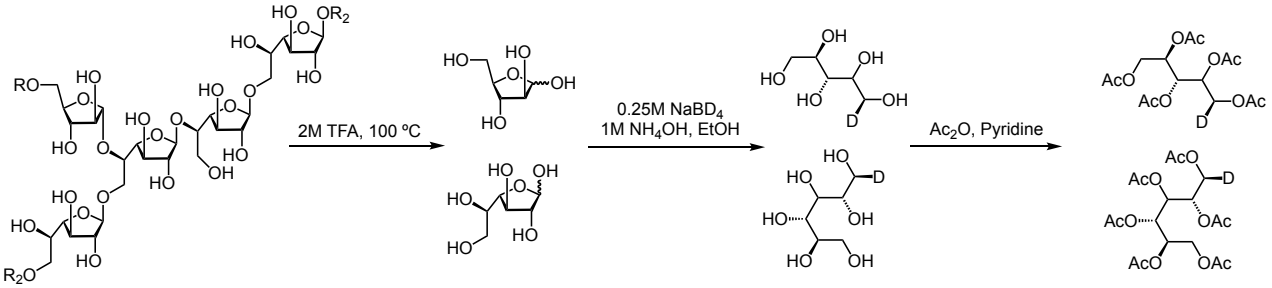

Scheme 3.1 Alditol acetate preparation from mAGP isolates. Mass spectrometry analysis performed by detecting $[M\text{-}OAc]^+$ signal of the products shown.

The resultant alditol acetate samples were analyzed by LC-MS to determine the arabinose:galactose ratio as a measure of arabinan truncation. Ratios were determined based on the area under the curve for the ion counts of the $[M\text{-}OAc]^+$ signals (**Figure 3.6**). We observed a statistically significant decrease in the arabinose:galactose ratio upon probe treatment indicating chain truncation.

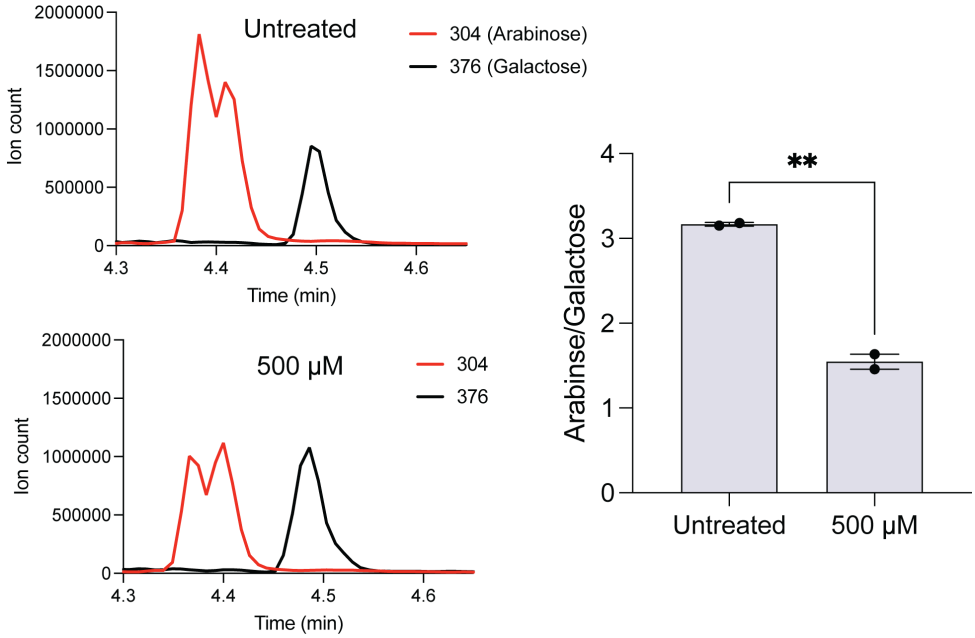

Figure 3.6 Extent of arabinose truncation determined by cell wall composition analysis. Composition analysis chromatograms (left) and the ratio of arabinose to galactose residues based on area under the curve (right) for untreated and 5-AzFPA treated *C. glutamicum* WT. Error bars denote the standard error of the mean (n=2). Statistical unpaired T-test is shown with $p \leq 0.005$ represented as **.

3.3.3.2 Treatment with 5-AzFPA Induces Phenotypic Changes

To investigate the phenotypic consequences of arabinan truncation via 5-AzFPA treatment in *C. glutamicum*, we visualized the cells via super-resolution microscopy.[33] Cells were grown in media supplement with high doses (500 µM or 1000 µM) of 5-AzFPA. Though there was significant cell death, enough cells were viable for downstream analysis. In order to ensure the effects observed weren't being confounded by the DBCO-conjugated dye, we visualized cell morphology using 7-hydroxycoumarin-

3-carboxylic acid-3-amino-D-alanine (HADA), a fluorescent D-alanine analog that is incorporated into peptidoglycan.[36] This commercial probe allowed for visualization of the cell wall. In the samples treated with high concentrations of 5-AzFPA, many of the cells contained multiple septa rather than forming a single septal plane prior to standard division (**Figure 3.7**). New cells appear to be starting to form but are unable to fully divide, resulting in long cells with several septal planes. Interestingly, in most cases the cells did not appear to be severely blebbed, a phenotype previously seen upon cell wall glycan truncation.[37]

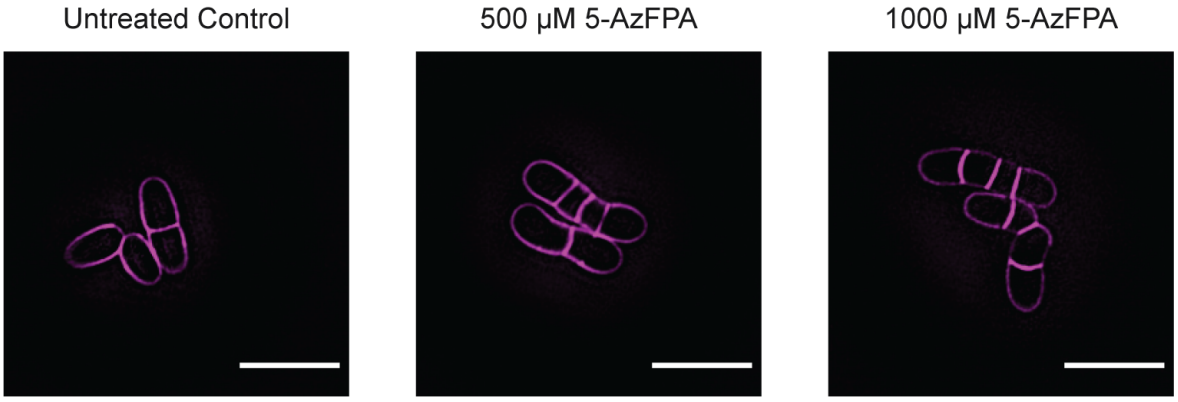

Figure 3.7 Super-resolution imaging of *C. glutamicum* treated with 5-AzFPA. The cell wall was visualized by staining the peptidoglycan with HADA (500 μM). (Scale bar = 3 μm).

We next tested a genetic analog to our proposed chemical perturbation. The enzyme responsible for the final condensation step in mycolic acid biosynthesis in *C. glutamicum* has been identified as Pks13 (**Figure 3.8A**).[38] *C. glutamicumΔpks13* cells are viable though *pks13* was shown to be essential for the viability of *M. smegmatis* and *Mtb*.[39] It was been demonstrated through lipid extractions[38] and electron microscopy[18] that *C. glutamicumΔpks13* cells lack an outer mycolate layer on their cell wall. To investigate the phenotypic consequences of mycolate deletion, we used HADA to visualize *C. glutamicum Δpks13* cells by SIM. These cells displayed a similar phenotype to those treated with 5-AzFPA, bearing multiple septa (**Figure 3.8B**). However, the *C.*

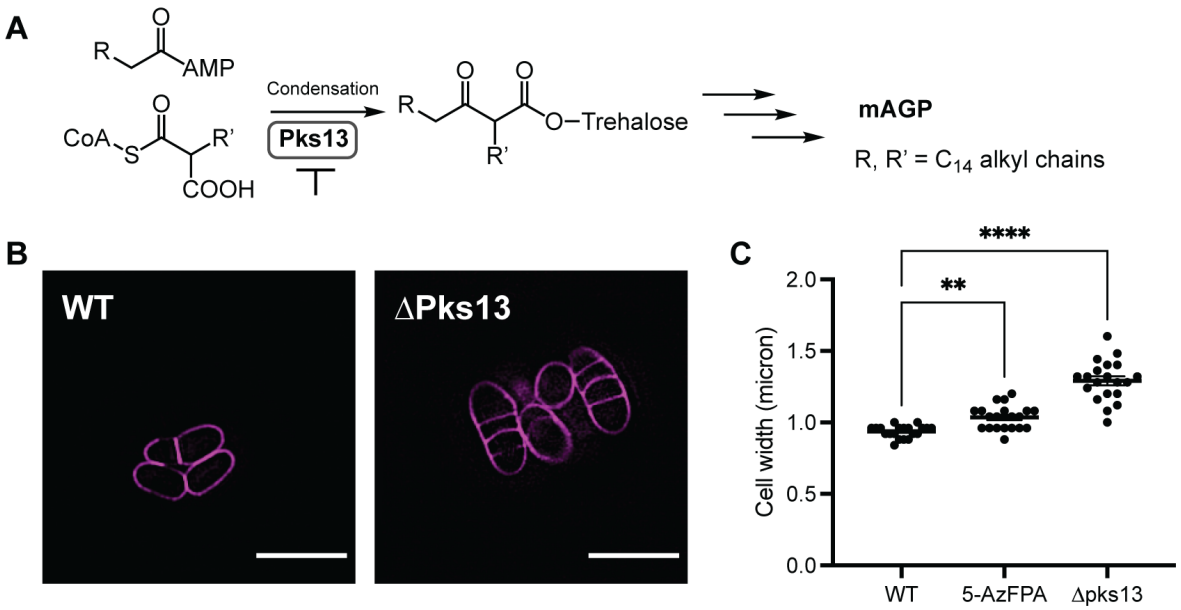

Figure 3.8 Super-resolution microscopy of *C. glutamicum Δpks13*. (A) Chemical step catalyzed by Pks13 in mycolic acid biosynthesis for mAGP assembly. **(B)** SIM images of WT and *Δpks13* cells and corresponding schematic depictions of cell wall structure. Cell wall was visualized by staining the peptidoglycan with HADA (500 μM). (Scale bar = 3 μm). **(C)** Based on SIM data, distance between maximum fluorescence was calculated to quantify cell length in wild-type *C. glutamicum*, wild-type *C. glutamicum* treated with 500 μM 5-AzFPA or *C. glutamicum Δpks13*. Error bars denote the standard error of the mean (n=20 cells). Statistical one-way ANOVA shown with $p \leq 0.005$ and 0.0001, represented as ** and **** respectively.

glutamicum Δpks13 cells exhibit a more dramatic phenotype, with the cells being shorter and, in some cases, blebbing. Furthermore, these cells are wider than wild-type cells and cells treated with 5-AzFPA (**Figure 3.8C**). A similar phenotype has been observed in the literature upon ethambutol treatment, an antibiotic used to treat *Mtb* infections that inhibits multiple arabinosyltransferases, as well as acting on other cell wall assembly enzymes including glutamate racemase.[40-42]

The difference in phenotype between our chemical perturbation and the genetic analog could be a consequence of the complete knockout of any mycolic acids in the genetic perturbation, as opposed to what is likely partial removal of this layer in the 5-AzFPA treated samples. The phenotypic differences between the *Δpks13* cells and 5-AzFPA treated samples could also indicate a mechanism for perturbation of the cell wall

that is distinct from the removal of the mycolic acid layer. In the literature, a similar multi-septate phenotype with minimal cell-widening was observed in a *C. glutamicum* mutant with deletion of a gene encoding NlpC/P60-like PG hydrolase (*Δcpg_1735)*.[43-44] The similarity of these phenotypes suggests a potential mechanistic explanation. The introduction of azide moieties into the arabinan could prevent recognition of the cell wall cleavage or biosynthesis machinery (PG hydrolase or otherwise), preventing complete cell division. This selective perturbation of the arabinan using a chemical probe may enable a number of exciting research directions. The 5-AzFPA probe is not significantly incorporated into the cell wall of *M. smegmatis* so this phenomenon cannot be observed in this species.[22] However, a similar multi-septate phenotype has been observed in *Mtb* cells treated with high concentrations of 5-AzFPA, indicating that this phenomenon is not specific to *C. glutamicum* (data not shown). The resultant altered cell division could be due to aberrant localization of cell wall synthesis machinery, lack of recognition of the perturbed substrate, or changes in signaling. Additional studies are required to better understand this phenomenon and its consequences.

3.3.3.3 Transmission Electron Microscopy Reveals Mild Changes in Cell Wall Thickness

We next investigated if changes induced by 5-AzFPA or the genetic analog result in changes in cell envelope morphology. Electron microscopy has previously been applied to directly visualize the cell wall of Corynebacterineae including *C. glutamicum* and *M. tuberculosis*.[43, 45] We used transmission electron microscopy (TEM) to compare the cell wall structure of *C. glutamicum* WT, *C. glutamicum Δpks13* and *C. glutamicum* WT treated with 5-AzFPA (**Figure 3.9**). This data confirmed that both mutants result in a significant decrease in cell wall thickness, consistent with previous studies.[18] At 250 μM 5-AzFPA treatment, no detectable changes in cell wall thickness are observed (**Figure**

3.9B). This is consistent with the observation that cells treated at this concentration maintain viability and show no abnormal phenotypes by confocal and super-resolution microscopy. However, upon treatment at 500 μM 5-AzFPA, the cells have a statistically significant decrease in cell wall thickness. This further corroborates that the chemical perturbation by 5-AzFPA is milder than the changes induced in the *Δpks13* cells. This highlights the value of specific chemical modulators to finetune phenotypic effects, in

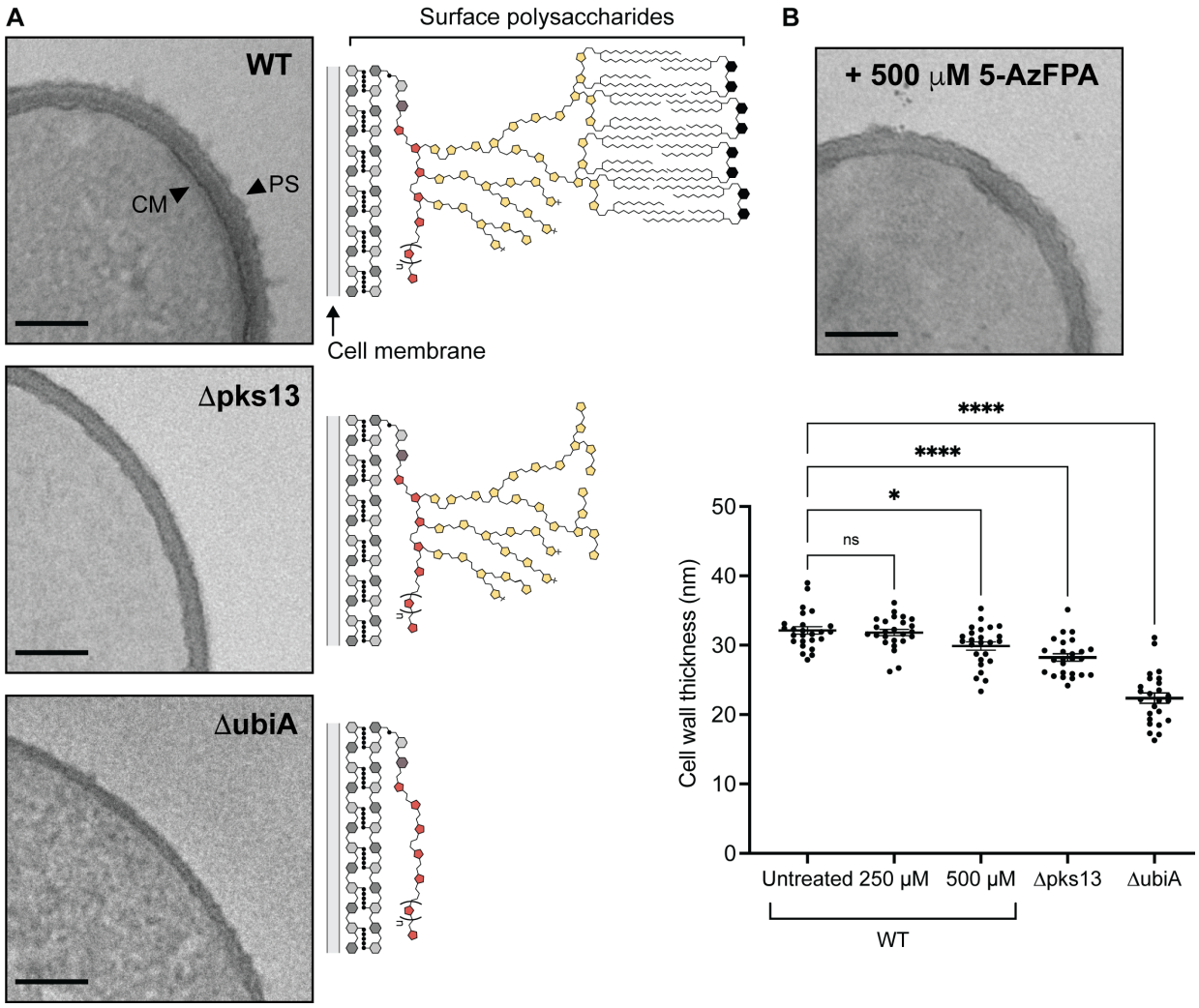

Figure 3.9 Transmission electron micrographs of *C. glutamicum*. (A) Ultrathin section of *C. glutamicum* WT, *C. glutamicum Δpks13* and *C. glutamicum ΔubiA* (Direct magnification = 23000x scale bars = 100 nm). **(B)** WT treated with 5-AzFPA (500 μM) and quantification of cell wall length based on electron micrographs. Error bars denote the standard error of the mean (n=25 cells). Statistical one-way ANOVA shown with $p \leq 0.05$ and 0.0001, represented as * and **** respectively.

contrast with genetic alternatives. Additionally, these TEM studies can serve as a platform for future work harnessing the azide handle to perform "Click-EM" for enhanced labeling at sites of probe incorporation.[46] This could illuminate the position of cell wall structures with new levels of precision.

3.4 Conclusions

The ubiquity and importance of bacterial cell surface glycans warrant a molecular-level understanding of their structure and function. The installation of modifiable chemical functionalities into glycans can enable a wide range of investigations including the facile purification for immunological studies, identification of glycan interactions with other biomolecules, or elucidation of polysaccharide trafficking and maintenance. We have developed a platform that can circumvent intracellular processes to allow for direct and specific labeling of the arabinan in the mAGP complex. This chapter highlights several examples of studies involving arabinan modification by AzFPA probes. The outlined examples demonstrate the utility of chemical probes that selectively perturb glycan structures of interest. These probes have proved useful for research directions being explored within the Kiessling group and to the broader scientific community.

3.5 Experimental Details

3.5.1 Strains and Growth Conditions

For bacterial assays, the strains employed include *Corynebacterium glutamicum ATCC13032, C. glutamicumΔpks13,* and *Mycobacterium tuberculosis H37Rv*. *C. glutamicum* was cultured in brain heart infusion (BHI) medium (BD, Franklin Lake, NJ) supplemented with 9% (w/v) sorbitol (BHIS) in a shaking incubator at 30 °C. *C. glutamicumΔpks13* was cultured in BHI media with 25 μg/ml kanamycin. *M. tuberculosis* was grown in Middlebrook 7H9 broth (HiMedia, Mumbai, India) supplemented with 0.2% (w/v) dextrose, 0.2% (v/v) glycerol, 0.5% bovine serum albumin (United States Biological, Salem, MA), catalase (4 mg/liter) (Sigma-Aldrich), 15 mM sodium chloride and 0.05 % (v/v) Tween 80 in a shaking incubator at 37 °C. Generally, starter cultures were incubated at the relevant temperature with shaking until saturation. Cells were then diluted into fresh media and grown to mid-logarithmic phase (determined by OD_{600} measurement on a BioMate 3S Spectrophotometer).

Mtb was grown in Middlebrook 7H9 broth (HiMedia, Mumbai, India) supplemented with 0.005% (w/v) oleic acid, 0.2% (w/v) dextrose, 0.2% (v/v) glycerol, 0.5% bovine serum albumin, catalase (4 mg/liter), 15 mM sodium chloride, and 0.05% (v/v) Tween 80 in a shaking incubator at 37 ºC. For growth with AzFPA probes, *Mtb* was passaged to an OD of 0.05 in Middlebrook 7H9 broth supplemented with 0.03% casitone, 0.08% sodium chloride, and 0.4% dextrose and allowed to grow for four doubling times.

3.5.2 mAGP Isolation

Cell envelope material was extracted similarly to previously described protocols.[18, 47] *C. glutamicum* was cultured in BHIS medium (1 mL) in a shaking incubator at 30 °C.

Cells were pelleted for 5 min at 3000 x g, normalizing across samples by OD. Cells were washed and reacted with AFDye™ 647 DBCO (Click Chemistry Tools #1302).[23] After staining and washing, cell pellets were resuspended in lysis buffer (2% Triton X-100 in phosphate-buffered saline (PBS)) and disrupted by sonication (6 x 20 s separated by 2 min off intervals on ice). The cell lysate was then pelleted by centrifugation at 15000 g for 15 min. The supernatant was removed and the pellet was taken up in 2% SDS in PBS and heated to 95 °C for 1 h before pelleting as above and discarding the supernatant. The pellet was then washed with water, 80% acetone/water, and then acetone.

3.5.3 mAGP Fluorescence Release Assay

Labelled mAGP was incubated with 1 μM of each enzyme in PBS (or PBS only) with rotation overnight at 37 °C. This insoluble suspension was pelleted by centrifugation at 15000 g for 15 min. Samples were washed three times with PBS. The remaining fluorescence was detected on a Tecan M1000 plate reader. Plates were shaken for 3 s (6 mm, orbital) immediately before the well fluorescence was read (λ_{ex} = 648 nm ±5, λ_{em} = 671 ± 5 nm).

3.5.4 Flow Cytometry

Cells were pelleted for 5 min at 3000 x g. The pellets were washed with ice-cold PBS supplemented with 0.05% Tween 80 (100 μL) once. Cells were washed an additional time with PBS supplemented with 0.05% Tween 80 and 0.5% (w/v) bovine serum albumin (BSA) once then taken up in fresh 7H9 media supplemented with 0.5% Tween 80 (150 μL). AFDye™ 647 DBCO (Click Chemistry Tools #1302) was added from a 10 mM stock solution in DMSO to a final concentration of 500 μM. The samples were

stained for 2 h rotating at 37 °C. When 1 h and 45 min minutes had passed, 0.1 µL (1500X dilution) of SytoBC™ Green Fluorescent Nucleic Acid Stain (ThermoFischer #S34855) was added for a 15-minute incubation period. The stained cells were pelleted for 5 min at 3000 x g. The supernatant was removed, and the pellet was washed with PBS supplemented with 0.05% Tween 80 and 0.5% (w/v) BSA twice.

For flow cytometry, stained cell pellets were taken up in 4% paraformaldehyde in PBS to be fixed at room temperature for 1 h. Following fixation, cells were pelleted then taken up in sterile PBS supplemented with 0.05% Tween 80 in flow tubes and analyzed using an Attune NxT Flow Cytometer (405 nm, 488 nm, 561 nm, and 640 nm lasers). 10,000 cells were counted at the low flow rate. Flow cytometry analysis was performed in triplicate, and representative scatter plots are shown. The unstained controls were analyzed first to set gates. Data were analyzed using the FlowJo software package (FlowJo LLC). Mean fluorescence intensity was calculated using a geometric mean.

3.5.5 Super-Resolution Microscopy

For analysis by microscopy, stained, fixed cells were pelleted and taken up in PBS supplemented with 1% w/v DABCO ((1,4-diazabicyclo[2.2.2]octane) as an antifading reagent. Each sample was spotted onto a glass-bottomed microwell dish (MatTek corporation # P35G-1.5-14-C), allowed to settle and covered with a pre-cooled 1% (w/v) agarose pad. Images were collected on an Applied Precision DeltaVision-OMXv4 Super-Resolution Microscope (60x/1.42 NA oil immersion lens, sequential imaging on two sCMOS cameras). SIM reconstruction and warp-based image alignments were performed with Applied Precision softWoRx. Multi-color image alignments were calculated from an Applied Precision grid test slide, checked with TetraSpeck beads (0.1

μm, Molecular Probes), and verified with an Argo-SIM test slide (Axiom Optics) prior to data collection. Brightness and contrast were identically adjusted with the open-source Fiji distribution of ImageJ. Images were then converted to an RGB format to preserve normalization and then assembled into panels.

3.5.6 Cell Viability Assay

Experiments were performed following standard reported procedures.[18] In brief, a saturated culture was diluted down to the desired starting OD_{600} = 0.05 and plated in triplicate in a Corning black 96-well plate. Probes were added at the indicated concentration from DMSO stock solutions. *C. glutamicum* was grown with shaking at 30 °C for 16 h. Alamar Blue reagent (6 μL, Invitrogen) was added to each well and the plates were incubated again for 1 h at 30 °C. The fluorescence emission of each well was then measured on a Tecan Infinite M1000 Pro microplate reader. Monitoring of resorufin fluorescence was achieved by exciting at 570 nm ± 5 nm and detecting at 585 nm ± 5 nm. Z-position was set to 2 mm, and the fluorimeter gain was optimized and then kept constant between plates. Data are reported in relative fluorescence units (RFU) normalized to untreated controls.

3.5.7 mAGP Isolation and Composition Analysis

C. glutamicum cells were grown under the described treatment conditions for 8 h at 30 °C. Cells were pelleted for 5 min at 3000 x g. The pellets were washed with ice-cold PBS supplemented with 0.05% Tween 80 (1 mL) once. Cells were washed an additional time with PBS supplemented with 0.05% Tween 80 and 0.5% (w/v) BSA once then taken up in fresh 7H9 media supplemented with 0.5% Tween 80 (1 mL). Cells were then

delipidated by treatment with 2:1 chloroform:methanol (1.2 mL total) rotating at room temperature overnight. Samples were pelleted for 5 min at 3000 x g followed by two additional delipidation treatments with 1:2 chloroform:methanol (1.2 mL total) rotating at 55 °C for 2 h each. Samples were pelleted for 5 min at 3000 x g. Samples were then boiled in 50% ethanol in water twice, first for 2 h, then 1.5 h. Samples were pelleted for 5 min at 3000 x g between each wash and after the final wash.

The resulting insoluble samples were taken as the mAGP complex for alditol acetate preparation.[48] Samples were taken up in 2M trifluoroacetic acid (250 µL) and hydrolyzed at 100 °C for 2 h. The suspension was then diluted in an additional 500 µL of water and filtered through syringe filters (PVDF, 0.2 µm pore size) and concentrated under reduced pressure. The resultant monosaccharides were then reduced with 0.25 M $NaBD_4$ in 1 M NH_4OH in ethanol (250 µL) overnight. The reactions were then quenched with 10% acetic acid in methanol (250 µL) and concentrated under reduced pressure. Three additional 250 µL aliquots of 10% acetic acid in methanol were added and removed by reduced pressure. The samples were then taken up in a 1:1 mixture of acetic anhydride:pyridine (500 µL) for reaction overnight at room temperature. The reactions were concentrated under reduced pressure and taken up in ethyl acetate and passed through a plug of $MgSO_4$ followed by concentration.

Samples were taken up in 1:1 acetonitrile:water (1 mL) and analyzed by LC-MS. The analysis was performed using MS2 scan mode on an Ultivo triple-quadrupole Agilent Mass Spectrometer, which is coupled with an Agilent 1260 Infinity II LC system fitted with a Zorbax RRHD Eclipse Plus C18 column (2.1 mm x 50 mm, 1.8 µM pore size). Gradient from 10 to 100 % acetonitrile in water containing 0.1% formic acid was used

over 10 min with a flow rate of 0.3 mL/min. An ESI ion source was used measuring total ion counts for the desired monosaccharides.

3.5.8 Transmission Electron Microscopy Sample Preparation

C. glutamicum cells were grown under the described treatment conditions for 8 h at 30 °C. Cells were pelleted for 5 min at 3000 x g. The pellets were washed with ice-cold PBS supplemented with 0.05% Tween 80 (1 mL) once. Cells were washed an additional time with PBS supplemented with 0.05% Tween 80 and 0.5% (w/v) BSA once then taken up in fresh 7H9 media supplemented with 0.5% Tween 80 (1 mL). Cells were then fixed at 4 °C for 1 h with freshly prepared fixative solution containing: 4% paraformaldehyde, 2.5% glutaraldehyde, 0.075% (w/v) Ruthenium red in 0.1 M cocadylate buffer. Following fixation, cells were pelleted for 5 min at 3000 x g and washed five times with 0.075% (w/v) Ruthenium red in 0.1 M cocadylate buffer. The washed cells were then postfixed with 1% (w/v) OsO_4 in 0.1 M cocadylate buffer with 0.075% (w/v) Ruthenium red at room temperature for 1 h. Cells were then rinsed with distilled water and resuspended in 1% aqueous uranyl acetate for 1 h and washed five times with water. Suspended cells were dehydrated through a graded ethanol series (50% to 100% ethanol in distilled water). Samples were embedded in Epon resin. Blocks were conventionally cut, stained and examined with a FEI Spirit T12 electron microscopy. Samples were prepared and imaged in collaboration with the Swanson Biotechnology Center at the Koch Institute.

3.5.9 Transmission Electron Microscopy Data Analysis

Images were analyzed with the open-source Fiji distribution of ImageJ. Cell wall width was measured at five independent points around each measured cell using the Plot Profile function. These measurements were averaged for each cell. For each condition, 25 cells were measured. One-way ANOVA with multiple comparisons were calculated versus WT cells to assess statistical significance.

3.6 References

1. Gringhuis, S. I.; den Dunnen, J.; Litjens, M.; van der Vlist, M.; Geijtenbeek, T. B., Carbohydrate-specific signaling through the DC-SIGN signalosome tailors immunity to Mycobacterium tuberculosis, HIV-1 and Helicobacter pylori. *Nat Immunol* **2009,** *10* (10), 1081-8.

2. Lee, S.; Inzerillo, S.; Lee, G. Y.; Bosire, E. M.; Mahato, S. K.; Song, J., Glycan-mediated molecular interactions in bacterial pathogenesis. *Trends Microbiol* **2021**.

3. Zhuo, L.; Kanamori, A.; Kannagi, R.; Itano, N.; Wu, J.; Hamaguchi, M.; Ishiguro, N.; Kimata, K., SHAP potentiates the CD44-mediated leukocyte adhesion to the hyaluronan substratum. *J Biol Chem* **2006,** *281* (29), 20303-14.

4. Dorr, T.; Moynihan, P. J.; Mayer, C., Editorial: Bacterial Cell Wall Structure and Dynamics. *Front Microbiol* **2019,** *10*, 2051.

5. Kiessling, L. L.; Marando, V. M.; Smelyansky, S. R.; Kim, D. E., Chapter 25: Chemical Microbiology. In *Advanced Chemical Biology*, Hang, H. C.; Pratt, M. R.; Prescher, J. A., Eds. Wiley-VCH: 2023.

6. Dube, D. H.; Bertozzi, C. R., Metabolic oligosaccharide engineering as a tool for glycobiology. *Curr Opin Chem Biol* **2003,** *7* (5), 616-25.

7. Luong, P.; Dube, D. H., Dismantling the bacterial glycocalyx: Chemical tools to probe, perturb, and image bacterial glycans. *Bioorg Med Chem* **2021,** *42*, 116268.

8. Lee, T. S.; Kim, Y.; Zhang, W.; Song, I. H.; Tung, C. H., Facile metabolic glycan labeling strategy for exosome tracking. *Biochim Biophys Acta Gen Subj* **2018,** *1862* (5), 1091-1100.

9. Siegrist, M. S.; Swarts, B. M.; Fox, D. M.; Lim, S. A.; Bertozzi, C. R., Illumination of growth, division and secretion by metabolic labeling of the bacterial cell surface. *Fems Microbiology Reviews* **2015,** *39* (2), 184-202.

10. Wang, H.; Mooney, D. J., Metabolic glycan labelling for cancer-targeted therapy. *Nat Chem* **2020,** *12* (12), 1102-1114.

11. Boons, G. J., Bioorthogonal chemical reporter methodology for visualization, isolation and analysis of glycoconjugates. *Carbohydr Chem* **2010,** *36*, 152-167.

12. Lopez Aguilar, A.; Briard, J. G.; Yang, L.; Ovryn, B.; Macauley, M. S.; Wu, P., Tools for Studying Glycans: Recent Advances in Chemoenzymatic Glycan Labeling. *ACS Chem Biol* **2017,** *12* (3), 611-621.

13. Cioce, A.; Malaker, S. A.; Schumann, B., Generating orthogonal glycosyltransferase and nucleotide sugar pairs as next-generation glycobiology tools. *Curr Opin Chem Biol* **2021,** *60*, 66-78.

14. Gilormini, P. A.; Batt, A. R.; Pratt, M. R.; Biot, C., Asking more from metabolic oligosaccharide engineering. *Chem Sci* **2018,** *9* (39), 7585-7595.

15. Adibekian, A.; Stallforth, P.; Hecht, M.-L.; Werz, D. B.; Gagneux, P.; Seeberger, P. H., Comparative bioinformatics analysis of the mammalian and bacterial glycomes. *Chem. Sci.* **2011,** *2* (2), 337-344.

16. Fraenkel, D. G.; Vinopal, R. T., Carbohydrate metabolism in bacteria. *Annu. Rev. Microbiol.* **1973,** *27*, 69-100.

17. Imperiali, B., Bacterial carbohydrate diversity - a Brave New World. *Curr Opin Chem Biol* **2019,** *53*, 1-8.

18. Calabretta, P. J.; Hodges, H. L.; Kraft, M. B.; Marando, V. M.; Kiessling, L. L., Bacterial Cell Wall Modification with a Glycolipid Substrate. *J Am Chem Soc* **2019,** *141* (23), 9262-9272.

19. Angala, S. K.; Joe, M.; McNeil, M. R.; Liav, A.; Lowary, T. L.; Jackson, M., Use of Synthetic Glycolipids to Probe the Number and Position of Arabinan Chains on Mycobacterial Arabinogalactan. *ACS Chem Biol* **2021,** *16* (1), 20-26.

20. Alderwick, L. J.; Seidel, M.; Sahm, H.; Besra, G. S.; Eggeling, L., Identification of a novel arabinofuranosyltransferase (AftA) involved in cell wall arabinan biosynthesis in Mycobacterium tuberculosis. *J Biol Chem* **2006,** *281* (23), 15653-61.

21. Joe, M.; Lowary, T. L., Synthesis of a homologous series of galactofuranose-containing mycobacterial arabinogalactan fragments. *Canadian Journal of Chemistry* **2016,** *94* (11), 976-988.

22. Marando, V. M.; Kim, D. E.; Calabretta, P. J.; Kraft, M. B.; Bryson, B. D.; Kiessling, L. L., Biosynthetic Glycan Labeling. *J Am Chem Soc* **2021,** *143* (40), 16337-16342.

23. Marando, V. M.; Kim, D. E.; Kiessling, L. L., Biosynthetic incorporation for visualizing bacterial glycans. *Methods Enzymol* **2022,** *665*, 135-151.

24. Al-Jourani, O.; Benedict, S.; Ross, J.; Layton, A.; van der Peet, P.; Marando, V. M.; Bailey, N. P.; Heunis, T.; Manion, J.; Mensitieri, F.; Franklin, A.; Abellon-Ruiz, J.; Oram, S. L.; Parsons, L.; Cartmell, A.; Wright, G. S. A.; Baslé, A.; Trost, M.; Henrissat, B.; Munoz-Munoz, J.; Hirt, R. P.; Kiessling, L. L.; Lovering, A.; Williams, S. J.; Lowe, E. C.; Moynihan, P. J., Mining the human gut microbiome identifies mycobacterial D-arabinan degrading enzymes. *Biorxiv* **2022**.

25. El Kaoutari, A.; Armougom, F.; Gordon, J. I.; Raoult, D.; Henrissat, B., The abundance and variety of carbohydrate-active enzymes in the human gut microbiota. *Nat Rev Microbiol* **2013,** *11* (7), 497-504.

26. Cartmell, A.; Munoz-Munoz, J.; Briggs, J. A.; Ndeh, D. A.; Lowe, E. C.; Basle, A.; Terrapon, N.; Stott, K.; Heunis, T.; Gray, J.; Yu, L.; Dupree, P.; Fernandes, P. Z.; Shah, S.; Williams, S. J.; Labourel, A.; Trost, M.; Henrissat, B.; Gilbert, H. J., A surface endogalactanase in Bacteroides thetaiotaomicron confers keystone status for arabinogalactan degradation. *Nat Microbiol* **2018,** *3* (11), 1314-1326.

27. Cuskin, F.; Lowe, E. C.; Temple, M. J.; Zhu, Y.; Cameron, E.; Pudlo, N. A.; Porter, N. T.; Urs, K.; Thompson, A. J.; Cartmell, A.; Rogowski, A.; Hamilton, B. S.; Chen, R.; Tolbert, T. J.; Piens, K.; Bracke, D.; Vervecken, W.; Hakki, Z.; Speciale, G.; Munoz-Munoz, J. L.; Day, A.; Pena, M. J.; McLean, R.; Suits, M. D.; Boraston, A. B.; Atherly, T.; Ziemer, C. J.; Williams, S. J.; Davies, G. J.; Abbott, D. W.; Martens, E. C.; Gilbert, H. J., Human gut Bacteroidetes can utilize yeast mannan through a selfish mechanism. *Nature* **2015,** *517* (7533), 165-169.

28. Grondin, J. M.; Tamurma, K.; Dejean, G.; Abbott, D. W.; Brumer, H., Polysaccharide Utilization Loci: Fueling Microbial Communities. *Journal of Bacteriology* **2017,** *199* (15), 1.

29. Luis, A. S.; Briggs, J.; Zhang, X.; Farnell, B.; Ndeh, D.; Labourel, A.; Basle, A.; Cartmell, A.; Terrapon, N.; Stott, K.; Lowe, E. C.; McLean, R.; Shearer, K.; Schuckel, J.; Venditto, I.; Ralet, M. C.; Henrissat, B.; Martens, E. C.; Mosimann, S. C.; Abbott, D. W.; Gilbert, H. J., Dietary pectic glycans are degraded by coordinated enzyme pathways in human colonic Bacteroides. *Nat Microbiol* **2018,** *3* (2), 210-219.

30. Martens, E. C.; Lowe, E. C.; Chiang, H.; Pudlo, N. A.; Wu, M.; McNulty, N. P.; Abbott, D. W.; Henrissat, B.; Gilbert, H. J.; Bolam, D. N.; Gordon, J. I., Recognition and degradation of plant cell wall polysaccharides by two human gut symbionts. *PLoS Biol* **2011,** *9* (12), e1001221.

31. Besra, G. S.; Khoo, K. H.; McNeil, M. R.; Dell, A.; Morris, H. R.; Brennan, P. J., A new interpretation of the structure of the mycolyl-arabinogalactan complex of Mycobacterium tuberculosis as revealed through characterization of oligoglycosylalditol fragments by fast-atom bombardment mass spectrometry and 1H nuclear magnetic resonance spectroscopy. *Biochemistry* **1995,** *34* (13), 4257-66.

32. Sparks, I. L.; Derbyshire, K. M.; Jacobs Jr, W. R.; Morita, Y. S., Mycobacterium smegmatis: The Vanguard of Mycobacterial Research. *Journal of Bacteriology* **2023,** *205* (1), 1-16.

33. Heintzmann, R.; Huser, T., Super-Resolution Structured Illumination Microscopy. *Chem Rev* **2017,** *117* (23), 13890-13908.

34. Pitarque, S.; Larrouy-Maumus, G.; Payre, B.; Jackson, M.; Puzo, G.; Nigou, J., The immunomodulatory lipoglycans, lipoarabinomannan and lipomannan, are exposed at the mycobacterial cell surface. *Tuberculosis (Edinb)* **2008,** *88* (6), 560-5.

35. Mikusova, K.; Slayden, R. A.; Besra, G. S.; Brennan, P. J., Biogenesis of the Mycobacterial Cell Wall and the Site of Action of Ethambutol. *Antimicrobial Agents and Chemotherapy* **1995,** *39* (11), 2484-2489.

36. Kuru, E.; Hughes, H. V.; Brown, P. J.; Hall, E.; Tekkam, S.; Cava, F.; de Pedro, M. A.; Brun, Y. V.; VanNieuwenhze, M. S., In Situ probing of newly synthesized peptidoglycan in live bacteria with fluorescent D-amino acids. *Angew Chem Int Ed Engl* **2012,** *51* (50), 12519-23.

37. Justen, A. M.; Hodges, H. L.; Kim, L. M.; Sadecki, P. W.; Porfirio, S.; Ultee, E.; Black, I.; Chung, G. S.; Briegle, A.; Azadi, P.; Kiessling, L. L., Polysaccharide length affects mycobacterial cell shape and antibiotic susceptibility. *Science Advances* **2020,** *6*, eaba4015.

38. Portevin, D.; De Sousa-D'Auria, C.; Houssin, C.; Grimaldi, C.; Chami, M.; Daffe, M.; Guilhot, C., A polyketide synthase catalyzes the last condensation step of mycolic acid biosynthesis in mycobacteria and related organisms. *Proc Natl Acad Sci U S A* **2004,** *101* (1), 314-9.

39. Bosch, B.; DeJesus, M. A.; Poulton, N. C.; Zhang, W.; Engelhart, C. A.; Zaveri, A.; Lavalette, S.; Ruecker, N.; Trujillo, C.; Wallach, J. B.; Li, S.; Ehrt, S.; Chait, B. T.; Schnappinger, D.; Rock, J. M., Genome-wide gene expression tuning reveals diverse vulnerabilities of M. tuberculosis. *Cell* **2021,** *184* (17), 4579-4592 e24.

40. Schubert, K.; Sieger, B.; Meyer, F.; Giacomelli, G.; Bohm, K.; Rieblinger, A.; Lindenthal, L.; Sachs, N.; Wanner, G.; Bramkamp, M., The Antituberculosis Drug Ethambutol Selectively Blocks Apical Growth in CMN Group Bacteria. *mBio* **2017,** *8* (1).

41. Pawar, A.; Jha, P.; Konwar, C.; Chaudhry, U.; Chopra, M.; Saluja, D., Ethambutol targets the glutamate racemase of Mycobacterium tuberculosis-an enzyme involved in peptidoglycan biosynthesis. *Appl Microbiol Biotechnol* **2019,** *103* (2), 843-851.

42. Xiang, X.; Gong, Z.; Deng, W.; Sun, Q.; Xie, J., Mycobacterial ethambutol responsive genes and implications in antibiotics resistance. *J Drug Target* **2021,** *29* (3), 284-293.

43. Zhou, X.; Rodriguez-Rivera, F. P.; Lim, H. C.; Bell, J. C.; Bernhardt, T. G.; Bertozzi, C. R.; Theriot, J. A., Sequential assembly of the septal cell envelope prior to V snapping in Corynebacterium glutamicum. *Nat Chem Biol* **2019,** *15* (3), 221-231.

44. Tsuge, Y.; Ogino, H.; Teramoto, H.; Inui, M.; Yukawa, H., Deletion of cgR_1596 and cgR_2070, encoding NlpC/P60 proteins, causes a defect in cell separation in Corynebacterium glutamicum R. *J Bacteriol* **2008,** *190* (24), 8204-14.

45. Chuang, Y. M.; Bandyopadhyay, N.; Rifat, D.; Rubin, H.; Bader, J. S.; Karakousis, P. C., Deficiency of the novel exopolyphosphatase Rv1026/PPX2 leads to metabolic downshift and altered cell wall permeability in Mycobacterium tuberculosis. *mBio* **2015,** *6* (2), e02428.

46. Ngo, J. T.; Adams, S. R.; Deerinck, T. J.; Boassa, D.; Rodriguez-Rivera, F.; Palida, S. F.; Bertozzi, C. R.; Ellisman, M. H.; Tsien, R. Y., Click-EM for imaging metabolically tagged nonprotein biomolecules. *Nat Chem Biol* **2016,** *12* (6), 459-65.

47. Besra, G. S.; Khoo, K.; McNeil, M. R.; Dell, A.; Morris, H. R.; Brennan, P. J., A New Interpretation of the Structure of the Mycolyl-Arabinogalactan Complex of *Mycobacterium tuberculosis* As Revealed through Characterization of Oligoglycosylalditol Fragments by Fast-Aton Bombardment Mass Spectrometry and 1H Nuclear Magnetic Resonance Spectroscopy. *Biochemistry* **1995,** *34*, 4257-4266.

48. Voiges, K.; Adden, R.; Rinken, M.; Mischnick, P., Critical re-investigation of the alditol acetate method for analysis of substituent distribution in methyl cellulose. *Cellulose* **2012,** *19* (3), 993-1004.

Chapter 4: Biosynthetic Glycan Labeling of Mannose-Containing Glycans in Mycobacteria

Contributions:
Compounds were synthesized by So Young Lee, Daria E. Kim, and Phillip J. Calabretta. Flow cytometry, microscopy and other cell-based assays were performed by Victoria M. Marando and So Young Lee. mCherry constructs were prepared and imaged by Victoria M. Marando. FRAP data was collected by Victoria M. Marando and analyzed by Teddy. C. Warner. Experiments in *Mtb* were peformed by Stephanie R. Smelyansky. Research designed by Victoria M. Marando, So Young Lee, Daria E. Kim, Phillip J. Calabretta and Laura L. Kiessling.

4.1 Abstract

Mycobacterium tuberculosis (*Mtb*) is one of the most successful human pathogens in history. By subverting typical immune responses, mycobacteria can persist within their host until conditions become favorable for their growth and proliferation. Key virulence factors that enable mycobacterial pathogens to modulate host immune systems include a suite of mannose-containing glycans namely, phosphatidylinositol mannosides (PIMs), lipomannan (LM), and lipoarabinomannan (LAM). Despite the importance of these structures, tools for their covalent capture, modification, and imaging remain very limited. By intervening at a late-stage biosynthetic step, a strategy termed biosynthetic incorporation, we have developed reagents to selectively modify a previously inaccessible glycan, the arabinan, in wild-type mycobacteria. In this report, we designed and evaluated a series of biosynthetic incorporation to target mannose-containing glycans for the first time, azido-(*Z,Z*)-farnesyl phosphoryl-β-D-mannose (AzFPM) probes. We demonstrate that these compounds enable the direct visualization of the localization and dynamics mannose-containing glycolipids in wild-type mycobacteria. These studies highlight the generality and utility of biosynthetic incorporation as a labeling method and that substructure-specific labeling can be dictated by probe structure. The disclosed reagents allowed for direct tracking of these immunomodulatory glycolipid dynamics *in cellulo* for the first time and we anticipate that these probes will be useful for future studies investigating the biological roles that these glycans play.

4.2 Introduction

Mycobacterium tuberculosis (*Mtb*) ranks among the most pernicious human pathogens.[1] Tuberculosis, the consequence of *Mtb* infection, remains one of the leading causes of death due to infectious disease, accounting for over one million casualties annually. This statistic is made more striking considering an estimated 3 billion people are infected with latent *Mtb* worldwide.[2] The ability of *Mtb* to suppress the host immune system during infection and persist in a latent form severely exacerbates the impact of this pandemic.[3-6] Mannose-containing glycans produced by mycobacteria, which include phosphatidylinositol mannosides (PIMs), lipomannan (LM), lipoarabinomannan (LAM), mannosylated lipoarabinomannan (ManLAM), and mannosylated glycoproteins, are known to play key roles in host immune modulation.[7-11] Although, host recognition of bacterial glycans is critical to the development of host immune responses and clearance of the pathogen, in the case of *Mtb*, mannose-containing glycans enable a number of immune evasion mechanisms. For instance, LAM inhibits liposome-phagosome fusion, allowing *Mtb* to form an intracellular niche within host macrophages.[12-13] In addition to important immunomodulatory functions, mannose containing glycolipids have been implicated in maintaining cellular integrity.[11-12]

Despite their importance, few direct methods exist to study the biosynthesis, trafficking, and biological function of these glycans. Monoclonal antibodies (mAbs) that recognize LAM or LM are much larger (180kDa) than the molecules of interest (LAM: 15kDa) and result in structural occlusion upon binding, minimizing the relevance of subsequent structure-function studies.[14-15] Furthermore, binding specificities of anti-LAM mAbs, particularly those targeting the mannan core, have been poorly defined.[15] Thus, there is a need for the development of new strategies for the selective structural

perturbation of the PIMs, LM, and LAM in order to probe the composition, function, and dynamics of mannose-containing glycans within the context of live cells and disease pathogenesis.

These structures have historically been challenging to study due to the fundamental difficulties achieving site-selective glycan modification. Unlike protein or polynucleotide synthesis, glycan biosynthesis is not directly genetically encoded, thus, there is no general template for perturbation through genetic manipulation.[16] Moreover, in contrast with protein bioconjugation where endogenous amino acid residues can be differentiated through complementary reactivity using small molecule reagents, naturally-derived monosaccharides often lack unique reactive functional groups. Given these challenges, chemical perturbation of glycans in a biological context is most commonly achieved through metabolic incorporation.[17-21] Metabolic incorporation relies on the multi-step, intracellular processing of simple monosaccharide building blocks by endogenous metabolic machinery, culminating in the presentation of the end products on the cell surface.[19] The application of this technique in prokaryotic systems poses several challenges due to the complexity of bacterial metabolism and catabolism, though several successful examples have been demonstrated.[17, 22-29]

To date, the only probe of the PIMs, LM and LAM was designed based on metabolic incorporation of azide-functionalized inositol.[30] This work highlights a key challenge of metabolic incorporation: due to competition with endogenous substrate at multiple steps, selective probe incorporation is contingent upon knock-out of endogenous inositol biosynthesis, preventing use of this probe in wild-type cells. There are currently no metabolic incorporation probes in use for mannose. Mannose is acquired by mycobacteria either through synthesis from fructose-6-phosphate or through import.[31-

[32] This intracellular mannose can be used for energy production or converted to fucose, rhamnose, or mannose sugar donors. Due to its central role in metabolism, we propose that a probe which relied on metabolic incorporation of derivatized mannose would be susceptible to non-specific incorporation or require genetic manipulation limiting applicability for labeling of the target structures.

Therefore, we instead turned to biosynthetic incorporation. Biosynthetic incorporation probes do not require activation in the cytosol; instead, they can be used directly by membrane-associated glycosyltransferases.[33] Direct utilization is advantageous as it limits competition with endogenous substrates to a single step. Previously, our group developed and applied biosynthetic incorporation probes in mycobacteria by synthesizing azido-(*Z,Z*)-farnesyl phosphoryl-β-D-arabinofuranose (AzFPA) derivatives as surrogates for the extended endogenous arabinofuranose donor decaprenyl phosphoryl-β-D-arabinofuranose (DPA).[34-35] The lipid truncation facilitated exogenous reagent delivery and the isomeric AzFPA probes with azide substitution at different positions on the sugar ring showed distinct incorporation trends in different species. Like the arabinogalactan, LM and LAM synthesis occurs in the periplasm and is accomplished by glycosyltransferase-C (GT-C) superfamily mannosyltransferases that utilize a polyprenyl phosphoryl-β-D-mannose (PPM), as their mannose donor.[36-37] We hypothesized that this strategy can be applied generally and the glycan target will mediated by glycosyltransferase-mediated recognition of the donor sugar structure. We anticipated that we could apply our optimized truncated lipid scaffold to deliver azido-mannose for selective labeling and subsequent bioconjugation of our mannose-containing glycans of interest.

Herein, we report the synthesis, validation and application of biosynthetic incorporation probes to study mannose-containing glycans in model mycobacterial organisms and *Mtb* (**Figure 4.1**). We prepared probes that contain azide handles for bioconjugation allowing for direct visualization of these structures of interest. This work highlights the generality of biosynthetic incorporation as a glycan bioconjugation strategy and represents the first development of specific, chemical probes of the PIMs, LM and LAM in wild-type cells. We investigated specificity of probe labeling and used these reagents to directly visualize membrane diffusion of these structures. We have also validated use of these probes in *Mtb* providing a new tool for the community to study the roles these glycans play in disease.

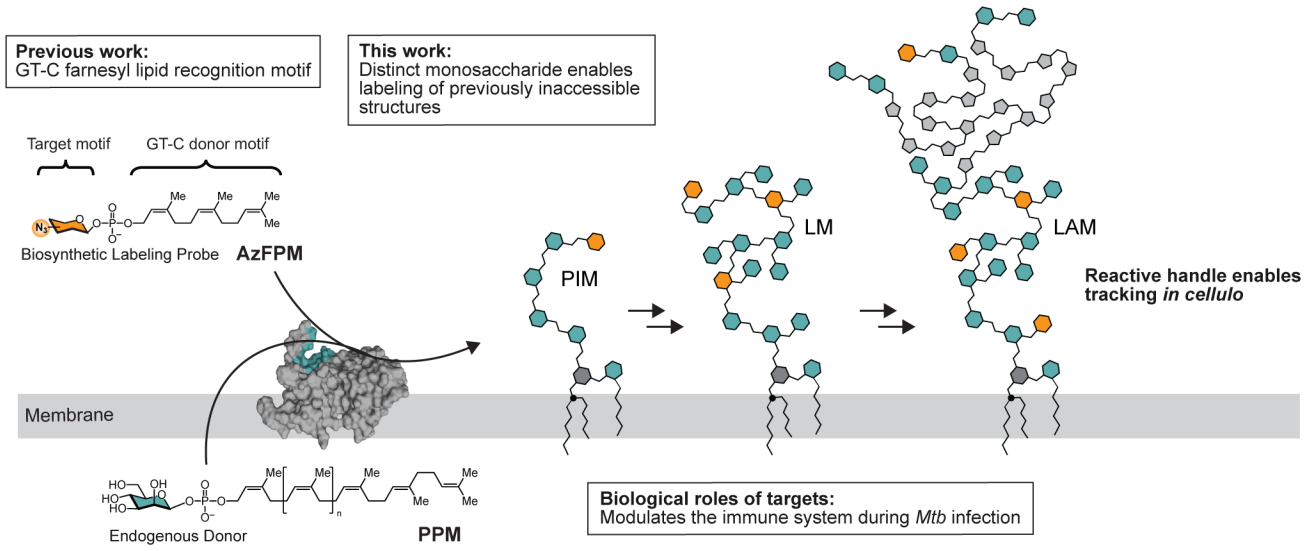

Figure 4.1 Overview schematic of biosynthetic labeling strategy targeting biologically important mannose-containing glycans. Previous work led to optimization of lipid motif for membrane associated glycosyltransferase recognition. This work demonstrates the modularity of this strategy by labeling new glycans with a novel suite of glycolipid probes (AzFPMs).

4.3 Results & Discussion

4.3.1 Design and Synthesis of Azido-Mannose Probes

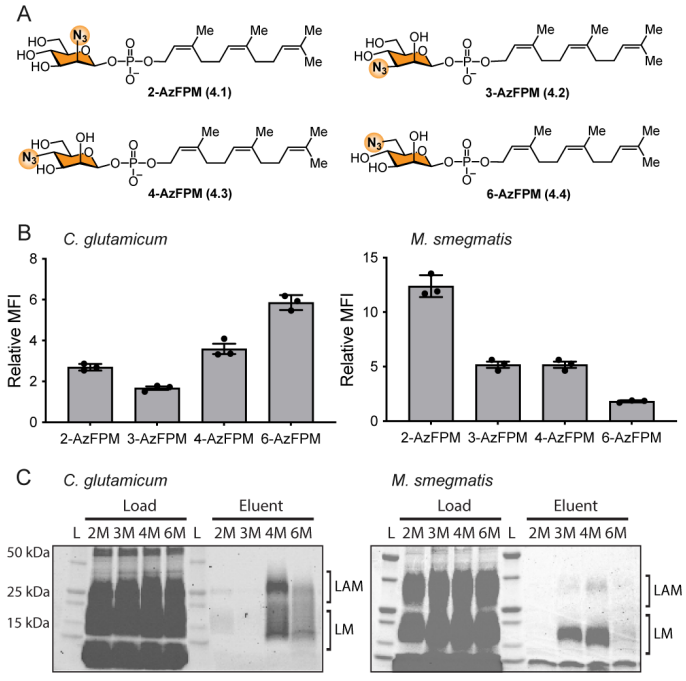

Figure 4.2 Validation of AzFPM labeling (A) The azide-modified substrate surrogates were designed based on structural homology to the endogenous mannose donor. Four azide regioisomers were produced (**4.1**–**4.4**). **(B)** Flow cytometry analysis of AzFPM (125 μM) labeled *C. glutamicum* and *M. smegmatis* treated with DBCO-AF647. Mean fluorescence intensity (MFI) was calculated using the geometric mean and plotted relative to a dye-only control. Error bars denote the standard error of the mean of three replicate experiments. **(C)** Streptavidin-enrichment of labeled structures from AzFPM (125 μM) labeled *C. glutamicum* and *M. smegmatis* reacted with DBCO-biotin. Load and eluent analyzed by SDS-PAGE using Pro-Q Emerald 300 glycan staining kit.

Though biosynthetic incorporation has only been previously applied to one target, arabinose within mycobacterial arabinogalactan,[33-34] we hypothesized that this approach is generalizable and be useful for labeling other glycans. Based on our previous success using a farnesyl motif to mimic the endogenous decaprenyl donor, we designed a panel of azido-(*Z,Z*)-farnesyl phosphoryl-β-D-mannose (AzFPM) derivatives (**Figure 4.2A**). We hypothesized that the efficiency of non-natural mannose incorporation may vary between different isomers and in different species as has been seen previously with biosynthetic incorporation probes.[34] We anticipated that the degree of incorporation may be affected by the specific enzyme-substrate complementarity for each substrate as well as the impact of chain truncation resulting from azides preventing further glycosylation. Moreover, a key target structure, the LAM, varies significantly between mycobacterial

model organisms. For instance, *Corynebacterium glutamicum* produces AraLAM which contains a mannan core that is capped by arabinose residues, whereas *Mycobacterium smegmatis* produces phosphoinositol-capped PILAM and *Mtb* produces mannose-capped ManLAM. Additional organism-specific tailoring of the LAM further includes the presence of succinate or methylthioxylofuranose caps which may be disrupted through the installation of azides. Accordingly, we prepared and evaluated all four possible regioisomeric AzFPM probes. The AzFPM regioisomers were synthesized from commercially available mannose derivatives and an inexpensive cellulose degradation product (Cyrene™) (**Scheme 4.1**). In all cases, the key azide functionality was installed through nucleophilic displacement or nucleophilic epoxide opening. We appended the (*Z,Z*)-farnesyl recognition motif and then removed the protecting groups to afford the target compounds (**4.1-4.4**).

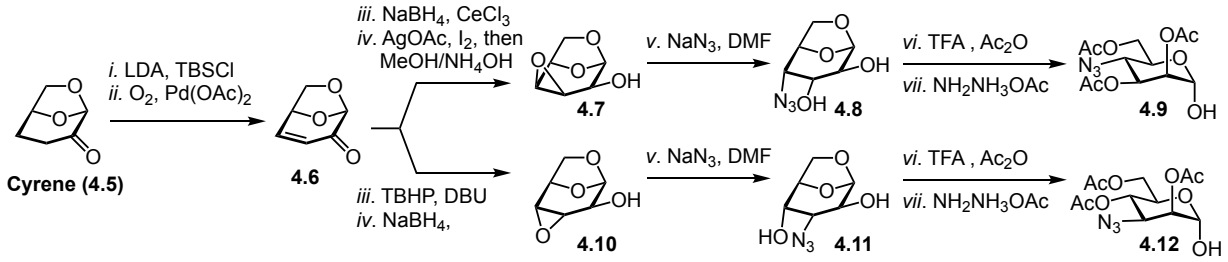

Scheme 4.1 Synthesis of AzFPM monomers from Cyrene

4.3.2 AzFPM Probes Label Mannose-Containing Glycans *In Cellulo*

We first confirmed incorporation of AzFPM probes *in cellulo* using model organisms of *Mtb*, *C. glutamicum* and *M. smegmatis*, using fluorescence labeling followed by flow cytometry (**Figure 4.2B**). Bacterial cultures were supplemented with 125 μM AzFPM in media and grown to late-logarithmic phase. At this concentration, the probes did not affect cell viability (**Figure 4.3**). Following growth, the labeled cells were washed to

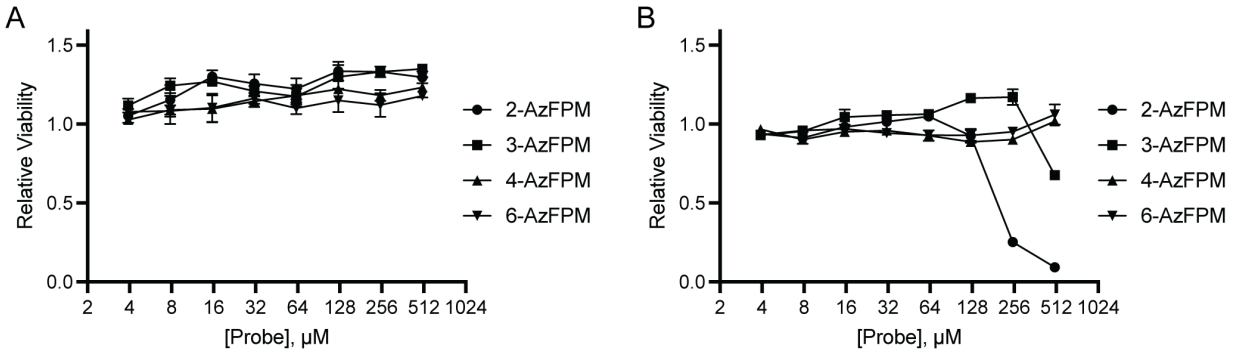

Figure 4.3 Cell viability upon AzFPM treatment. Growth of *C. glutamicum* **(A)** and *M. smegmatis* **(B)** measured via the Alamar Blue assay following serial dilution of AzFPM probes from 500 μM. The Y axis depicts the relative fluorescence compared to an untreated control sample. Error bars denote the standard error of the mean (n=3).

remove unincorporated probe followed by reaction with Alexa Fluor647 (AF647)-conjugated dibenzocyclooctyne (DBCO) via a strain-promoted azide-alkyne cycloaddition (SPAAC). Fixed samples were analyzed by flow cytometry. Increased fluorescence in AzFPM treated cells was observed relative to untreated controls. The degree of AzFPM incorporation, measured by relative Mean Fluorescence Intensity (MFI) levels, varied across organism. In *M. smegmatis*, the 2-AzFPM probe showed the highest levels of incorporation, whereas incorporation of the 6-AzFPM probe was negligible. In *C. glutamicum*, the 6-AzFPM probe showed the highest levels of incorporation, whereas the 3-AzFPM probe did not show significant incorporation. These data indicate AzFPM probes are competent substrates for mycobacterial mannosyltransferases and can be incorporated into mannose-containing cell surface glycans. We validated that the observed fluorescence by flow cytometry correlated with membrane localized labeling using super-resolution structured illumination microscopy (SIM) (**Figure 4.4**). These results demonstrate, for the first time, the generality of biosynthetic incorporation probes bearing farnesyl lipid motifs. Furthermore, our data show that glycosyltransferases even tolerate sugar substrates with azide-substitution on

secondary carbons, in contrast to what has been reported in studies of glycosidase promiscuity.[38]

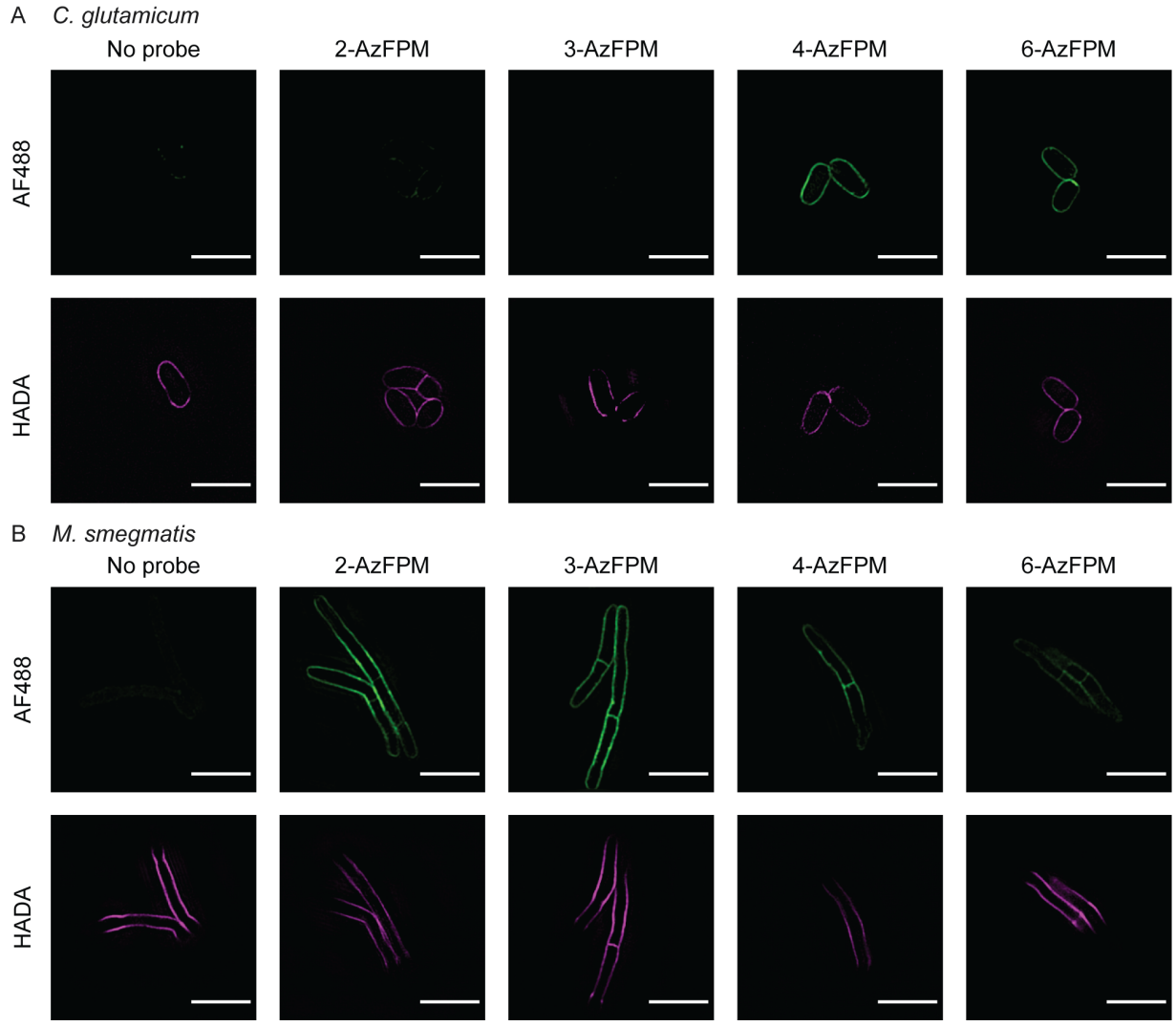

Figure 4.4 Super-resolution microscopy of AzFPM labeled cells. Fluorescence SIM images of live AzFPM-labeled (125 μM) *C. glutamicum* **(A)** and *M. smegmatis* **(B)** reacted with DBCO-AF488. Cell walls were identified using a commercial peptidoglycan stain HADA. (Scale bars: 3 μm).

We next aimed to isolate the labeled structures to assess the specificity of our strategy. Cells were grown in media supplemented with 125 μM AzFPM. Azide-modified biomolecules were then labeled for enrichment by reacting with DBCO-biotin. Upon washing, the cells were lysed and the cell lysate was incubated with Dynabeads™ M-270 Streptavidin for enrichment. Enriched samples were analyzed by gel electrophoresis. We

observed glycans using a Pro-Emerald Q stain which allowed for detection of bands consistent with the expected molecular weight for LAM and LAM when cells were grown with AzFPM probes (**Figure 4.2C**) but not when cells were grown with AzFPA probes (**Figure 4.5**).

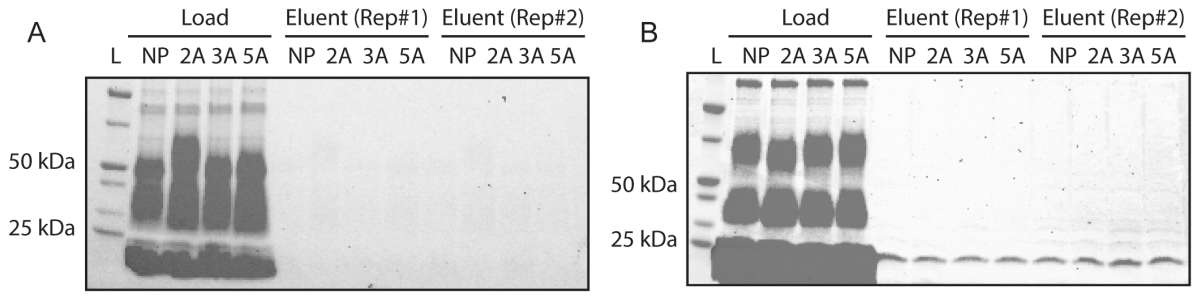

Figure 4.5 SDS-PAGE analysis of glycans from streptavidin enrichment upon biotin labeling following AzFPA labeling. Gel images of samples loaded onto streptavidin beads and eluted samples for cell *C. glutamicum* **(A)** and *M. smegmatis* **(B)** cells grown with all AzFPA probes and reacted with DBCO-biotin. Upon enrichment, samples were run on 10-20% gradient gels and were visualized via Pro-Emerald Q300. L: ladder, NP: no probe, 2A: 2-AzFPA, 3A: 3-AzFPA, 5A: 5-AzFPA. Data is representative of two independent experiments.

In *C. glutamicum* 4- and 6-AzFPM label the LAM best and in *M. smegmatis* 3- and 4-AzFPM label the LM robustly with minor labeling of the LAM. Though 2-AzFPM labeled *M. smegmatis*, it does not seem to label LM and LAM. We investigated the target of this labeling further in the following section. Additionally, though the LAM contains arabinose residues in addition to mannose residues, the AzFPA probes are selectively incorporated into the arabinogalactan. When we visualized the enriched samples using a highly sensitive silver stain, we did not observe any enriched proteins (**Figure 4.6**). This indicates that our probes are specifically processed by mannosyltransferases responsible for glycolipid biosynthesis and not protein-*O*-mannosyltransferases. This is of note as there is a known mycobacterial membrane associated protein-*O*-mannosyltransferase (Msmeg_5447) with sequence homology to eukaryotic protein-*O*-mannosyltransferases which accept lipid carrier substrates

(dolichyl-phosphate). The data we have obtained suggests that despite similarity in these biosynthetic precursors, AzFPM probes retain specificity for our targets. Dolichyl and polyprenyl donors vary in the degree of β-γ saturation, suggesting that preservation of this motif in farnesyl-bearing probes may be key to specific modification of glycolipid targets or selectivity could be dictated by probe localization at the membrane.

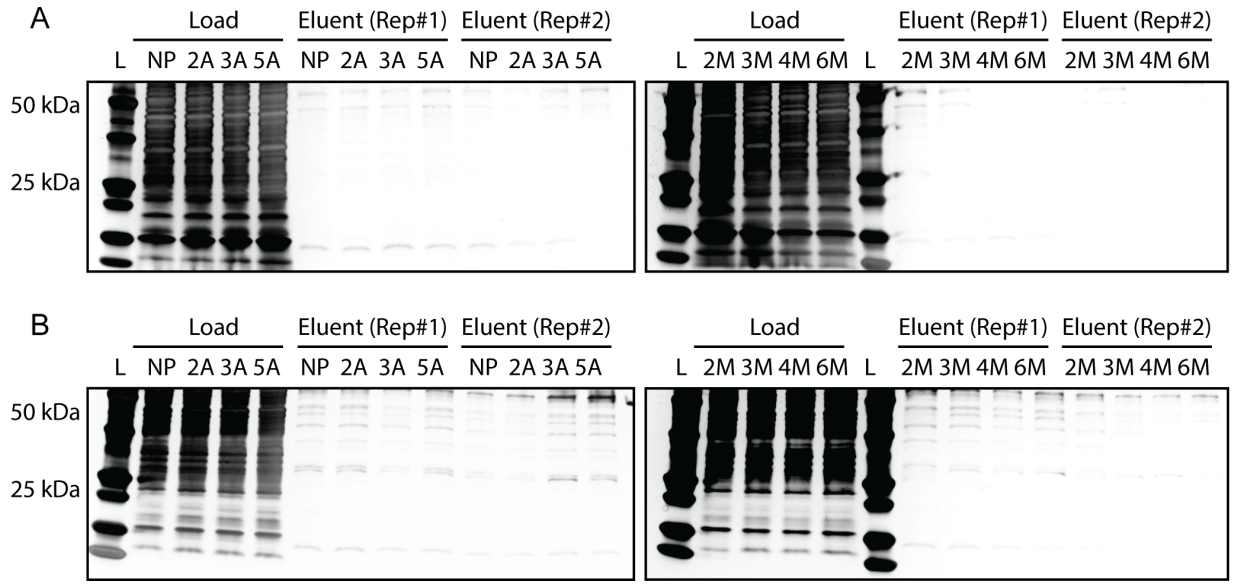

Figure 4.6 SDS-PAGE analysis of proteins from streptavidin enrichment upon biotin labeling following AzFPA or AzFPM labeling. Gel images of samples loaded onto streptavidin beads and eluted samples for cell *C. glutamicum* **(A)** and *M. smegmatis* **(B)** cells grown with all AzFPA and AzFPM probes and reacted with DBCO-biotin. Upon enrichment, samples were run on 10-20% gradient gels and were visualized via Silver Staining. L: ladder, NP: no probe, 2A: 2-AzFPA, 3A: 3-AzFPA, 5A: 5-AzFPA, 2M: 2-AzFPM, 3M: 3-AzFPM, 4M: 4-AzFPM, 6M: 6-AzFPM. Data is representative of two independent experiments.

4.3.3 Position of Azide Substitution Mediates Selectivity of Labeling for PIMs

Despite bright, membrane localized cellular labeling of *M. smegmatis* by 2-AzFPM, we were unable to detect probe incorporation into the LAM or LM. We therefore hypothesized that this probe is labeling another mannose-containing structure, phosphatidylinositol mannosides (PIMs). PIMs have been implicated as an important virulence factor and are a known ligand for C-type lectin dendritic cell (DC)-specific

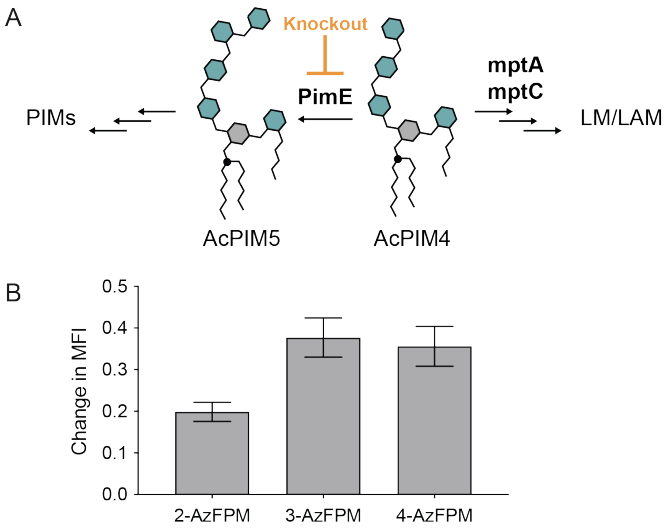

Figure 4.7 Demonstration of azide position dictating target glycan. (A) Point of divergence in the biosynthesis of PIMs vs LM and LM highlight point of PimE knockout. **(B)** Change in relative MFI calculated from flow cytometry analysis of AzFPM (125 μM) labeled *M. smegmatis* wild-type and ΔpimE cells treated with DBCO-AF647. Error bars denote the standard error of the mean (n=2).

intercellular adhesion molecule 3-grabbing nonintegrin (DC-SIGN).[39] We hypothesized that 2-AzFPM may be serving as a surrogate for DPM in the final steps of PIM biosynthesis. To test this, we acquired a knockout cell line of *M. smegmatis* lacking the lipid-dependent glycosyltransferase PimE (**Figure 4.7A**). This enzyme catalyzes the first step at which extended PIM biosynthesis and LAM/LM biosynthesis diverges.[40] *C. glutamicum* lacks extended PIMs and a PimE ortholog suggesting that this is why we did not see a similar discrepancy between staining and LAM/LM pulldown.[24, 27] Consistent with our hypothesis, we saw a stark decrease in staining with 2-AzFPM in *M. smegmatis ΔpimE* cells compared to wild-type, in contrast with a minor decrease in staining with our probes that show greater incorporation into LM and LAM, 3- and 4-AzFPM (**Figure 4.7B**). This demonstrates the first labeling of PIMs in wild-type *M. smegmatis* and showcases that biosynthetic incorporation probes not only enable monomer specificity in labeling but also biomolecule specificity based on the structure of the probe.

4.3.4 Understanding Biosynthesis of Mannose-Containing Glycans

We next applied these tools to investigate the sites of mannose-containing glycan biosynthesis *in cellulo*. It is known that peptidoglycan, arabinogalactan and mycolic acid

biosynthesis all occur at the poles and septa of actively dividing cells. To date, due to a lack of chemical tools, there have been no reports investigating the sites of LM and LAM biosynthesis and localization. To address this, we labeled *C. glutamicum* with the probe that stained to the greatest extent, 6-AzFPM, and visualized localization of incorporation after a short incubation via confocal fluorescence microscopy (**Figure 4.8**). The results were compared to our previously described 5-AzFPA probe as a control for known biosynthesis patterns. While 5-AzFPA labeled arabinose localized to the bacterial septa and poles at short time points, 6-AzFPM labeled mannose along the entire cell wall. This annular staining suggests that the localization of mannose-containing glycans is decoupled known areas of cell wall biosynthesis. To better understand the biosynthesis of these targets, we therefore generated C-terminal mCherry fusions of two *M. smegmatis* mannosyltransferases, one which forms ***α***-1,6 linkages, mptA (Msmeg_4241), and one which forms ***α***-1,2 branching linkages mptC (Msmeg_4247) (**Figure 4.9**). Using these strains, we assessed protein localization (**Figure 4.10**). It was observed that fluorescent proteins localized primarily at the septa, rather than displaying homogenous

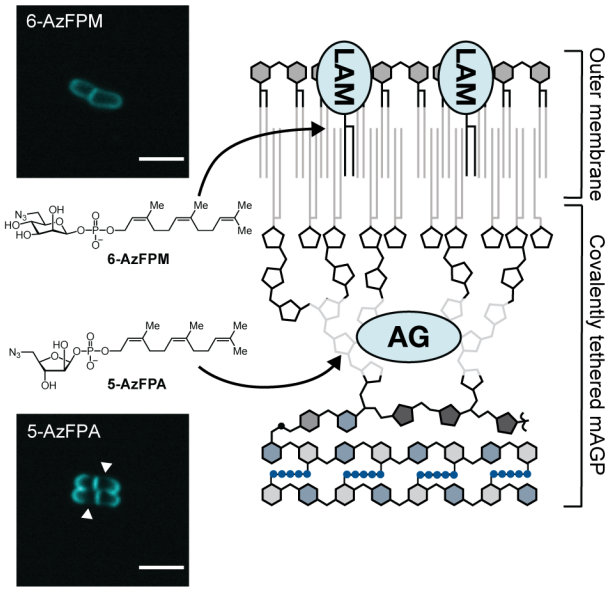

Figure 4.8 Analysis of localization of AzFPM and AzFPA probes was visualized via confocal fluorescence microscopy. Diagram points to corresponding structures that are labeled by each probe. Arabinogalactan (AG) is covalently connected to the peptidoglycan, whereas LAM structures are non-covalently embedded in the mycolic acid (MA) layer. mAGP: mycolyl-arabinogalactan-peptidogalactan, PM: plasma membrane.

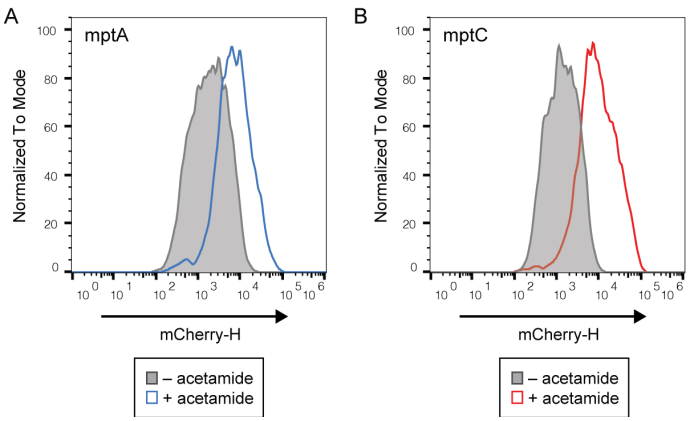

Figure 4.9 Flow cytometry histograms of mCherry-fusion expressing *M. smegmatis*. Histogram depicts data from bacteria containing mCherry-fusion plasmid, mptA **(A)** or mptC **(B)**, with or without induction with 0.2% acetamide for 4 h. Cells were stained with Syto-BC.

fluorescence along the entire cell wall. This observation that the localization of the labeled mannose-containing glycans is not coupled to the localization of the biosynthetic enzymes is suggestive that these structures are able to freely diffuse.

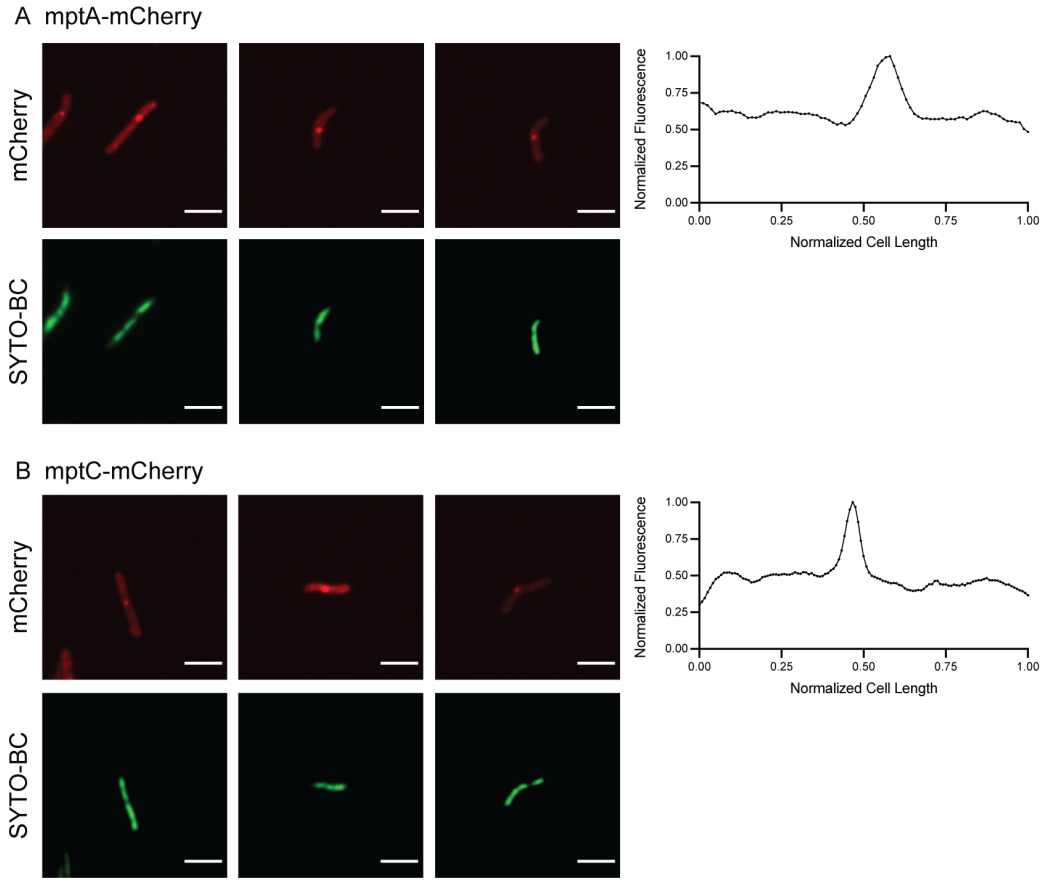

Figure 4.10 Fluorescence microscopy of mCherry-fusion expressing *M. smegmatis*. Representative images of bacteria containing mCherry-fusion plasmid, mptA **(A)** or mptC **(B)**, with or without induction with 0.2% acetamide for 4 h. Cells were stained with Syto-BC. Representative quantification of mCherry signal shown on the right.

4.3.5 Tracking Diffusion of Mannose-Containing Glycans

Unlike the components of the core cell wall structure, i.e. the inner mycolate and arabinogalactan, that are covalently linked to the peptidoglycan, the PIMs, LM and LAM are thought to be to be non-covalently embedded in the outer and inner lipid membranes. Based on our observations that the localization of our probes and the biosynthetic enzyme constructs are decoupled, we hypothesized that the LM and LAM are able to rapidly diffuse throughout the cell membrane in the tested model organisms. Using our chemical probes, we sought to test this hypothesis by tracking diffusion of these structures, employing fluorescence recovery after photobleaching (FRAP). In this FRAP experiment, a portion of the labeled cell is photobleached and then the cell is visualized over a recovery period. If the fluorophore is attached to a diffusible structure, the fluorescence at the photobleached site will be restored as fluorescent molecules that

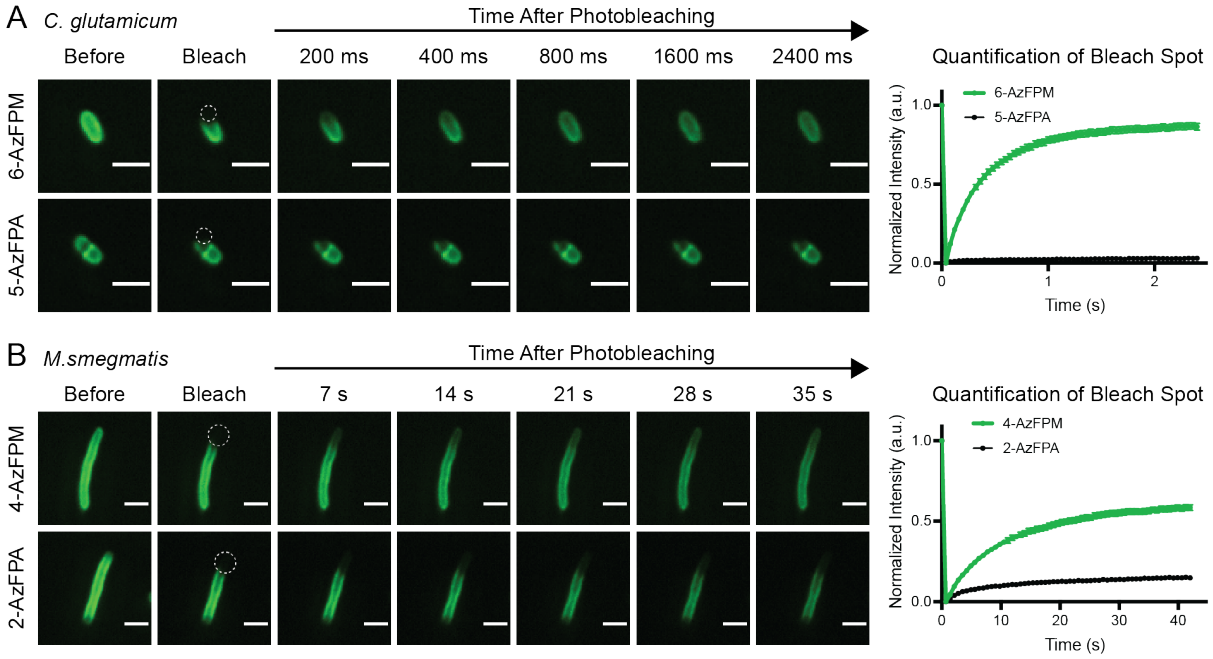

Figure 4.11 FRAP analysis to track glycan diffusion. Representative FRAP profiles FPM or FPA treated *C. glutamicum* (A) and *M. smegmatis* cells (B). White dashed circles indicate the areas of photobleaching. On the right fluorescence recovery traces for the cells shown. Error bars denote the standard error of the mean (n=50 cells).

have not been photobleached move freely to that area of the cell membrane. However, if the labeled structure is unable to diffuse (i.e., covalently tethered) or diffuses slowly, the photobleached region will remain dark over time and no recovery will be observed. We performed FRAP in both *C. glutamicum* and *M. smegmatis* with LAM and LM labeled by AzFPM and compared the results to arabinogalacan labeled by AzFPA probes (**Figure 4.11**). As anticipated, the covalently bound arabinan was unable to recover fluorescence at a site of photobleaching. In contrast, the mannosylated structures were able to diffuse and recover fluorescence. Moreover, the rate of diffusion varied between model organisms, with longer mycolic acids correlating with slower diffusion. This trend is consistent with previous work studying mycolate probes in different model organisms of *Mtb*.[41] Consistent with glycolipid labeling rather than glycoprotein labeling, upon formaldehyde fixation, which reacts with any available amines immobilizing labeled proteins, the labeled structures retain the ability to diffuse (**Figure 4.12**).

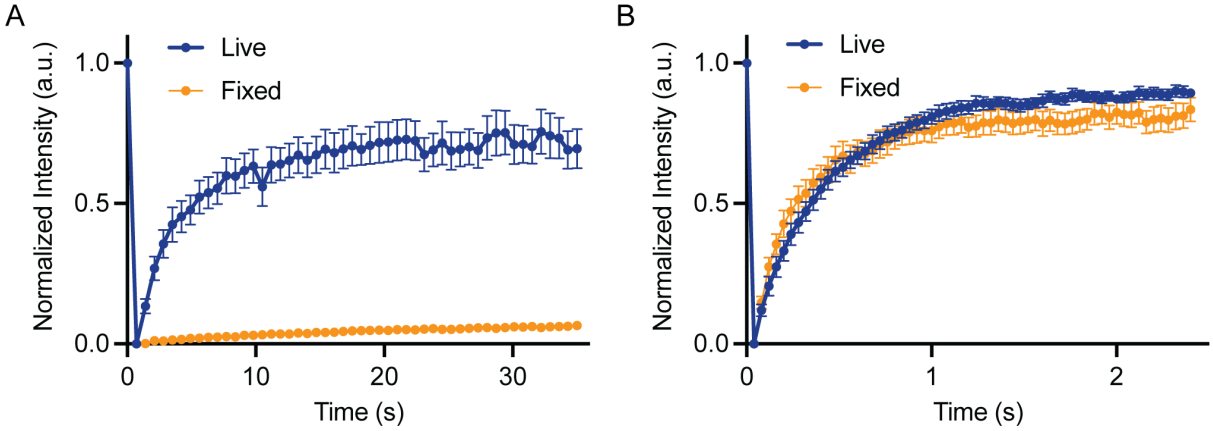

Figure 4.12 Fluorescence recovery traces for live and fixed cells. Normalized fluorescence recovery of photobleached area for *M. smegmatis* expressing fluorescent GFP-UGM comparing live cells to cells fixed in 4% Formaldhyde for 15 min at room temperature (A). Normalized fluorescence recovery of photobleached area for *C. glutamicum* labeled with 6-AzFPM and reacted with DBCO-AF488 comparing live cells to cells fixed in 4% Formaldhyde for 15 min at room temperature (B). Error bars denote the standard error of the mean of 10 cells.

To the best of our knowledge, this is the first direct visualization of LAM or LM diffusion on the surface of mycobacterial cells. Moreover, we performed similar studies using 2-AzFPM to label PIMs in *M. smegmatis*. These new reagents allowed for the direct observation of diffusion of this additional structure (**Figure 4.13**). We found that the rates of PIM diffusion were similar to those of the LAM and LM in *M. smegmatis* indicating that the organisms' cell wall structure and lipid anchor dictate the rate of diffusion, rather than the elaborated glycan (**Figure 4.14**).

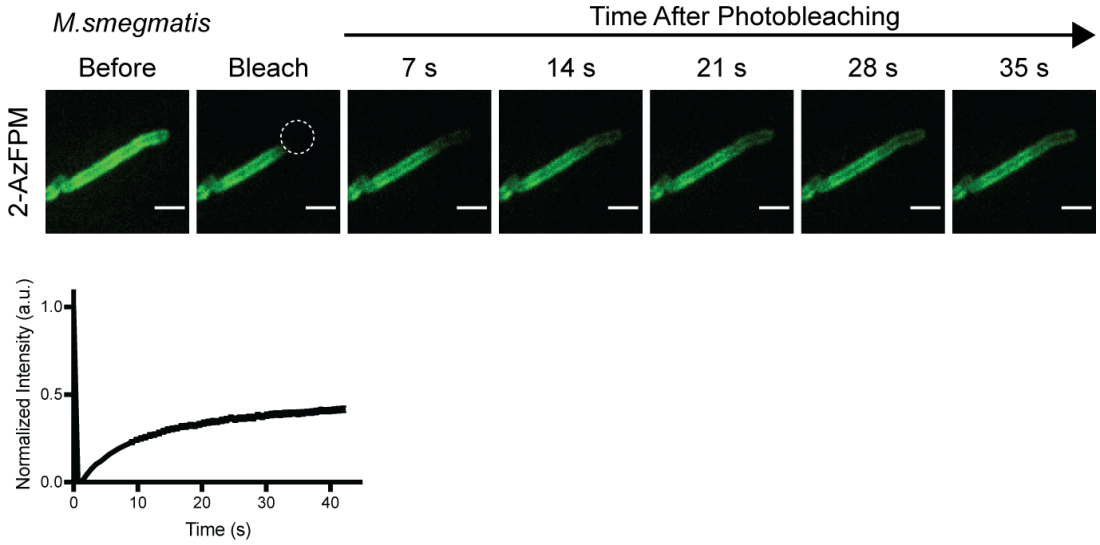

Figure 4.13 Representative FRAP profile of 2-AzFPM treated *M. smegmatis*. White dashed circles indicate the areas of photobleaching. Fluorescence recovery traces for the cells shown. Error bars denote the standard error of the mean (n=50 cells).

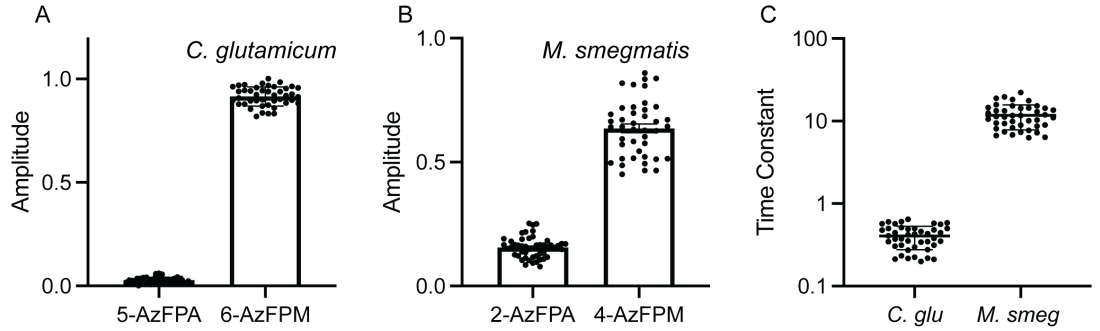

Figure 4.14 Quantification of fluorescence recovery. Timecourses were fit using a one-phase exponential association equation (ExpAssoc1) in OriginLab to calculate an amplitude (A-B) and time constant (C). Outliers two or more standard deviations from the mean were manually removed.

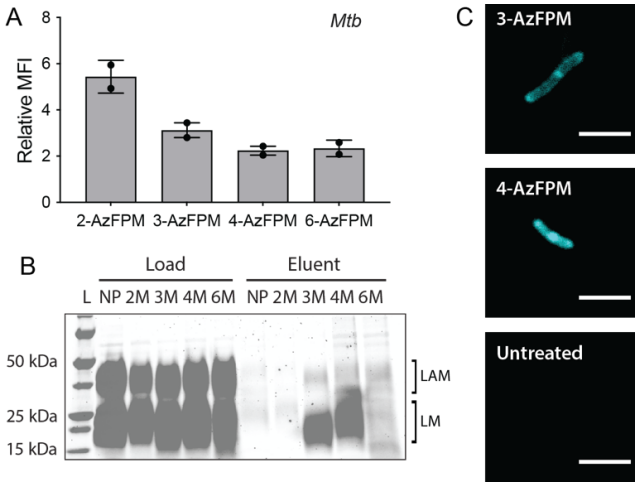

Figure 4.15 AzFPM probes label *Mtb*. (A) Flow cytometry analysis of AzFPM (125 μM) labeled *Mtb* treated with DBCO-AF647. Mean fluorescence intensity (MFI) was calculated using the geometric mean and plotted relative to a dye-only control. Error bars denote the standard error of the mean of two replicate experiments. **(B)** Streptavidin enriched labeled structures from AzFPM (125 μM) labeled *Mtb* reacted with DBCO-biotin. Load and eluent analyzed by SDS-PAGE using Pro-Q Emerald 300 glycan staining kit. **(C)** Confocal fluorescence microscopy images of *Mtb* grown with 3-AzFPA or 4-AzFPM (125 μM).

4.3.6 Applying FPM Probes in *Mtb*

Though much important mycobacterial research is performed in nonpathogenic and fast growing species within the genus,[42] we were interested in assessing the utility of our probes in *Mtb* itself. Towards this end, we first assessed incorporation by flow cytometry (**Figure 4.15A**). In *Mtb*, we observed a similar relationship between probe regioisomer and level of incorporation to what was seen in *M. smegmatis*. This is the first application of biosynthetic incorporation probes in *Mtb*. We next performed enrichment of labeled structures by clicking on DBCO-biotin and performing streptavidin pulldowns (**Figure 4.15B**). Again, similar results were observed as in *M. smegmatis*. Though bright staining is observed upon treatment with 2-AzFPM, we were unable to detect probe incorporation into the LAM or LM. In contract, 3-AzFPM and 4-AzFPM robustly label both the LAM and LM. We postulate that, similar to *M. smegmatis,* 2-AzFPM may be labeling PIMs in *Mtb*. Finally, we performed confocal microscopy on 3-AzFPM and 4-AzFPM as these probes labeled the LAM and LM (**Figure 4.15C**). Taken together, these data highlight the versatility of these probes in a number of bacteria within the suborder of *Corynebacterianeae* and we

anticipate these new tools will provide further insight into the role of mannose-containing glycans in pathogenic mycobacteria.

4.4 Conclusions

This work discloses a new suite of biosynthetic incorporation probes which can be used to visualize mannose containing glycans in mycobacteria. These results demonstrate the first visualization of the PIMs, LM and LAM on the cell surface of wild-type mycobacteria. When aiming to label specific glycan structures, probes that require extensive intracellular processing are susceptible to competition with endogenous substrate at multiple steps and divergence down undesired paths. By applying a biosynthetic incorporation strategy, we were able to specifically target immunomodulatory structures on the cell surface of mycobacteria, without engaging the variety of biochemical pathways involved in mannose metabolism. We observed that the site of labeling is dictated by the monosaccharide structure and the position of the installed azides. Moreover, these reagents allowed for tracking of glycan diffusion on the cell surface. This work demonstrates the generality and utility of biosynthetic incorporation as a glycan labeling method. The targeted GT-C class of glycosyltransferases exist in humans, yeast, archaea and bacteria. This highlights the potential for a wide range of future targets that can become accessible for modification by biosynthetic incorporation.

4.5 Experimental Details

4.5.1 Chemical Synthesis and Characterization

All chemicals were purchased from Sigma Aldrich unless otherwise stated. Dry solvents were obtained from a solvent purification system (Pure Process Technologies) under argon unless otherwise stated. DMF, MTBE and pyridine were used from sure seal bottles (Sigma Aldrich) without further purification. Triethylamine was distilled from CaH_2 just prior to use.

Analytical thin layer chromatography (TLC) was performed on EMD Millipore TM TLC silica gel 60 F254 (glass-backed). Plates were visualized under UV light and by staining with *p*-anisaldehyde stain with charring. Flash chromatography was performed on SiliCycle ® SiliaFlash ® P60 silica gel and Biotage ® Selekt using Biotage Sfär silica cartridges.

Nuclear magnetic resonance spectra were recorded on a 300 MHz spectrometer (acquired at 300 MHz for ^{1}H and 75 MHz for ^{13}C), 400 MHz spectrometer (acquired at 400 MHz for ^{1}H and 100 MHz for ^{13}C), a 500 MHz spectrometer (acquired at 500 MHz for ^{1}H and 125 MHz for ^{13}C) or a 600 MHz spectrometer (acquired at 600 MHz for ^{1}H and 151 MHz for ^{13}C). Chemical shifts are reported relative to residual solvent peaks in parts per million ($CHCl_3$: ^{1}H, 7.26, ^{13}C, 77.16; MeOH: ^{1}H, 3.31, ^{13}C, 49.00; C_6D_6: ^{1}H, 7.16, ^{13}C, 128.06). High-resolution mass spectra (HRMS) were obtained on an electrospray ionization-time of flight (ESI-TOF) mass spectrometer. All IR spectra were taken on an FT-IR Bruker Alpha II.

4.5.2 Strains and Growth Conditions

For bacterial assays, the strains employed include *Mycobacterium smegmatis mc²155*, *Corynebacterium glutamicum ATCC13032,* and *Mycobacterium tuberculosis* H37Rv. *M. smegmatis* was grown in Middlebrook 7H9 broth (HiMedia, Mumbai, India) supplemented with 0.2% (w/v) dextrose, 0.2% (v/v) glycerol, 0.5% bovine serum albumin (United States Biological, Salem, MA), catalase (4 mg/L) (Sigma-Aldrich), 15 mM sodium chloride and 0.05 % (v/v) Tween 80 in a shaking incubator at 37 °C. *C. glutamicum* was cultured in brain heart infusion (BHI) medium (BD, Franklin Lake, NJ) supplemented with 9% (w/v) sorbitol (BHIS) in a shaking incubator at 30 °C. *Mtb* was grown in Middlebrook 7H9 broth supplemented with 0.005% (w/v) oleic acid, 0.5% bovine serum albumin, 0.2% (w/v) dextrose, 0.2% (v/v) glycerol, catalase (4 mg/L), 15 mM sodium chloride, and 0.05% (v/v) Tween 80 in a shaking incubator at 37 °C. Generally, starter cultures were incubated at the relevant temperature with shaking until saturation. Cells were then diluted into fresh media and grown to mid to late-logarithmic phase (determined by OD_{600} measurement on a BioMate 3S Spectrophotometer).

4.5.3 Growth Inhibition Experiments

Experiments were performed following reported procedures.[33] In brief, a saturated culture was diluted down to the desired starting OD and plated in triplicate in a Corning black 96-well plate. Probes were added at the indicated concentration from DMSO stock solutions. *M. smegmatis* were grown with shaking at 37 °C for 24 h. *C. glutamicum* were grown with shaking at 30 °C for 16 h. Alamar Blue reagent (6 μL, Invitrogen) was added

to each well and the plates were incubated again for 1 h at 37 °C or 30 °C. The fluorescence emission of each well was then measured on a Tecan Infinite M1000 Pro microplate reader. Monitoring of resorufin fluorescence was achieved by exciting at 570 nm ± 5 nm and detecting at 585 nm ± 5 nm. Z-position was set to 2 mm, and the fluorimeter gain was optimized and then kept constant between plates. Data are reported in relative fluorescence units (RFU) normalized to untreated controls.

4.5.4 Flow Cytometry and Fluorescence Microscopy

Cells were plated from saturated starter cultures (OD_{600} = 0.05) in a Corning black 96-well plate. *M. smegmatis* was cultured in Middlebrook 7H9 containing 0.2% (v/v) glycerol and 0.05 % Tween 80. *C. glutamicum* was cultured in BHIS medium containing 0.05 % Tween 80. *E. coli* was cultured in LB liquid medium containing 0.05 % Tween 80. AzFPA derivatives were added to the desired concentrations from 85 mM stocks in DMSO. Cultures were grown to mid-log (OD_{600} = 1.0-1.2) at 37 °C or 30 °C with shaking. Samples were immediately prepared for flow cytometry or microscopy.

Cells were pelleted for 5 min at 3000 x g. The pellets were washed with ice-cold phosphate-buffered saline (PBS) supplemented with 0.05% Tween 80 (100 µL) once. Cells were washed an additional time with PBS supplemented with 0.05% Tween 80 and 0.5% (w/v) bovine serum albumin (BSA) once then taken up in fresh 7H9 media supplemented with 0.5% Tween 80 (150 µL). AFDye™ 647 DBCO (Click Chemistry Tools #1302) was added from a 10 mM stock solution in DMSO to a final concentration of 500 µM. The samples were stained for 2 h rotating at 37 °C. When 1 h and 45 min minutes had passed, 0.1 µL (1500X dilution) of SytoBC™ Green Fluorescent Nucleic Acid Stain (ThermoFischer #S34855) was added for a 15-minute incubation period. The

stained cells were pelleted for 5 min at 3000 x g. The supernatant was removed, and the pellet was washed with PBS supplemented with 0.05% Tween 80 and 0.5% (w/v) BSA twice.

For flow cytometry, stained cell pellets were taken up in 4% paraformaldehyde in PBS to be fixed at room temperature for 20 min. Following fixation, cells were pelleted then taken up in sterile PBS supplemented with 0.05% Tween 80 in flow tubes and analyzed using an Attune NxT Flow Cytometer (405 nm, 488 nm, 561 nm, and 640 nm lasers). 10,000 cells were counted at the low flow rate. Flow cytometry analysis was performed in triplicate, representative scatter plots are shown. The unstained controls were analyzed first to set gates. Data were analyzed using the FlowJo software package (FlowJo LLC). Mean fluorescence intensity was calculated using a geometric mean.

For analysis by microscopy, stained cell pellets were taken up in 7H9 supplemented with 0.5% Tween 80 (100 uL). Each sample was spotted onto a glass-bottomed microwell dish (MatTek corporation # P35G-1.5-14-C) and covered with a pre-cooled and 0.6% (w/v) agarose pad. Images were collected on a RPI spinning-disk confocal microscope (100x oil immersion lens, 1.4 NA). Brightness and contrast were identically adjusted with the open-source Fiji distribution of ImageJ. Images were then converted to an RGB format to preserve normalization and then assembled into panels.

4.5.5 Super-Resolution Microscopy

For SIM, stained cell were pellets and taken up in taken up in 7H9 supplemented with 0.5% Tween 80 and 1% w/v DABCO (1,4-diazabicyclo[2.2.2]octane) as an antifading reagent. Each sample was spotted onto a glass-bottomed microwell dish, and covered with a pre-cooled 1% (w/v) agarose pad. Images were collected on an Applied

Precision DeltaVision-OMXv4 Super-Resolution Microscope (60x/1.42 NA oil immersion lens, sequential imaging on two sCMOS cameras). SIM reconstruction and dwarp-based image alignments were performed with Applied Precision softWoRx. Multi-color Image alignments were calculated from an Applied Precision grid test slide, checked with TetraSpeck beads (0.1 μm, Molecular Probes), and verified with an Argo-SIM test slide (Axiom Optics) prior to data collection. Brightness and contrast were identically adjusted with the open-source Fiji distribution of ImageJ. Images were then converted to an RGB format to preserve normalization and then assembled into panels.

4.5.6 Dynabead Streptavidin Enrichment

Cells were grown from saturated starter cultures (OD_{600} = 0.05) in 10 mL culture flasks under standard conditions. AzFPA and AzFPM derivatives were added to the desired concentrations from 85 mM stocks in DMSO. Cells were grown for 24 h at 37 °C (*M. smegmatis*) or 9 h at 30 °C (*C. glutamicum*). Cells were pelleted for 5 min at 3000 x g, normalizing across samples by OD. The pellets were washed with ice-cold PBS supplemented with 0.05% Tween 80 once. Cells were washed an additional time with PBS supplemented with 0.05% Tween 80 and 0.5% (w/v) BSA once then taken up in fresh 7H9 media supplemented with 0.5% Tween 80. DBCO-PEG_4-Biotin (Sigma Aldrich) was added from a 10 mM stock solution in DMSO to a final concentration of 250 μM. The samples reacted for 2 h rotating at 37 °C. The stained cells were pelleted for 5 min at 3000 x g. The supernatant was removed, and the pellet was washed with PBS supplemented with 0.05% Tween 80 and 0.5% (w/v) BSA twice.

Cell pellets were resuspended in 1x RIPA lysis buffer (diluted from 10x stock) and disrupted by bead beating (5 x 30 s separated by 5 min off intervals on ice). The lysate

was removed from the beads via centrifugation. Dynabeads™ M-270 Streptavidin (Invitrogen, REF#65305) were washed with PBS three times (50 uL). Cell lysate was added to two sets of beads (250 uL). A fraction of the cell lysate was saved as load sample. Bead suspensions were incubated overnight at 4 °C with rotation. Using a magnetic tube rack, supernatant was collected as unbound samples. Beads were washed with PBS three times (250 uL). 50 uL elution buffer (1X SDS loading dye, 1X BXT in MQ H2O) was added to the beads and heated to 95 °C for 10 min. Supernatant was collected as elution samples.

LM and LAM were separated by SDS-polyacrylamide gel electrophoresis (10 to 20% gradient gel) and visualized using the ProQ Emerald300 carbohydrate staining kit (Molecular Probes).

4.5.7 Fluorescence Recovery After Photobleaching

Samples were prepared as previously described for imaging. Each sample was spotted onto a glass-bottomed microwell dish (MatTek corporation # P35G-1.5-14-C) and covered with a pre-cooled and 1% (w/v) agarose pad. Images were collected on an Andor Revolution spinning-disk confocal microscope (100x oil immersion lens, 1.49 NA). Cells were photobleached with a dwell time of 250 μs, twice. Images were collected prior to bleaching and following bleaching at the reported interval. Brightness and contrast were identically adjusted with the open-source Fiji distribution of ImageJ. Images were then converted to an RGB format to preserve normalization and then assembled into panels. Recovery was calculated by normalizing using the following equation as previously reported.[43] The values were initialized at 1 and immediately after

photobleaching, the value was 0. The resulting timecourses were fit according to ExpAssoc1 in OriginLab.

$$F(t)_{norm} = \frac{F(t)_{ROI} - F_{background}}{F(t)_{cell} - F_{background}} \times \frac{F(i)_{cell} - F_{background}}{F(i)_{ROI} - F_{background}}$$

4.5.8 Cloning Vectors Encoding C-terminal mCherry *M. smegmatis* Mannosyltransferase Fusion Proteins

To generate C-termial mCherry fusions of *M. smegmatis* mannosyltransferases, a linker-mCherry containing pLAM12 vector (codon optimized for *M. smegmatis*) was used as previously described.[44] Each mannosyltransferase gene was amplified from isolated genomic DNA from *M. smegmatis* mc²155. DNA fragments were joined to a linearized pLAM12-mcherry vector via isothermal annealing with Gibson Assembly master mix. Assembled plasmids were transformed into DH5*α E. coli* and vector identity was verified by sanger sequencing analysis by Quintaro Biosciences. Plasmids were then transformed into electrocompetent *M. smegmatis* mc²155 for homologous expression.

Table 4.1 Primers used to generate mCherry fusions of *M. smegmatis* mannosyltransferases.

Template	Primers
Genomic DNA (targeting MSMEG_4241, mptA)	5'-GATAAGAGAAAGGGAGTCCAatgacaccgacggaaacccac-3' 5'- GGACCCGGACGCACCgctcgccgtcgcctcag-3'
Genomic DNA (targeting MSMEG_4247, mptC)	5'-GATAAGAGAAAGGGAGTCCAatgagtaagcggcagtcgcc-3' 5'- GGACCCGGACGCACCgccgcgtgcgagcg-3'
pLAM12-mCherry vector	5'-GGTGCGTCCGGGTCC-3' 5'-TGGACTCCCTTTCTCTTATCGGGTG-3'

4.5.9 mCherry *M. smegmatis* Mannosyltransferase Fusion Protein Microscopy

M. smegmatis harboring Mpt-mCherry fusion plasmids was cultured in complete 7H9 + ADC + 0.05% Tween- 80 and induced in early logarithmic phase, with 0.2% acetamide for 4 hours 37°C. Syto-BC, 0.2 µL (5000X dilution), was added to cultures for

the final 10 min of growth. For analysis by microscopy, cell pellets were taken up in 7H9 supplemented with 0.5% Tween 80 (100 uL). Each sample was spotted onto a glass-bottomed microwell dish (MatTek corporation # P35G-1.5-14-C) and covered with a pre-cooled and 1% (w/v) agarose pad. Images were collected on a spinning-disk confocal microscope (100x oil immersion lens, 1.4 NA). Brightness and contrast were identically adjusted with the open-source Fiji distribution of ImageJ. Images were then converted to an RGB format to preserve normalization and then assembled into panels.

4.5.10 *Mtb* Flow Cytometry and Microscopy

Experiments in *Mtb* were performed according to the following procedure. Cells were diluted from a late-logarithmic phase starter culture to OD 0.05 in a non-tissue culture treated multiwell plate in Middlebrook 7H9 supplemented with 0.03% casitone (DIBCO), 0.08% sodium chloride, and 0.4% dextrose. AzFPM derivatives were added to cultures at 125 uM from an 8.5 mM stock in DMSO. Cultures were grown for 72 hours (three doubling times). Samples were immediately prepared for flow cytometry or microscopy.

Cells were pelleted for 5 min at 3000 x g. The pellets were washed phosphate-buffered saline (PBS) supplemented with 0.05% Tween 80 (500 µL) once. Cells were washed an additional time with PBS supplemented with 0.05% Tween 80 and 0.5% (w/v) bovine serum albumin (BSA) once then taken up in fresh 7H9 media supplemented with 0.5% Tween 80 (500 µL). AFDye™ 647 DBCO (Click Chemistry Tools #1302) was added from a 10 mM stock solution in DMSO to a final concentration of 250 µM. The samples were stained for one hour in a shaking incubator at 37 °C. The stained cells were pelleted for 5 min at 3000 x g. The supernatant was removed, and the

pellet was washed with PBS supplemented with 0.05% Tween 80 and 0.5% (w/v) BSA twice. To remove Mtb from the BSL3, the cells were resuspended in 4% paraformaldehyde in PBS and fixed for one hour at room temperature. Following fixation, cells were pelleted and taken up in PBS supplemented with 0.5% Tween-80.

For flow cytometry, cells were aliquoted in flow tubes and analyzed using an Attune NxT Flow Cytometer (405 nm, 488 nm, 561 nm, and 640 nm lasers). 10,000 cells were counted at the low flow rate. Flow cytometry analysis was performed in duplicate. The unstained controls were analyzed first to set gates. Data were analyzed using the FlowJo software package (FlowJo LLC). Mean fluorescence intensity was calculated using a geometric mean.

For microscopy, 100 µl of each sample was spotted onto a glass-bottomed microwell dish (MatTek corporation # P35G-1.5-14-C) and covered with a pre-cooled and 1% (w/v) agarose pad. Images were collected on an RPI spinning-disk confocal microscope (100x oil immersion lens, 1.4 NA). Brightness and contrast were identically adjusted with the open-source Fiji distribution of ImageJ. Images were then converted to an RGB format to preserve normalization and then assembled into panels.

4.6 References

1. Chakaya, J.; Petersen, E.; Nantanda, R.; Mungai, B. N.; Migliori, G. B.; Amanullah, F.; Lungu, P.; Ntoumi, F.; Kumarasamy, N.; Maeurer, M.; Zumla, A., The WHO Global Tuberculosis 2021 Report - not so good news and turning the tide back to End TB. *Int J Infect Dis* **2022,** *124 Suppl 1*, S26-S29.

2. Ding, C.; Hu, M.; Guo, W.; Hu, W.; Li, X.; Wang, S.; Shangguan, Y.; Zhang, Y.; Yang, S.; Xu, K., Prevalence trends of latent tuberculosis infection at the global, regional, and country levels from 1990-2019. *Int J Infect Dis* **2022,** *122*, 46-62.

3. Chandra, P.; Grigsby, S. J.; Philips, J. A., Immune evasion and provocation by Mycobacterium tuberculosis. *Nat Rev Microbiol* **2022,** *20* (12), 750-766.

4. Mir, M. A.; Mir, B.; Kumawat, M.; Alkhanani, M.; Jan, U., Manipulation and exploitation of host immune system by pathogenic Mycobacterium tuberculosis for its advantage. *Future Microbiol* **2022,** *17*, 1171-1198.

5. Kumar, A.; Shivangi; Agarwal, P.; S. Meena, L., Interconnection of Mycobacterium tuberculosis with host immune system. *Journal of Respiratory Diseases and Medicine* **2020,** *2* (2).

6. Flynn, J. L.; Chan, J., Immune evasion by Mycobacterium tuberculosis: living with the enemy. *Curr Opin Immunol* **2003,** *15* (4), 450-5.

7. Liu, C. F.; Tonini, L.; Malaga, W.; Beau, M.; Stella, A.; Bouyssie, D.; Jackson, M. C.; Nigou, J.; Puzo, G.; Guilhot, C.; Burlet-Schiltz, O.; Riviere, M., Bacterial protein-O-mannosylating enzyme is crucial for virulence of Mycobacterium tuberculosis. *Proc Natl Acad Sci U S A* **2013,** *110* (16), 6560-5.

8. Zhou, K. L.; Li, X.; Zhang, X. L.; Pan, Q., Mycobacterial mannose-capped lipoarabinomannan: a modulator bridging innate and adaptive immunity. *Emerg Microbes Infect* **2019,** *8* (1), 1168-1177.

9. Briken, V.; Porcelli, S. A.; Besra, G. S.; Kremer, L., Mycobacterial lipoarabinomannan and related lipoglycans: from biogenesis to modulation of the immune response. *Mol Microbiol* **2004,** *53* (2), 391-403.

10. Barnes, P. F.; Chatterjee, D.; Abrams, J. S.; Lu, S.; Wang, E.; Yamamura, M.; Brennan, P. J.; Modlin, R. L., Cytokine production induced by Mycobacterium tuberculosis lipoarabinomannan. Relationship to chemical structure. *The Journal of Immunology* **1992,** *149* (2), 541-547.

11. Torrelles, J. B.; Schlesinger, L. S., Diversity in Mycobacterium tuberculosis mannosylated cell wall determinants impacts adaptation to the host. *Tuberculosis (Edinb)* **2010,** *90* (2), 84-93.

12. Fukuda, T.; Matsumura, T.; Ato, M.; Hamasaki, M.; Nishiuchi, Y.; Murakami, Y.; Maeda, Y.; Yoshimori, T.; Matsumoto, S.; Kobayashi, K.; Kinoshita, T.; Morita, Y. S., Critical roles for lipomannan and lipoarabinomannan in cell wall integrity of mycobacteria and pathogenesis of tuberculosis. *mBio* **2013,** *4* (1), e00472-12.

13. Hayakawa, E.; Tokumasu, F.; Nardone, G. A.; Jin, A. J.; Hackley, V. A.; Dvorak, J. A., A Mycobacterium tuberculosis-derived lipid inhibits membrane fusion by modulating lipid membrane domains. *Biophys J* **2007,** *93* (11), 4018-30.

14. Kaur, D.; Lowary, T. L.; Vissa, V. D.; Crick, D. C.; Brennan, P. J., Characterization of the epitope of anti- lipoarabinomannan antibodies as the terminal hexaarabinofuranosyl motif of mycobacterial arabinans. *Microbiology* **2002,** *148*, 3049-3057.

15. Nakayama, H.; Oshima, E.; Hotta, T.; Hanafusa, K.; Nakamura, K.; Yokoyama, N.; Ogawa, H.; Takamori, K.; Iwabuchi, K., Identification of anti-lipoarabinomannan antibodies against mannan core and their effects on phagocytosis of mycobacteria by human neutrophils. *Tuberculosis (Edinb)* **2022,** *132*, 102165.

16. Bertozzi, C. R.; Kiessling, L. L., Chemical Glycobiology. *Science* **2001,** *291*, 2357-2364.

17. Andolina, G.; Wei, R.; Liu, H.; Zhang, Q.; Yang, X.; Cao, H.; Chen, S.; Yan, A.; Li, X. D.; Li, X., Metabolic Labeling of Pseudaminic Acid-Containing Glycans on Bacterial Surfaces. *ACS Chem Biol* **2018,** *13* (10), 3030-3037.

18. Barrett, K.; Dube, D. H., Chemical Tools to Study Bacterial Glycans: A Tale from Discovery of Glycoproteins to Disruption of Their Function. *Israel Journal of Chemistry* **2022**.

19. Dube, D. H.; Bertozzi, C. R., Metabolic oligosaccharide engineering as a tool for glycobiology. *Curr Opin Chem Biol* **2003,** *7* (5), 616-25.

20. Liang, H.; DeMeester, K. E.; Hou, C. W.; Parent, M. A.; Caplan, J. L.; Grimes, C. L., Metabolic labelling of the carbohydrate core in bacterial peptidoglycan and its applications. *Nat Commun* **2017,** *8*, 15015.

21. Zheng, Q.; Chang, P. V., Shedding Light on Bacterial Physiology with Click Chemistry. *Israel Journal of Chemistry* **2022**.

22. Gilormini, P. A.; Batt, A. R.; Pratt, M. R.; Biot, C., Asking more from metabolic oligosaccharide engineering. *Chem Sci* **2018,** *9* (39), 7585-7595.

23. Banahene, N.; Kavunja, H. W.; Swarts, B. M., Chemical Reporters for Bacterial Glycans: Development and Applications. *Chem Rev* **2022,** *122* (3), 3336-3413.

24. Cashmore, T. J.; Klatt, S.; Yamaryo-Botte, Y.; Brammananth, R.; Rainczuk, A. K.; McConville, M. J.; Crellin, P. K.; Coppel, R. L., Identification of a Membrane Protein

Required for Lipomannan Maturation and Lipoarabinomannan Synthesis in Corynebacterineae. *J Biol Chem* **2017,** *292* (12), 4976-4986.

25. Liang, H.; DeMeester, K. E.; Hou, C. W.; Parent, M. A.; Caplan, J. L.; Grimes, C. L., Metabolic labelling of the carbohydrate core in bacterial peptidoglycan and its applications. *Nature Communications* **2017,** *8*.

26. Nilsson, I.; Grove, K.; Dovala, D.; Uehara, T.; Lapointe, G.; Six, D. A., Molecular characterization and verification of azido-3,8-dideoxy-d-manno-oct-2-ulosonic acid incorporation into bacterial lipopolysaccharide. *J Biol Chem* **2017,** *292* (48), 19840-19848.

27. Rainczuk, A. K.; Yamaryo-Botte, Y.; Brammananth, R.; Stinear, T. P.; Seemann, T.; Coppel, R. L.; McConville, M. J.; Crellin, P. K., The lipoprotein LpqW is essential for the mannosylation of periplasmic glycolipids in Corynebacteria. *J Biol Chem* **2012,** *287* (51), 42726-38.

28. Wang, Y.; Li, L.; Yu, J.; Hu, H.; Liu, Z.; Jiang, W.; Xu, W.; Guo, X.; Wang, F.; Sheng, J., Imaging of Escherichia coli K5 and glycosaminoglycan precursors via targeted metabolic labeling of capsular polysaccharides in bacteria. *Science Advances* **2023,** *9*, ead4770.

29. Yi, W.; Liu, X.; Li, Y.; Li, J.; Xia, C.; Zhou, G.; Zhang, W.; Zhao, W.; Chen, X.; Wang, P. G., Remodeling bacterial polysaccharides by metabolic pathway engineering. *Proc Natl Acad Sci U S A* **2009,** *106* (11), 4207-12.

30. Hodges, H.; Obeng, K.; Avanzi, C.; Ausmus, A. P.; Angala, S. K.; Kalera, K.; Palcekova, Z.; Swarts, B. M.; Jackson, M., Azido Inositol Probes Enable Metabolic Labeling of Inositol-Containing Glycans and Reveal an Inositol Importer in Mycobacteria. *ACS Chem Biol* **2023,** *18* (3), 595-604.

31. Morita, Y. S.; Fukuda, T.; Sena, C. B.; Yamaryo-Botte, Y.; McConville, M. J.; Kinoshita, T., Inositol lipid metabolism in mycobacteria: biosynthesis and regulatory mechanisms. *Biochim Biophys Acta* **2011,** *1810* (6), 630-41.

32. Patterson, J. H.; Waller, R. F.; Jeevarajah, D.; Billman-Jacobe, H.; McConville, M., J., Mannose metabolism is required for mycobacterial growth. *Biochem. J.* **2003,** *372*, 77-86.

33. Calabretta, P. J.; Hodges, H. L.; Kraft, M. B.; Marando, V. M.; Kiessling, L. L., Bacterial Cell Wall Modification with a Glycolipid Substrate. *J Am Chem Soc* **2019,** *141* (23), 9262-9272.

34. Marando, V. M.; Kim, D. E.; Calabretta, P. J.; Kraft, M. B.; Bryson, B. D.; Kiessling, L. L., Biosynthetic Glycan Labeling. *J Am Chem Soc* **2021,** *143* (40), 16337-16342.

35. Marando, V. M.; Kim, D. E.; Kiessling, L. L., Biosynthetic incorporation for visualizing bacterial glycans. *Methods Enzymol* **2022,** *665*, 135-151.

36. Kaur, D.; Berg, S.; Dinadayala, P.; Gicquel, B.; Chatterjee, D.; McNeil, M. R.; Vissa, V. D.; Crick, D. C.; Jackson, M.; Brennan, P. J., Biosynthesis of mycobacterial lipoarabinomannan: role of a branching mannosyltransferase. *Proc Natl Acad Sci U S A* **2006,** *103* (37), 13664-9.

37. Mishra, A. K.; Krumbach, K.; Rittmann, D.; Appelmelk, B.; Pathak, V.; Pathak, A. K.; Nigou, J.; Geurtsen, J.; Eggeling, L.; Besra, G. S., Lipoarabinomannan biosynthesis in Corynebacterineae: the interplay of two alpha(1-->2)-mannopyranosyltransferases MptC and MptD in mannan branching. *Mol Microbiol* **2011,** *80* (5), 1241-59.

38. Liu, F.; Chen, H. M.; Armstrong, Z.; Withers, S. G., Azido Groups Hamper Glycan Acceptance by Carbohydrate Processing Enzymes. *ACS Cent Sci* **2022,** *8* (5), 656-662.

39. Driessen, N. N.; Ummels, R.; Maaskant, J. J.; Gurcha, S. S.; Besra, G. S.; Ainge, G. D.; Larsen, D. S.; Painter, G. F.; Vandenbroucke-Grauls, C. M.; Geurtsen, J.; Appelmelk, B. J., Role of phosphatidylinositol mannosides in the interaction between mycobacteria and DC-SIGN. *Infect Immun* **2009,** *77* (10), 4538-47.

40. Morita, Y. S.; Sena, C. B.; Waller, R. F.; Kurokawa, K.; Sernee, M. F.; Nakatani, F.; Haites, R. E.; Billman-Jacobe, H.; McConville, M. J.; Maeda, Y.; Kinoshita, T., PimE is a polyprenol-phosphate-mannose-dependent mannosyltransferase that transfers the fifth mannose of phosphatidylinositol mannoside in mycobacteria. *J Biol Chem* **2006,** *281* (35), 25143-55.

41. Rodriguez-Rivera, F. P.; Zhou, X.; Theriot, J. A.; Bertozzi, C. R., Visualization of mycobacterial membrane dynamics in live cells. *J Am Chem Soc* **2017,** *139* (9), 3488-3495.

42. Sparks, I. L.; Derbyshire, K. M.; Jacobs Jr, W. R.; Morita, Y. S., Mycobacterium smegmatis: The Vanguard of Mycobacterial Research. *Journal of Bacteriology* **2023,** *205* (1), 1-16.

43. Day, C. A.; Kraft, L. J.; Kang, M.; Kenworthy, A. K., Analysis of protein and lipid dynamics using confocal fluorescence recovery after photobleaching (FRAP). *Curr Protoc Cytom* **2012,** *Chapter 2*, Unit2 19.

44. Hodges, H. L.; Brown, R. A.; Crooks, J. A.; Weibel, D. B.; Kiessling, L. L., Imaging mycobacterial growth and division with a fluorogenic probe. *Proc Natl Acad Sci U S A* **2018,** *115* (20), 5271-5276.

Chapter 5: Mechanistic Investigation into N-QTF, Harnessing Carbamate-Containing Probes

Contributions:
Carbamate-containing compounds were synthesized by Victoria M. Marando. Compound 5.14 was prepared by Teddy C. Warner. Cell-based assays were performed by Victoria M. Marando and Alby Joseph. Research designed by Victoria M. Marando and Laura L. Kiessling.

5.1 Abstract

Approximately one-quarter of the world's population is infected with *Mycobacterium tuberculosis* (*Mtb*), the etiological agent of tuberculosis (TB). Most current antibiotics administered to treat TB target enzymes involved in cell envelope biosynthesis. However, new *Mtb* strains have emerged that are multidrug-resistant and potentially lack these target enzymes, emphasizing that the pathogenesis and persistence of *Mtb* is not yet fully understood. To address these challenges and reveal critical biological insights into *Mtb* infection, there is a need for new tools, with-characterized biological activity, to study mycobacterial cell wall assembly enzymes. In particular, the mycolyltransferases play a central role in the biosynthesis of key components of the mycobacterial outer membrane, including trehalose dimycolate (TDM) and mycolylarabinogalactan (mAG). Our group has previously disclosed a series of fluorogenic probes that report on mycolyltransferase activity in live cells. These probes function based on enzyme-mediated ester hydrolysis to release a fluorophore. In this work, carbamate-containing probes were rationally designed to form a more stable covalent adduct to form upon enzymatic processing. These probes enable better characterization of *in cellulo* targets of the ester-containing probes. Testing a collection of probes with varying carbonyl reactivity highlights fundamental physical organic differences principles and will enhance our understanding of mycobacterial cell wall assembly enzymes.

5.2 Introduction

Mycobacterium tuberculosis, *Mtb*, remains one of the world's most deadly single infectious agents.[1] The increased emergence of multi-drug-resistant TB underscores the urgent need for novel strategies to drug this pathogen.[2] Many antibiotics, including current *Mtb* treatments, target the enzymes involved in cell wall biosynthesis.[3-6] Mycobacterial cell envelope biogenesis and remodeling are dynamic processes and though they are critical to infectivity and thus targeted by antibiotics, these processes are also central resistance to current front-line antibiotics.[7-9] However, the enzymes responsible for *Mtb* cell wall assembly are often poorly characterized as their removal or manipulation in genetic models is deleterious to the organism.[10-11] Without sufficient characterization, it remains unclear to what extent targeting cell wall enzymes with other therapeutics, in isolation or in combination, would lead to more efficacious treatments.

To overcome this barrier, chemical approaches have been powerful tools to evaluate mycobacterial membrane biosynthesis and remodeling dynamics.[12-13] Chemical probes have enabled many important discoveries ranging from fundamental *Mtb* biology to understanding mechanisms of resistance.[14-16] Previously, our group disclosed a fluorogenic substrate analog probe to reveal real-time mycomembrane dynamics and illuminate mycobacterial growth and division.[14, 17] This probe was designed to leverage the biosynthetic activity of secreted mycolyltransferases that assemble the outermost bilayer encasing mycobacteria via the transfer of trehalose monomycolate (TMM).[18] These enzymes function via a catalytic triad beginning with a neighboring group-assisted nucleophilic attack by serine and formation of an acyl-enzyme intermediate, followed by attack of a second substrate facilitating transfer to assemble the cell wall.[19-21]

The quencher-trehalose-fluorophore (QTF) probe was designed to exploit this mechanism by installing a quencher with a tandem fluorophore on the substrate which can be decoupled upon enzymatic processing to enable fluorescence. To improve hydrolytic stability, a second-generation probe was designed with a single atom substitution at the trehalose C6-position to yield an amide-containing derivative, N-QTF.[14] This probe has already proved useful in visualizing spatial and temporal fluorogenic phenotypes in response to antibiotic stress. The key functionality of QTF and N-QTF is the ester moiety that reacts with the enzymes of interest. The resulting acyl-enzyme intermediates are labile and therefore are hydrolyzed rather than being retained in the enzyme active site or transferred. There remains a need for a fluorogenic probe that is retained in the active site of mycobacterial cell wall assembly enzymes to enable tracking and understanding of these important drug targets.

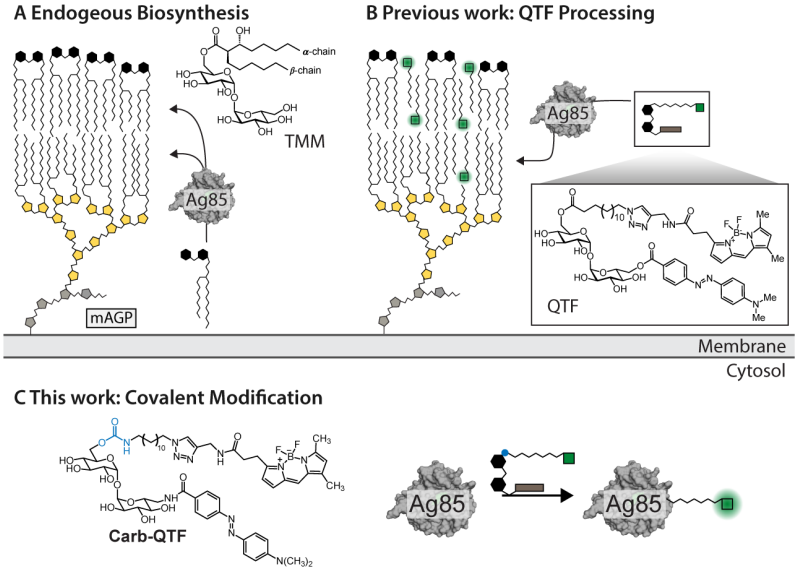

Figure 5.1 Overview schematic of endogenous biosynthetic donor and probes. (A) Endogenous biosynthesis of the mAGP is facilitated by transfer of mycolic acids from a TMM donor. **(B)** QTF was designed to mimic the structure of TMM and enable real-time reporting on enzyme activity. **(C)** Covalent probe designed based on QTF scaffold.

Herein, we design and employ a carbamate-containing QTF-based probe with attenuated reactivity that was rationally designed to enable stable covalent modification of the enzymes responsible for fluorogenesis of N-QTF *in cellulo* (**Figure 5.1**). We envisioned this probe to be useful for mechanistic investigations to verify the cellular

target of N-QTF and track enzymes. As expected based on fundamental carbonyl electrophilicity trends, substitution of the reactive ester with a carbamate resulted in lower, but still significant, cellular activity in *Corynebacteria glutamicum* and *Mycobacterium smegmatis*, model organisms of *Mtb*. The carbamate-containing probe shared a common mechanism with N-QTF, confirmed using a known mycolyltransferase inhibitor. The improved stability enabled the enrichment of reactive partners from cellular lysate for the identification of the modified protein targets. Diversification of the carbonyl substructure within QTF probes in this work revealed differences in reactivity and retention rates of labeling, enhancing our ability to track and therefore understand mycobacterial cell wall assembly enzymes.

5.3 Results & Discussion

5.3.1 Probe Design and Synthesis

The rapid reactivity of N-QTF allows for real-time imaging of mycobacterial cells. However, this rapid reactivity complicates mechanistic investigation due to the short-lived nature of the acyl-enzyme intermediate which forms. Moreover, the rapid hydrolysis allows tracking of enzyme activity but does not allow tracking of enzyme localization. We therefore sought to design a probe that would form a stable covalent adduct. We hypothesized that a carbamate functional group was an ideal target due to the increased stability and the ability to react with a catalytic serine residue.[22-23] Carbamate stability stems from the available resonance structures.[24] The oxygen adjacent to the carbonyl contributes electronically to enhanced reactivity compared to analogous amides. This manifests in a rotational barrier about the C–N bond of about 3-4 kcal/mol (15-20% lower than that of an equivalent amide). The structural similarity

between esters and carbamates suggests that enzyme-substrate complementarity would be retained. We anticipated that a resultant carbamoyl-enzyme intermediate is expected to be much more stable than the acyl-enzyme analog. For instance, the activity of cholesterol esterase has been shown to be inhibited by substrate mimics containing carbamate moieties.[23]

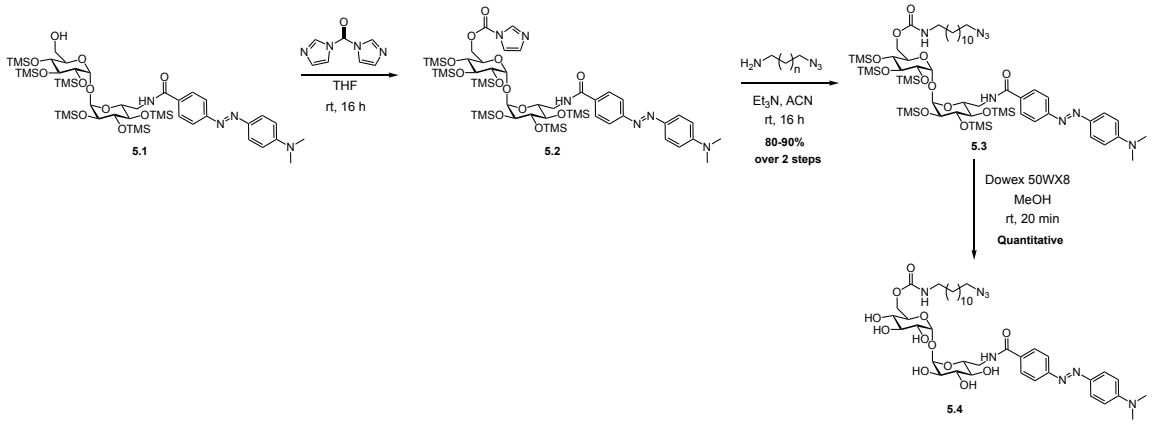

Scheme 5.1 Formation of the key carbamate moiety in Carb-QTF probes and synthesis of Carb-QT-N_3 for target enrichment.

The desired carbamate-containing probes were prepared by carbonyl-diimidazole-mediated activation of the 6-hydroxyl of trehalose (**Scheme 5.1**). This reactive intermediate could then be functionalized with an azide-bearing linker to attach the fluorophore in the next step via copper catalyzed alkyne-azide click chemistry (CuAAC) (**Scheme 5.2**). This synthetic sequence serves as a platform to incorporate a variety of azide-bearing linkers, fluorophores or additional functionality. A BODIPY fluorophore-bearing probe was synthesized to facilitate fluorescent turn-on upon enzymatic processing, Carb-QTF (**Scheme 5.2**). Another probe was prepared to retain an unreacted azide group that would allow for functionalization and enrichment post-processing (**Scheme 5.1**). Finally, an analogous ester-containing probe was produced

to provide a direct comparison of how the reactivity of the carbonyl impacts enrichment studies (**Scheme 5.3**). Taken together, a curated collection of carbamate and ester-bearing proves were prepared for biochemical and biological testing.

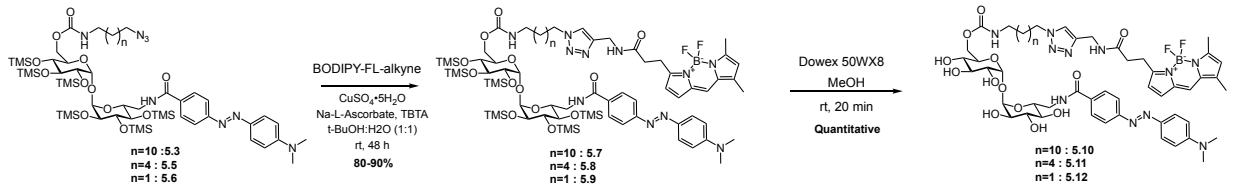

Scheme 5.2 Synthesis of Carb-QTF for fluorescence read-out assays.

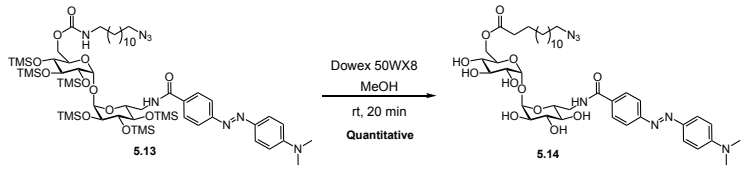

Scheme 5.3 Synthesis of QT-N_3.

5.3.2 Carb-QTF is Processed *in cellulo*

Though reduced electrophilicity was expected with the carbamate probe design relative to the ester derivatives, we hypothesized that pre-organization in the enzyme active site would be sufficent for probe processing in live cells. We evaluated Carb-QTF processing by measuring end-point fluorescence following probe incubation with live cells. We anticipated that, upon cell growth, probe-processing enzymes would be secreted and facilitate liberation of the fluorophore from the quencher and

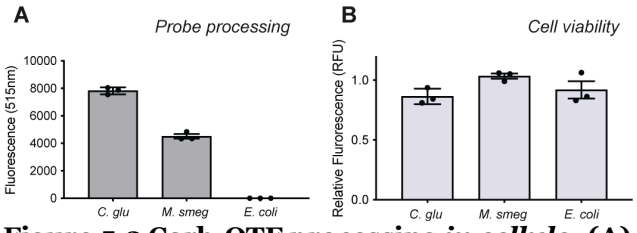

Figure 5.2 Carb-QTF processing *in cellulo*. (A) Fluorescence resulting from incubation with compound 1 with cells for 16 h. Error bars represent the standard error of the mean, $n = 3$. **(B)** Bacterial viability after full probe incubation measured by Alamar blue. Relative fluorescence calculated based on an untreated control of each organism. Error bars represent the standard error of the mean, $n = 3$.

therefore signal. Upon treatment with two model organisms for *Mtb*, *C. glutamicum* and *M. smegmatis*, Carb-QTF (**5.10**) produced a significant fluorescent turn-on (**Figure 5.2A**). Reaction in *C. glutamicum* showed greater fluorescence than *M. smegmatis*, consistent with what has been previously observed with QTF.[17] No fluorescence was observed upon treatment of a negative control organism, *E. coli*, as these cells lack mycolyltransferases and related enzymes. These data indicate that the carbamate-based probes can be processed by enzymes produced by mycobacterial species. Additionally, in all cases, treatment with probe did not significantly affect cell viability, compared to an untreated control, as measured by an endpoint Alamar Blue assay (**Figure 5.2B**).[25]

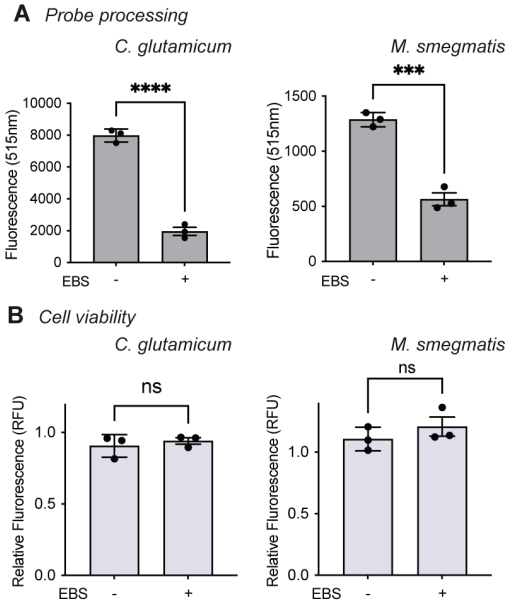

Figure 5.3 Inhibition of Carb-QTF processing by co-treatment with Ebselen. (A) Fluorescence resulting from incubation with Carb-QTF (1 μM) with cells with or without Ebselen, EBS (*C. glutamicum* = 30 μM, *M. smegmatis* = 50 μM). An asterisk denotes a statistically significant difference (****p < 0.0001, ***p < 0.0005) between samples with and without Ebselen. Error bars represent the standard error of the mean, *n* = 3. **(B)** Bacterial viability after full probe incubation measured by Alamar blue. Relative fluorescence calculated based on an untreated control of each organism. n.s.: no significant difference based on t-test. Error bars represent the standard error of the mean, *n* = 3.

5.3.3 Understanding the Mechanism of Carb-QTF Processing

To probe the *in cellulo* mechanism of action of Carb-QTF, we took advantage of a commercial inhibitor of mycolyltransferase activity, Ebselen, utilizing a similar experiment as reporter for QTF. [17, 20] If Carb-QTF fluorescence is dependent on mycolyltransferase processing, then co-treatment with Ebselen would result in decreased fluorescence. We co-treated *C. glutamicum* or *M. smegmatis* with a sublethal

concentration of Ebselen (30 μM and 50 μM, respectively) and Carb-QTF treatment (1 μM) and detected endpoint fluorescence. We observed a significant decrease in fluorescence by Carb-QTF in the sample co-treated with Ebselen relative to samples with Carb-QTF only consistent with a mycolyltransferase-dependent mechanism (**Figure 5.3A**). The observed minimal signal retention could either be a result of alternative targets or due to incomplete inhibition at the tested sublethal inhibitor concentration. There was no significant change in cell viability in the co-treated samples, confirming that the decrease in fluorescence signal is not due to cell death (**Figure 5.3B**). Though Ebselen is not an entirely selective inhibitor, these data support that Carb-QTF is processed, at least in part, by mycolyltransferases or related enzymes.

Next, confocal fluorescence microscopy was used to verify that fluorescence generated by Carb-QTF was localized at the cell wall. As anticipated, bright staining was observed localized at the cell membrane in both *C. glutamicum* and *M. smegmatis* (**Figure 5.4**), consistent with probe processing being facilitated by cell wall associating enzymes. Taken together, these data suggest that carbamate-containing QTF-based probes are processed similarly to the first and second-generation QTF probes *in cellulo*. Moreover, this experiment can serve as a proof of concept that Carb-QTF may be used to tracking of target localization via microscopy.

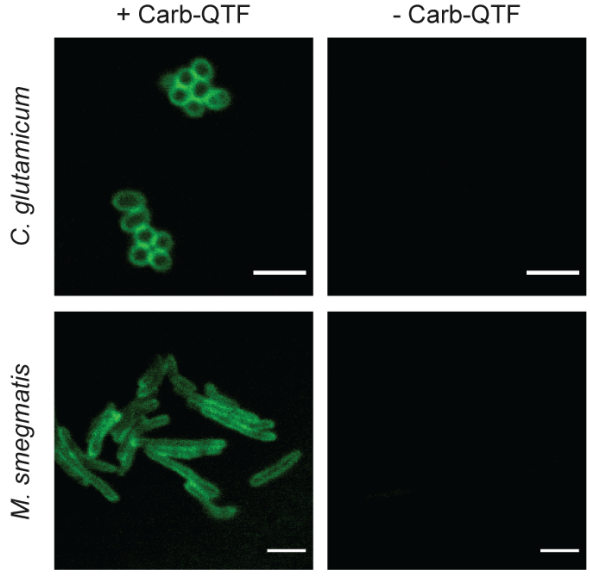

Figure 5.4 Confocal fluorescence microscopy images of *C. glutamicum* and *M. smegmatis* grown with Carb-QTF. Probe treatment at 10 μM for 16 h and 20 h, respectively. (Scale bars: 3 μm).

5.3.4 Carb-QTF Structure-Activity Relationship Analysis

We next aimed to leverage the modularity of our synthetic route to test a small library of Carb-QTF probes to understand structure-activity relationships (**Figure 5.5A**). Probes were synthesized with alkyl linkers between the trehalose and the fluorophore that varied in length. We hypothesized that a longer alkyl chain would be a better mimic of the endogenous donor, TMM which bears a long mycolic acid, and therefore manifests in enhanced enzyme binding. To test this, cells were treated with 500 nM of each probe, and endpoint fluorescence was measured. There was a preference for a longer linker, and this effect was more pronounced in *C. glutamicum* (**Figure 5.5B**). There was minimal variation in cell viability with any of the tested probes at the concentration reported (**Figure 5.5C**). This preference is consistent with what is known about the endogenous substrate structure as well as the enzyme active site.[18] In *C. glutamicum* the endogenous alkyl chains are 22-28 carbons and in *M. smegmatis* they are 64-79 carbons long.[26-27] In addition, based on structural data of the endogenous donor bound to the *Mtb*

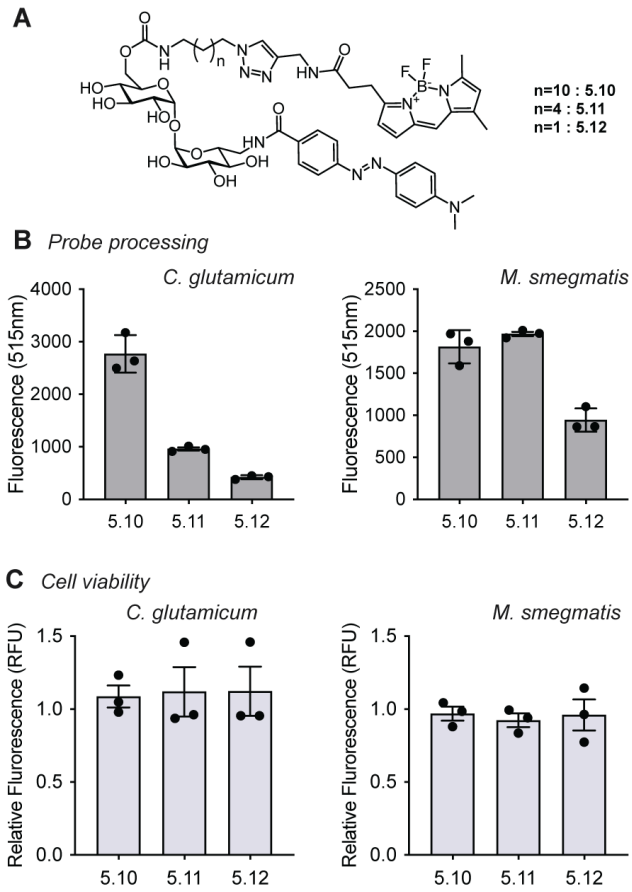

Figure 5.5 Structure-activity relationship of linker length in Carb-QTF probes. (A) Structures of Carb-QTF derivatives tested. **(B)** Fluorescence resulting from incubation with compounds (500 nM). Error bars represent the standard error of the mean, $n = 3$. **(C)** Bacterial viability after full probe incubation measured by Alamar blue. Relative fluorescence calculated based on an untreated control of each organism. Error bars represent the standard error of the mean, $n = 3$.

enzyme, we postulate that a shorter linker would place the charged fluorophore on a hydrophobic patch of the mycolyltrasferase surface, disfavoring binding.[28]

5.3.5 Carb-QTF Allows for Target Protein Enrichment

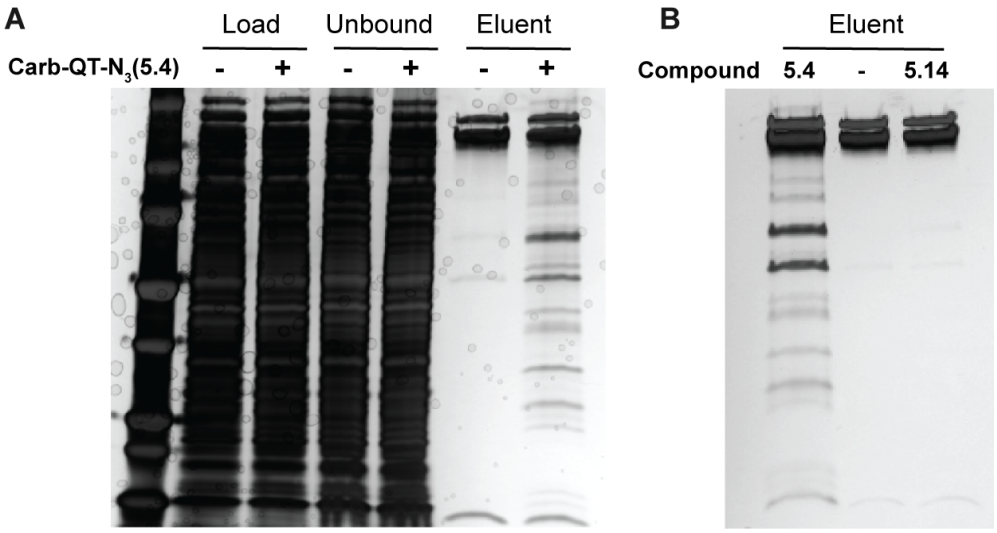

Figure 5.6 SDS-PAGE analysis of streptavidin enrichment of Carb-QT-N_3 targets. (A) Gel visualized by Silver Stain showing enrichment work flow from lysate (load), unbound and eluent. **(B)** Eluents for DMSO control, Carb-QT-N_3 (**5.4**) and ester control QT-N_3 (**5.14**).

C. glutamicum has been identified to express six mycolyltransferase genes (Myt A to F).[29-30] Myt A and Myt B are the major Myts expressed in *C. glutamicum* and are both involved in cell wall assembly processes, transferring mycolates group onto trehalose and AG acceptors. In order to identify the enzymes responsible for Carb-QTF processing and thereby N-QTF processing, we designed a probe derivative bearing a free azide for capture (Carb-QT-N_3, **5.4**). We anticipated that the key recognition motifs of our probe were retained with this compound: trehalose, the alkyl chain at C6, and the hydrophobic quencher moiety. Following growth with Carb-QT-N_3, DBCO-Biotin was added to react with the resultant conjugates and install biotin for enrichment. Cells were lysed and streptavidin-coated magnetic Dynabeads were used to enrich modified proteins. Eluents were analyzed by SDS-PAGE and visualized by silver stain. We observed distinct bands

only in samples containing Carb-QT-N_3, not the DMSO control or an ester-bearing derivative (**5.14**) (**Figure 5.6**). The molecular weights of several of these bands are consistent with Myts expressed in *C. glutamicum*. Future studies will work to identify these proteins by mass spectrometry and verify target engagement.

5.4 Conclusions

There is an imminent need for new, well-characterized tools to study mycobacterial cell wall assembly enzymes. In this work, we investigated the mechanisms of N-QTF processing *in cellulo* by preparing a probe that forms a more stable enzyme adduct. N-QTF is known to function based on enzyme-mediated ester hydrolysis to release a fluorophore. Leveraging knowledge of carbamate-containing probes, we demonstrated the reduced reactivity and increased stability of a new Carb-QTF probe. This probe was validated using model organisms of *Mtb* and a known mycolyltransferase inhibitor. Once Carb-QTF was validated to be processed as expected, an enrichment was performed for the identification of all protein targets in an unbiased fashion. Ultimately, we anticipate that these probes will highlight the utility of the differences in reactivity rates between esters and carbamates, which can be useful for a wide range of applications.

5.5 Experimental Details

5.5.1 Chemical Synthesis and Characterization

All chemicals were purchased from Millipore Sigma unless otherwise stated. Dry solvents were obtained from a solvent purification system (Pure Process Technologies) under argon. DMF, triethylamine and pyridine were used from sure seal bottles (Sigma Aldrich) without further purification. Analytical thin layer chromatography (TLC) was performed on EMD Millipore TM TLC silica gel 60 F254 (glass-backed). Plates were visualized under UV light and by heating after staining with *p*-anisaldehyde. Flash chromatography was performed on SiliCycle ® SiliaFlash ® P60 silica gel and Biotage ® Selekt using Biotage Sfär silica cartridges.

Nuclear magnetic resonance spectra were recorded on a 300 MHz spectrometer, 400 MHz spectrometer, a 500 MHz spectrometer or a 600 MHz spectrometer. Chemical shifts are reported relative to residual solvent peaks in parts per million ($CHCl_3$: ^1H, 7.26, ^{13}C, 77.16; MeOH: ^1H, 3.31, ^{13}C, 49.00; C_6D_6: ^1H, 7.16, ^{13}C, 128.06). High-resolution mass spectra (HRMS) were obtained on an electrospray ionization-time of flight (ESI-TOF) mass spectrometer. All IR spectra were taken on an FT-IR Bruker Alpha II.

*Synthesis of 6-O-(12-azidododecyl)-6'-NH-DABCYL-2,3,4,2',3',4'-hexakis-O-(trimethylsilyl)-**α**,**α**-trehalose* (**5.3**)

*6'-NH-DABCYL-2,3,4,2',3',4'-hexakis-O-(trimethylsilyl)- **α**,**α**-trehalose* **5.1** (50 mg, 0.048 mmol) was dissolved in dry THF (0.5 mL). Carbodiimidazole (CDI, 16 mg, 0.099 mmol) was added and the reaction mixture stirred at room temperature for 20 h. An additional portion of CDI (20 mg, 0.124 mmol) was added for 4 h. The reaction was quenched by pouring into water (100 mL). The product was extracted into Et_2O (4 x 100 mL). The combined organic layers were dried over anhydrous Na_2SO_4, filtered, and concentrated under reduced pressure by rotary evaporation.

The resultant orange film (**5.2**) was dissolved in MeCN (0.5 mL). 12-Azido-1-dodecylamine (40 mg, 0.179 mmol) was added followed by triethylamine (17 µl, 0.148 mmol). The reaction mixture stirred at room temperature for 20 h and then concentrated under reduced pressure. Purification of the resulting residue by column chromatography (SiO_2, 5→45% EtOAc/hexanes) afforded the title compound **5.3** (19 mg, 42%) as an orange solid.

^{1}H NMR (600 MHz, $CDCl_3$) δ 7.92 – 7.82 (m, 6H), 6.76 (d, *J* = 9.3 Hz, 2H), 6.47 (s, 1H), 4.98 (d, *J* = 3.1 Hz, 1H), 4.93 (d, *J* = 3.2 Hz, 1H), 4.71 (t, *J* = 6.0 Hz, 1H), 4.27 (d, *J* = 11.6 Hz, 1H), 4.09 – 4.06 (m, 1H), 4.01 – 3.88 (m, 5H), 3.50 – 3.33 (m, 5H), 3.27 – 3.12 (m, 4H), 3.11 (s, 6H), 1.60 (s, 14H), 1.47 (t, *J* = 6.8 Hz, 3H), 1.39 – 1.34 (m, 3H), 0.20 (s, 9H), 0.15 (dd, *J* = 8.7, 5.4 Hz, 36H), 0.03 (s, 9H).

^{13}C NMR (151 MHz, $CDCl_3$) δ 171.10, 166.76, 156.12, 155.13, 152.62, 143.59, 134.35, 127.78, 125.41, 122.06, 111.45, 93.94, 93.71, 74.03, 72.86, 72.64, 71.67, 71.50, 71.23, 63.72, 60.34, 53.40, 51.42, 41.52, 40.35, 40.20, 30.24, 29.39, 29.07, 26.64, 21.03, 1.08, 0.45, -0.08.

IR (cm^{-1}): 2926, 2896, 2848, 2074, 1708, 1635, 1578, 1490, 1342, 1233, 1111, 1049, 978, 874, 820.

HRMS (DART): calc. for $C_{58}H_{108}N_8O_{12}Si_6$ (M + H^+): 1277.6702, found 1277.6158.

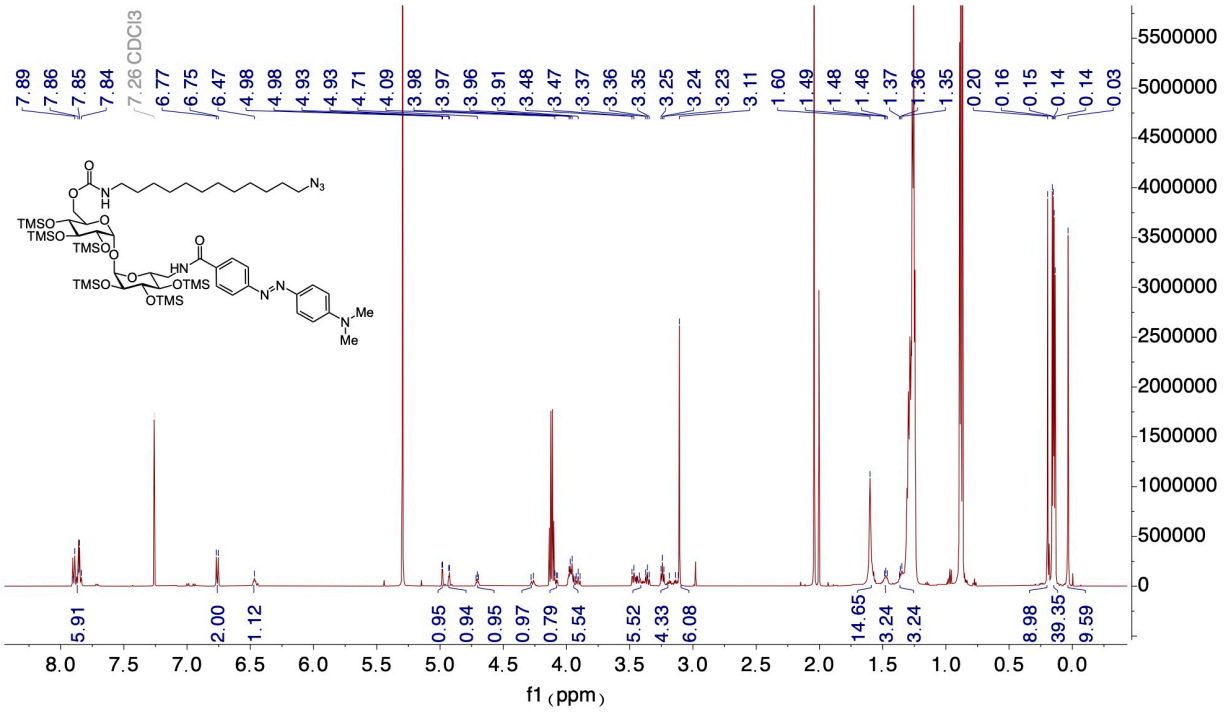
7.89
7.86
7.85
7.84
7.26 CDCl3
6.77
6.75
6.47
4.98
4.98
4.93
4.93
4.71
4.09
3.98
3.97
3.96
3.91
3.48
3.47
3.37
3.36
3.35
3.25
3.24
3.23
3.11
1.60
1.49
1.48
1.46
1.37
1.36
1.35
0.20
0.16
0.15
0.14
0.14
0.03
TMSO
TMSO
TMSO
TMSO
OTMS
OTMS
HN
N
N
Me
Me
N3
5.91
2.00
1.12
0.95
0.94
0.95
0.97
0.79
5.54
5.52
4.33
6.08
14.65
3.24
3.24
8.98
39.35
9.59
f1 (ppm)

*Synthesis of 6-O-(12-azidododecyl)-6'-NH-DABCYL-**α**,**α**-trehalose* (**5.4**)

Dowex-50WX8-200 ion exchange resin (10 mg) was added to a solution of compound **5.3** (5 mg, 0.004 mmol) in dry methanol (0.5 mL) and stirred at room temperature for 1 h. The resin was removed by filtration with methanol washes and the filtrate was concentrated under reduced pressure to afford the title compound **5.4** (3 mg, quantitative) as an orange solid.

^{1}H NMR (600 MHz, MeOD) δ 7.95 (d, *J* = 8.4 Hz, 2H), 7.85 (d, *J* = 8.7 Hz, 4H), 6.85 (d, *J* = 9.1 Hz, 2H), 5.08 (dd, *J* = 13.6, 3.8 Hz, 2H), 4.77 – 4.72 (m, 1H), 4.28 – 4.17 (m, 2H), 4.05 – 3.90 (m, 4H), 3.83 – 3.75 (m, 2H), 3.75 – 3.68 (m, 3H), 3.66 – 3.58 (m, 2H), 3.57 – 3.44 (m, 2H), 3.34 (d, *J* = 9.1 Hz, 2H), 3.28 – 3.20 (m, 3H), 3.12 (s, 6H), 3.07 (t, *J* = 7.1 Hz, 2H), 1.68 – 1.39 (m, 7H), 1.36 (d, *J* = 11.8 Hz, 2H), 0.96 – 0.80 (m, 4H).

^{13}C NMR (151 MHz, MeOD) δ 193.42, 186.79, 167.74, 166.34, 156.43, 146.62, 144.29, 129.43, 126.70, 126.45, 125.86, 123.00, 119.64, 118.40, 114.42, 112.63, 96.62, 95.77, 76.16, 40.38, 30.63.

IR (cm^{-1}): 2902, 2828, 2078, 1685, 1579, 1522, 1442, 1409, 1339, 1241, 1120, 1001, 964, 796.

HRMS (MALDI): calc. for $C_{40}H_{60}N_8O_{12}$ ($M + Na^+$): 867.423, found 867.280.

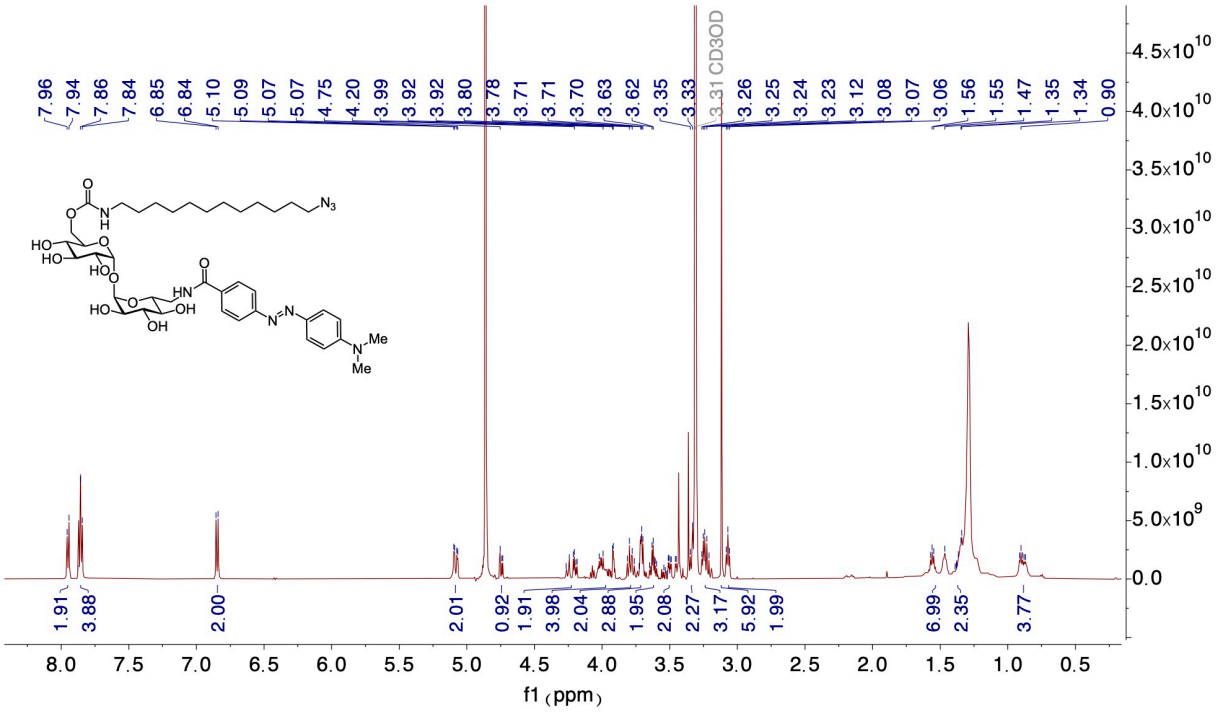
7.96
7.94
7.86
7.84
6.85
6.84
5.10
5.09
5.07
5.07
4.75
4.20
3.99
3.92
3.92
3.80
3.78
3.71
3.71
3.70
3.63
3.62
3.35
3.33
3.31 CD3OD
3.26
3.25
3.24
3.23
3.12
3.08
3.07
3.06
1.56
1.55
1.47
1.35
1.34
0.90
4.5x10^10
4.0x10^10
3.5x10^10
3.0x10^10
2.5x10^10
2.0x10^10
1.5x10^10
1.0x10^10
5.0x10^9
0.0
1.91
3.88
2.00
2.01
0.92
1.91
3.98
2.04
2.88
1.95
2.08
2.27
3.17
5.92
1.99
6.99
2.35
3.77
8.0
7.5
7.0
6.5
6.0
5.5
5.0
4.5
4.0
3.5
3.0
2.5
2.0
1.5
1.0
0.5
f1 (ppm)

*Synthesis of 6-O-(6-azidohexanyl)-6'-NH-DABCYL-2,3,4,2',3',4'-hexakis-O-(trimethylsilyl)-**α**,**α**-trehalose* (**5.5**)

*6'-NH-DABCYL-2,3,4,2',3',4'-hexakis-O-(trimethylsilyl)- **α**,**α**-trehalose* **5.1** (50 mg, 0.048 mmol) was dissolved in dry THF (0.5 mL). Carbodiimidazole (CDI, 16 mg, 0.099 mmol) was added and the reaction mixture stirred at room temperature for 20 h. An additional portion of CDI (20 mg, 0.124 mmol) was added for 4 h. The reaction was quenched by pouring into water (100 mL). The product was extracted into Et_2O (4 x 100 mL). The combined organic layers were dried over anhydrous Na_2SO_4, filtered, and concentrated under reduced pressure by rotary evaporation.

The resultant orange film (**5.2**) was dissolved in MeCN (0.5 mL) and 6-azido-1-hexanylamine (7 mg, 0.049 mmol) was added followed by triethylamine (17 µl, 0.148 mmol). The reaction mixture stirred at room temperature for 20 h and then concentrated under reduced pressure. Purification of the resulting residue by column chromatography (SiO_2, 5→45% EtOAc/hexanes) afforded the title compound **5.5** (48 mg, 91%) as an orange solid.

^{1}H NMR (600 MHz, $CDCl_3$) δ 7.92 – 7.82 (m, 6H), 6.76 (s, 2H), 6.46 (s, 1H), 4.98 (d, *J* = 2.9 Hz, 1H), 4.93 (d, *J* = 3.3 Hz, 1H), 4.71 (t, *J* = 6.0 Hz, 1H), 4.27 (d, *J* = 9.1 Hz, 1H), 4.09 (dd, *J* = 11.4, 4.5 Hz, 1H), 4.01 – 3.87 (m, 5H), 3.50 – 3.32 (m, 5H), 3.28 – 3.13 (m, 4H), 3.11 (s, 6H), 1.50 (t, *J* = 7.4 Hz, 2H), 1.43 – 1.27 (m, 6H), 0.20 (s, 9H), 0.15 (dd, *J* = 8.5, 5.3 Hz, 36H), 0.04 (s, 9H).

^{13}C NMR (151 MHz, $CDCl_3$) δ 166.77, 165.59, 157.19, 155.04, 152.75, 143.60, 134.41, 127.78, 125.34, 122.16, 111.40, 105.09, 104.57, 104.44, 103.41, 103.07, 102.75, 102.42, 101.59, 100.54, 94.08, 93.72, 73.97, 73.31, 72.73, 71.62, 71.07, 63.74, 51.26, 41.53, 40.23, 29.78, 28.68, 26.19, 0.99, 0.91, 0.08.

IR (cm^{-1}): 2912, 2887, 2091, 1708, 1599, 1591, 1473, 1432, 1364, 1333, 1073, 1009, 840.

HRMS (DART): calc. for $C_{52}H_{96}N_8O_{12}Si_6$ ($M + H^+$): 1193.5763, found 1193.5765.

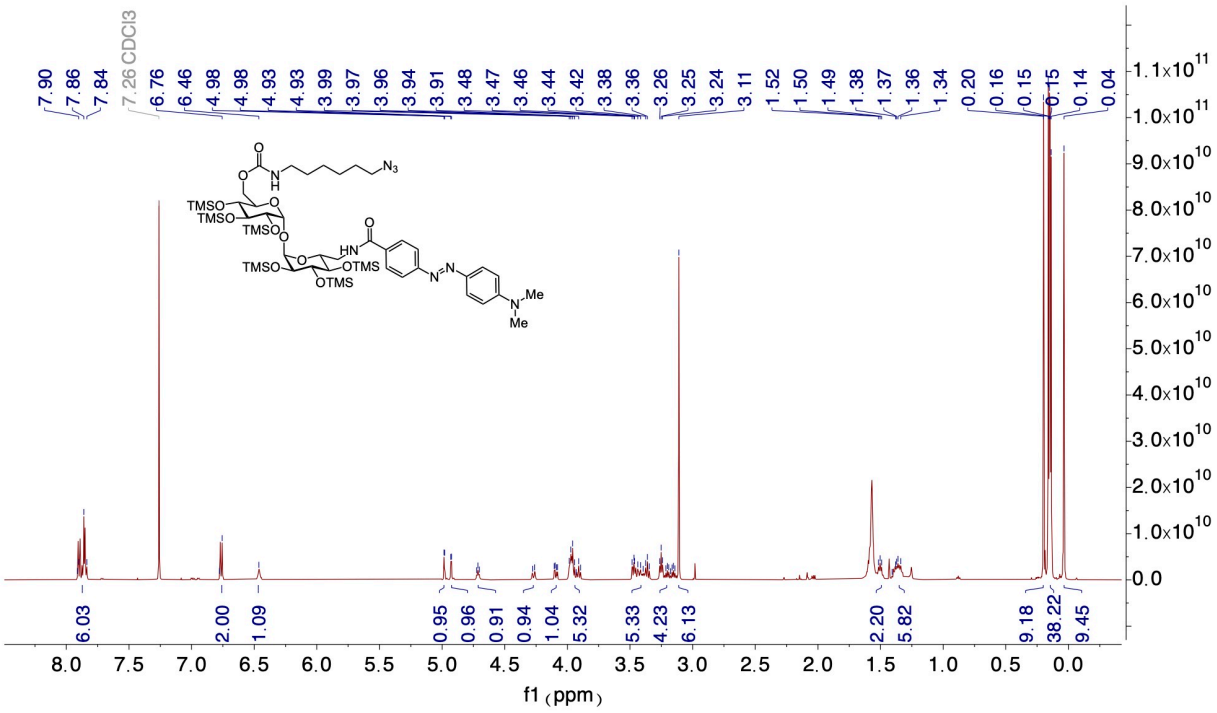
7.90
7.86
7.84
7.26 CDCl3
6.76
6.46
4.98
4.98
4.93
4.93
3.99
3.97
3.96
3.94
3.91
3.48
3.47
3.46
3.44
3.42
3.38
3.36
3.26
3.25
3.24
3.11
1.52
1.50
1.49
1.38
1.37
1.36
1.34
0.20
0.16
0.15
0.15
0.14
0.04
1.1x10^11
1.0x10^11
9.0x10^10
8.0x10^10
7.0x10^10
6.0x10^10
5.0x10^10
4.0x10^10
3.0x10^10
2.0x10^10
1.0x10^10
0.0
6.03
2.00
1.09
0.95
0.96
0.91
0.94
1.04
5.32
5.33
4.23
6.13
2.20
5.82
9.18
38.22
9.45
8.0
7.5
7.0
6.5
6.0
5.5
5.0
4.5
4.0
3.5
3.0
2.5
2.0
1.5
1.0
0.5
0.0
f1 (ppm)
TMSO
TMSO
TMSO
OTMS
TMSO
OTMS
HN
N=N
N
Me
Me
N3

*Synthesis of 6-O-(3-azidopropyl)-6'-NH-DABCYL-2,3,4,2',3',4'-hexakis-O-(trimethylsilyl)-**α**,**α**-trehalose* (**5.6**)

*6'-NH-DABCYL-2,3,4,2',3',4'-hexakis-O-(trimethylsilyl)- **α**,**α**-trehalose* **5.1** (50 mg, 0.048 mmol) was dissolved in dry THF (0.5 mL). Carbodiimidazole (CDI, 16 mg, 0.099 mmol) was added and the reaction mixture stirred at room temperature for 20 h. An addition portion of CDI (20 mg, 0.124 mmol) was added for 4 h. The reaction was quenched poured into water (100 mL). The product was extracted into Et_2O (4 x 100 mL). The combined organic layers were dried over anhydrous Na_2SO_4, filtered, and concentrated under reduced pressure by rotary evaporation.

The resultant orange film (**5.2**) was dissolved in MeCN (0.5 mL) and 3-azido-1-propylamine (4.8 μL, 0.049 mmol) was added followed by triethylamine (17 μl, 0.148 mmol). The reaction mixture stirred at room temperature for 20 h and then concentrated under reduced pressure. Purification of the resulting residue by column chromatography (SiO_2, 5→45% EtOAc/hexanes) afforded the title compound **5.6** (40 mg, 80%) as an orange solid.

^{1}H NMR (400 MHz, $CDCl_3$) δ 7.94 – 7.81 (m, 6H), 6.76 (d, *J* = 9.3 Hz, 2H), 6.47 (t, *J* = 4.5 Hz, 1H), 4.98 (d, *J* = 3.1 Hz, 1H), 4.92 (d, *J* = 3.2 Hz, 1H), 4.90 – 4.81 (m, 1H), 4.27 (d, *J* = 12.2 Hz, 1H), 3.93 (dt, *J* = 18.4, 9.6 Hz, 5H), 3.57 – 3.17 (m, 10H), 3.11 (s, 6H), 1.79 (p, *J* = 6.7 Hz, 2H), 0.20 (s, 9H), 0.15 (dd, *J* = 6.0, 3.1 Hz, 36H), 0.04 (s, 9H).

^{13}C NMR (151 MHz, CDCl3) δ 168.52, 160.02, 159.34, 153.75, 153.55, 152.92, 152.67, 144.46, 132.59, 127.56, 124.71, 121.27, 110.83, 102.51, 101.30, 76.33, 75.82, 73.35, 72.62, 72.31, 63.39, 38.98, 34.07, 29.33, 28.94, 28.73, 25.37, 25.29, 10.75, 9.88.

IR (cm^{-1}): 2956, 2090, 1652, 1624, 1599, 1514, 1349, 1360, 1251, 1007, 984.

HRMS (DART): calc. for $C_{49}H_{90}N_8O_{12}Si_6$ ($M + H^+$): 1151.5294, found: 1151.5351.

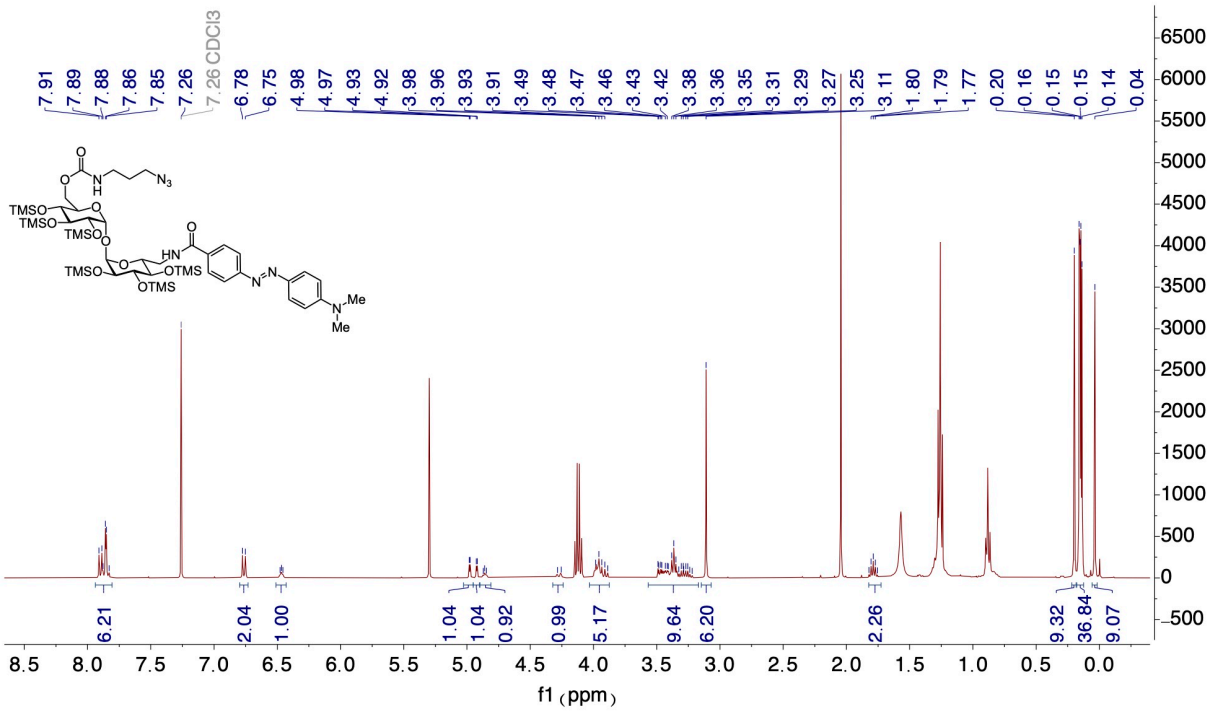
7.91
7.89
7.88
7.86
7.85
7.26
7.26 CDCl3
6.78
6.75
4.98
4.97
4.93
4.92
3.98
3.96
3.93
3.91
3.49
3.48
3.47
3.46
3.43
3.42
3.38
3.36
3.35
3.31
3.29
3.27
3.25
3.11
1.80
1.79
1.77
0.20
0.16
0.15
0.15
0.14
0.04
TMSO
TMSO
TMSO
TMSO
OTMS
OTMS
HN
N=N
N
Me
Me
6.21
2.04
1.00
1.04
1.04
0.92
0.99
5.17
9.64
6.20
2.26
9.32
36.84
9.07
f1 (ppm)

*Synthesis of 6-O-(12-[BODIPY-FL]-dodecyl)-6'-NH-DABCYL-2,3,4,2',3',4'-hexakis-O-(trimethylsilyl)- **α**,**α**-trehalose* (**5.7**)

Compound **5.3** (16 mg, 0.013 mmol) and BODIPY-FL alkyne (4.4 mg, 0.013 mmol) were dissolved in 5:5:1 *t*-BuOH:H_2O:CH_2Cl_2 (0.5 mL total). To this solution tris(benzyltriazolylmethyl)amine (TBTA, 1.4 mg in CH_2Cl_2, 0.001 mmol), sodium ascorbate (0.4 mg in aqueous solution, 0.003 mmol), and $CuSO_4 \cdot 5H_2O$ (0.2 mg in aqueous solution, 0.001 mmol) were added. The resulting mixture was stirred vigorously in the dark for 16 h, and then concentrated under reduced pressure. Purification of the resulting residue by column chromatography (SiO_2, 50→90% EtOAc/hexanes) afforded the title compound **5.7** (20 mg, quantitative) as an orange solid.

^{1}H NMR (400 MHz, $CDCl_3$) δ 7.93 – 7.81 (m, 6H), 7.45 (s, 1H), 7.06 (s, 1H), 6.83 (d, *J* = 4.1 Hz, 1H), 6.75 (d, *J* = 9.3 Hz, 2H), 6.48 (t, *J* = 5.0 Hz, 1H), 6.31 (s, 1H), 6.22 (d, *J* = 4.1 Hz, 1H), 6.11 (s, 1H), 4.98 (d, *J* = 3.1 Hz, 1H), 4.93 (d, *J* = 3.3 Hz, 1H), 4.72 (s, 1H), 4.47 (d, *J* = 5.7 Hz, 2H), 4.27 (t, *J* = 7.4 Hz, 3H), 4.15 – 3.87 (m, 7H), 3.53 – 3.32 (m, 5H), 3.26 (s, 2H), 3.23 – 3.13 (m, 2H), 3.10 (s, 6H), 2.63 (t, *J* = 7.6 Hz, 2H), 2.54 (s, 3H), 2.24 (s, 3H), 1.84 (s, 2H), 1.47 (s, 2H), 1.26 (d, *J* = 17.6 Hz, 18H), 0.20 (s, 9H), 0.15 (dd, *J* = 5.8, 3.9 Hz, 36H), 0.03 (s, 9H).

^{13}C NMR (101 MHz, $CDCl_3$) δ 171.95, 166.93, 160.61, 152.94, 144.91, 143.79, 134.58, 127.99, 125.53, 123.90, 122.35, 122.19, 120.61, 117.33, 111.60, 94.27, 93.91, 74.16, 73.52, 73.25, 72.92, 71.83, 71.54, 71.29, 50.47, 41.73, 41.22, 40.42, 35.91, 35.19, 29.39, 29.11, 24.91, 15.08, 1.18, 0.97, 0.24.

HRMS (MALDI): calc. for $C_{75}H_{126}BF_2N_{11}O_{13}Si_6$ ($M + Na^+$): 1628.8111, found 1629.7050.

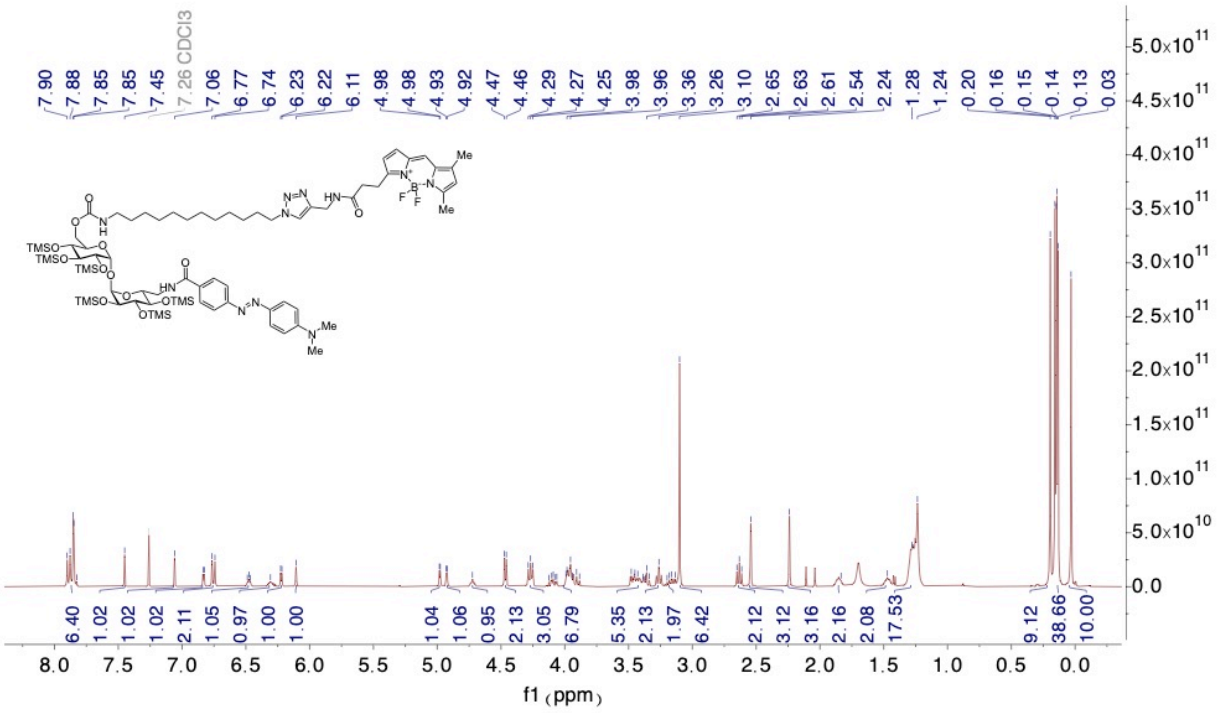
7.90 7.88 7.85 7.85 7.45 7.26 CDCl3 7.06 6.77 6.74 6.23 6.22 6.11 4.98 4.98 4.93 4.92 4.47 4.46 4.29 4.27 4.25 3.98 3.96 3.36 3.26 3.10 2.65 2.63 2.61 2.54 2.24 1.28 1.24 0.20 0.16 0.15 0.14 0.13 0.03
5.0x10^11
4.5x10^11
4.0x10^11
3.5x10^11
3.0x10^11
2.5x10^11
2.0x10^11
1.5x10^11
1.0x10^11
5.0x10^10
0.0
6.40 1.02 1.02 1.02 2.11 1.05 0.97 1.00 1.00 1.04 1.06 0.95 2.13 3.05 6.79 5.35 2.13 1.97 6.42 2.12 3.12 3.16 2.16 2.08 17.53 9.12 38.66 10.00
8.0 7.5 7.0 6.5 6.0 5.5 5.0 4.5 4.0 3.5 3.0 2.5 2.0 1.5 1.0 0.5 0.0
f1 (ppm)

Synthesis of 6-O-(6-[BODIPY-FL]-hexanyl)-6'-NH-DABCYL-2,3,4,2',3',4'-hexakis-O-(trimethylsilyl)- ***α,α****-trehalose* (**5.8**)

Compound **5.5** (4 mg, 0.003 mmol) and BODIPY-FL alkyne (1.1 mg, 0.003 mmol) were dissolved in 5:5:1 *t*-BuOH:H_2O:CH_2Cl_2 (0.2 mL total). To this solution tris(benzyltriazolylmethyl)amine (TBTA, 0.4 mg in CH_2Cl_2, 0.001 mmol), sodium ascorbate (0.4 mg in aqueous solution, 0.001 mmol), and $CuSO_4$•$5H_2O$ (0.1 mg in aqueous solution, 0.001 mmol) were added. The resulting mixture was stirred vigorously in the dark for 16 h, and then concentrated under reduced pressure. Purification of the resulting residue by column chromatography (SiO_2, 60→90% EtOAc/hexanes) afforded the title compound **5.8** (4 mg, 80%) as an orange solid.

^{1}H NMR (600 MHz, $CDCl_3$) δ 7.92 – 7.80 (m, 6H), 7.44 (s, 1H), 7.06 (s, 1H), 6.83 (d, *J* = 4.0 Hz, 1H), 6.75 (d, *J* = 6.9 Hz, 2H), 6.47 (s, 1H), 6.31 (s, 1H), 6.22 (d, *J* = 4.4 Hz, 1H), 6.10 (s, 1H), 4.97 (d, *J* = 3.3 Hz, 1H), 4.91 (d, *J* = 2.9 Hz, 1H), 4.76 (s, 1H), 4.46 (d, *J* = 5.8 Hz, 2H), 4.31 – 4.19 (m, 4H), 4.05 (d, *J* = 6.5 Hz, 3H), 3.96 (d, *J* = 20.0 Hz, 6H), 3.49 – 3.32 (m, 5H), 3.25 (t, *J* = 7.4 Hz, 2H), 3.21 – 3.11 (m, 2H), 3.09 (s, 6H), 2.62 (t, *J* = 7.4 Hz, 2H), 2.53 (s, 3H), 2.31 (d, *J* = 7.6 Hz, 1H), 2.23 (s, 3H), 1.08 – 1.00 (m, 3H), 0.19 (s, 9H), 0.17 – 0.10 (m, 36H), 0.02 (s, 9H).

^{13}C NMR (151 MHz, $CDCl_3$) δ 127.78, 125.31, 123.70, 122.13, 111.39, 93.67, 73.94, 73.04, 50.07, 40.20, 34.58, 29.65, 28.97, 25.19, 11.22, 0.96, 0.06, 0.02.

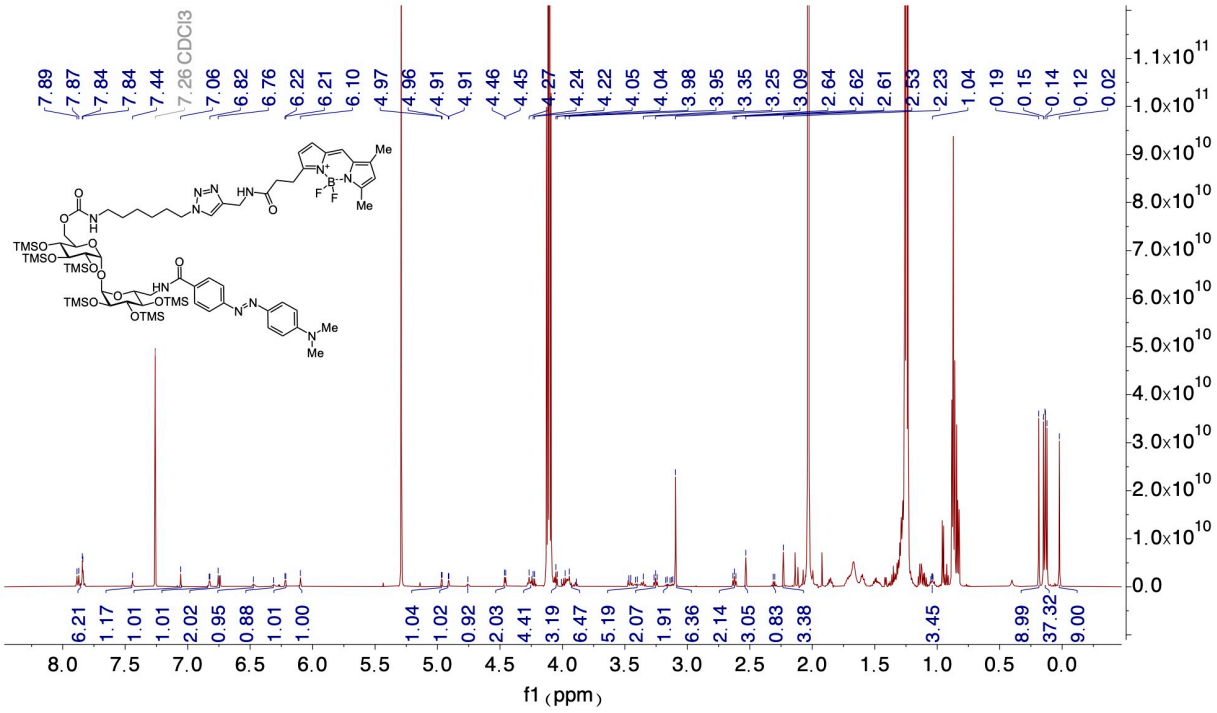
7.89
7.87
7.84
7.84
7.44
7.26 CDCl3
7.06
6.82
6.76
6.22
6.21
6.10
4.97
4.96
4.91
4.91
4.46
4.45
4.27
4.24
4.22
4.05
4.04
3.98
3.95
3.35
3.25
3.09
2.64
2.62
2.61
2.53
2.23
1.04
0.19
0.15
0.14
0.12
0.02
6.21
1.17
1.01
1.01
2.02
0.95
0.88
1.01
1.00
1.04
1.02
0.92
2.03
4.41
3.19
6.47
5.19
2.07
1.91
6.36
2.14
3.05
0.83
3.38
3.45
8.99
37.32
9.00
f1 (ppm)

*Synthesis of 6-O-(3-[BODIPY-FL]-propyl)-6'-NH-DABCYL-2,3,4,2',3',4'-hexakis-O-(trimethylsilyl)- **α**,**α**-trehalose* (**5.9**)

Compound **5.6** (5 mg, 0.004 mmol) and BODIPY-FL alkyne (1.4 mg, 0.004 mmol) were dissolved in 5:5:1 *t*-BuOH:H_2O:CH_2Cl_2 (0.2 mL total). To this solution tris(benzyltriazolylmethyl)amine (TBTA, 0.6 mg in CH_2Cl_2, 0.001 mmol), sodium ascorbate (0.4 mg in aqueous solution, 0.001 mmol), and $CuSO_4$•$5H_2O$ (0.1 mg in aqueous solution, 0.001 mmol) were added. The resulting mixture was stirred vigorously in the dark for 16 h, and then concentrated under reduced pressure. Purification of the resulting residue by column chromatography (SiO_2, 35→90% EtOAc/hexanes) afforded the title compound **5.9** (4 mg, 80%) as an orange solid.

^{1}H NMR (400 MHz, $CDCl_3$) δ 7.92 – 7.81 (m, 6H), 7.49 (s, 1H), 7.07 (s, 1H), 6.84 (d, *J* = 4.0 Hz, 1H), 6.76 (d, *J* = 9.2 Hz, 2H), 6.49 (s, 1H), 6.25 (dd, *J* = 14.9, 4.8 Hz, 2H), 6.10 (s, 1H), 5.03 (s, 1H), 4.98 (d, *J* = 3.1 Hz, 1H), 4.92 (d, *J* = 3.1 Hz, 1H), 4.47 (d, *J* = 5.9 Hz, 2H), 4.36 (t, *J* = 6.7 Hz, 2H), 4.27 (d, *J* = 12.0 Hz, 1H), 4.12 (dd, *J* = 11.6, 4.3 Hz, 1H), 4.01 – 3.87 (m, 6H), 3.51 – 3.33 (m, 6H), 3.30 – 3.13 (m, 4H), 3.10 (s, 6H), 2.54 (s, 3H), 2.24 (s, 3H), 1.43 (d, *J* = 5.6 Hz, 2H), 0.20 (s, 9H), 0.15 (dd, *J* = 6.3, 3.1 Hz, 36H), 0.04 (s, 9H).

^{13}C NMR (101 MHz, $CDCl_3$) δ 154.14, 150.28, 146.82, 128.33, 125.86, 123.33, 122.64, 119.14, 116.74, 116.52, 113.85, 111.94, 97.48, 73.03, 69.98, 64.31, 56.46, 55.64, 52.05, 51.34, 47.80, 42.78, 40.60, 37.50, 35.97, 32.82, 30.17, 1.51, 0.65.

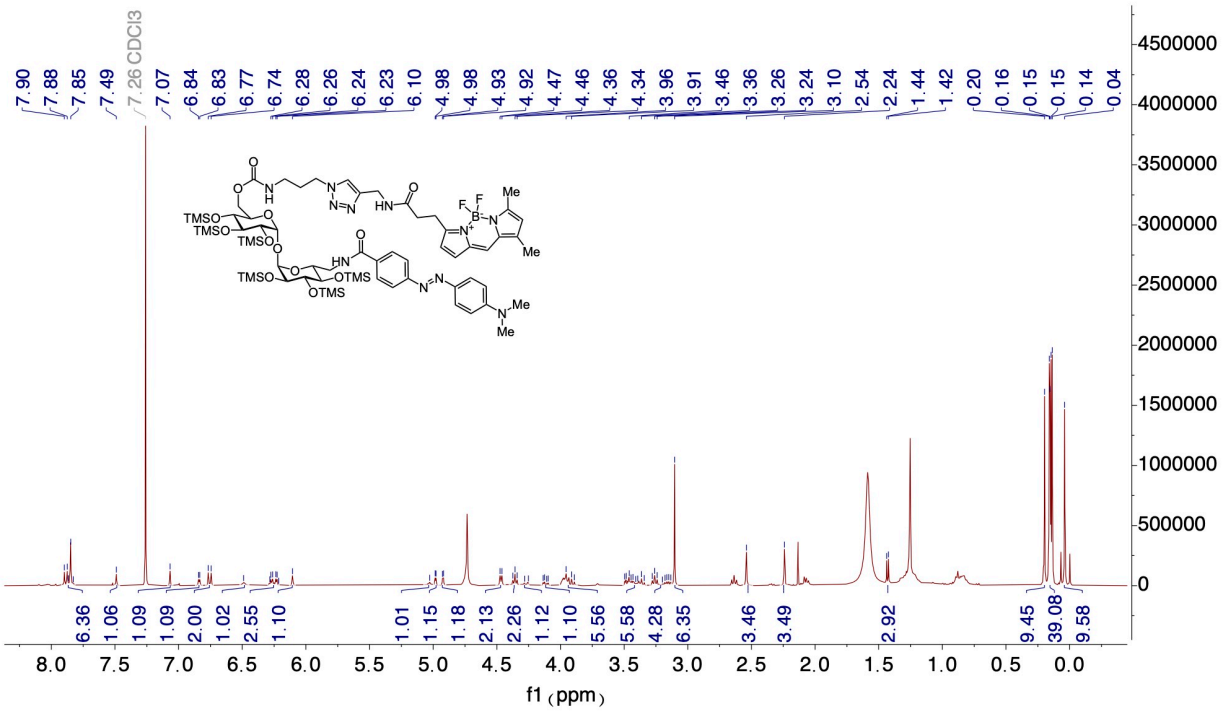
7.90
7.88
7.85
7.49
7.26 CDCl3
7.07
6.84
6.83
6.77
6.74
6.28
6.26
6.24
6.23
6.10
4.98
4.98
4.93
4.92
4.47
4.46
4.36
4.34
3.96
3.91
3.46
3.36
3.26
3.24
3.10
2.54
2.24
1.44
1.42
0.20
0.16
0.15
0.15
0.14
0.04
TMSO
TMSO
TMSO
TMSO
OTMS
OTMS
HN
HN
F
F
Me
Me
Me
Me
4500000
4000000
3500000
3000000
2500000
2000000
1500000
1000000
500000
0
6.36
1.06
1.09
1.09
2.00
1.02
2.55
1.10
1.01
1.15
1.18
2.13
2.26
1.12
1.10
5.56
5.58
4.28
6.35
3.46
3.49
2.92
9.45
39.08
9.58
8.0
7.5
7.0
6.5
6.0
5.5
5.0
4.5
4.0
3.5
3.0
2.5
2.0
1.5
1.0
0.5
0.0
f1 (ppm)

*Synthesis of 6-O-(12-[BODIPY-FL]-dodecyl)-6'-NH-DABCYL-**α**,**α**-trehalose* (**5.10**)

Dowex-50WX8-200 ion exchange resin (20 mg) was added to a solution of compound **5.7** (5 mg, 0.005 mmol) in dry methanol (1 mL) and stirred at room temperature for 3 h. The resin was removed by filtration with methanol washes and the filtrate was concentrated under reduced pressure. Purification of the resulting residue by column chromatography (SiO_2, 10→20% MeOH/CH_2Cl_2) afforded the title compound **5.10** (4.9 mg, quantitative) as an orange solid.

^{1}H NMR (600 MHz, MeOD) δ 7.94 (d, *J* = 8.4 Hz, 2H), 7.84 (t, *J* = 7.6 Hz, 4H), 7.72 (s, 1H), 7.40 (s, 1H), 6.96 (d, *J* = 4.4 Hz, 1H), 6.83 (d, *J* = 9.4 Hz, 2H), 6.28 (d, *J* = 4.4 Hz, 1H), 6.20 (s, 1H), 5.08 (dd, *J* = 12.9, 3.8 Hz, 2H), 4.91 (s, 8H), 4.42 (s, 2H), 4.35 – 4.16 (m, 4H), 4.04 – 3.95 (m, 2H), 3.84 – 3.65 (m, 4H), 3.10 (s, 6H), 3.06 (t, *J* = 6.7 Hz, 2H), 2.50 (s, 3H), 2.27 (s, 3H), 2.03 (d, *J* = 13.1 Hz, 3H), 1.90 – 1.76 (m, 2H), 1.45 (d, *J* = 7.3 Hz, 2H), 1.28 (d, *J* = 12.7 Hz, 13H).

^{13}C NMR (151 MHz, MeOD) δ 129.58, 126.58, 123.14, 112.78, 92.88, 89.68, 89.14, 88.92, 85.95, 81.46, 81.22, 74.71, 72.85, 64.88, 40.54, 30.73, 30.18, 27.42, 25.64, 20.32, 11.58, 11.34.

HRMS (DART): calc. for $C_{57}H_{78}BF_2N_{11}O_{13}$ (M + Na^+): 1196.5661, found 1195.8327.

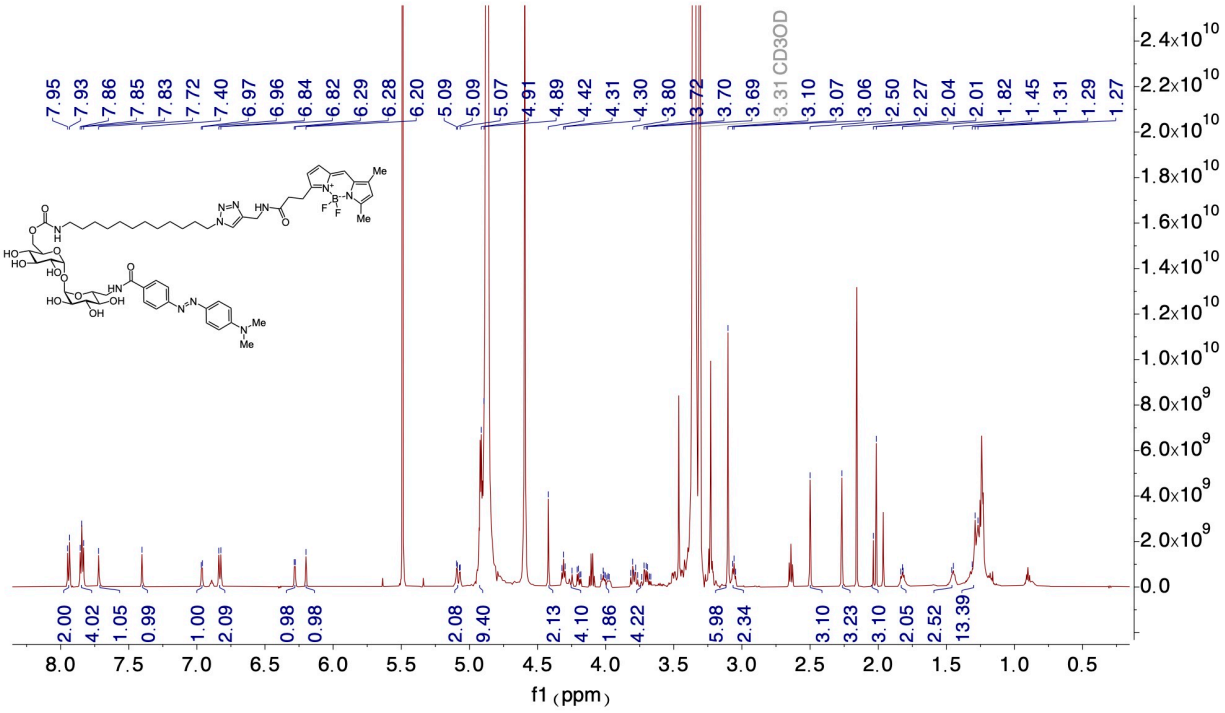
7.95
7.93
7.86
7.85
7.83
7.72
7.40
6.97
6.96
6.84
6.82
6.29
6.28
6.20
5.09
5.09
5.07
4.91
4.89
4.42
4.31
4.30
3.80
3.72
3.70
3.69
3.31 CD3OD
3.10
3.07
3.06
2.50
2.27
2.04
2.01
1.82
1.45
1.31
1.29
1.27
2.00
4.02
1.05
0.99
1.00
2.09
0.98
0.98
2.08
9.40
2.13
4.10
1.86
4.22
5.98
2.34
3.10
3.23
3.10
2.05
2.52
13.39
f1 (ppm)

*Synthesis of 6-O-(6-[BODIPY-FL]-hexanyl)-6'-NH-DABCYL-**α**,**α**-trehalose* (**5.11**)

Dowex-50WX8-200 ion exchange resin (20 mg) was added to a solution of compound **5.8** (2 mg, 0.002 mmol) in dry methanol (0.5 mL) and stirred at room temperature for 1 h. The resin was removed by filtration with methanol washes and the filtrate was concentrated under reduced pressure. Purification of the resulting residue by column chromatography (SiO_2, 5→25% MeOH/CH_2Cl_2) afforded the title compound **5.11** (1.1 mg, quantitative) as an orange solid.

^{1}H NMR (600 MHz, MeOD) δ 7.88 (d, *J* = 8.7 Hz, 2H), 7.79 (dd, *J* = 11.3, 8.7 Hz, 4H), 7.61 (s, 1H), 7.24 (s, 1H), 6.88 (d, *J* = 4.0 Hz, 1H), 6.75 (d, *J* = 9.1 Hz, 2H), 6.21 (d, *J* = 4.0 Hz, 1H), 6.11 (s, 1H), 5.02 (d, *J* = 8.0 Hz, 2H), 4.38 (d, *J* = 17.1 Hz, 4H), 4.25 (t, *J* = 7.1 Hz, 2H), 4.22 – 4.15 (m, 2H), 4.01 – 3.88 (m, 2H), 3.77 – 3.67 (m, 2H), 3.60 (d, *J* = 17.8 Hz, 1H), 3.47 – 3.41 (m, 2H), 3.20 – 3.17 (m, 2H), 3.06 (s, 6H), 3.02 (t, *J* = 7.1 Hz, 2H), 2.59 (t, *J* = 7.6 Hz, 2H), 2.46 (s, 3H), 2.21 (s, 3H), 1.81 (d, *J* = 7.3 Hz, 2H), 1.41 (t, *J* = 7.3 Hz, 2H), 0.89 – 0.76 (m, 5H).

^{13}C NMR (151 MHz, MeOD) δ 155.60, 154.25, 148.74, 134.21, 134.08, 129.18, 126.29, 122.85, 112.46, 102.89, 40.58, 35.73, 30.86, 30.58, 30.40, 26.87, 12.37, 11.40.

HRMS (DART): calc. for $C_{51}H_{66}BF_2N_{11}O_{13}$ ($M + Na^+$): 1112.4800, found 1112.1231.

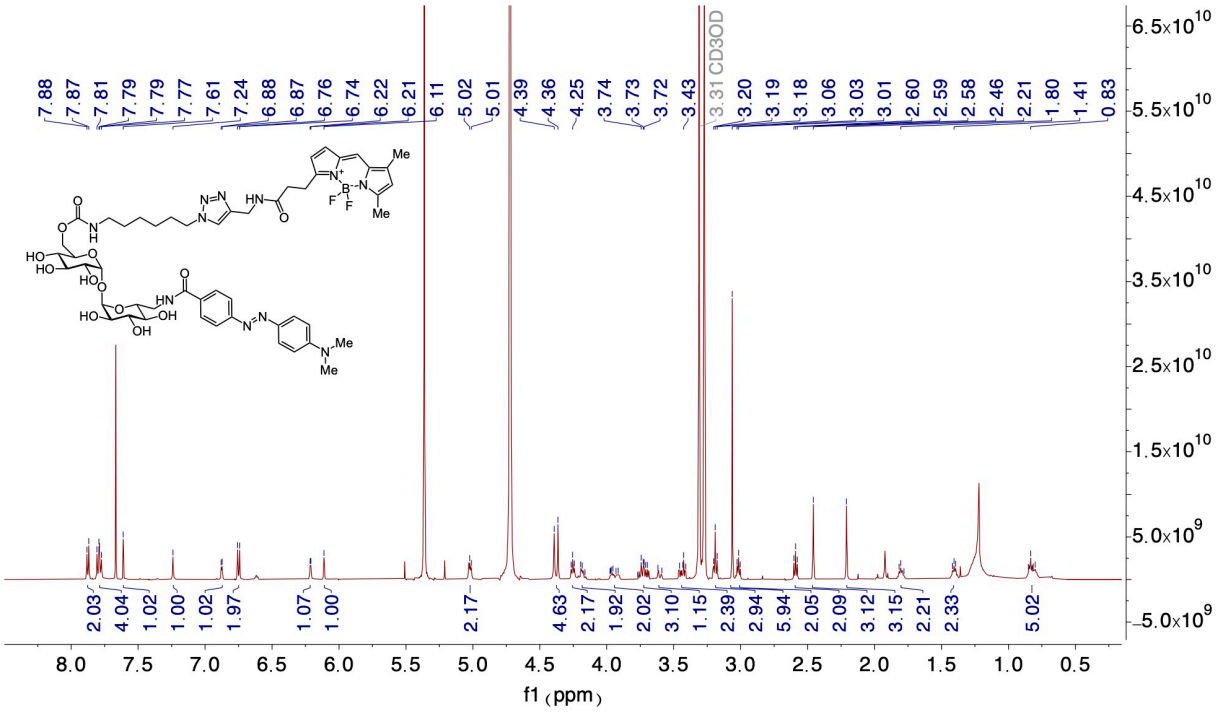
7.88
7.87
7.81
7.79
7.79
7.77
7.61
7.24
6.88
6.87
6.76
6.74
6.22
6.21
6.11
5.02
5.01
4.39
4.36
4.25
3.74
3.73
3.72
3.43
3.31 CD3OD
3.20
3.19
3.18
3.06
3.03
3.01
2.60
2.59
2.58
2.46
2.21
1.80
1.41
0.83
2.03
4.04
1.02
1.00
1.02
1.97
1.07
1.00
2.17
4.63
2.17
1.92
2.02
3.10
1.15
2.39
2.94
5.94
2.05
2.09
3.12
3.15
2.21
2.33
5.02
f1 (ppm)

*Synthesis of 6-O-(3-[BODIPY-FL]-propyl)-6'-NH-DABCYL-**α**,**α**-trehalose* (**5.12**)

Dowex-50WX8-200 ion exchange resin (20 mg) was added to a solution of compound **5.9** (2 mg, 0.002 mmol) in dry methanol (0.5 mL) and stirred at room temperature for 1 h. The resin was removed by filtration with methanol washes and the filtrate was concentrated under reduced pressure. Purification of the resulting residue by column chromatography (SiO_2, 5→25% MeOH/CH_2Cl_2) afforded the title compound **5.12** (1.1 mg, quantitative) as an orange solid.

^{1}H NMR (600 MHz, MeOD) δ 7.93 (d, *J* = 8.7 Hz, 2H), 7.84 (t, *J* = 9.4 Hz, 4H), 7.78 (s, 1H), 7.39 (s, 1H), 6.96 (d, *J* = 4.7 Hz, 1H), 6.83 (d, *J* = 9.4 Hz, 2H), 6.28 (d, *J* = 4.0 Hz, 1H), 6.18 (s, 1H), 5.08 (dd, *J* = 13.1, 3.6 Hz, 2H), 4.44 – 4.35 (m, 4H), 4.33 – 4.17 (m, 2H), 4.04 – 3.96 (m, 2H), 3.79 (q, *J* = 9.1 Hz, 2H), 3.69 (d, *J* = 7.6 Hz, 2H), 3.51 – 3.39 (m, 6H), 3.11 (s, 6H), 2.64 (t, *J* = 7.6 Hz, 2H), 2.49 (s, 3H), 2.26 (s, 3H), 2.07 – 2.02 (m, 2H), 1.94 (s, 2H).

HRMS (DART): calc. for $C_{48}H_{60}BF_2N_{11}O_{13}$ ($M + Na^+$):1070.4331, found 1070.1450.

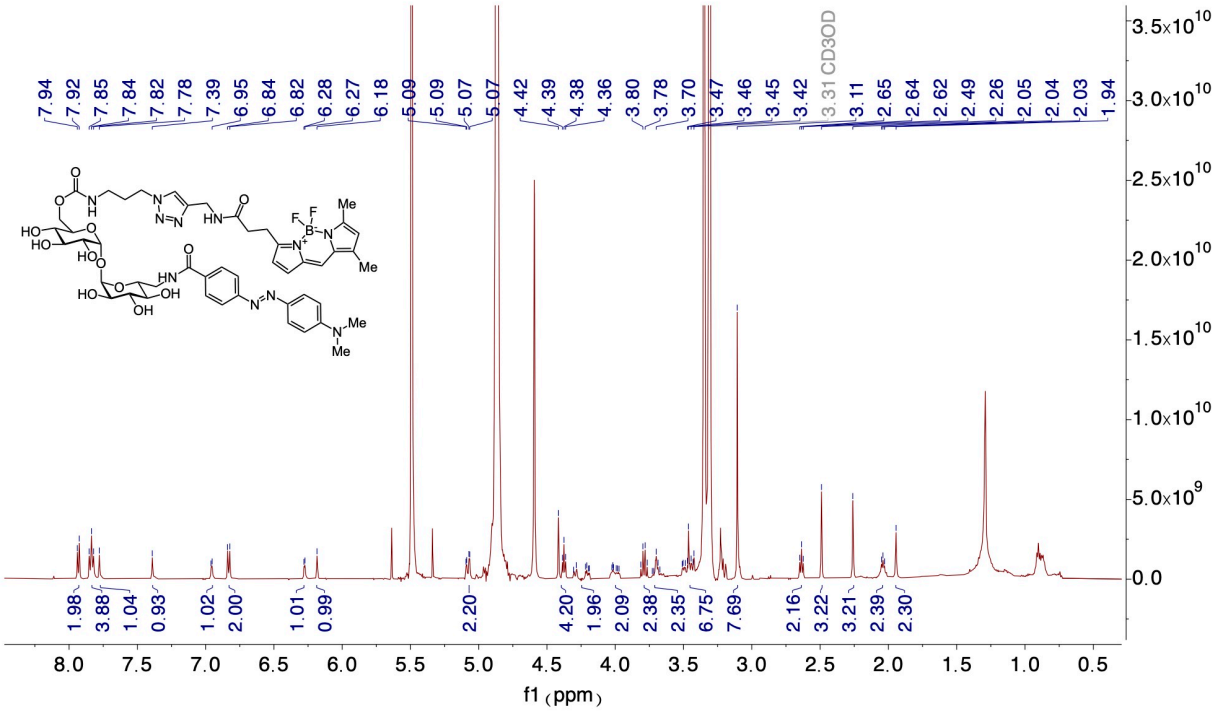
7.94
7.92
7.85
7.84
7.82
7.78
7.39
6.95
6.84
6.82
6.28
6.27
6.18
5.09
5.09
5.07
5.07
4.42
4.39
4.38
4.36
3.80
3.78
3.70
3.47
3.46
3.45
3.42
3.31 CD3OD
3.11
2.65
2.64
2.62
2.49
2.26
2.05
2.04
2.03
1.94
1.98
3.88
1.04
0.93
1.02
2.00
1.01
0.99
2.20
4.20
1.96
2.09
2.38
2.35
6.75
7.69
2.16
3.22
3.21
2.39
2.30
f1 (ppm)

5.5.2 Strains and Growth Conditions

For bacterial assays, the strains employed include *Mycobacterium smegmatis mc²155*, *Corynebacterium glutamicum ATCC13032*, and *Escherichia coli BL21*. *M. smegmatis* was grown in Middlebrook 7H9 broth (HiMedia, Mumbai, India) supplemented with 0.2% (w/v) dextrose, 0.2% (v/v) glycerol, 0.5% bovine serum albumin (United States Biological, Salem, MA), catalase (4 mg/liter) (Sigma-Aldrich), 15 mM sodium chloride and 0.05 % (v/v) Tween 80 in a shaking incubator at 37 °C. *C. glutamicum* was cultured in brain heart infusion (BHI) medium (BD, Franklin Lake, NJ) supplemented with 9% (w/v) sorbitol (BHIS) and *E. coli* was cultured in Luria broth (LB) liquid medium (Sigma-Aldrich) in a shaking incubator at 30 °C and 37 °C, respectively. Generally, starter cultures were incubated at the relevant temperature with shaking until saturation. Cells were then diluted into fresh media and grown to mid-logarithmic phase (determined by OD_{600} measurement on a BioMate 3S Spectrophotometer).

5.5.3 In-Culture Fluorescence Assays

Cultures of *M. smegmatis* or *C. glutamicum* were grown in LB media to mid-logarithmic phase and diluted to an $OD_{600} = 0.05$. A black 96-well plate was set up to monitor fluorescence following bacterial growth. Wells ($n = 3$) were filled with diluted bacteria (99 μL), and 1 μL of a 100 μM QTF DMSO stock solution (or 1 μL DMSO for negative control wells) was added to give a final QTF concentration of 1 μM, a final well volume of 100 μL, and DMSO concentration of 1%. The plate was incubated with shaking at 37 °C for reported time. Fluorescence emission at 515 nm was recorded.

5.5.4 Cell Viability Assays

Experiments were performed following reported procedures.[25, 31] In brief, a saturated culture was diluted down to the desired starting OD and plated in triplicate in a Corning black 96-well plate. Probes were added at the indicated concentration from DMSO stock solutions. *M. smegmatis* were grown with shaking at 37 °C for 24 h. *C. glutamicum* were grown with shaking at 30 °C for 16 h. Alamar Blue reagent (6 µL, Invitrogen) was added to each well and the plates were incubated again for 1 h at 37 °C or 30 °C. The fluorescence emission of each well was then measured on a Tecan Infinite M1000 Pro microplate reader. Monitoring of resorufin fluorescence was achieved by exciting at 570 nm ± 5 nm and detecting at 585 nm ± 5 nm. Z-position was set to 2 mm, and the fluorimeter gain was optimized and then kept constant between plates. Data are reported in relative fluorescence units (RFU) normalized to untreated controls.

5.5.5 Confocal Microscopy

Cells were plated from saturated starter cultures (OD_{600} = 0.05) in a Corning black 96-well plate. *M. smegmatis* was cultured in Middlebrook 7H9 containing 0.2% (v/v) glycerol and 0.05% Tween 80. *C. glutamicum* was cultured in LB liquid medium containing 0.05% Tween 80. *E. coli* was cultured in LB liquid medium containing 0.05 % Tween 80.

For analysis by microscopy, stained cell pellets were taken up in 7H9 supplemented with 0.5% Tween 80 (100 uL). Each sample was spotted onto a glass-bottomed microwell dish (MatTek corporation # P35G-1.5-14-C) and covered with a pre-cooled and 0.6% (w/v) agarose pad. Images were collected RPI spinning-disk confocal microscope (100x oil immersion lens, 1.4 NA). Brightness and contrast were identically

adjusted with the open-source Fiji distribution of ImageJ. Images were then converted to an RGB format to preserve normalization and then assembled into panels.

5.5.6 Dynabead Streptavidin Target Enrichment

Cells were grown for 16 h at 30 °C in 1 mL cultures. 700 µL of cell culture was diluted to 1 mL with 7H9 supplemented with 0.5% Tween 80. DBCO-PEG_4-Biotin (Sigma Aldrich) was added from a 10 mM stock solution in DMSO to a final concentration of 50 µM. The samples reacted for 2 h rotating at 37 °C. The stained cells were then immediately prepared for lysis. RIPA lysis buffer was added (100 µL of a 10x stock) and samples were disrupted by bead beating (5 x 30 s separated by 5 min off intervals on ice). The lysate was removed from the beads via centrifugation.

Dynabeads™ M-270 Streptavidin (Invitrogen, REF#65305) were washed with PBS three times (50 µL). Cell lysate was added. A fraction of the cell lysate was saved as load sample for SDS-PAGE analysis. Bead suspensions were incubated for 6 h at 4 °C with rotation. Using a magnetic tube rack, supernatant was collected as unbound samples. Beads were washed with PBS three times (500 uL). 30 µL elution buffer (1X SDS loading dye, 1X BXT in MQ H2O) was added to the beads and heated to 95 °C for 10 mins. Supernatant was collected as elution samples for SDS-PAGE analysis.

5.6 References

1. Petersen, E.; Al-Abri, S.; Chakaya, J.; Goletti, D.; Parolina, L.; Wejse, C.; Mucheleng'anga, L. A.; Khalili, S. A.; Yeboah-Manu, D.; Chanda-Kapata, P.; Nasiri, M. J.; Lungu, P. S.; Maeurer, M.; Tiberi, S.; Ntoumi, F.; Battista-Migliori, G.; Zumla, A., World TB Day 2022: Revamping and Reshaping Global TB Control Programs by Advancing Lessons learnt from the COVID-19 pandemic. *Int J Infect Dis* **2022,** *124 Suppl 1*, S1-S3.

2. Sun, W.; Gui, X.; Wu, Z.; Zhang, Y.; Yan, L., Prediction of drug resistance profile of multidrug-resistant Mycobacterium tuberculosis (MDR-MTB) isolates from newly diagnosed case by whole genome sequencing (WGS): a study from a high tuberculosis burden country. *BMC Infect Dis* **2022,** *22* (1), 499.

3. Batt, S. M.; Burke, C. E.; Moorey, A. R.; Besra, G. S., Antibiotics and resistance: the two-sided coin of the mycobacterial cell wall. *Cell Surf* **2020,** *6*, 100044.

4. Brennan, P. J.; Crick, D. C., The cell-wall of Mycobacterium tuberculosis in the context of drug discovery. *Current Topics in Medicinal Chemistry* **2007,** *7*, 475-488.

5. Maitra, A.; Munshi, T.; Healy, J.; Martin, L. T.; Vollmer, W.; Keep, N. H.; Bhakta, S., Cell wall peptidoglycan in Mycobacterium tuberculosis: An Achilles' heel for the TB-causing pathogen. *FEMS Microbiol Rev* **2019,** *43* (5), 548-575.

6. Vilchèze, C., Mycobacterial Cell Wall: A Source of Successful Targets for Old and New Drugs. *Applied Sciences* **2020,** *10* (7).

7. Dulberger, C. L.; Rubin, E. J.; Boutte, C. C., The mycobacterial cell envelope — a moving target. *Nature Reviews Microbiology* **2019,** *18* (1), 47-59.

8. Puech, V.; Chami, M.; Lemassu, A.; Lanéelle, M.-A.; Schiffler, B.; Gounon, P.; Bayan, N.; Benz, R.; Daffé, M., Structure of the cell envelope of corynebacteria: importance of the non-covalently bound lipids in the formation of the cell wall permeability barrier and fracture plane. *Microbiology* **2001,** *147* (5), 1365-1382.

9. Favrot, L.; Ronning, D. R., Targeting the mycobacterial envelope for tuberculosis drug development. *Expert Rev. Anti Infect. Ther.* **2012,** *10* (9), 1023-1036.

10. Alderwick, L. J.; Radmacher, E.; Seidel, M.; Gande, R.; Hitchen, P. G.; Morris, H. R.; Dell, A.; Sahm, H.; Eggeling, L.; Besra, G. S., Deletion of Cg-emb in corynebacterianeae leads to a novel truncated cell wall arabinogalactan, whereas inactivation of Cg-ubiA results in an arabinan-deficient mutant with a cell wall galactan core. *J Biol Chem* **2005,** *280* (37), 32362-71.

11. Bosch, B.; DeJesus, M. A.; Poulton, N. C.; Zhang, W.; Engelhart, C. A.; Zaveri, A.; Lavalette, S.; Ruecker, N.; Trujillo, C.; Wallach, J. B.; Li, S.; Ehrt, S.; Chait, B. T.; Schnappinger, D.; Rock, J. M., Genome-wide gene expression tuning reveals diverse vulnerabilities of M. tuberculosis. *Cell* **2021,** *184* (17), 4579-4592 e24.

12. Banahene, N.; Kavunja, H. W.; Swarts, B. M., Chemical Reporters for Bacterial Glycans: Development and Applications. *Chem Rev* **2022,** *122* (3), 3336-3413.

13. Luong, P.; Dube, D. H., Dismantling the bacterial glycocalyx: Chemical tools to probe, perturb, and image bacterial glycans. *Bioorg Med Chem* **2021,** *42*, 116268.

14. Wuo, M. G.; Dulberger, C. L.; Brown, R. A.; Sturm, A.; Ultee, E.; Bloom-Ackermann, Z.; Choi, C.; Garner, E. C.; Briegel, A.; Hung, D. T.; Rubin, E. J.; Kiessling, L. L., Antibiotic action revealed by real-time imaging of the mycobacterial membrane. *Biorxiv* **2022**.

15. Ding, Y.; Li, Z.; Xu, C.; Qin, W.; Wu, Q.; Wang, X.; Cheng, X.; Li, L.; Huang, W., Fluorogenic Probes/Inhibitors of beta-Lactamase and their Applications in Drug-Resistant Bacteria. *Angew Chem Int Ed Engl* **2021,** *60* (1), 24-40.

16. Levine, S. R.; Beatty, K. E., Investigating beta-Lactam Drug Targets in Mycobacterium tuberculosis Using Chemical Probes. *ACS Infect Dis* **2021,** *7* (2), 461-470.

17. Hodges, H. L.; Brown, R. A.; Crooks, J. A.; Weibel, D. B.; Kiessling, L. L., Imaging mycobacterial growth and division with a fluorogenic probe. *Proc Natl Acad Sci U S A* **2018,** *115* (20), 5271-5276.

18. Ronning, D. R.; Vissa, V.; Besra, G. S.; Belisle, J. T.; Sacchettini, J. C., Mycobacterium tuberculosis antigen 85A and 85C structures confirm binding orientation and conserved substrate specificity. *J Biol Chem* **2004,** *279* (35), 36771-7.

19. Cook, P. F.; Cleland, W. W., *Enzyme Kinetics and Mechanism*. Garland Science: 2007.

20. Favrot, L.; Grzegorzewicz, A. E.; Lajiness, D. H.; Marvin, R. K.; Boucau, J.; Isailovic, D.; Jackson, M.; Ronning, D. R., Mechanism of inhibition of Mycobacterium tuberculosis antigen 85 by ebselen. *Nat Commun* **2013,** *4*, 2748.

21. Ronning, D. R.; Klabunde, T.; Besra, G. S.; Vissa, V. D.; Belisle, J. T.; Sacchettini, J. C., Crystal structure of the secreted form of antigen 85C reveals potential targets for mycobacterial drugs and vaccines. *Nature Structural Biology* **2000,** *7*, 141-146.

22. Ghosh, A. K.; Brindisi, M., Organic carbamates in drug design and medicinal chemistry. *J Med Chem* **2015,** *58* (7), 2895-940.

23. Lin, G.; Shieh, C.-T.; Tsai, Y.-C.; Hwang, C.-I.; Lu, C.-P.; Chen, G.-H., Structure-reactivity probes for active site shapes of cholesterol esterase by carbamate inhibitors. *Biochimica et Biophysica Acta* **1999,** *1431*, 500-511.

24. Deetz, M. J.; Forbes, C. C.; Jonas, M.; Malerich, J. P.; Smith, B. D.; Wiest, O., Unusually Low Barrier to Carbamate C-N Rotation. *J. Org. Chem.* **2002,** *67*, 3949-3952.

25. Shiloh, M. U.; Ruan, J.; Nathan, C., Evaluation of bacterial survival and phagocyte function with a fluorescence-based microplate assay. *Infection and Immunity* **1997,** *65* (8), 3193.

26. Liu, J.; Nikaido, H., A mutant of Mycobacterium smegmatis defective in the biosynthesis of mycolic acids accumulates meromycolates. *Proc Natl Acad Sci U S A* **1999,** *96*, 4011-4016.

27. Pacheco, S. A.; Hsu, F.-F.; Powers, K. M.; Purdy, G. E., MmpL11 Protein Transports Mycolic Acid-containing Lipids to the Mycobacterial Cell Wall and Contributes to Biofilm Formation in Mycobacterium smegmatis. *Journal of Biological Chemistry* **2013,** *288* (33), 24213-24222.

28. Favrot, L.; Lajiness, D. H.; Ronning, D. R., Inactivation of the Mycobacterium tuberculosis antigen 85 complex by covalent, allosteric inhibitors. *J Biol Chem* **2014,** *289* (36), 25031-40.

29. Brand, S.; Niehaus, K.; Puhler, A.; Kalinowski, J., Identification and functional analysis of six mycolyltransferase genes of Corynebacterium glutamicum ATCC 13032: the genes cop1, cmt1, and cmt2 can replace each other in the synthesis of trehalose dicorynomycolate, a component of the mycolic acid layer of the cell envelope. *Arch Microbiol* **2003,** *180* (1), 33-44.

30. Dietrich, C.; Li de la Sierra-Gallay, I.; Masi, M.; Girard, E.; Dautin, N.; Constantinesco-Becker, F.; Tropis, M.; Daffe, M.; van Tilbeurgh, H.; Bayan, N., The C-terminal domain of Corynebacterium glutamicum mycoloyltransferase A is composed of five repeated motifs involved in cell wall binding and stability. *Mol Microbiol* **2020,** *114* (1), 1-16.

31. Calabretta, P. J.; Hodges, H. L.; Kraft, M. B.; Marando, V. M.; Kiessling, L. L., Bacterial Cell Wall Modification with a Glycolipid Substrate. *J Am Chem Soc* **2019,** *141* (23), 9262-9272.

Appendix 1: Investigation of Binding and Internalization of Synthetic N-Terminal Domain of Pyocin S2 in *Pseudomonas aeruginosa*

Reproduced with permission from:
Saebi A*, Brown JS*, Marando VM, Hartrampf N, Chumbler NM, Hanna S, Poskus M, Loas A, Kiessling LL, Hung DT, Pentelute BL. Rapid Single-Shot Synthesis of the 214 Amino Acid-Long N-Terminal Domain of Pyocin S2. *ACS Chemical Biology*. **2023**, 18, *3*, 518-527.
* denotes authors contributed equally

Contributions:
Protein was synthesized and folded by Azin Saebi with protocols optimized by Azin Saebi and Nina Hartrampf. Cell lines were provided by Nicole M. Chumbler. Flow cytometry, microscopy and other cell-based assays were performed by Victoria M. Marando and Joseph S. Brown. Research designed by Azin Saebi, Joseph S. Brown, Victoria M. Marando, Andrei Loas and Bradley L. Pentelute.

A1.1 Abstract

The impermeable outer membrane of *Pseudomonas aeruginosa* is bypassed by antibacterial proteins known as S-type pyocins. Because of their properties, pyocins are investigated as a potential new class of antimicrobials against *Pseudomonas* infections. Their production and modification, however, remains challenging. To address this limitation, we employed automated fast-flow peptide synthesis (AFPS) for the rapid production of a pyocin S2 import domain. The N-terminal domain sequence ($PyS2^{NTD}$) was synthesized in under 10 hours and purified to yield milligram quantities of the desired product. To our knowledge, the 214 amino acid sequence of $PyS2^{NTD}$ is among the longest peptides produced from a "single-shot" synthesis, i.e., made in a single stepwise route without the use of ligation techniques. Fluorescently labeled $PyS2^{NTD}$ binds to *P. aeruginosa* expressing the cognate ferripyoverdine receptor (FpvA) and is taken up into the periplasm. This selective uptake was validated with confocal and super resolution microscopy, flow cytometry, and fluorescence recovery after photobleaching (FRAP). These modified, synthetic S-type pyocins domains can be used to probe import mechanisms of *P. aeruginosa* and leveraged to develop selective antimicrobial agents that bypass the outer membrane.

A1.2 Introduction

Chemical synthesis is a powerful approach to access proteins and study their function. This strategy sidesteps biological expression bottlenecks to yield proteins that would be otherwise difficult to obtain (e.g., unstable, or toxic proteins).[1–3] Chemical protein synthesis also allows for unmatched flexibility in the incorporation of noncanonical residues. Thus, chemical protein synthesis can provide access to proteins with a plethora of chemical modifications to optimize their properties and activity, including efficacy, bioavailability, and half-life.[4,5]

Most methods towards chemical protein synthesis rely on solid-phase peptide synthesis (SPPS).[6] This process involves synthesis of the peptide backbone, cleavage, and deprotection of the side chains followed by purification and folding to yield a functional protein. While this method is generally successful, the accumulation of side products during SPPS can limit the purity and isolated yield of the desired full-length peptide. To maintain a straightforward purification, peptide synthesis is often limited to a chain length of 30-50 residues, which is significantly smaller than the average length of a single-domain protein.[7–10] Chemical protein synthesis has therefore relied heavily on ligation of shorter peptide fragments prepared in convergent SPPS. Most commonly, native chemical ligation (NCL) or α-ketoacid-hydroxylamine ligation (KAHA) strategies are employed to this end.[11,12]

Ligation strategies have delivered an impressive number of proteins, with the primary challenges being the production of multiple fragments and efficacy of the ligation assembly steps. These approaches have yielded proteins including mirror-image Pfu DNA polymerase with 775 amino acids,[13] tetra-ubiquitin-α-globin with 472 amino acids,[14] the Lys11/Lys48-branched hexaubiquitin chain with 456 amino acids,[15] P2 DNA

polymerase IV with 358 amino acids,[16] DapA with 312 amino acids,[17] and the F-ATPase subunit γ with 286 residues.[18]

These studies are a testament to the power of chemical protein synthesis; however, ligation strategies remain limited by the time to produce and assemble multiple fragments. Fragments can have poor solubility properties compared to the full intact protein, which has given rise to the design and use of solubility tags in ligation.[19,20] As protein length increases toward single-domain proteins and beyond, the challenge of chemical synthesis and ligation can become demanding and require multiple approaches to be explored to identify high yielding routes. Approaches including possible mutations to accommodate ligation sites, sequential deprotection of cysteines, and/or desulfurization after ligation can be considered. Moreover, purification of individual fragments or ligated fragments can be time-consuming and potentially introduce yield limiting steps even before approaching final protein folding and purification.[21]

The rapid and routine access to large synthetic proteins can be streamlined by technological and chemical advances to generate longer peptide sequences, thus decreasing the number of ligations required. Significant time-saving could be achieved if protein synthesis were completed in a "single-shot," wherein the full-length polypeptide was produced in a single SPPS effort at sufficient purity and yield. This approach would minimize intermediate handling steps, reactions, and purifications, prior to folding. However, single-shot peptide synthesis of long sequences has historically been limited by steric hindrance of protecting groups, formation of secondary structures, and intra- and/or intermolecular aggregation on resin. All of these barriers interfere with synthesis, reducing purity and yield.[9,22–24] Approaches to improve SPPS by focusing on

overcoming on-resin aggregation, including use of backbone protected monomers,[25,26] alternative solvents,[27] and microwave heating.[28,29] If known, structural information can also inform the optimization of the protein sequence to improve synthesis efficiency.[30–32] Overall, these strategies have led to the robust synthesis of difficult peptides with decreased synthesis time and increased crude peptide purity.

Flow chemistry has advanced SPPS by improving the synthesis rate and quality of long peptides.[33–38] The Pentelute group recently implemented automated fast-flow peptide synthesis (AFPS), a technology for rapid synthesis of peptides in flow.[39] Rigorous optimization of reaction parameters including use of amine-free *N*,*N*-dimethylformamide (DMF), increased amino acid concentration to 0.4 M, and increased reagent activation and coupling temperature to 90 °C led to improved results. The use of formic acid as an additive for fluorenylmethyloxycarbonyl (Fmoc) deprotection,[40] and optimization of cysteine and histidine couplings led to reduction in aspartimide formation and epimerization, respectively. These changes thereby minimize some of the known challenges of peptide synthesis at elevated temperature. Further residue-specific optimization for coupling agents resulted in the establishment of a general protocol for AFPS.[41,42] This protocol led to the successful syntheses of single-domain proteins in a single-shot approach, including murine double minute 2 protein domain (MDM2 domain, 127 AA), lysozyme (129 AA), fibroblast growth factor 1 (FGF1, 140 AA), and sortase A* (164 AA).

These initial successes prompted us to apply this optimized AFPS protocol to produce a protein over 200 residues long in a single-shot synthesis. Our objective was to assess whether this approach could yield workable amounts (>1 mg) of biologically active material for functional studies. To this end, we describe here the single-shot

synthesis of the 214-mer N-terminal receptor binding domain of the bacteriocin pyocin S2 ($PyS2^{NTD}$) produced by the Gram-negative bacterium *Pseudomonas aeruginosa*.[43] Full-length pyocin S2 is an interspecies competition protein that mimics the pyoverdine siderophore, binds to the ferripyoverdine Type 1 receptor (FpvA), crosses both the outer and inner membranes, and subsequently acts as a toxic nuclease in the cytoplasm of *P. aeruginosa*.[44] Within the full-length protein, the C-terminal region of the protein displays nuclease activity, which is mitigated by co-expressed immunity proteins to prevent self-harm. Thus, pyocin S2 promotes intraspecies competition between *Pseudomonas* strains. On its own, the nontoxic N-terminal domain ($PyS2^{NTD}$) binds FpvA and only achieves periplasmic internalization, as portions of the C-terminal of pyocin S2 are also responsible for cytoplasmic entry.[45] While it demonstrates the utility of the optimized AFPS technology, $PyS2^{NTD}$ was chosen for its potential biological application, specifically for its ability to enter the periplasm of the Gram-negative bacterium *P. aeruginosa*.[43] With global antibiotic resistance rate on the rise, there is an urgent need for new strategies to target pathogenic bacteria. Thus, in this work, we synthesize and demonstrate the expected biological function of synthetically produced $PyS2^{NTD}$. Given that the low permeability of the outer membrane is a major contributor to antibiotic resistance of *P. aeruginosa*,[46,47] we envision the production and bioconjugation of $PyS2^{NTD}$ will enable the development of novel antipseudomonal therapeutics and further improve the understanding of pyocin transport.[48,49]

A1.3 Results & Discussion

A1.3.1 AFPS Enables Rapid Single-Shot Synthesis of PyS2^{NTD}

The N-terminal domain of pyocin S2 (PyS2^{NTD}, Q06584, M1-K209) has been previously produced using recombinant DNA technology and shown to translocate across the outer membrane of *P. aeruginosa* via its native FpvA receptor.[44,45] We hypothesized this protein fragment could be feasibly produced in a single-shot synthesis, rather than through ligation (**Figure A1.1A**) due to advancements made in automated flow technology for peptide and protein synthesis. Structural and functional data in the literature provide a direct comparison to understand and verify the integrity and function of synthetic PyS2^{NTD}.[45] To minimize any disruption in the ability of the N-terminal domain to undergo internalization, a cysteine handle for site-selective bioconjugation was incorporated near the C-terminus (Cys216) of the PyS2^{NTD} sequence. Furthermore, to reduce the possibility of methionine oxidation side products, methionine residues were mutated to norleucine (Nle),[30] resulting in a synthetic PyS2^{NTD} construct 214 residues in length (**Figure A1.1B**).

PyS2^{NTD} was synthesized in an automated flow sequence of *in situ* amino acid activation, residue incorporation via amide coupling on solid-phase H-Rink ChemMatrix resin, and deprotection of the newly incorporated residue. The efficiency of residue incorporation was monitored in real time via an in-line UV-Vis absorbance detector. At 310 nm, the release of fluorene-containing compounds was observed, allowing for quantification of the deprotection step as a measure of residue incorporation.[41,42,50] Any irregularities, such as a decrease in deprotection peak height, could be indicative of aggregation of the nascent chain.[23,50] Analysis of the peak area resulting from the amine deprotection during the synthesis of PyS2^{NTD} suggested no

major aggregation events (**Figure A1.1C**). This synthesis protocol was previously developed for the production of shorter sequences and used here with no further optimization, supporting its robustness and general applicability.[42] Synthesis of PyS2^{NTD} proceeded for 9.2 hours with 434 steps, where each residue was incorporated in approximately 2.5 minutes.

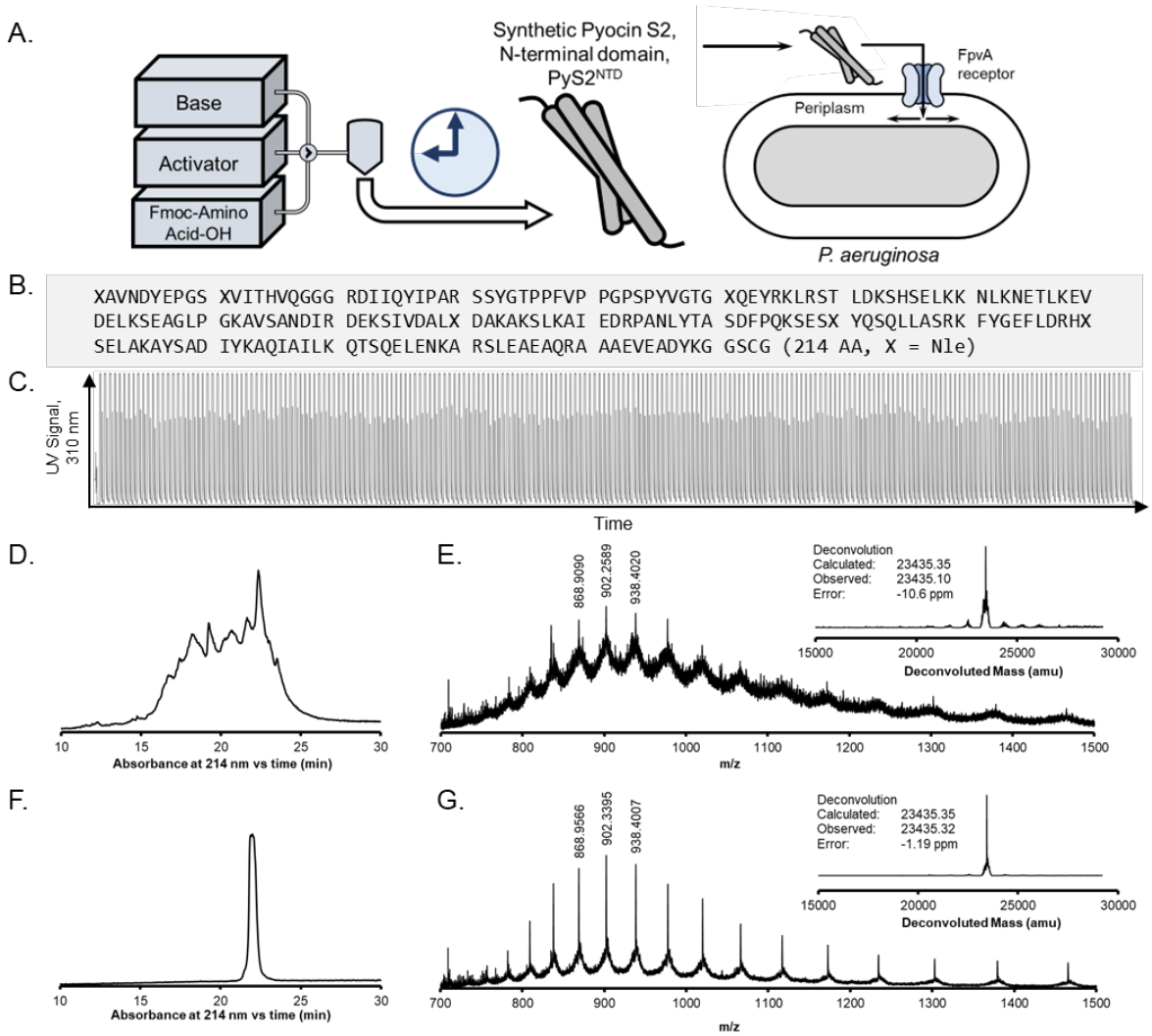

Figure A1.1 PyS2^{NTD} was rapidly synthesized in 9.2 hours using automated fast-flow peptide synthesis (AFPS). (A) Schematic representation of the automated flow synthesis and biological function of PyS2^{NTD}. **(B)** The sequence of PyS2^{NTD} with cysteine (Cys216) added for bioconjugation. **(C)** The UV absorbance trace at 310 nm from flow synthesis showed the Fmoc-deprotection peaks remained comparable in height and width throughout the synthesis. Coupling steps are also shown and produce a saturated signal, just before each Fmoc-deprotection peak. **(D)** Analytical reverse-phase high-performance liquid chromatography (RP-HPLC) from absorbance at 214 nm and **(E)** Liquid chromatography–mass spectrometry (LC-MS) mass spectrum of crude PyS2^{NTD} with deconvoluted mass spectrum inset. **(F)** RP-HPLC of purified PyS2^{NTD} with absorbance at 214 nm and **(G)** LC-MS mass spectrum of the purified PyS2^{NTD} with deconvoluted mass spectrum inset.

After synthesis, the crude PyS2^{NTD} clearly exhibited the expected mass corresponding to the intact protein, and preparative reverse-phase purification was able to isolate >10 mg of the unfolded PyS2^{NTD} polypeptide. When starting synthesis with 100 mg of low-loading resin (0.17 mmol/g), cleavage from the resin provided 197 mg of crude PyS2^{NTD} material as the trifluoroacetate salt (47% yield). The synthesis quality of the crude PyS2^{NTD} was examined by analytical liquid chromatography and liquid chromatography-mass spectrometry (LC-MS). Analytical reverse-phase chromatography of the crude PyS2^{NTD} provided a quality assessment of potential synthesis issues including truncations, deletions, and isomers. Though the PyS2^{NTD} exhibited multiple peaks (**Figure A1.1D**), the presence of some distinct peaks indicated that optimized preparative chromatography could potentially yield pure fractions. Using LC-MS, the crude synthesis quality was evaluated to determine if the calculated mass of the fully assembled N-terminal domain was present. When integrating the entire mass chromatogram peak from the crude PyS2^{NTD}, a charge-state series of ions were observed in the raw mass chromatogram (**Figure A1.1E**). From this raw chromatogram, a deconvoluted mass spectrum clearly exhibited the expected calculated molecular weight of the fully assembled PyS2^{NTD} (**Figure A1.1E inset**). PyS2^{NTD} was purified by preparative reverse-phase high-performance liquid chromatography (RP-HPLC). A preparative-grade C18 column was used at elevated temperature (60 °C) to isolate 10.3 mg of pure PyS2^{NTD} as the trifluoroacetate salt. LC-MS was again used for confirming the molecular weight of the product (**Figure A1.1G, inset**) and analytical HPLC confirmed isolation of PyS2^{NTD} from multiple side products (**Figure A1.1F**).

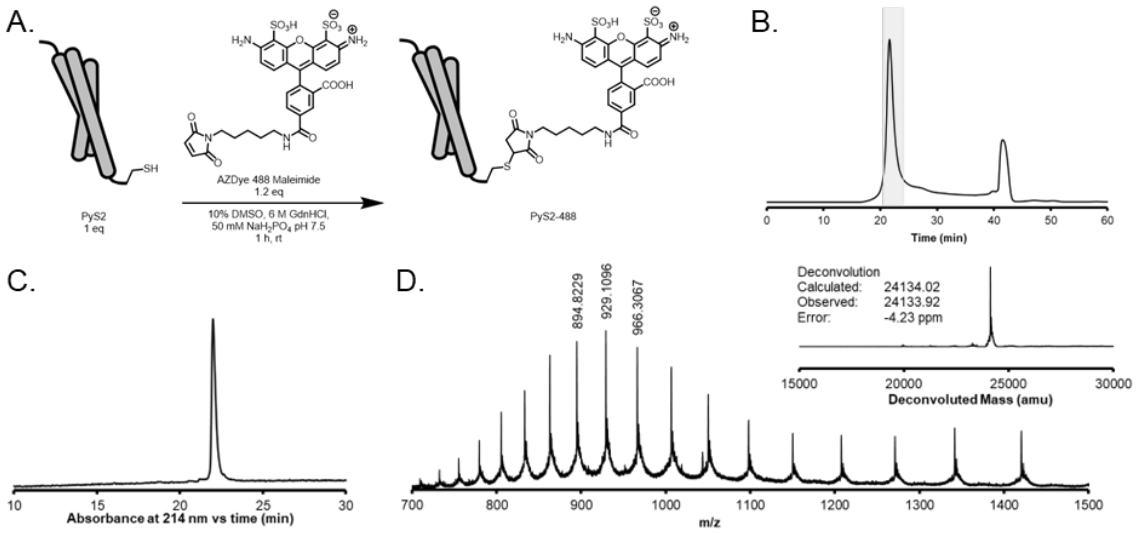

Figure A1.2 Synthetic PyS2^{NTD} was conjugated to fluorophore AZDye 488 and folded. (A) Conjugation and folding scheme of PyS2^{NTD}. **(B)** Chromatogram of size exclusion chromatography (SEC) purification of PyS2-488, showing fluorescence signal with excitation at 280 nm and emission at 325 nm, where the fractions containing the protein (shaded in gray) were pooled to yield 234 μg of material corresponding to 24% combined reaction and folding recovery yield. **(C)** RP-HPLC of folded PyS2-488 conjugate showing absorbance at 214 nm and **(D)** LC-MS of the folded PyS2-488 conjugate with deconvoluted mass spectrum inset.

A1.3.2 Site-Specific PyS2^{NTD} Labeling with AZDye 488

For biological characterization, we prepared PyS2^{NTD}-fluorophore conjugate by reacting the installed cysteine residue with a fluorophore maleimide to complete conversion and purify by size exclusion chromatrography (SEC). Fluorescence microscopy has been previously used to assess the import of recombinant PyS2^{NTD} into live *P. aeruginosa* cells.[45] Although folded synthetic PyS2^{NTD} can be labeled under aqueous conditions, we sought to combine the conjugation and folding processes to streamline the procedure and maximize PyS2^{NTD} yield. Accordingly, HPLC-purified synthetic PyS2^{NTD} was simultaneously denatured and labeled with AZDye 488 (1.2 equiv.) via cysteine-maleimide conjugation (**Figure A1.2A**). The reaction was monitored by LC-MS for the expected mass shift of +698 Da corresponding to the addition of the AZDye to the PyS2^{NTD} and the complete labeling of all PyS2^{NTD} with

AZDye 488 (PyS2-488). SEC purification was then used to remove excess fluorophore maleimide from the reaction and simultaneously fold the protein (**Figure A1.2B**). Combining the labeling and folding steps afforded the desired folded PyS2-488, corresponding to 24% isolated yield (234 µg from 1.17 mg reacted). The purity of the PyS2-488 post-folding and conjugation was high as evaluated by analytical RP-HPLC and LC-MS (**Figure A1.2C,D**).

A1.3.3 PyS2^{NTD}-Fluorophore Conjugate Binds and Internalizes into the *P. aeruginosa* Periplasm

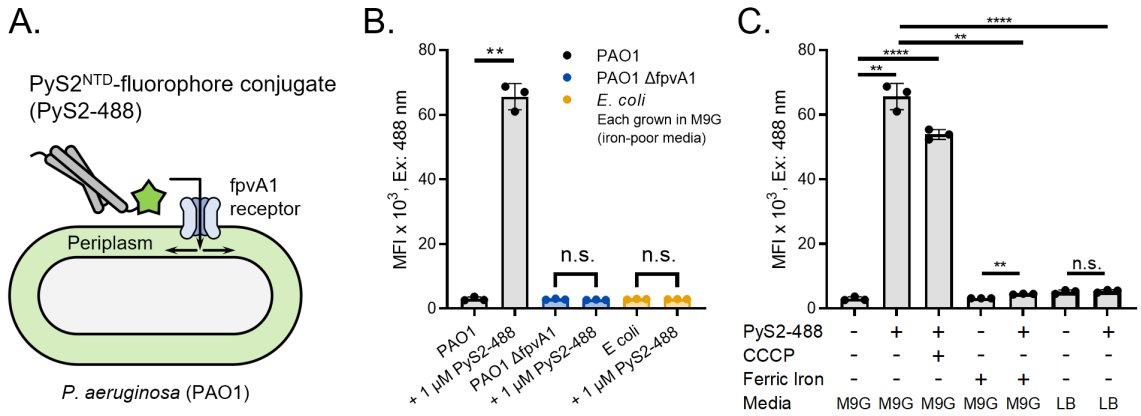

Figure A1.3 Synthetic PyS2^{NTD}-488 binds *P. aeruginosa* with expected species- and receptor-specificity. **(A)** The FpvA-dependent internalization of PyS2^{NTD}-fluorophore conjugate can be monitored by the emitted fluorescence signal via flow cytometry. **(B)** Flow cytometry indicates species specificity staining of PyS2-488 with only PAO1 positively stained in comparison to control (p = 0.0011), whereas knockout strain PAO1 Δ*fpvA* and *E. coli* (ATCC 25922) showed no staining when grown in iron-poor minimal M9 Glucose (M9G) media (p = 0.297 and p = 0.837, respectively). **(C)** Growth and staining conditions known to affect the abundance and function of FpvA further confirmed that PyS2-488 is binding to FpvA. Positive staining is observed in minimal M9G compared to control (p = 0.0011). The addition of the CCCP internalization inhibitor (100 µM pretreatment) minimally affected PyS2-488 staining as it only affects periplasmic internalization and accumulation, leaving FpvA abundance and thus PyS2-488 staining unaffected (p < 0.0001 compared to control PAO1). Limited staining was observed if ferric iron is added to M9G or iron-rich media (Luria Broth, LB) is used because the iron scavenging function of the FpvA is less critical (p = 0.0014 and < 0.0001 compared to PAO1 in M9G, respectively).[57] All experimental conditions were completed with n = 3 biological replicates with individual data points shown and all statistical t-tests shown are paired t-test, two-tailed with Welch's correction with $p \leq 0.01$, 0.001, 0.0001, represented as **, ***, and **** respectively.

The uptake of the PyS2^{NTD}-AZDye488 conjugate (PyS2-488) into *P. aeruginosa* was then evaluated using flow cytometry and fluorescence microscopy (**Figure A1.3A**). Natively, PyS2 binds to the ferripyoverdine receptor (FpvA) with high affinity (dissociation constant, K_D < 1 nM)[45] and undergoes internalization through a process in which the proton motive force coupled to the inner membrane protein TonB1 facilitates transport after FpvA binding. Thus, PyS2-488 should demonstrate species specificity for *P. aeruginosa* and receptor specificity for FpvA. PAO1 was used as an FpvA-positive strain, with FpvA-negative controls including *E. coli* (ATCC 25922) and a PAO1 FpvA null (Δ*fpvA* deletion, see Supporting Information). Treatment of the bacteria with PyS2-488 revealed species and receptor-specific staining with PAO1 only demonstrating a positive signal (**Figure A1.3B**).

Additional media conditions were examined to further test the receptor binding specificity and internalization of PyS2-488 (**Figure A1.3C**). The regulation of FpvA receptor expression depends on the bacterial environment: iron-poor conditions promote the production of the ferripyoverdine iron scavenger and its cognate receptor FpvA.[54] Thus, the PAO1 and PAO1 Δ*fpvA* were grown in either a minimal media M9 Glucose (M9G) containing no iron or M9G supplemented with 17 μM ferric (+3) iron chloride to replicate iron-rich conditions (e.g., Luria broth).[55,56] For control experiments, the proton motive force was diminished by the pre-treatment of PAO1 with protonophore carbonyl cyanide m-chlorophenyl hydrazone (CCCP). The use of CCCP thus inhibits PyS2-488 internalization, while leaving FpvA binding unaffected. Treatment of the bacteria with PyS2-488 revealed staining consistent with the environment- and proton motive force-dependent presence of the FpvA-TonB transport system. Specifically, the presence of ferric iron in the growth media ablated PyS2-488

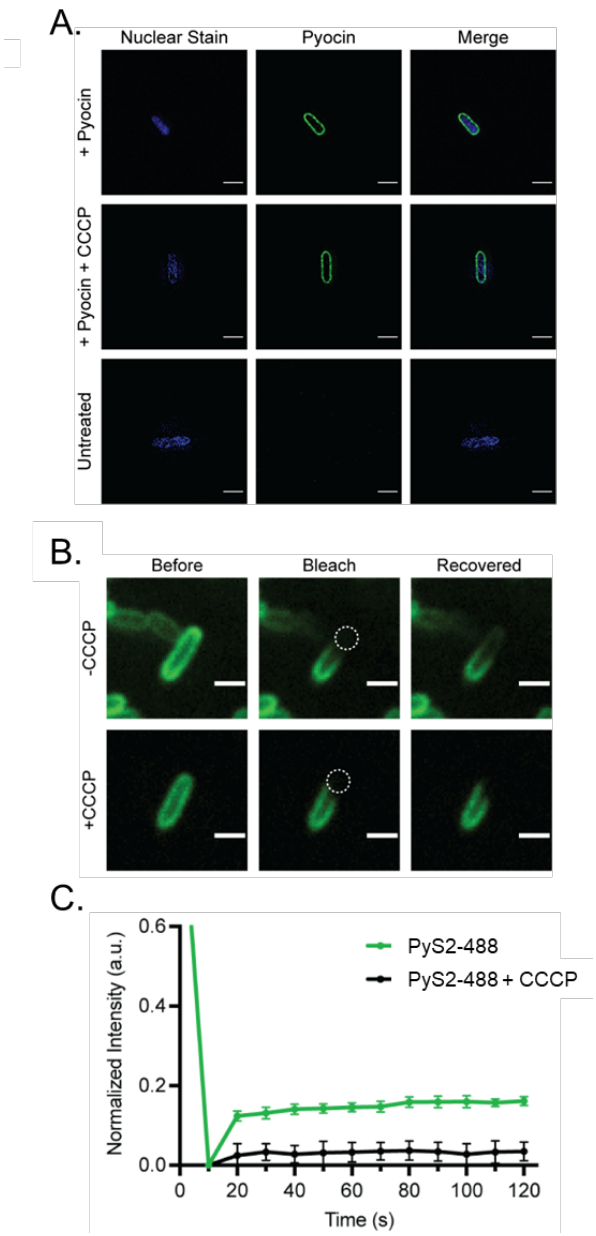

Figure A1.4 PyS2-488 binds *P. aeruginosa* and achieves periplasmic localization. (A) Super resolution structured illumination microscopy (SIM) confirming periplasmic and outer membrane localization of PyS2-488 (Scale bar = 3 μm). **(B)** Confocal fluorescence microscopy demonstrated localization of PyS2-488 to the outer membrane and periplasm and fluorescence recovery after photobleaching (FRAP) (Scale bar = 3 μm). **(C)** FRAP analysis illustrates PyS2-488 achieves periplasmic localization as a result of CCCP-dependent recovery.

staining, likely because of the lack of FpvA expression and survival dependence on iron-scavenging. CCCP had a minimal effect to reduce the strong staining of PyS2-488, likely because FpvA binding was uninhibited, but internalization and accumulation of PyS2-488 in the periplasm was slowed.

To evaluate FpvA-based binding and internalization of PyS2-488 further, fluorescence microscopy techniques were used to assess periplasmic localization of PyS2-488 of the positively stained samples (PAO1 and PAO1 + the internalization inhibitor CCCP). PAO1 cells stained with PyS2-488 are expected to achieve periplasmic internalization.[45] However, the PyS2-488-stained PAO1 cells pretreated with the internalization inhibitor CCCP should only show outer membrane localization because CCCP diminishes the proton motor force utilized by PyS2 for internalization. PyS2-488-stained PAO1 cells examined by confocal

microscopy and super resolution structured illumination microscopy (SIM) revealed that the staining was localized to the outer envelope of PAO1 (**Figure A1.4A**) as expected. However, these observations did not discriminate between the outer membrane and periplasmic localization of PyS2-488.

To gain further insight into subcellular localization of PyS2-488, fluorescence recovery after photobleaching (FRAP) was used to determine if this staining was a result of binding at the outer membrane to FpvA or within the periplasm after internalization (**Figure A1.4B,C**). If internalized to the periplasm, PyS2-488 would diffuse and recovery from FRAP would be observed. In contrast, the diffusion of outer membrane proteins is limited, therefore, FRAP recovery would not be observed if the fluorescently labeled protein is bound to FpvA on the outer membrane. PAO1 stained with PyS2-488 demonstrated partial rapid recovery, indicative of localization within the periplasm and ability to diffuse. In contrast, PAO1 cells pretreated with CCCP did not recover (Figure 5B), likely because most PyS2-488 was bound to the diffusion-limited outer membrane protein FpvA. Thus, we conclude that synthetic PyS2-488 was able to internalize into the *P. aeruginosa* periplasm. A large fraction of the fluorescence signal was bleached and did not recover relative to the original signal, suggesting that the majority of the PyS2-488 may remain bound to the FpvA receptor or undergoing transport. This recovery level is similar to those observed for recombinant $PyS2^{NTD}$.[45]

A1.4 Conclusions

We report the single-shot solid-phase peptide synthesis of a 214 residue-long protein. The $PyS2^{NTD}$ was manufactured in under 10 hours with an academic laboratory-scale automated fast-flow synthesizer and folded with and without fluorophore conjugation. The chemical synthesis of $PyS2^{NTD}$ proceeded rapidly with high fidelity to

yield a protein of unprecedented sequence length. This work further demonstrates the capabilities of automated flow synthesis technology and should further inspire the use of chemically synthesized proteins to interrogate biology.

The synthetic PyS2^{NTD} had similar biophysical and biological function to those reported for the recombinant protein. Moreover, fluorophore-labeled PyS2-488 showed species- and FpvA receptor-specific binding and internalization. PyS2-488 staining supported the binding of PyS2-488 specifically to the FpvA receptor, evidenced by the limited staining of PAO1 Δ*fpvA*, *E. coli*, and PAO1 when grown with iron supplementation compared to the strong staining seen from PAO1 grown in iron-poor media. After FpvA-binding, synthetic PyS2-488 was localized in the periplasm, which required FpvA-coupled transport. Evidence for this transport was the transport inhibition by proton motive force inhibitor CCCP and its FRAP recovery in comparison to untreated PAO1.

Access to this class of pyocin proteins enables the exploration and potential development of non-traditional species-specific antimicrobials against *P. aeruginosa* infections. The low permeability of the outer membrane of *P. aeruginosa* is a major roadblock in developing new antibiotics. Although there are environment-dependent (ferric iron) effects of the internalization efficiency of PyS2^{NTD}, the expression level of the ferripyoverdine receptor is related to the virulence of *P. aeruginosa*. At a minimum, pyocin-based antimicrobials stand to add selection pressure against the ferripyoverdine receptor, like inhibitors that have improved survival of the host *in vivo*.[57]

A1.5 Experimental Details

A1.5.1 Protein Synthesis and Purification

The PyS2^{NTD} sequence synthesized on 100 mg of pre-swollen LL ChemMatrix Rink Amide resin (0.17 mmol/g) using the published optimized protocol for automated flow peptide synthesis (AFPS) as described previously.[42] Briefly, utilizing an automated synthesizer, amine-free DMF washed the resin before coupling, after coupling, and after deprotection. Coupling was performed with HATU, except C, H, N, Q, R, V, T with PyAOP. Deprotection was completed with 20% piperidine in amine-free DMF with 2% formic acid (2 pumps, 40 mL/min). Amino acids were iteratively coupled and deprotected until finished. After synthesis, the resin was washed with DMF and dichloromethane (3 x 5 mL each) and dried. Reagent K solution (82.5% TFA, 5% water, 5% phenol, 5% thioanisole, 2.5% EDT) was used for global cleavage for 4 h at room temperature (RT, 15 mL + 5 mL washes), triturated with cold diethyl ether (3 x 45 mL), suspended in 50% acetonitrile in water (0.1% TFA), and lyophilized.

The lyophilized crude sample of PyS2^{NTD} was weighed, dissolved in 10 mL of 6 M guanidinium chloride, 0.1 M dithiothreitol (DTT), in 50 mM sodium phosphate pH 7.5, vortexed briefly, 0.2 μm filtered, and subjected to RP-HPLC purification using a Agilent Zorbax 300SB-C18 PrepHT (21.2 × 250 mm, 7 μm) heated at 60 °C at 20.0 mL/min with the following optimized gradient: isocratic 5% B from 0–5 min; linear gradient from 5–35% B from 5–12 min; isocratic 35% B from 12–15 min; linear gradient from 35–45% B from 15–45 min; linear gradient from 45–65% B from 45–50 min; isocratic 65% B from 50–55 min. Fractions showing high purity charge state series were combined and lyophilized, leading to the purification of 182 mg of crude to isolate 10.3 mg of HPLC-purified PyS2^{NTD} (6% yield).

A1.5.2 Staining of *P. aeruginosa* with PyS2-488

E. coli (ATCC 25922), PAO1, and *ΔfpvA* were grown overnight in Luria broth (LB), M9 glucose (M9G), or M9G supplemented with 17 μM ferric iron chloride at 37 °C to stationary phase. The cultures were spun for 10 minutes at 3.2 k rcf, resuspended, and washed with blocking buffer (0.5% BSA in M9G, 0.01% Tween80) three times. Bacteria were stained with 1 μM PyS2-488 and 5 μM cell-permeant SYTO 40 Blue at an OD_{600} = 3.6 in 100 μL for 30 minutes at RT and washed three times with blocking buffer. If used, 100 μM CCCP was added 10 minutes before staining and maintained through all washes as was 5 μM SYTO 40 Blue. After the last wash, cells were resuspended in 0.5% BSA in M9G with 0.05% Tween80 with 5 μM SYTO 40 Blue.

A1.5.3 Flow Cytometry

Stained and unstained bacteria-only controls were diluted ten-fold in 0.5% BSA in M9G with 0.05% Tween80 with 5 μM SYTO 40 Blue and placed into flow tubes (Corning Cat. 352235), if used, 100 μM of CCCP was added to all buffers. An Attune NxT Flow Cytometer with 405 nm, 488 nm, 561 nm, and 640 nm lasers analyzed 10,000 cells at low flow rate in biological triplicate after using the unstained controls first to set gates. Data were analyzed using the FlowJo software package (FlowJo LLC). Mean fluorescence intensity was calculated using a geometric mean.

A1.5.4 Fluorescence Microscopy

Stained and unstained bacteria-only controls were dispensed (3-5 μL) on to pre-prepared pads of 1% agarose in M9G (with CCCP if needed) assembled using a 125 μL (1.7 x 2.8 cm) Gene Frames on 1.0 mm glass microscope slides (2.5 x 7.5 cm) and then sealed with a coverslip (thickness 1 1/2, 2.4 x 40 cm). Samples were then visualized

using an Andor Revolution Spinning Disk Confocal using a 100× oil immersion objective with 1.4 N.A. Differential Interference Contrast (brightfield). Fluorescent confocal images excited at 405 nm and 488 nm to observe the SYTO 40 Blue at 447/60 nm and AzDye488 ($PyS2^{NTD}$-fluorophore conjugate) at 525/40 nm, respectively, on a Andor iXon 897E back-illuminated EM-CCD camera. FRAP was completed using the Andor FRAPPA photomanipulation system, capturing multiple bacteria (n = 10) for analysis. A portion of each cell was photobleached with a dwell time of 250 μs, twice. Images were acquired before FRAP and recovery was observed afterward every 10 seconds for 2 minutes and analyzed with ImageJ using previously reported methods.[58] The values were initialized at 1 and immediately after photobleaching, the value was 0.

A1.6 Acknowledgments

The authors thank A. Callahan for helpful discussions on protein folding. This research was supported by a grant from the National Institute of Allergy and Infectious Diseases (U19 AI142780). A. Saebi gratefully acknowledges support from the National Science Foundation Graduate Research Fellowship under Grant no. 1122374. J.S. Brown acknowledges support from the Pharmaceutical Research and Manufacturers of America (PhRMA) through the Postdoctoral Fellowship in Drug Discovery. V.M. Marando acknowledges support from the Natural Sciences and Engineering Research Council of Canada (NSERC) through the PGSD Fellowship. We thank the MIT Koch Institute's Robert A. Swanson (1969) Biotechnology Center for technical support (NCI Cancer Center Support Grant P30 CA14051), specifically The Microscopy Core Facility and J.R. Kuhn. Also, we thank the W.M. Keck imaging facility at the Whitehead Institute for access to the ANDOR FRAPPA confocal microscope.

A1.7 References

1. Kent, S. B. H. Novel Protein Science Enabled by Total Chemical Synthesis. *Protein Sci.* **2019**, *28* (2), 313–328.

2. Rosano, G. L.; Ceccarelli, E. A. Recombinant Protein Expression in Escherichia Coli: Advances and Challenges. *Front Microbiol* **2014**, *5* (APR), 172.

3. Nilsson, B. L.; Soellner, M. B.; Raines, R. T. Chemical Synthesis of Proteins. *Annu Rev Biophys Biomol Struct* **2005**, *34* (1), 91–118.

4. Tan, Y.; Wu, H.; Wei, T.; Li, X. Chemical Protein Synthesis: Advances, Challenges, and Outlooks. *J. Am. Chem. Soc.* **2020**, *142* (48), 20288–20298.

5. Kulkarni, S. S.; Sayers, J.; Premdjee, B.; Payne, R. J. Rapid and Efficient Protein Synthesis through Expansion of the Native Chemical Ligation Concept. *Nat Rev Chem* **2018**, *2* (4), 0122.

6. Merrifield, R. B. Solid Phase Peptide Synthesis. I. The Synthesis of a Tetrapeptide. *J Am Chem Soc* **1963**, *85* (14), 2149–2154.

7. Frederick, M. O.; Boyse, R. A.; Braden, T. M.; Calvin, J. R.; Campbell, B. M.; Changi, S. M.; Coffin, S. R.; Condon, C.; Gowran, O.; McClary Groh, J.; Groskreutz, S. R.; Harms, Z. D.; Humenik, A. A.; Kallman, N. J.; Klitzing, N. D.; Kopach, M. E.; Kretsinger, J. K.; Lambertus, G. R.; Lampert, J. T.; Maguire, L. M.; Moynihan, H. A.; Mullane, N. S.; Murphy, J. D.; O'Mahony, M. E.; Richey, R. N.; Seibert, K. D.; Spencer, R. D.; Strege, M. A.; Tandogan, N.; Torres Torres, F. L.; Tsukanov, S. v.; Xia, H. Kilogram-Scale GMP Manufacture of Tirzepatide Using a Hybrid SPPS/LPPS Approach with Continuous Manufacturing. *Org Process Res Dev* **2021**, *25* (7), 1628–1636.

8. Bray, B. L. Innovation: Large-Scale Manufacture of Peptide Therapeutics by Chemical Synthesis. *Nat Rev Drug Discov* **2003**, *2* (7), 587–593.

9. Coin, I.; Beyermann, M.; Bienert, M. Solid-Phase Peptide Synthesis: From Standard Procedures to the Synthesis of Difficult Sequences. *Nat Protoc* **2007**, *2* (12), 3247–3256.

10. Tan, Y.; Wu, H.; Wei, T.; Li, X. Chemical Protein Synthesis: Advances, Challenges, and Outlooks. *J Am Chem Soc* **2020**, *142* (48), 20288–20298.

11. Dawson, P. E.; Muir, T. W.; Clark-Lewis, I.; Kent, S. B. H. Synthesis of Proteins by Native Chemical Ligation. *Science (1979)* **1994**, *266* (5186), 776–779.

12. Pattabiraman, V. R.; Ogunkoya, A. O.; Bode, J. W.; Pattabiraman, V. R.; Ogunkoya, A. O.; Bode, J. W. Chemical Protein Synthesis by Chemoselective α-Ketoacid–Hydroxylamine (KAHA) Ligations with 5-Oxaproline. *Angewandte Chemie International Edition* **2012**, *51* (21), 5114–5118.

13. Fan, C.; Deng, Q.; Zhu, T. F. Bioorthogonal Information Storage in L-DNA with a High-Fidelity Mirror-Image Pfu DNA Polymerase. *Nat Biotechnol* **2021**, *39* (12), 1548–1555.

14. Sun, H.; Brik, A. The Journey for the Total Chemical Synthesis of a 53 KDa Protein. *Acc Chem Res* **2019**, *52* (12), 3361–3371.

15. Tang, S.; Liang, L. J.; Si, Y. Y.; Gao, S.; Wang, J. X.; Liang, J.; Mei, Z.; Zheng, J. S.; Liu, L. Practical Chemical Synthesis of Atypical Ubiquitin Chains by Using an Isopeptide-Linked Ub Isomer. *Angewandte Chemie International Edition* **2017**, *56* (43), 13333–13337.

16. Xu, W.; Jiang, W.; Wang, J.; Yu, L.; Chen, J.; Liu, X.; Liu, L.; Zhu, T. F. Total Chemical Synthesis of a Thermostable Enzyme Capable of Polymerase Chain Reaction. *Cell Discov* **2017**, *3* (1), 17008.

17. Weinstock, M. T.; Jacobsen, M. T.; Kay, M. S. Synthesis and Folding of a Mirror-Image Enzyme Reveals Ambidextrous Chaperone Activity. *Proc Natl Acad Sci U S A* **2014**, *111* (32), 11679–11684.

18. Wintermann, F.; Engelbrecht, S. Reconstitution of the Catalytic Core of F-ATPase (Aβ)3γ from Escherichia Coli Using Chemically Synthesized Subunit γ. *Angewandte Chemie International Edition* **2013**, *52* (4), 1309–1313.

19. Eid, E.; Boross, G. N.; Sun, H.; Msallam, M.; Singh, S. K.; Brik, A. Total Chemical Synthesis of ISGylated-Ubiquitin Hybrid Chain Assisted by Acetamidomethyl Derivatives with Dual Functions. *Bioconjug Chem* **2020**, *31* (3), 889–894.

20. Jacobsen, M. T.; Petersen, M. E.; Ye, X.; Galibert, M.; Lorimer, G. H.; Aucagne, V.; Kay, M. S. A Helping Hand to Overcome Solubility Challenges in Chemical Protein Synthesis. *J Am Chem Soc* **2016**, *138* (36), 11775–11782.

21. Anfinsen, C. B. Principles That Govern the Folding of Protein Chains. *Science (1979)* **1973**, *181* (4096), 223–230.

22. Bacsa, B.; Horváti, K.; Bõsze, S.; Andreae, F.; Kappe, C. O. Solid-Phase Synthesis of Difficult Peptide Sequences at Elevated Temperatures: A Critical Comparison of Microwave and Conventional Heating Technologies. *Journal of Organic Chemistry* **2008**, *73* (19), 7532–7542.

23. Atherton, E.; Woolley, V.; Sheppard, R. C. Internal Association in Solid Phase Peptide Synthesis. Synthesis of Cytochrome C Residues 66–104 on Polyamide Supports. *J Chem Soc Chem Commun* **1980**, No. 20, 970–971.

24. Bedford, J.; Hyde, C.; Johnson, T.; Jun, W.; Owen, D.; Quibell, M.; Sheppard, R. C. Amino Acid Structure and "Difficult Sequences" in Solid Phase Peptide Synthesis. *Int J Pept Protein Res* **2009**, *40* (3–4), 300–307.

25. White, P.; Keyte, J. W.; Bailey, K.; Bloomberg, G. Expediting the Fmoc Solid Phase Synthesis of Long Peptides through the Application of Dimethyloxazolidine Dipeptides. *Journal of Peptide Science* **2004**, *10* (1), 18–26.

26. Cardona, V.; Eberle, I.; Barthélémy, S.; Beythien, J.; Doerner, B.; Schneeberger, P.; Keyte, J.; White, P. D. Application of Dmb-Dipeptides in the Fmoc SPPS of Difficult and Aspartimide-Prone Sequences. *Int J Pept Res Ther* **2008**, *14* (4), 285–292.

27. Jad, Y. E.; Acosta, G. A.; Khattab, S. N.; de La Torre, B. G.; Govender, T.; Kruger, H. G.; El-Faham, A.; Albericio, F. Peptide Synthesis beyond DMF: THF and ACN as Excellent and Friendlier Alternatives. *Org Biomol Chem* **2015**, *13* (8), 2393–2398.

28 Pedersen, S. L.; Tofteng, A. P.; Malik, L.; Jensen, K. J. Microwave Heating in Solid-Phase Peptide Synthesis. *Chem Soc Rev* **2012**, *41* (5), 1826–1844.

29. Collins, J. M.; Porter, K. A.; Singh, S. K.; Vanier, G. S. High-Efficiency Solid Phase Peptide Synthesis (HE -SPPS). *Org Lett* **2014**, *16* (3), 940–943.

30. Johnson, E. C. B.; Malito, E.; Shen, Y.; Rich, D.; Tang, W. J.; Kent, S. B. H. Modular Total Chemical Synthesis of a Human Immunodeficiency Virus Type 1 Protease. *J Am Chem Soc* **2007**, *129* (37), 11480–11490.

31. Mueller, L. K.; Baumruck, A. C.; Zhdanova, H.; Tietze, A. A. Challenges and Perspectives in Chemical Synthesis of Highly Hydrophobic Peptides. *Front Bioeng Biotechnol* **2020**, *8*, 162.

32. Schmidt, M.; Toplak, A.; Rozeboom, H. J.; Wijma, H. J.; Quaedflieg, P. J. L. M.; van Maarseveen, J. H.; Janssen, D. B.; Nuijens, T. Design of a Substrate-Tailored Peptiligase Variant for the Efficient Synthesis of Thymosin-A1. *Org Biomol Chem* **2018**, *16* (4), 609–618.

33. Sletten, E. T.; Nuño, M.; Guthrie, D.; Seeberger, P. H. Real-Time Monitoring of Solid-Phase Peptide Synthesis Using a Variable Bed Flow Reactor. *Chemical Communications* **2019**, *55* (97), 14598–14601.

34. Atherton, E.; Brown, E.; Sheppard, R. C.; Rosevear, A. A Physically Supported Gel Polymer for Low Pressure, Continuous Flow Solid Phase Reactions. Application to Solid Phase Peptide Synthesis. *J Chem Soc Chem Commun* **1981**, No. 21, 1151–1152.

35. Farkas, V.; Ferentzi, K.; Horváti, K.; Perczel, A. Cost-Effective Flow Peptide Synthesis: Metamorphosis of HPLC. *Org Process Res Dev* **2021**, *25* (2), 182–191.

36. Miranda, L. P.; Alewood, P. F. Accelerated Chemical Synthesis of Peptides and Small Proteins. *Proc Natl Acad Sci U S A* **1999**, *96* (4), 1181–1186.

37. Merrifield, R. B.; Stewart, J. M.; Jernberg, N. Instrument for Automated Synthesis of Peptides. *Anal Chem* **1966**, *38* (13), 1905–1914.

38. Lukas, T. J.; Prystowsky, M. B.; Erickson, B. W. Solid-Phase Peptide Synthesis under Continuous-Flow Conditions. *Proceedings of the National Academy of Sciences* **1981**, *78* (5), 2791–2795.

39. Mijalis, A. J.; Thomas, D. A.; Simon, M. D.; Adamo, A.; Beaumont, R.; Jensen, K. F.; Pentelute, B. L. A Fully Automated Flow-Based Approach for Accelerated Peptide Synthesis. *Nat Chem Biol* **2017**, *13* (5), 464–466.

40. Michels, T.; Dölling, R.; Haberkorn, U.; Mier, W. Acid-Mediated Prevention of Aspartimide Formation in Solid Phase Peptide Synthesis. *Org Lett* **2012**, *14* (20), 5218–5221.

41. Gates, Z. P.; Hartrampf, N. Flow-based SPPS for Protein Synthesis: A Perspective. *Peptide Science* **2020**, *112* (6) 1-16.

42. Hartrampf, N.; Saebi, A.; Poskus, M.; Gates, Z. P.; Callahan, A. J.; Cowfer, A. E.; Hanna, S.; Antilla, S.; Schissel, C. K.; Quartararo, A. J.; Ye, X.; Mijalis, A. J.; Simon, M. D.; Loas, A.; Jessen, C.; Nielsen, T. E.; Pentelute, B. L. Synthesis of Proteins by Automated Flow Chemistry. *Science (1979)* **2020**, *987* (May), 1–20.

43. Michel-Briand, Y.; Baysse, C. The Pyocins of Pseudomonas Aeruginosa. *Biochimie* **2002**, *84* (5–6), 499–510.

44. Denayer, S.; Matthijs, S.; Cornelis, P. Pyocin S2 (Sa) Kills Pseudomonas Aeruginosa Strains via the FpvA Type I Ferripyoverdine Receptor. *J Bacteriol* **2007**, *189* (21), 7663–7668.

45. White, P.; Joshi, A.; Rassam, P.; Housden, N. G.; Kaminska, R.; Goult, J. D.; Redfield, C.; McCaughey, L. C.; Walker, D.; Mohammed, S.; Kleanthous, C. Exploitation of an Iron Transporter for Bacterial Protein Antibiotic Import. *Proc Natl Acad Sci U S A* **2017**, *114* (45), 12051–12056.

46. Lister, P. D.; Wolter, D. J.; Hanson, N. D. Antibacterial-Resistant Pseudomonas Aeruginosa: Clinical Impact and Complex Regulation of Chromosomally Encoded Resistance Mechanisms. *Clin Microbiol Rev* **2009**, *22* (4), 582–610.

47. Hancock, R. E. W. Resistance Mechanisms in Pseudomonas Aeruginosa and Other Nonfermentative Gram-Negative Bacteria. *Clinical Infectious Diseases* **1998**, *27* (Supplement_1), S93–S99.

48. Shao, X.; Xie, Y.; Zhang, Y.; Liu, J.; Ding, Y.; Wu, M.; Wang, X.; Deng, X. Novel Therapeutic Strategies for Treating Pseudomonas Aeruginosa Infection. *Expert Opin Drug Discov* **2020**, *15* (12), 1403–1423.

49. Behrens, H. M.; Six, A.; Walker, D.; Kleanthous, C. The Therapeutic Potential of Bacteriocins as Protein Antibiotics. *Emerg Top Life Sci* **2017**, *1* (1), 65–74.

50 Mohapatra, S.; Hartrampf, N.; Poskus, M.; Loas, A.; Gómez-Bombarelli, R.; Pentelute, B. L. Deep Learning for Prediction and Optimization of Fast-Flow Peptide Synthesis. *ACS Cent Sci* **2020**, acscentsci.0c00979.

51 Yamaguchi, H.; Miyazaki, M. Refolding Techniques for Recovering Biologically Active Recombinant Proteins from Inclusion Bodies. *Biomolecules 2014, Vol. 4, Pages 235-251* **2014**, *4* (1), 235–251.

52. Greenfield, N. J. Using Circular Dichroism Spectra to Estimate Protein Secondary Structure. *Nat Protoc* **2006**, *1* (6), 2876–2890.

53. Greenfield, N. J. Using Circular Dichroism Collected as a Function of Temperature to Determine the Thermodynamics of Protein Unfolding and Binding Interactions. *Nat Protoc* **2007**, *1* (6), 2527–2535.

54. Butaitė, E.; Kramer, J.; Wyder, S.; Kümmerli, R. Environmental Determinants of Pyoverdine Production, Exploitation and Competition in Natural Pseudomonas Communities. *Environ Microbiol* **2018**, *20* (10), 3629–3642.

55. Abdul-Tehrani, H.; Hudson, A. J.; Chang, Y. S.; Timms, A. R.; Hawkins, C.; Williams, J. M.; Harrison, P. M.; Guest, J. R.; Andrews, S. C. Ferritin Mutants of Escherichia Coli Are Iron Deficient and Growth Impaired, and Fur Mutants Are Iron Deficient. *J Bacteriol* **1999**, *181* (5), 1415–1428.

56. Yang, Y.; Harris, D. P.; Luo, F.; Xiong, W.; Joachimiak, M.; Wu, L.; Dehal, P.; Jacobsen, J.; Yang, Z.; Palumbo, A. v.; Arkin, A. P.; Zhou, J. Snapshot of Iron Response in Shewanella Oneidensis by Gene Network Reconstruction. *BMC Genomics* **2009**, *10* (1), 1–17.

57. Kang, D.; Revtovich, A. v.; Chen, Q.; Shah, K. N.; Cannon, C. L.; Kirienko, N. v. Pyoverdine-Dependent Virulence of Pseudomonas Aeruginosa Isolates From Cystic Fibrosis Patients. *Front Microbiol* **2019**, *10*, 2048.

58. Day, C. A.; Kraft, L. J.; Kang, M.; Kenworthy, A. K. Analysis of Protein and Lipid Dynamics Using Confocal Fluorescence Recovery After Photobleaching (FRAP). *Curr Protoc Cytom* **2012**, *62* (1), 2.19.1-2.19.29.

Appendix 2: Identifying New Inhibitors of UDP-galactofuranose Mutase

Contributions:
Enzyme prepared by Victoria M. Marando and Nutchapong Suwanwong. NMR samples prepared by Victoria M. Marando, Nutchapong Suwanwong and Alby Joseph. NMR data collected and analyzed in collaboration with Yann Ayotte, Steven R. LaPlante and the Harvard Medical School Bio-molecular NMR Facility. Research designed by Victoria M. Marando and Laura L. Kiessling.

A2.1 Abstract

Approximately one quarter of the world's population is infected by *Mtb*, the etiological agent of Tuberculosis (TB). *Mtb* has been particularly difficult to eradicate largely due to its elaborate and protective cell wall. Several enzymes involved in *Mtb* cell wall assembly are targeted by existing anti-TB drugs, but efficacy and drug resistance remain major challenges. Despite previous successes targeting cell wall assembly, UGM, an enzyme involved in the biosynthesis of the galactan remains undrugged. UGM is essential and predicted to be highly vulnerable as a drug target based on CRISPRi screening. Previous inhibitor scaffolds suffer from poor potency limiting downstream drug development. We therefore applied a fragment-based approach to develop novel UGM inhibitors. We performed a fragment-based screen measuring binding by orthogonal NMR assays. We identified preliminary structure-activity relationships based on screening data. Finally, we have validated an orthogonal binding assay to validate elaborated fragments. Ultimately, we anticipate that the efforts described in this chapter will serve as a starting point for further development of potent UGM inhibitors.

A2.2 Introduction

Mycobacterium tuberculosis (*Mtb*), the etiological agent of tuberculosis (TB), has plagued humanity for millennia and remains a prominent global health threat.[1] Combating mycobacterial infections is particularly challenging in large part because these bacteria possess a uniquely thick hydrophobic cell wall that is impenetrable to many broad-spectrum antibiotics.[2] The distinct mycobacterial cell envelope is composed of many building blocks unique to microbes, providing exciting opportunities to target biosynthetic enzymes that assemble this structure as therapeutic targets.[3] For instance, front-line antitubercular drugs ethambutol and isoniazid target the formation of the arabinan and mycolic acid components of mycobacteria. However, multidrug-resistant strains of *Mtb* are on the rise and there is a need for new drug targets.[4] There is one component of the cell envelope whose biosynthesis is not inhibited by existing drugs or potent chemical probes, the galactan.

The galactan is a linear polysaccharide of D-galactofuranose (Gal*f*) residues with alternating β-1-5, β-1-6 linkages, that serves to connect the peptidoglycan to the arabinan polysaccharide chains, which in turn provide covalent attachment points for the lipophilic mycolic acids.[5-6] In the absence of the galactan, cell wall construction is halted and mycobacterial growth is compromised. Recent work from our group has highlighted an additional role the galactan may play in mycobacteria as a regulator of cell shape and antibiotic susceptibility further supporting this polysaccharide as an exciting drug target.[7] Indeed, based on a CRISPRi screen in mycobacteria, all key biosynthetic enzymes involved in galactan biosynthesis were found to be essential and predicted to be highly vulnerable as drug targets (**Table A2.1**).[8]

Table A2.1 CRISPRi Screen Results for Galactan Biosynthesis Enzymes. Vulnerability index defined as the total fitness cost associated with all theoretical sgRNAs summed into one value.

Enzyme	Gene	TnSeq Gene Essentiality	Vulnerability Index
UDP-galactopyranose mutase (UGM)	*glf*	Essential	-13.4070
UDP-galactofuranoseyltrasnferase (Glft1)	*glfT1*	Essential	-6.8830
UDP-galactofuranoseyltrasnferase (Glft2)	*glfT2*	Essential	-12.7510

Galactan biosynthesis is dependent on the production of uridine 5′-diphosphate galactofuranose (UDP-Galf) by the enzyme UDP-galactopyranose mutase (UGM, also referred to as Glf).[9-10] UGM catalyzes the interconversion of UDP-galactopyranose (UDP-Galp) and UDP-Galf (**Figure A2.1**). Our group and others have sought to identify potent and selective UGM inhibitors.[11-14] A class of 2-aminothiazoles was previously designed by the Kiessling group, that inhibits *M. tuberculosis* UGM (*Mtb*UGM) activity and blocks the growth of *M. smegmatis*. The most potent compound of this inhibitor set displays modest antimycobacterial activity. The next series of compounds produced by our group were designed to improve cell permeability by replacing the carboxylate with a functional group mimic, N-acylsulfonamide.[15] Though these compounds allowed for improved inhibition, they still lacked sufficient potency for downstream applications.

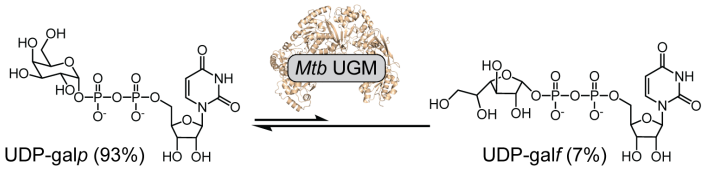

Figure A2.1 Nucleotide-sugar donor isomerization reaction catalyzed by UGM. Equilibrium of this reaction heavily favors the pyranose form of the reaction (~93:7).

In order to modify the current scaffold and significantly improve potency, we turned to fragment-based drug discovery (FBDD).[16] FBDD has emerged over the past few decades as a powerful approach to inhibitor discovery and design.[17] This approach involves assessing small molecule fragments approximately half the size of typically

screened compounds. By screening smaller molecules, there are fewer possible chemical perturbations and therefore it is possible to search through a larger chemical space with fewer compounds and less material. We thought this strategy was particularly relevant to our target as many front-line antibiotics against *Mtb* are similar in complexity to conventional fragments (i.e., ethambutol, pyrazinamide and isoniazid) and therefore similarly effective compounds may not require as much elaboration. We therefore sought to apply this strategy to screen for new binding motifs for *Mtb*UGM. Previously the LaPlante Group has demonstrated the utility of NMR to detect binding between fragments and a wide range of target proteins.[18-19] Herein, we describe progress towards the identification novel inhibitor scaffolds of UGM using NMR-based fragment screening.

A2.3 Results & Discussion

A2.3.1 NMR Fragment-based screen

In order to ensure that the binding data collected by NMR was relevant to a folded UGM, initial target enablement studies were run to assess protein stability over time, DMSO tolerance and protein promiscuity. The ^{1}H NMR spectra suggest that the protein is folded in the assay conditions based on dispersed resonances in the aromatic and aliphatic regions (**Figure A2.2A**). Moreover, the protein was found to be stable over 96 h (**Figure A2.2B**) and tolerates up to 3.6% DMSO with only minor perturbations in the aromatic region (**Figure A2.2C**). We performed these studies in the absence and presence of sodium dithionite as UGM has been shown to occupy two distinct conformations depending on if it is in a reduced or oxidized state.[20]

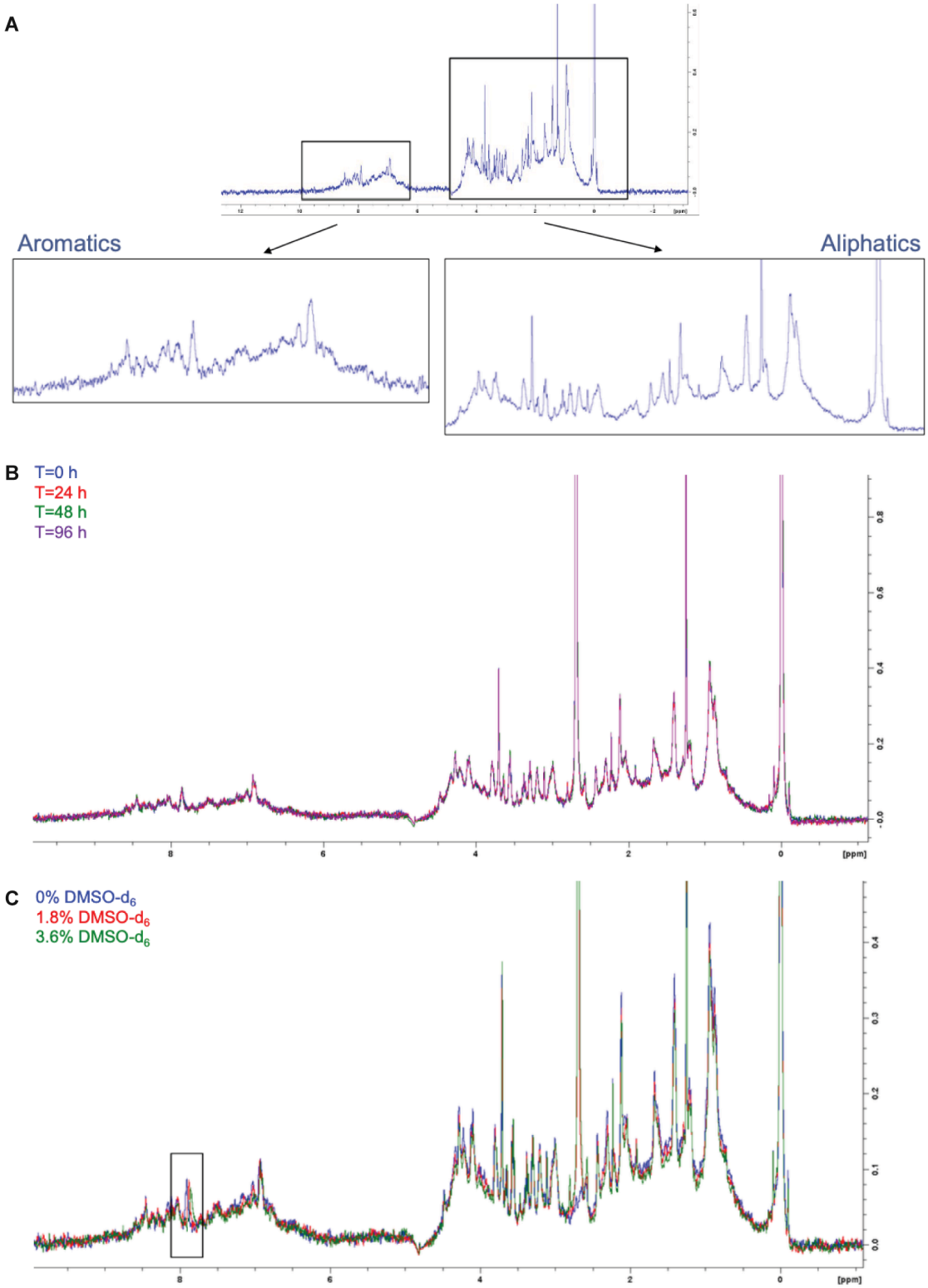

Figure A2.2 Summary of enablement study for *Mtb*UGM fragment-based screen by NMR. **(A)** Protein resonances were observed to be dispersed suggesting that the protein is folded. **(B)** No significant changes were observed in shifts or peak intensity over 96 h. **(C)** No significant changes were observed in shifts or peak intensity with up to 3.6% DMSO with only minor perturbations in the aromatic region.

Following this, *Mtb* UGM was screened against the NMX Fast-Screen ^{19}F fragment library.[21] We screened pools of compounds (31 pools of 7-12 compounds each) for a total of 461 compounds. These fragments pools were designed to prevent signal overlap which allows for analysis of pools. Pooled analysis is critical to reduce NMR time and increase screening throughput. To determine binding, we used two orthogonal experiments: differential line broadening (DLB) and spin–spin relaxation Carr–Purcell–Meiboom–Gill (T2-CPMG) experiments. DLB reports on differences in NMR signals as a result of changes in chemical environment for free molecules relative to bound molecules. T2-CPMG exploits differences in NMR relaxation properties of free molecules relative to bound molecules based on differences in size and tumbling rates. In addition to testing for binding in this screen, compounds are assessed for signs of aggregation based on changes in relaxation by T2-CPMG NMR.[22] This is important as these and other small molecule fragments have been shown to form nano-entities or aggregates in various screening buffers and conditions. A set of top 10 binders were identified (**Figure A2.3**).

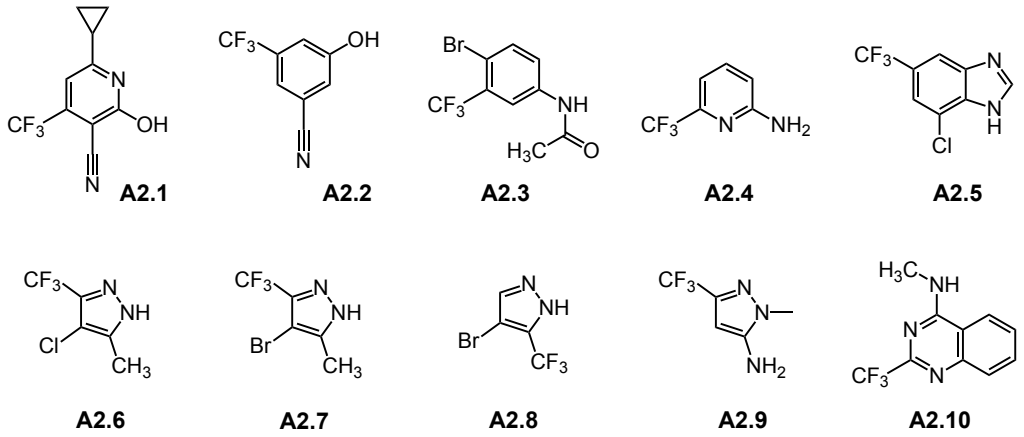

Figure A2.3 Top 10 hits from initial NMR screen against *Mtb*UGM.

A2.3.2 Fragment singleton follow-up

Following this, we deconvoluted the pools using a proprietary program and confirmed binding in singleton assays. This is important as there could be artifacts of the pooled screening that affects binding. We tested the 10 compounds that showed the best binding in the initial screen. All of the tested compounds confirmed binding activity. Four of the tested compounds showed structurally similar motifs providing initial SAR information. 51 additional fragments were purchased and tested in our NMR binding assay for SAR exploration.

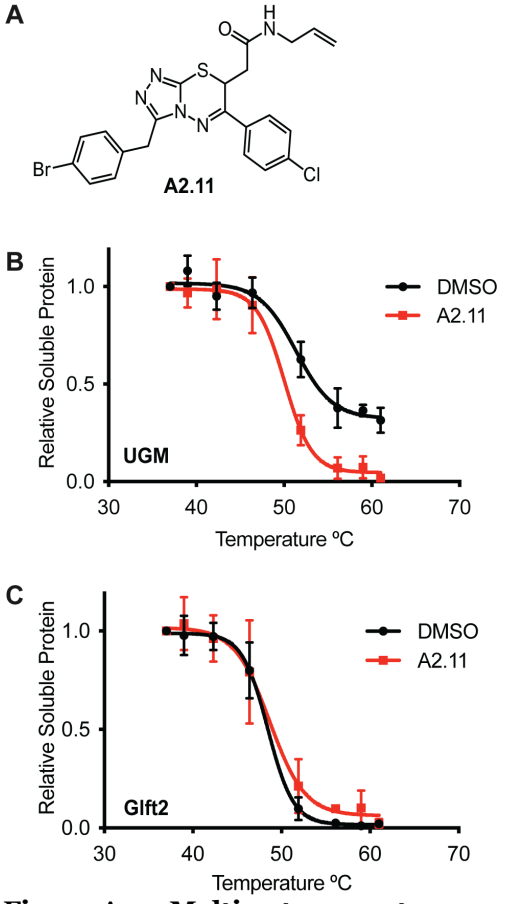

Figure A2.4 Melting temperature binding assay validation. (A) Previous inhibitor of UGM. **(B)** Change in UGM melting temperature upon compound treatment. **(C)** Negative control demonstrating no change in Glft2 melting temperature upon compound treatment.

A2.3.3 Orthogonal assay development

To complement the NMR-screening efforts, we developed an alternative binding assay to validate lead compounds as they are optimized. This assay was designed based on a CETSA workflow.[23-24] Initial studies were performed using a structurally related ortholog of *Mtb* UGM, *C. diphtheria* UGM. Using a previously identified inhibitor (**Figure A2.4A**), we observed destabilization of the protein based on melting temperature curves (**Figure A2.4B**). To further validate this assay, a distinct protein (*Mycobacterium smegmatis* Glft2) that should not bind this compound was tested and showed no changes in melting temperatures (**Figure A2.4C**). We anticipate that this assay will be

useful in characterizing elaborated fragments *in vitro* before moving to cell viability assays.

A2.4 Conclusions

The studies outlined in this chapter can serve as a starting point for the development of novel *Mtb* UGM inhibitors. We demonstrated that NMR-fragment based screening is a viable method for lead discovery in this system based on our enablement study. We then identified and validated fragment hits using two orthogonal binding techniques. These fragments can serve as starting points for elaboration and validation studies. One assay that can be used to develop SAR on elaborated fragments has been validated in this work using *C. diphtheria* UGM. We anticipate that by using fragments as the starting point for this inhibitor discovery campaign, we can more rapidly identify potent inhibitors with good pharmacological properties. Given the importance of galactan biosynthesis for mycobacteria, we anticipate such inhibitors will be important in treatment of TB infections and overcoming antibiotic resistance to current front-line drugs.

A2.5 Experimental Details

A2.5.1 Expression and purification of *Mtb* UGM

*Mtb*UGM was expressed in *E. coli* using recombinant DNA methods and purified as previously described.[11, 13] In brief, *E. coli* BL21 (DE3) cells containing the desired plasmid (MtUGM-pET-29b) were grown in Luria broth (LB) media with 50 μg/mL kanamycin at 37 °C. Cells were cultured to mid-log phase and gene expression was then induced with 0.1 mM IPTG at 18 °C overnight. Cells were then harvested and lysed by cell disruption. His-tagged proteins were purified via Ni-affinity chromatography.

A2.5.2 NMR sample preparation

Samples were prepared in 50 mM sodium phosphate, 10 % D_2O, pH 7.0, with and without 10 mM sodium dithionite and were stored and measured at 278 K. Compounds were tested at 240 μM (8.3 mM stock in DMSO-d_6). Protein was tested at 15 μM.

A2.5.3 NMR methods

NMR spectra were acquired on a 600 MHz NMR spectrometer (probe temperature: 298 K). 1D ^1H NMR spectra, 1D ^{19}F NMR spectra were acquired along with ^{19}F T_2-CPMG for size-filtering aggregation analyses. CPMG experiments employed a sweep width (SW)=20.0263 ppm, recycle delay (D1)=3 s, number of points (TD)=32 000, and four scans for each spectrum. Water suppression was applied using excitation sculpting with gradients.[25] Data were visualized using Bruker's TopSpin software and peak alignment was done using DMSO peak set at 2.49 ppm.

A2.5.4 Melting temperature assay

Procedure was modified from a literature protocol for cellular assays.[23] Protein was prepared as a 1.1 μM stock in 50 mM sodium phosphate, pH 7.0 with 10 mM dithionite (added fresh). Compound A2.11 was tested at 50 μM (10 mM stock in DMSO). Once the

compound was added, samples were incubated at room temperature for 5 min. Samples were aliquoted into PCR tubes and headed in a thermocycler at the indicated temperature for 10 min. Samples were transferred to Eppendorf tubes and denatured protein was removed by centrifugation (12 000 g, 4 °C, 20 min). Following centrifugation, 25 µL of supernatant was mixed with 5 µL 6X SDS loading buffer with DTT and boiled for 5 min. Samples were analyzed by SDS-PAGE and gel was stained using SYPRO™ Protein Gel Stain (Invitrogen Cat. #S6650). Band intensities were quantified using a ChemiDoc™ Imaging System and intensities were calculated relative to the lowest tested temperature (37 °C).

A2.6 References

1. Petersen, E.; Al-Abri, S.; Chakaya, J.; Goletti, D.; Parolina, L.; Wejse, C.; Mucheleng'anga, L. A.; Khalili, S. A.; Yeboah-Manu, D.; Chanda-Kapata, P.; Nasiri, M. J.; Lungu, P. S.; Maeurer, M.; Tiberi, S.; Ntoumi, F.; Battista-Migliori, G.; Zumla, A., World TB Day 2022: Revamping and Reshaping Global TB Control Programs by Advancing Lessons learnt from the COVID-19 pandemic. *Int J Infect Dis* **2022,** *124 Suppl 1*, S1-S3.

2. Dulberger, C. L.; Rubin, E. J.; Boutte, C. C., The mycobacterial cell envelope — a moving target. *Nature Reviews Microbiology* **2019,** *18* (1), 47-59.

3. Besra, G. S.; Khoo, K. H.; McNeil, M. R.; Dell, A.; Morris, H. R.; Brennan, P. J., A new interpretation of the structure of the mycolyl-arabinogalactan complex of Mycobacterium tuberculosis as revealed through characterization of oligoglycosylalditol fragments by fast-atom bombardment mass spectrometry and 1H nuclear magnetic resonance spectroscopy. *Biochemistry* **1995,** *34* (13), 4257-66.

4. Yadav, P., Challenges and Solutions for Recent Advancements in Multi-Drug Resistance in Tuberculosis: A Review. *Microbiology Insights* **2023,** *16*, 1-9.

5. Pan, F.; Jackson, M.; Ma, Y.; McNeil, M., Cell wall core galactofuran synthesis is essential for growth of mycobacteria. *J Bacteriol* **2001,** *183* (13), 3991-8.

6. Angala, S. K.; Joe, M.; McNeil, M. R.; Liav, A.; Lowary, T. L.; Jackson, M., Use of Synthetic Glycolipids to Probe the Number and Position of Arabinan Chains on Mycobacterial Arabinogalactan. *ACS Chem Biol* **2021,** *16* (1), 20-26.

7. Justen, A. M.; Hodges, H. L.; Kim, L. M.; Sadecki, P. W.; Porfirio, S.; Ultee, E.; Black, I.; Chung, G. S.; Briegle, A.; Azadi, P.; Kiessling, L. L., Polysaccharide length affects mycobacterial cell shape and antibiotic susceptibility. *Science Advances* **2020,** *6*, eaba4015.

8. Bosch, B.; DeJesus, M. A.; Poulton, N. C.; Zhang, W.; Engelhart, C. A.; Zaveri, A.; Lavalette, S.; Ruecker, N.; Trujillo, C.; Wallach, J. B.; Li, S.; Ehrt, S.; Chait, B. T.; Schnappinger, D.; Rock, J. M., Genome-wide gene expression tuning reveals diverse vulnerabilities of M. tuberculosis. *Cell* **2021,** *184* (17), 4579-4592 e24.

9. Soltero-Higgin, M.; Carlson, E. E.; Gruber, T. D.; Kiessling, L. L., A unique catalytic mechanism for UDP-galactopyranose mutase. *Nat Struct Mol Biol* **2004,** *11* (6), 539-43.

10. Sanders, D. A. R.; Staines, A. D.; McMahon, S. A.; McNeil, M. R.; Whitfield, C.; Naismith, J. H., UDP-galactopyranose mutase has a novel structure and mechanism. *Nature Structural Biology* **2001,** *8* (10), 858-863.

11. Carlson, E. E.; May, J. F.; Kiessling, L. L., Chemical probes of UDP-galactopyranose mutase. *Chem Biol* **2006,** *13* (8), 825-37.

12. Dykhuizen, E. C.; May, J. F.; Tongpenyai, A.; Kiessling, L. L., Inhibitors of UDP-Galactopyranose Mutase Thwart Mycobacterial Growth. *J. Am. Chem. Soc.* **2006,** *130*, 6706-6707.

13. Kincaid, V. A.; London, N.; Wangkanont, K.; Wesener, D. A.; Marcus, S. A.; Heroux, A.; Nedyalkova, L.; Talaat, A. M.; Forest, K. T.; Shoichet, B. K.; Kiessling, L. L., Virtual Screening for UDP-Galactopyranose Mutase Ligands Identifies a New Class of Antimycobacterial Agents. *ACS Chem Biol* **2015,** *10* (10), 2209-18.

14. Soltero-Higgin, M.; Carlson, E. E.; Phillips, J. H.; Kiessling, L. L., Identification of Inhibitors for UDP-Galactopyranose Mutase. *J. Am. Chem. Soc.* **2004,** *128*, 10532-10533.

15. Winton, V. J.; Aldrich, C.; Kiessling, L. L., Carboxylate Surrogates Enhance the Antimycobacterial Activity of UDP-Galactopyranose Mutase Probes. *ACS Infect Dis* **2016,** *2* (8), 538-43.

16. Li, Q., Application of Fragment-Based Drug Discovery to Versatile Targets. *Front Mol Biosci* **2020,** *7*, 180.

17. Murray, C. W.; Rees, D. C., The rise of fragment-based drug discovery. *Nat Chem* **2009,** *1* (3), 187-92.

18. Ayotte, Y.; Bernet, E.; Bilodeau, F.; Cimino, M.; Gagnon, D.; Lebughe, M.; Mistretta, M.; Ogadinma, P.; Ouali, S. L.; Sow, A. A.; Chatel-Chaix, L.; Descoteaux, A.; Manina, G.; Richard, D.; Veyrier, F.; LaPlante, S. R., Fragment-Based Phenotypic Lead Discovery To Identify New Drug Seeds That Target Infectious Diseases. *ACS Chem Biol* **2021,** *16* (11), 2158-2163.

19. Ayotte, Y.; Bilodeau, F.; Descoteaux, A.; LaPlante, S. R., Fragment-Based Phenotypic Lead Discovery: Cell-Based Assay to Target Leishmaniasis. *ChemMedChem* **2018,** *13* (14), 1377-1386.

20. Partha, S. K.; van Straaten, K. E.; Sanders, D. A., Structural basis of substrate binding to UDP-galactopyranose mutase: crystal structures in the reduced and oxidized state complexed with UDP-galactopyranose and UDP. *J Mol Biol* **2009,** *394* (5), 864-77.

21. Ayotte, Y.; Woo, S.; LaPlante, S. R., Practical Considerations and Guidelines for Spectral Referencing for Fluorine NMR Ligand Screening. *ACS Omega* **2022,** *7* (15), 13155-13163.

22. Ayotte, Y.; Marando, V. M.; Vaillancourt, L.; Bouchard, P.; Heffron, G.; Coote, P. W.; Larda, S. T.; LaPlante, S. R., Exposing Small-Molecule Nanoentities by a Nuclear Magnetic Resonance Relaxation Assay. *J Med Chem* **2019,** *62* (17), 7885-7896.

23. Molina, D. M.; Jafari, R.; Ignatushchenko, M.; Seki, T.; Larsson, E. A.; Dan, C.; Sreekumar, L.; Cao, Y.; Nordlund, P., Monitoring Drug Target Engagement in Cells and Tissues Using the Cellular Thermal Shift Assay. *Science* **2013,** *341*, 84-87.

24. Jensen, A. J.; Molina, D. M.; Lundback, T., CETSA: a target engagement assay with potential to transform drug discovery. *Future Med. Chem* **2015,** *7* (8), 975-978.

25. Hwang, T. L.; Shaka, A. J., Water Supression That Works. Excitation Sculpting Using Arbitraty Wave-Forms and Pulsed Field Gradients. *Joutnal of Magnetic Resonance, Series A* **1995,** *112* (2), 275-279.